How a meristem cell senses its own size

Marco D'Ario

John Innes Centre

Norwich

Department of Cell and Developmental Biology

A thesis submitted to the

University of East Anglia for the degree of

Doctor of Philosophy

December 2021

Abstract

Despite many advances made in the field of cell biology, the molecular mechanism for cell size regulation remains a subject of intense study across biological kingdoms. In this study, I used plant meristematic cells as a model to address this question and proposed a mechanism for cell size control that acts at the G1/S transition and uses DNA as an internal metric. To test this hypothesis, I developed a novel live imaging technique that allowed me to follow growth and cell cycle progression in meristem cells for long periods of time and high time resolution. I also showed how total protein and nuclear size scale with cell size and analysed the cellular behaviour of inhibitors of the S-phase transition, identifying KIP RELATED 4 (KRP4) as a candidate regulator of cell size during the G1-S transition. KRP4 bound to chromatin during mitosis, suggesting a possible mechanism that uses chromosome segregation as a mean for equal inheritance, followed by dilution of KRP4 to a threshold that triggers S-phase entry. The protein F-BOX LIKE 17 (FBL17) was identified as a component used for targeted proteolysis of excess KRP4, ensuring that production of the latter matched chromatin content. To better understand the dynamics of KRP4 production and dilution, a mathematical model was produced, which predicted the behaviour of various mutants, solidifying the understanding of cell size control using DNA as an internal metric. Additionally, data for a possible size regulatory machinery acting during G2 are presented, with the hope to guide future research in this topic, suggesting a different mechanism that utilises microtubules as the measuring structure. Finally, I discuss the broader implications of this study, suggesting ways in which it could be implemented by plants during their development and consequences for the evolutionary history of cell size control in this kingdom of life.

"The scientist is not a person who gives the right answers, they are one who asks the right questions."

Claude Lévi-Strauss

Acknowledgments

First and foremost, I would like to thank my primary PhD supervisor Professor Robert Sablowski for his support, guidance, and mentoring. Thank you for always challenging my ideas and for always being open to accept my opinions. I will treasure the philosophy with which you conduct your science.

I would like to thank my secondary PhD supervisor Professor Martin Howard for giving me the change to develop my skills in mathematical modelling. Thank you for trusting me with learning and treasuring this discipline.

I would like to thank all the members of Professor Sablowski and Professor Howard laboratories for helping me throughout my PhD. In particular, I would like to thank Dr Max Bush for being there every time I needed something, Dr Rafael Tavares for the help finalising the manuscript, and Dr Emma McKechnie-Welsh for our hypothesis discussions and her moral support.

I would also like to thank Dr Laila Moubayidin whose scientific help and moral support during my career will be unreplaceable.

I would also like to thank Dr Giuseppe Facchetti for the many discussions on the mathematics of cell size regulation, and for teaching me it is never too late to learn if you are eager to know.

A special thanks to all the people involved in the rotation programme, including students and advisors, who contribute to such a wonderful environment for early scientists to develop. In particular, I would like to thank Dr Stephen Bornemann for his moral support over the years, who always found the time to listen to me. I would also like to thank Dr Antony Dodd whose help during the pandemic was timely and essential.

I would like to thank all the members of the JIC Bioimaging department whose help and support was critical for the success of this work. In particular, I would like to thank Grant Calder for teaching me half of what I know about confocal microscopy, and Dr Eva Wegel

for teaching me the other half. I would also like to thank Kim Findlay for all their patience in dealing with my requests, as well as the professional support.

Finally, I would like to thank the members of The 1Kb Band for the fun, exploratory time in the science of musical performance.

Abbreviations

ATP = adenosine triphosphate

CDK = CYCLIN DEPENDENT KINASE

CDS = coding sequence

CDT = CHROMATIN LICENSING AND DNA REPLICATION FACTOR

CFP = CYAN FLUORESCENT PROTEIN

CYC = CYCLIN

Col = Columbia

DAPI = 4',6-diamidino-2-phenylindole

DNA = deoxyribonucleic acid

E2F = E2 FACTOR

EDTA = Ethylenediaminetetraacetic acid

FBL17 = F-BOX-LIKE PROTEIN 17

G1 = Gap 1

G2 = Gap 2

GFP GREEN FLUORESCENT PROTEIN

JAG = JAGGED

KRP = KIP-RELATED PROTEIN

M = mitosis

dNTP = deoxynucleotide triphosphates

PPB = preprophase band

RBR = RETINOBLASTOMA RELATED

RCF = relative centrifugal force

RFP = RED FLUORESCENT PROTEIN

RNA = ribonucleic acid

S = synthesis

SAM = shoot apical meristem

SDS = sodium dodecyl sulphate

SMR = SIAMISE-RELATED

SNP = single nucleotide polymorphism

TOR = TARGET OF RAPAMICYN

Wt = wild type

YFP = YELLOW FLUORESCENT PROTEIN

Table of Contents

Chapter 3: G1-S size control using KRPs as proxy for chromatin content

57

Chapter 1: An introduction to cell size

1.1 Evidence for cell size control

"Omnis cellula e cellula": every cell comes from a cell, one of the paradigms of cellular life (Virchow, 1858), implies that every cell in existence is the product of the division of a mother cell. While the endless cycle of growth and division spans across generations as well as within the same multicellular organism, evidence for regulation of cell size has long been noted (Fantes *et al.*, 1975). Cell size homeostasis is an active feature of cell populations to counteract accumulated size variability. Increase of cell size variability can result from cellular growth (Hervieux *et al.*, 2017) and asymmetric division, so both phenomena need to be taken into account when studying cell size homeostasis. More broadly, both the average in cell size and cell size variability can be controlled by molecular mechanisms. I will refer to the collection of mechanisms that regulate cell size and cell size variability as "cell size control" – in this way, cell size control contains cell size homeostasis, which is specifically the process of correcting perturbation in cell size, by the reduction of variability and convergence to a target cell size.

One question that should come to mind when trying to address the problem of cell size control is what internal metric can cells use to measure their size. Ultimately, the concepts of "big" and "small" are meaningless, unless a comparison is made between two quantities. Evidence connecting growth and average cell size have long been identified (Schaechter, Maaloe and Kjeldgaard, 1958) and, whilst mechanisms to connect growth and size have been suggested (Cadart *et al.*, 2018), the nature of the internal standard used by these mechanisms remains ambiguous. In contrast, early studies on sea urchin embryos suggested that average cell size is proportional to genomic content, leading to the hypothesis that DNA itself might be used as metric for measuring cell size (Boveri, 1902).

The appealing role of DNA as internal standard is further emphasised by the plethora of examples in biology in which genomic content is quantitatively associated with increase in average cell size. In early experiments on *Nicotiana* and other *Solanaceae*, heteroploidy, the presence of an heterogenous amount of copies of the genome, was induced by the application of colchicine, and an increase in the size of various organs as the result of cell size enlargement was observed (Smith, 1943). Similarly, aneuploid stems, those whose cells possess extra chromosomes, show increase in width (Henry *et al.*, 2010). In salamander

larvae, cell size also increases in proportion to chromosome number, but the overall size of the organism is unaffected by heteroploidy (Fankhauser, 1945), perhaps suggesting a different interaction between the mechanisms that measure organ size and cell size in animals compared to plants. Critically, manipulating genomic content as a means to influence average cell size is a mechanism that evolved multiple times and it is used in many developmental programs across kingdoms. For example, many tissues of organisms in the fungi kingdom are heteroploid, a characteristic that plays diverse functions in cell size variability during development, from mycelia to spore size (Tolmsoff, 1983). Plants also provide great examples in which genome content is used to generate larger cells, particularly in the process of endoreduplication. Endoreduplication is a controlled event by which cells skip the division step of their cell cycle, but continue to progress in further phases as normal, resulting in the duplication of the genomic contents in individual cells (Melaragno, Mehrotra and Coleman, 1993). A plausible advantage of endoreduplication is the ability of increasing cell size variability within the tissue, whilst preserving size homeostasis of each lineage. Endoreduplication is well documented in leaves, although its function is debated because some plant species show no endoreduplication in their organs, and there is a high variability in endoreduplication events between species that do (Barow and Meister, 2003). Nevertheless, the connection between genomic content and cell size across kingdoms shows how mechanisms for cell size control are likely to involve processes that measure genomic content.

Studies aimed to address the question of size control, cell size homeostasis and its connection to cell cycle progression have been the focus of genetic studies for many years, particularly through the use of various cell cycle model systems, most famously *Schizosaccharomyces pombe* (Nurse, 1975). The advantage of this organism in carrying single cell studies allowed for the first observations to be made on cell variability, which was reported to reach its minimum prior to division, and increase to its maximum just after that (Mitchison, 1957). In parallel, studies conducted on bacteria produced the idea that cell size at division was under some "physiological control" (Schaechter *et al.*, 1962), and eventually, a series of studies on mouse fibroblasts highlighted that cell cycle progression through S-phase was coupled to cellular mass (Killander and Zetterberg, 1965a, 1965b; Zetterberg and Killander, 1965). These series of studies were the progenitors of studies on cell size homeostasis and cell size control, which have been carried out on a plethora of different biological systems since then. In plants, the past decade of studies has focused on

the characterisation of size homeostasis in the meristems, and have used genetic manipulation as a means to understand homeostasis *per se* (Serrano-Mislata, Schiessl and Sablowski, 2015; Willis *et al.*, 2016). The plant meristem offers a unique opportunity to study cell size homeostasis and cell size control in a multicellular context, because meristem cells are easily trackable by live imaging and their volume can be quantified accurately by image analysis. Additionally, the spatial variation of cell types in the plant meristem can be easily accounted for, giving the opportunity to study large populations of rapidly dividing cells of the same kind. For example, via overexpression of KRP4, an inhibitor of cell cycle progression which will be discussed in great details in this text, the average cell size in the central zone of the meristem was increased by four fold (Serrano-Mislata, Schiessl and Sablowski, 2015). However, cells leaving the overexpression domain in the central zone underwent multiple rounds of division to reach a target cell size (Serrano-Mislata, Schiessl and Sablowski, 2015), suggesting that plant meristem cells have cell autonomous information on their size, which is independent from lineage history and neighbouring effects. This indirectly suggested that plant meristem cells actively reduce size variability by division to reach a certain target size. In line with this observation, time lapse experiments on shoot apexes showed a negative correlation between size at birth and size at division, indicative of a mechanism for size homeostasis able to reduce ~75% of variably per round of division (Willis *et al.*, 2016). This study also confirmed the cell autonomous nature of cell size control in the meristem (Willis *et al.*, 2016), adding to the appeal of this system for the study of cell size control.

The role of cell size homeostasis is clear by its definition: it is a mechanism responsible for the reduction of accumulated variability, to prevent built up effects. However, mechanisms for cell size control can adjust both average cell size and cell size variably, the importance of which is distinct and still a subject of intense research. In the interest of understanding the role of any possible mechanisms for cell size control, I will introduce the known roles that these two quantitates have in development and evolution.

1.2 Importance of cell size

The evidence for cell size control opens the question of what might be the role of cell size and whether there is an optimal cell size. The laws that govern allometry, the study of scaling of biological features with size, have been the subject of research for long time – the observed relationship between body size and metabolism have produced the idea that

metabolic rates scale more slowly than body size does (Kleiber, 1932), so that bigger cells have slower metabolic rates. This relationship was extended in a study showing that cellular allometry scales with mitochondrial functionality, so that cellular respiration sets the limits for optimal cell size (Miettinen and Björklund, 2016).

Considering the expected impact of diffusion on respiration, it is important to consider how cell shape might impact allometric scaling. Indeed, surface and volume do not scale linearly to each other, with surface scaling quadratically and volume scaling cubically. Supporting the idea of an optimal surface to volume ratio (SV), experimental evolution-based approaches in *E. coli* showed that cells with faster growth rates and higher SV have higher fitness (Gallet *et al.*, 2017) – therefore, it might be more meaningful to talk about optimal SV, rather than optimal cell size. Metabolic allometry is particularly important for biological processes like endothermy, the physiological regulation of body heat seen in some animals, which requires high rate of gas exchange between red blood cells and their surroundings, necessary to meet tissue demand for oxygen (Szarski, 1983). Mammals may have evolved enucleation, the cellular process of removing the nucleus of a cell, as a means to optimize red blood cell SV (Szarski, 1983). Enucleation is accountable for the characteristic donut shape of red blood cells, that have higher SV than spherical cells (Szarski, 1983).

Interestingly, convergent evolution of endothermy is found in the avian lineage, but bird red blood cells do not enucleate, so high SV is accomplished by different means. Avian genomes are much smaller compared to those of mammals (Organ *et al.*, 2007), a feature thought to be under selection to maintain small red blood cells and favour endothermy (Hughes and Hughes, 1995). To support this idea, a drastic reduction in cell size occurred in the theropod lineage, long hypothesised to be endothermic, and maintained as such throughout the evolutionary trajectory of birds (Organ *et al.*, 2007). Further emphasizing the impact that selective pressure can have on cell size and on the genome size of organisms, modelling approaches have suggested that accumulation of noncoding DNA in the avian genome is under selection to optimise metabolic rates dependent on body size (Kozłowski, Konarzewski and Gawelczyk, 2003). Therefore, because of the relationship between cellular genomic content and cell size, genome size seems to be one of the traits under selection to ensure optimal cell size.

This phenomenon is also observed in the plant lineage, where cell and genome size that initially increased following whole genome duplication (WGD) events, are subsequentially reduced through evolution (Butterfass, 1987). As the name suggests, WGD are instances in which the whole genome of an organism is duplicated in one generation. WGD events are major drivers of evolution, particularly of plants, and impact a myriad of physiological and molecular processes, through direct changes in gene regulations but also through changes in cell size (for an excellent review see (Bomblies, 2020)). Unfortunately, the pleiotropic impact of WGD, which ranges from stomata transpiration to vascular transport, make it difficult to uncouple effect of cell size increase from other molecular effects. However, WGD illustrates that not only the selective pressure on cell size shapes the genomic landscape of organisms, but the opposite is true and sudden changes in genome size can have a major impact on the cell size and physiology of an organism. To further this observation, angiosperms genomes are amongst the smallest of all land plants (Simonin and Roddy, 2018), so an hypothesis has been forwarded in which the smaller angiosperm cells might favour diffusion within the cell and contribute to the success of this lineage (Benton, Wilf and Sauquet, 2021).

This tight relationship between genome and cell size raises the question of whether DNA content itself has any impact on cellular fitness. To better understand this relationship, mathematical modelling approaches have suggested that DNA concentration can become limiting to growth due to increased cell size (Lin and Amir, 2018). This phenomenon is hypothesised to result from competition between the components of the RNA transcription machinery to bind to promoter sequences, which in turn are made scarce by dilution (Lin and Amir, 2018). A fascinating, although still speculative, consequence of this idea is that some genes could be expressed in size dependent or independent manners, just by changing the affinity between the regulatory sequences of a gene to transcription factor binding (Heldt *et al.*, 2018). Thus far the technical difficulties associated with testing these hypotheses left a gap between speculation and paradigm, but experiments on yeast have shown that dilution of genomic content alone can limit growth and trigger senescence (Neurohr *et al.*, 2019). Therefore, the connection between cell size and genomic content might be not only linked to a putative role of DNA in size control, but also be the result of selective pressure on optimal growth.

Thus far, only growth and metabolic allometry have been discussed, but cell size also impacts other physiological aspects, many examples of which come from the plant lineage. Due to their function in gas exchange, stomata have a strong effect on photosynthetic efficiency and fitness (Jones, 1998). However, the size of stomatal guard cells, their concentration on the epidermis (Franks, Drake and Beerling, 2009) and their mechanical properties (Franks and Farquhar, 2007) impact plant growth non-linearly, so predicting their effect requires non-trivial biophysical models. Indeed, studies combining paleobotanical data and mathematical modelling have shown that guard cell size and stomata density have changed during the 400My of plant evolutionary history in relation to carbon dioxide availability (Franks and Beerling, 2009), showing that the size of specialised cells can be under the selective pressures of forces other than those related to cellular metabolism.

Another example is what we could call aerodynamic allometry, i.e. how aerodynamics scales with cell size. Spores of non-seeded plants are unicellular, and dispersal has a major impact on plant fitness (Haig and Westoby, 1988). The impact of force of aerodynamic drag on settling velocity, known as Stoke's law, sets optimal spore size for dispersal around $8\times10^3 \mu m^3$ (Hemsley, Scott and Collinson, 1999), well above the size of proliferating cells, which range between 100 and 200 μm^3 in the case of the plant meristem. However, the spore size of earlier land plants, those that lived 430My ago, was much smaller and evolution of larger spores occurred over 50My (Chaloner, 1967), from 430My to 390My ago (Bonacorsi *et al.*, 2021). Changes in the environment have been suggested to play a major role in the increase in average size during this period (Leslie and Bonacorsi, 2021), giving an example of how the optimal size of specialised cells might change over evolutionary time.

Another important role of cell size can be seen in flower development, where cell size within the boundary region of the developing organ preserves the cellular resolution necessary for accurate organ initiation (Serrano-Mislata, Schiessl and Sablowski, 2015). When aberration in cell size has been generated in developing flowers, defects in the number of organs produced were observed, accompanied by an increase in the variability of number of individual organs (Serrano-Mislata, Schiessl and Sablowski, 2015). This suggests that a minimum size in the boundary region is required to preserve the correct resolution of domain establishment. To confirm this view, when cell size increase is

accompanied by an increase in the whole organ, for example as result of increased ploidy (Robinson *et al.*, 2018), loss of resolution is prevented because the size of the organ relative to cell size in the boundary is preserved.

Given the many consequences of cell size for cell physiology and function, it should be therefore not surprising that cells within multicellular organisms show heterogeneity in size, reflecting their functional diversification. However, heterogeneity is also observed within cells of the same type, suggesting a more complex role for cell size variability.

1.3 Cell size variability in development

The major intrinsic sources of cell size variability in the meristem come from asymmetric division and growth variability (Nurse, 1975). The latter can be controlled by the cell (see below), but intrinsic heterogeneity in growth likely results from mechanical constraints on plant cells, which grow by generating pressure to push the cell wall (Zimmermann, Hüsken and Schulze, 1980). The variability in cell size and wall thickness generate differences in pressure and contributes to growth anisotropy (Lockhart, 1965). Additionally, variability in the cell size at division and heterogeneity in division rates across tissues contribute to heterogeneity in cell size, growth and mechanical stress (Alim, Hamant and Boudaoud, 2012). Such variability can be generated by endoreduplication events, by the inherent variability of cell cycle progression or enforced by mechanisms for cell size control. Therefore, variability in cell size and division rate feedback on growth and mechanical stress, which plays a major role in plant development.

At tissue level, the interaction between growth and mechanical stress has been studied by physical models for over 50 years and it is recognised as the "Lockhart's strain-based growth model" (Lockhart, 1965). The interactions between numerous cells in three dimensions can be very complex, especially if cell divisions are included. However, thanks to advances in computation power of the last two decades, digital frameworks for 3D mechanical modelling have emerged during the past years (Boudon *et al.*, 2015). These approaches are helping to understand how tissues behave under mechanical stress and how differences in cell size might contribute to it. The neighbouring effect of growth heterogeneity can be observed at the base of trichomes, where cells are arranged perpendicularly to the direction of maximal tensile strength (Hervieux *et al.,* 2017). The mechanical stress generated as the consequence of increase in cell size of the trichome

primordium, in respect to its neighbours, is required for bulging of this cell away from the plane of the tissue (Hervieux *et al.*, 2017). Indeed, trichomes that do not endoreduplicate and divide stop protruding outwards and resume growth as epidermal cells (Bramsiepe *et al.*, 2010). Critically, it is the difference in size generated by absence of division between the trichome and its neighbours that is responsible for this phenomenon (Hervieux *et al.*, 2017). Another example of the impact of cell size variability in plant development comes from sepals, where random fluctuation of AtML1, a transcription factor required to initiate the developmental program of giant cells in sepals, generates heterogeneity in cell size by endoreduplication (Meyer *et al.*, 2017). The role of giant cells in the sepals is to create tension in the tissue and curve of the sepal outwards upon flower maturity (Roeder *et al.*, 2010). The degree of curving is determine by the proportion of giant cells versus diploid cells (Roeder *et al.*, 2010), in a system that controls cell size variability to determine the degree of flower opening.

Locally, cell size impacts mechanical stress, with bigger cells being subjected to larger mechanical forces – this stress can be dissipated either by changing the shape of the cells, like puzzle cells on the leaf epidermis do (Sapala *et al.*, 2018), or by divisions (Alim, Hamant and Boudaoud, 2012). Therefore, the effect of cell size homeostasis can act to release mechanical stress by causing homogeneity in division across the tissue and contributing to the generation of uniform mechanical stress. Additionally, division orientation in the meristem is dependent on mechanical cues (Louveaux *et al.*, 2016), so size variability at birth is an inescapable issue the tissues are forced to deal with. However, any mechanism that prevents flexibility, thus heterogeneity, might act against reproducibility of organs shape – indeed, homogeneity in growth and cell size act against reproducibility of organ morphology (Hong *et al.*, 2016), because mechanical feedback and adjustable growth are part of the mechanisms that ensures reproducible development (Hervieux *et al.*, 2017). In a way, considering the impact of variability in division in generating noise in growth (Alim, Hamant and Boudaoud, 2012), cell size control can act to homogenise or heterogenise growth within a tissue. This phenomenon can be observed in sepal emergence, where blockage of cell division by oryzalin treatment prevents tissue folding, as the result of a lack of anisotropic growth (Zhao *et al.*, 2020). However, the interpretation of these experiments is complicated by the fact that destabilisation of microtubules by oryzalin treatment affects cell division and mechanical feedback on growth, both mediated by the cortical microtubule arrays

In *jagged* (*jag*) mutants, aberrant sepal emergence is also associated with lack of folding (Schiessl *et al.*, 2012). In these mutants, the coordination between cell size and cell cycle progression in sepal primordia is comparable to that of meristem cells (Schiessl *et al.*, 2012), where division is more homogeneous and the tissue does not fold. During the process of sepal development, *JAGGED* is specifically responsible for decoupling the relationship between cell size and S-phase progression, partly via suppression of the cell cycle inhibitor KRP4 (Schiessl, 2014; Schiessl, Muino and Sablowski, 2014). Taken together, these results might suggest that homogeneity of division, generated through cell size homeostasis in the meristem tissue, could account for the dome shape of this tissue, whilst heterogeneity in division rate and cell size might be part of the growth changes that shape organ primordia.

The discrete difference in cell size between distinctive cell types have a more evident role than continuous variability within tissues, as seen for spore size compared with proliferating tissue, or as visible in the vascular system of plants, where specialised cells show a diverse array in cell sizes (Etchells and Turner, 2010). In this context however, mechanical constraints imposed by the geometry that result from differences in cell size is responsible for the modulation of growth patterns, as seen in the case of the radicle during embryo development (Bassel *et al.*, 2014). Therefore, variability in the size of different cells across tissues might have less obvious implications related to variability in size across domains, not related to the optimal size of each cell type.

A further role in cell size variability can be seen during reproduction, where the well-known differences in the size of gametes (Matsuda and Abrams, 1999) is not only the result of differences between the optimal size of male versus female, but of the evolutionary trajectory of one in relation to the other (Togashi *et al.*, 2012). In fact, studies on the evolution of differently sized gametes in green algae have highlighted that evolutionary trends that connect size and sex might be more complex than the simple implication of optimal cell size of individual cells (Togashi *et al.*, 2012). The evolutionary history of individual sexes and how these relates to each other during the evolutionary process plays a major role in the selection of this trait (Togashi *et al.*, 2012). Plants offers unique opportunities to study the relationship between cell size and sex because of their unique reproductive cycles that involve alternation of generation and the production of the

multicellular gamete-producing phase: the gametophyte. Indeed, many spore producing plant have evolved the unique reproductive strategy of producing differently sized spores for each sex (Williamson and Scott, 1894), achieved through differential cell growth and survival between male and female spores (Simpson, 2019). Interestingly, experiments involving abiotic stress-induced cell size manipulation have suggested that cell size alone can account for difference in sex identity of developing spores (Shattuck, 1910). Early hypotheses on the evolution of differently size spores, heterospory, have suggested that fixed optimal sizes are accountable for this phenomenon, but left open the question of what evolved first, cell size variability (Haig and Westoby, 1988) or sex determination (DiMichele, Davis and Olmstead, 1989). However, recently discovered fossils have challenged both of these visions, presenting an extinct specimen with an intermediate phenotype of highly variable spores (Bonacorsi *et al.*, 2020, 2021), in which the relationship between spore size and sex is less obvious. Heterospory evolved multiple times in the plant lineage and is a critical trait for plant evolution, as it is required for the evolution of seeds (Bateman and DiMichelle, 1994). This topic is still a subject of intense research and a better understanding of the evolutionary landscape that influences spore size (Leslie and Bonacorsi, 2021), as well as a better understanding of the role of cell size variability on this landscape, will be critical to understand how plants took this important evolutionary step multiple times in their history.

In conclusion, the ability to generate and reduce variability is an important aspect of plant development and has critical repercussions on the evolutionary history of this kingdom. Ideally, any mechanism for cell size control should be able to regulate both: average cell size and cell size variability. In populations of proliferating cells, such as the meristems, any information on these will have to be delivered to the cell cycle machinery, which will act upon this information to progress towards division. Therefore, understanding the components of the cell cycle is paramount in the search for a mechanism for cell size regulation.

1.4 The plant cell cycle

The plant cell cycle has been studied for many years, and description of the individual details is beyond the scope of this text. Nevertheless, an introduction of the functional role and interaction of the major components of the cell cycle machinery will be critical for understanding the experimental design in this work. The overlap between the cell cycle

components amongst eukaryotes is substantial, so the understanding generated over the years is often similar across organisms. Therefore, I will present work carried out on various organisms, emphasising unique differences of the plant cell cycle when appropriate.
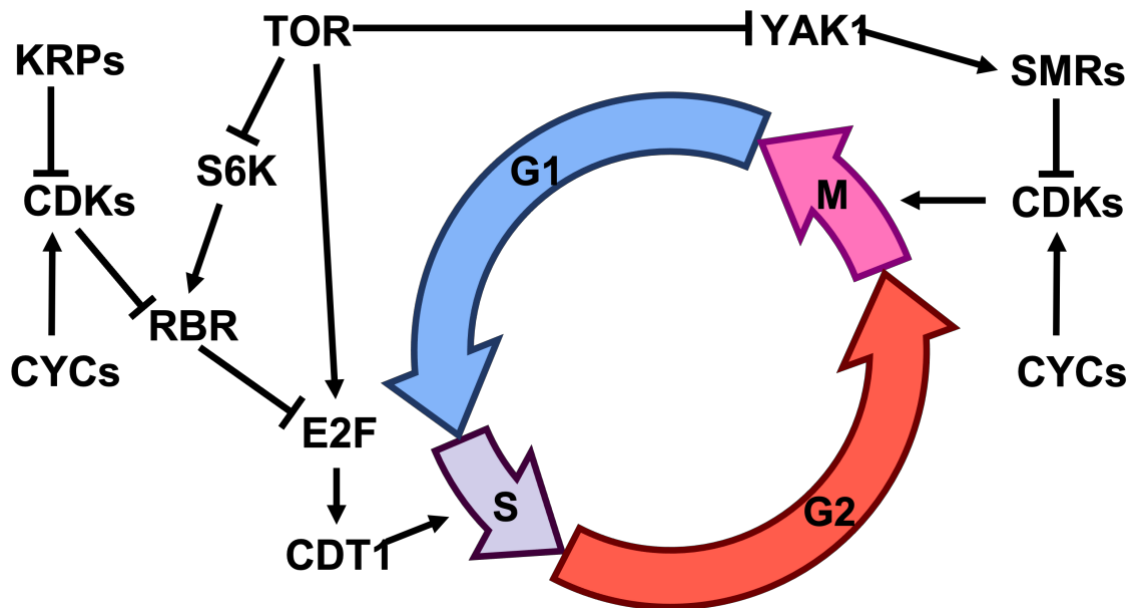
Figure 1.1: Simplified cell cycle progression in plants. New-born cells undergo a period of growth during the first Gap phase (G1) before committing to DNA synthesis, which happens during S-phase (S). They then grow again, during the second Gap phase (G2) and then divide, a process that occurs during mitosis (M). See text for more information on the individual proteins that trigger these events and how they interact with each other's.

The dawn of molecular studies of cell cycle progression is marked by the discovery of a family of proteins, the expression of which was observed to oscillate with cell cycle progression (Evans *et al.*, 1983). For this reason, those were called the CYCLINs (CYCs) and their large families, which in plants is divided into 7 subclasses of at least 49 individual genes (Verkest *et al.*, 2005), continue to be a core subject of study. The main role of CYCs is to interact with CYCLIN DEPENDENT KINASEs (CDKs) (Cdc2 in yeasts) (Fig. 1.1), to form heterodimers for the phosphorylation of a diverse set of substrates (Murray and Kirschner, 1989). The conservation of these proteins in the eukaryotic kingdom is apparent from experiments showing that the plant CDK to rescue the *cdc2* yeast mutant (Nowack *et al.*, 2012). In plants, the CDKa subfamily controls commitment to division phase as well as DNA replication (Nowack *et al.*, 2012), whilst the plant specific CDKb is only expressed during G2 and plays a role in promoting mitosis (Boudolf *et al.*, 2004) and supressing endoreduplication (Boudolf *et al.*, 2009).

Entry into S-phase is accomplished by phosphorylation and deactivation of the cell cycle inhibitor RETINOBLASTOMA RELATED (RBR) (Xie *et al.*, 1996), which is highly conserved

hotspot of eukaryotic cell cycle regulation (De Veylder, Beeckman and Inzé, 2007) (Fig. 1.1). Whilst CDKa phosphorylates RBR, it is the physical protein-protein interaction with CYCs that allows the event to occur (Soni *et al.*, 1995). Specifically, the amino acid motif LxCxE, found on the D class of cyclins, the CYCDs, is responsible for this interaction (Soni *et al.*, 1995), which is conserved across kingdoms (Dahl *et al.*, 1995). The role of RBR binding to the LxCxE motif in S-phase entry is so critical that geminiviruses evolved a mechanism to bypass the G1/S checkpoint by binding RBR via the LxCxE motif on their viral RepA protein (Xie, Suárez-López and Gutiérrez, 1995). Inhibition of RBR by RepA can even induce S-phase transition in terminally differentiated cells (Nagar *et al.*, 1995), highlighting the important role of RBR in preventing DNA replication. The importance of the LxCxE motif is further emphasised in plant development, where some transcription factors, notably SCARECROW, can interacting with RBR by this motif, (Cruz-Ramírez *et al.*, 2012) showing how deeply the plant developmental programs can interact with the cell cycle machinery.

Once phosphorylated, RBR releases the transcription factor E2F from its inhibitory binding (Hirano *et al.*, 2008), which initiates the S-phase transition (Ramirez-Parra, Fründt and Gutierrez, 2003) (Fig. 1.1). Initiation of DNA replication involves many factors, often different amongst eukaryotes (for a review, see (Dutta and Bell, 1997)). In plants, initiation of DNA replication primarily involves CDT1, but changes in chromatin condensation are also important to allow access to the DNA-replication machinery (Reiser, Sanchez-Baracaldo and Hake, 2000). Once S-phase is initiated, the E3-ligase F-BOX PROTEIN LIKE 17 (FBL17) targets CDT1 for degradation to prevent the initiation of further rounds of DNA duplication (Desvoyes *et al.*, 2019). However, the pleiotropic effects of shown by the *fbl17* mutant suggest a diverse role of this protein, ranging from reproduction to cell proliferation (Noir *et al.*, 2015). To summarise, the interaction between CYCDs and CDKa releases RBR inhibition of E2F, which activates DNA replication partially through the licensing factor CDT1 (Fig. 1.1).

Regulation of the G1/S transition, and of cell cycle progression in general, can occur at any stage of this cascade, but the phosphorylation activity of CDKa seems to be the main regulatory point. This observation partially explains the vast diversity of CYC proteins, thought to allow phosphorylation of specific subsets of targets and accounts for developmental plasticity to environmental responses (Shimotohno *et al.*, 2021). For example, CYCD3;1 is rate limiting for G1/S transition (Menges *et al.*, 2006) and its levels

drops upon sucrose starvation (Planchais, Samland and Murray, 2004), whilst CYCD6;1 promotes periclinal division in roots (Cruz-Ramírez *et al.*, 2012). Further highlighting the role of cyclin diversity in plant development, CYCD5;1 timely expression during stomata development is necessary for switching from asymmetric division symmetric division in the last division that generates the guard cells (Han *et al.*, 2018), and CYCA2;3 supresses endoreduplication and its normally downregulated in leaves to promote the endocycle (Boudolf *et al.*, 2009).

Another less abundant family of proteins binds to CDKs, but, in contrast with CYCs, their role is to inhibit CDK activity. The KIP-RELATED PROTEINs (KRPs) were originally identified via a yeast two-hybrid screen using CDKa1;1 as bait (Wang, Fowke and Crosby, 1997; Lui *et al.*, 2000; De Veylder *et al.*, 2001; Jasinski *et al.*, 2002). Seven of them can be found in the Arabidopsis genome via *in silico* analysis and were called INHIBITOR OF CDKs (ICKs) for obvious reasons, but are now widely recognised as KRP 1 to 7, due to short amino acid sequences similarity with the mammalian KIP inhibitors (De Veylder *et al.*, 2001). As their mammalian and yeast counterparts, KRPs inhibit CDK activity, but yeast two-hybrid and co-expression phenotypic rescuing have shown that KRPs inhibit CDKa but no CDKb (Schnittger *et al.*, 2003), implying that KRPs primary function as inhibitors of the G1/S transition (Fig. 1.1). KRPs can be broadly organised in two distinct families, based on their number of exons (Torres-Acosta, Fowke and Wang, 2011) and distinct subcellular localisation (Bird *et al.*, 2007), and different KRPs have been shown to perform specific functions. For example, KRP6 and KRP7 arrest cell cycle progression in the vegetative cell during pollen development, and FBL17 releases their inhibition to allow the development of the sperm cell (Kim *et al.*, 2008). Instead, KRP2 is involved in gibberellin acid signalling and determination of meristem size (Serrano-Mislata *et al.*, 2017). Additionally, transcription of KRP4 and KRP2 is suppressed by JAGGED (Schiessl, Muino and Sablowski, 2014) to repress growth in floral organs during sepal development (Schiessl *et al.*, 2012). Due to their role as inhibitors of the cell cycle, KRPs will be discussed much further in this text, particularly using KRP4 as a representative protein of this family. Additionally, KRPs stabilisation is regulated by FBL17 (Noir *et al.*, 2015), so the role of this E3-ligase in cell size control and cell cycle progression will also be the major subject of this text.

CYCs have been shown to have roles both in G1 and during G2, but KRPs seem to only function in inhibiting the S-phase entry (Schnittger *et al.*, 2003). Another plant specific

family of proteins perform the inhibitory role during G2: the SIAMESE RELATED PROTEINs (SMRs) (Churchman *et al.*, 2006) (Fig. 1.1). The role of SIAMESE (SIM), which gave the name to the family, in promoting endoreduplication of developing trichomes (Walker *et al.*, 2000) by downregulation of CYCB1;2 transcription (Schnittger *et al.*, 2002), shows that the SMRs inhibitory role can act both via physical interaction of with CDKs and via transcriptional regulation of cell cycle related genes. Similarly, SMR1, previously called LOSS OF GIANT CELLS FROM ORGANS (LGO), promotes endoreduplication in the sepals and is required for giant cell formation via major transcriptional changes (Schwarz and Roeder, 2016). However, the SMRs belong to a large family of proteins, with 17 distinct members in Arabidopsis (Kumar *et al.*, 2015), some of which have other suggested roles, like regulation of a DNA damage checkpoint (Yi *et al.*, 2014). SMR11 is of particular interest because is the only SMR found to be expressed in the meristem by *in situ* hybridisation experiments (Yang, Wightman and Meyerowitz, 2017), but its role is unknown – presumably, the role of SMR11 in the meristem does not involve endoreduplication, since this phenomenon is not observed in this organ, so perhaps it might have other functions related to cell cycle progression.

All in all, the cell cycle machinery is certainly complicated and many of its regulatory proteins have adopted unique roles in plant development. Interestingly, most of the diversity in terms of family size occurs through interaction of CDKa, in line with this being the major point of regulation of the cell cycle. However, cell size depends not only on the timing of cell cycle progression, but also on the cellular growth rate. Regulation of cell growth is a complex topic that has many repercussions for the mechanisms for cell size control.

1.5 Cell growth

To understand how fast cells grow and how this rate of growth relates to cell size, the concept of growth rate has been used over the years. However, different definitions of growth rate, which generally describes of how cell size changes over time, can express very different concepts. For example, absolute growth rate is expressed as the rate of change of size over a period of time, and in the case of cells, it is measured as $\mu m^3 h^{-1}$ (micrometre cubed per hour). In contrast, relative growth rate is the increase in size relative to the starting size per unit of time, and is measured in h^{-1} (per hour). In fact, there are various ways to measure those quantities, all of which result in a different scale. In my opinion, the

naming system, which uses the word absolute but then it is measured using volume, when relative growth does not, can generate some confusion in this topic. Importantly, if absolute growth is constant over time, it is said that cells grow linearly. Instead, if relative growth is constant over time, cells are said to grow exponentially – in this case, the rate of absolute size accumulation increases over time. In Chapter 5 I will discuss the mathematical definition of these two quantities, and I will give an explanation of how linear and exponential growth relates to size control, but here these definitions will be useful to understand the controversy generated over the years regarding the way cells grow. I will also mainly refer to relative growth rate, as it has more meaningful consequences.

During classic experiments on *S. pombe* cell size regulation, different arguments were made that cells growth exponentially (Fantes and Nurse, 1977) or linearly (Kubitschek and Clay, 1986), depending on the studies. Importantly, if linear growth were true, there would not be the need for a mechanism for cell size homeostasis (Facchetti, Chang and Howard, 2017), because the fixed amount of growth per unit of time would be smaller in comparison to large cells and larger relative to small cells, causing the sizes to converge over time. It was later suggested that growth rate of *S. pombe* would change between G1 and G2, with the latter being faster (Baumgärtner and Tolić-Nørrelykke, 2009). In this "bilinear" growth habit, cells would grow linearly at lower rates, then speed up after DNA replication has occurred. Meanwhile, studies explained how hard is to distinguish between different growth modes, because when considering variability, either curve can fit the experimental data (Cooper, 2006). However, it is now widely excepted that *S. pombe* cells grow exponentially (Cooper, 2013), with multiple reports in other organisms supporting this view, ranging from bacteria (Schaechter, Maaloe and Kjeldgaard, 1958) to budding yeast (Tyson, Lord and Wheals, 1979) and mammalian cells (Hola and Riley, 1987).

Of course exponential growth is also supported for plant proliferating tissues, in which the average relative growth rate across the meristem is independent of cell size (Willis *et al.*, 2016) even in the case of artificially enlarged cells (Serrano-Mislata, Schiessl and Sablowski, 2015). However, the relative growth rate seems to be different across tissues and organs, like in flower buds, where the larger the cells, the faster the growth rate (Jones *et al.*, 2017). Whether there is a correlation between cell size and growth rates of siter cells is controversial, as some report have found such a correlation (Willis *et al.*, 2016), whilst others, including this study, have not (D'Ario *et al.*, 2021). However, a correlation between

growth rate and the average size in a cell population is well documented, for example in plant meristem cells that increase in size when exposed to sucrose, which increases relative growth rates (Jones *et al.*, 2017). Note that the opposite is often wrongly assumed, but meristem cells have comparable relative growth rates even over a wide range of cell sizes (Serrano-Mislata, Schiessl and Sablowski, 2015), and growth can be impaired due to excessive cell size in yeast (Neurohr *et al.*, 2019). Therefore, this evidence would indicate that cell size and the mechanism for cell cycle progression have no impact on relative growth rate, but the opposite is true, suggesting that information on growth rate can be integrated by cells to control cell cycle progression and cell size.

A further complication in the analysis of how cell growth relates to cell size is that some plant tissues have a unique way to drive cell expansion, driven mostly by expansion of the vacuole, a plant specific organelle which by rapid fluid intake can cause growth by turgor pressure (Zimmermann, Hüsken and Schulze, 1980). Although this mechanism is very important in some organs like leaves (Marty, 1999) and for the dynamic regulation of cell size in specialised cells like stomata (Tanaka *et al.*, 2007), a similar function cannot be expected for the meristem cells. Indeed, meristematic tissues show almost no vacuolar volume (Priestley, 1929), so must regulate growth by protein synthesis like in other systems. Perhaps, vacuolar expansion in emerging flower primordia can explain the increase in growth rate observe in these organs when compared to the meristem (Jones *et al.*, 2017).

Part of the controversy in growth rate may relate to the fact that cell growth rate can be regulated molecularly through ribosome biogenesis across kingdoms of life (Arsham and Neufeld, 2006). Intrinsic variability in this regulation can impact measurements and result in complex growth behaviour. TARGET OF RAPAMYCIN (TOR) is a conserved protein across eukaryotic kingdoms, which functions as a central hub for regulation of growth rates in yeast (Heitman, Movva and Hall, 1991), animals (Sabers *et al.*, 1995) and plants (Menand *et al.*, 2002). TOR is a kinase that acts in complex with REGULATORY-ASSOCIATED PROTEIN OF TOR (RAPTOR) (Salem *et al.*, 2017) and the LETHAL WITH SEC THIRTEEN 8/G PROTEIN β SUBUINIT-like (LST8) (Moreau *et al.*, 2012) to phosphorylate a partially conserved subset of targets and promote cellular growth. TOR downregulation causes growth arrest (Deprost *et al.*, 2007), indicating that constant TOR activity is required for regular growth (Fig. 1.1).

Amongst the conserved targets of TOR phosphorylation, the TAP46 subunit of PROTEIN PHOSPHATASE 2A (PP2A) modulates growth and metabolism (Ahn *et al.*, 2011). PP2A is a phosphatase with multiple targets, including ribosomal subunits and cell cycle progression proteins (reviewed in (Janssens and Goris, 2001)). Another conserved phosphorylation cascade that leads to increased ribosome activity, triggered by TOR, starts from the phosphorylation of the S6 KINASE (S6K) (Mahfouz *et al.*, 2006), which in turn phosphorylates the ribosomal protein S6 to promote translation (Chung *et al.*, 1992). Interestingly, S6K forms a complex with RBR and E2F, promoting the nuclear localization of RBR to enhance its repressor activity (Henriques *et al.*, 2010), showing how the TOR pathway can interact with the cell cycle machinery (Fig. 1.1). Corroborating this idea, TOR integrates information on glucose availability via direct phosphorylation of E2F (Xiong *et al.*, 2013), suggesting that TOR not only regulates growth rate, but also division rate by facilitating cell cycle progression. Phosphorylation of E2F by TOR is also triggered by auxin to initiate S-Phase in root and shoot meristem via E2F (Li *et al.*, 2017). TOR can also communicate to the cell cycle machinery in G2 by suppressing SMR expression trough phosphorylation of YET ANOTHER KINESE 1 (YAK1) (Van Leene *et al.*, 2019), and activate CDK activity in the roots (Barrada *et al.*, 2019) (Fig. 1.1). Indeed, TOR signalling might be what links cell size to growth rate, by interacting with the molecular thresholds required for cell cycle progression. To my knowledge, the opposite relationship, one communicating from the cell cycle to TOR, has not been described to date (Pérez-Hidalgo and Moreno, 2017; McCready, Spencer and Kim, 2020), a paradigm that would further support the idea that changes in growth rate can modulate cell size, but information from cell size cannot be relayed back to the growth rate machinery. Importantly, a mechanism for cell size control has to take into account how the machinery behind growth regulation interacts with it.

1.6 Molecular mechanisms for cell size homeostasis

With the established molecular mechanism linking the growth rate machinery to cell cycle progression, it is not surprising that means for cell size homeostasis that involve regulation of growth have been suggested. One such mechanism was shown in mammalian cell cultures, which the smaller they are, the faster they grow in order to offset their size at birth (Cadart *et al.*, 2018). However, a mechanism that regulates cell cycle duration is also in play, suggesting that control over growth rate is only part of the mechanism for size homeostasis in mammalian cells (Cadart *et al.*, 2018). Interestingly, in this case the

relationship between cell size and growth rate, with smaller cells having higher relative growth rates, is the opposite to the one observed in other cases (Jones *et al.*, 2017), where higher relative growth correlated with larger cells – this would suggest that mechanisms that use growth rate to control size homeostasis are different from the mechanisms that link growth rate to increase in cell size. A similar mechanism to the one shown in mammalian cells was suggested in plants (Willis *et al.*, 2016), but the corresponding data on growth rate are incongruent with other reports, including this study (D'Ario *et al.*, 2021). Nevertheless, advances have been made in the description of molecular mechanisms for cell size regulation, many of which converge on similar pathways of the cell cycle.

The search for molecular mechanisms for cell size homeostasis has been a tortuous one, with some of the proposed mechanisms later shown to regulate target cell size but not cell size homeostasis. Notably, the protein Pom1 in *S. pombe* was suggested to measure the length of fission yeast cells, through a molecular gradient from either end of the cell that negative regulates cell cycle progression (Martin and Berthelot-Grosjean, 2009). Such gradient would be lowest in the middle of the cell and its effect would be reduced by cell enlargement, eventually releasing its inhibitory effect and allowing the cell to divide (Martin and Berthelot-Grosjean, 2009). It was later shown however, that mutants in *pom1* were smaller, but have similar cell size variability to the wild type, meaning that *S. pombe* can achieve cell size homeostasis regardless of Pom1 (Wood and Nurse, 2013). For this reason, forward genetic approaches have been taken in yeast to find components of the cell size homeostasis machinery, screening for mutation in cell size variability (Scotchman *et al.*, 2021). It will be interesting to see in the near future what role these genes might play in size homeostasis.

In budding yeast, the relationship between genomic content and cell size inspired a titration-based model involving Cln3 (Polymenis and Schmidt, 1997), which is a G1 cyclin analogous to plant CYCD3. In this system, accumulation of Cln3 would increase as cell size increased, together with protein number, and interact with the cell cycle progression machinery on specific sites on DNA (Wang *et al.*, 2009), effectively using information on DNA concentration as metric for measuring cell size. However, lack of size homeostasis-related phenotypes moved the attention towards other cell cycle proteins (for a review of the Cln3 hypothesis and its testing, see (Turner, Ewald and Skotheim, 2012)).

One such mechanisms is the area sensing mechanism that regulates cell size homeostasis in *S. pombe* (Pan *et al.*, 2014). In this mechanism, accumulation of the kinase Cdr2, a promoter of cell division, was shown to be proportional to surface area of the cell (Pan *et al.*, 2014). Fission yeast can accomplish this thanks to a subcellular structure, called the cortical band, that surrounds the nucleus and is proportional to the diameter of the cell, which remains constant during growth (Streiblová and Wolf, 1972). Cdr2 accumulates on the cortical band, therefore using this structure as internal scale. The dynamics of binding and unbinding to the band have been shown to result in the measurement of a surface area-like quantity, called pseudo area, which effectively is a measurement of volume over the cell perimeter (Pan *et al.*, 2014; Facchetti, Knapp, Flor-Parra, *et al.*, 2019). Through mathematical modelling and targeted genetic manipulation, it was possible to modify the geometric scaling of Cdr2 from area to length (Facchetti, Knapp, Flor-Parra, *et al.*, 2019), showing that modification of the molecular dynamics might have large impact on mechanisms for cell size homeostasis, particularly on the geometric sensing of size. Interestingly, it is thought that another mechanism for size homeostasis, which measures volume, runs in the background of the Cdr2 pathway (Facchetti, Knapp, Flor-Parra, *et al.*, 2019), so further work will need to take place to understand homeostasis to the full extent in *S. pombe*. Nevertheless, these studies have highlighted the importance of the geometric definition of cell size, as volume, area or length, especially because apparent increased variability can be masked when measuring the wrong geometric quantity (Facchetti, Knapp, Chang, *et al.*, 2019).

All reported mechanisms for cell size homeostasis, apart from Cdr2 and the one described in this text, involve the inhibitor of the G1/S transition RBR, or a functionally analogous protein. The first of such systems was reported in the unicellular green alga *Chlamydomonas reinhardtii*, referred here as Chlamydomonas, in which the RBR homologue MAT3 regulates cell size homeostasis (Umen and Goodenough, 2001). The unique vegetative growth behaviour of Chlamydomonas offers a new way to study cell size homeostasis, because the Chlamydomonas cell cycle is much different from the ones discussed thus far. Chlamydomonas cells grow during the day, accumulating volume without dividing – at night, Chlamydomonas cells undergo multiple rounds of S-phase and division without further growth, and the number of these rounds is dependent on their size at dusk (Umen and Goodenough, 2001) (Fig. 1.2). In this way, the number of divisions counteracts cell size variability accumulated during growth. MAT3 is required for

determining the number of division cycles that Chlamydomonas undergoes at night (Umen and Goodenough, 2001). Supporting the role of MAT3 in size homeostasis, not only the cell size for commitment to S-phase is reduced in *mat3* mutants, but the cell size variability is increased in the mutant (when calculated as coefficient of variation from (Umen and Goodenough, 2001)). The proposed mechanism of homeostasis via MAT3 involves the green algae unique class of CKDs, CDKGs, which has been proposed to act as proxy to measure DNA content in dividing cells (Li *et al.*, 2016) (Fig. 1.2). CDKGs promote cell cycle progression by inhibitory phosphorylation of MAT3, which in turn is associated with chromatin (Olson *et al.*, 2010). While CDKGs concentration is constant throughout Chlamydomonas life cycle, DNA concentration increases per each division, effectively reducing the ratio between CDKG and DNA content (Li *et al.*, 2016) (Fig. 1.2). Eventually, the concentration of MAT3 binding sites overwhelms CDKG concentration and division cycles stop (Li *et al.*, 2016) (Fig. 1.2). Although the CDKG titration model seems similar to the one suggested for Cln3, CDKG works the opposite way, with constant CDKG during growth and titration performed by increased concentration of DNA. In this way, the role as internal standard performed by DNA is much more obvious in the CDKG model, than in the one proposed for Cln3. However, the unique way in which cell cycle progresses in Chlamydomonas, combined with the fact that CDKGs are not found outside green algae,
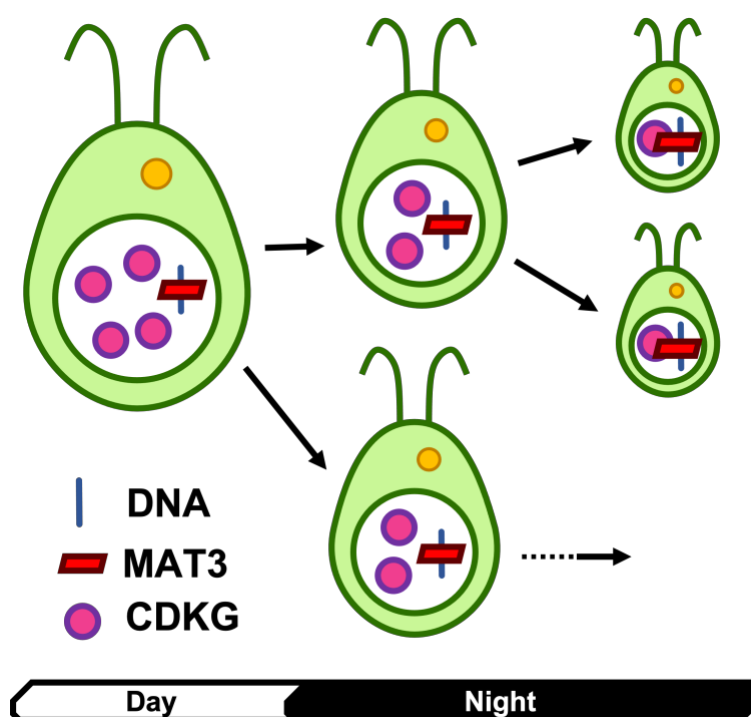
Figure 1.2: Cell size homeostasis in *Chlamydomonas reinhardtii*. Chlamydomonas cells grow during the day and divide at night, where they undergo multiple rounds of division. While the concentration of CDKG (purple circle) remains constant, the concentration of DNA (blue line) increases, because of DNA replication. MAT3 (red parallelogram) is associated with DNA so when the ratio of MAT3 and CDKG increases until further division are inhibited.

suggests that this is a highly derived mechanism for size homeostasis, that might as well be unique to this taxon. Nevertheless, the role of DNA content as internal standard and the involvement of protein dilution might be a more conserved feature of cell size homeostasis.

In *S. cerevisiae*, the suggested model for cell size homeostasis involves dilution of the inhibitor Whi5, which is a functional analogue to the plant RBR (Schmoller *et al.*, 2015). Whi5 concentration is highest at birth, and growth-driven dilution results in the release of the inhibitory action of Whi5, triggering S-phase transition (Schmoller *et al.*, 2015) (Fig. 1.3). This system requires that the same amount of Whi5 is inherited at birth regardless of size at division, to counteract accumulated variability. To do so, it has been proposed that Whi5 accumulates in a size-independent way during G2, due to the specific affinity of the Whi5 promoter to transcriptional regulators (Heldt *et al.*, 2018). Indeed, the synthesis rate of proteins expressed under the Whi5 promoter is not dependent on cell size (Swaffer *et al.*, 2021). Note that a fixed duration of G2 is required by this system to ensure consistent accumulation of Whi5 before division (Schmoller *et al.*, 2015), so that variability in G2 duration impacts Whi5 production. Finally, equal partitioning of Whi5 between sister cells has been suggested to occur via chromatin based interactions (Swaffer *et al.*, 2021) (Fig. 1.3). In this way, DNA in *S. cerevisiae* is used as segregating agent, rather than internal metric for measuring size. A similar model has been suggested in mammalian cells, performed by Retinoblastoma (Rb), mammalian homologue of the plant RBR, although mechanisms for volume independent production have not been described yet (Zatulovskiy *et al.*, 2020). Additionally, although mammalian Rb has been shown to associate with chromatin after division, it appeared dispersed in the cytoplasm during chromosome inheritance (Zatulovskiy *et al.*, 2020), thus a role for chromatin in equal partitioning of Rb is not fully established. I will discuss the implications and nature of dilution mechanisms throughout this text and in the final chapter I will examine the controversy behind these models (Barber, Amir and Murray, 2020).

The important observation to be made on the search of molecular mechanisms for cell size homeostasis is that many mutants affecting the cell cycle have shown phenotypic differences in average cell size, but this feature does not directly imply a role of such proteins in size homeostasis. Indeed, only phenotypes in the variability of cell size can indicate such a relationship. Finally, in light of the information presented thus far, I would like to review my specific goals during this study.
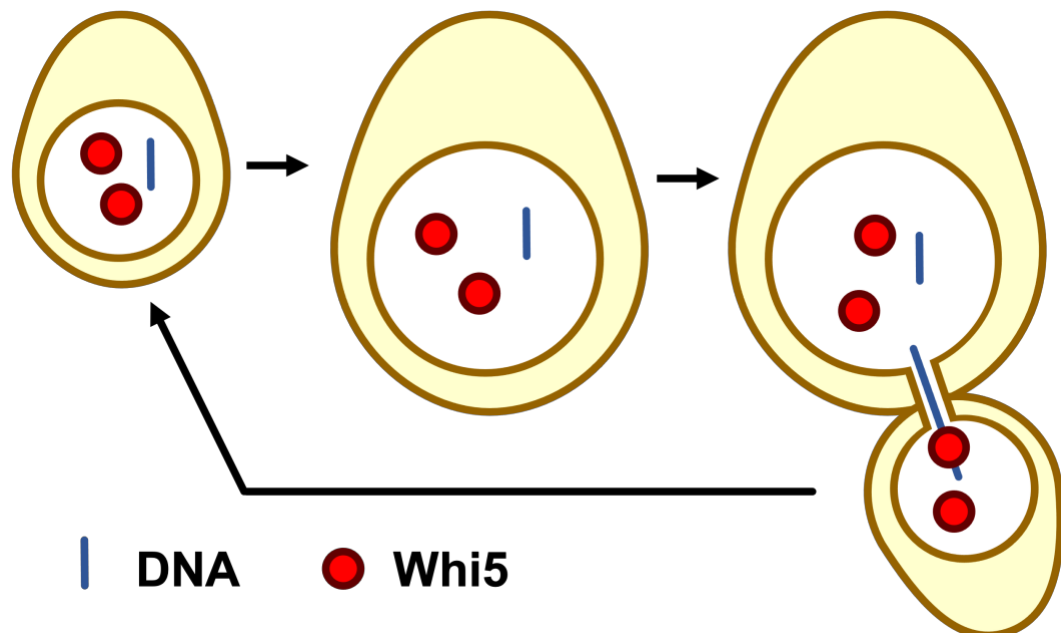
Figure 1.3: Cell size homeostasis in *Saccharomyces cerevisiae*. Budding yeast cells grow to dilute the inhibitor Whi5 (red circle), until its inhibitory effect is released, and the cell enters S-phase and eventually buds. Whi5 is transported to the budding cells via interaction with DNA. The cycle starts again after mitosis is completed.

1.7 The focus of this work

"What is the molecular mechanism used by cells to measure their size?" this was the main research question that guided this study. I used plant meristem cells as model system to answer this question, taking advantage of the many molecular resources developed for the model species *Arabidopsis thaliana*. Additionally, meristem cells are easy to track and proliferate constantly and quickly, providing a reliable system to observe cells growing and dividing. To tackle the question on the mechanism behind size homeostasis, I firstly sought to study how cell size variability changed during the cell cycle. My hypothesis was that a reduction of the cell size variability accumulated at birth would have either occurred at the G1/S transition or at division. Answering this question first was critical to select which group of cell cycle regulators to focus on. Once I identified the G1/S transition as the phase during which size homeostasis is achieved, inspired by previous work on cell size homeostasis my objective was to find a protein with the necessary characteristic of a size-dependent inhibitor of cell cycle progression. To study the behaviour of various proteins and identify the best candidates, I employed a novel approach involving live imaging of growing apexes, carried out at high time resolution. This type of approach was necessary because the objective was not simply to observe protein concentration and subcellular localisation, but how those changed in relation of cell cycle progression.

Once KRP4 was identified to be the proteinaceous component linking cell size to cell cycle progression, my main objective was to understand the molecular mechanism that allows cell size-independent accumulation of this protein. Using previously developed understanding of the plant cell cycle, my approach was to combine molecular and genetic techniques to show the involvement of FBL17 in the volume independent accumulation of KRP4, a process required for achieving homeostasis. Again, live imaging and image analysis technique were critical approaches for answering this question. To corroborate the observation obtained for KRP4, FBL17 and their role in size homeostasis, I produced a mathematical model, with the objective of recapitulating observed behaviour and predict the phenotype of mutants in the genes described so far. This approach allowed me to verify the hypothesis regarding the role of KRP4 in size homeostasis, as well as better understanding the role of FBL17 in controlling how cell size variability is counteracted by this system.

1.8 References

Ahn, C. S. *et al.* (2011) 'The PP2A regulatory subunit Tap46, a component of the TOR signaling pathway, modulates growth and metabolism in plants', *The Plant cell*. 2011/01/07. American Society of Plant Biologists, 23(1), pp. 185–209. doi: 10.1105/tpc.110.074005.

Alim, K., Hamant, O. and Boudaoud, A. (2012) 'Regulatory role of cell division rules on tissue growth heterogeneity', *Frontiers in plant science*. Frontiers Research Foundation, 3, p. 174. doi: 10.3389/fpls.2012.00174.

Arsham, A. M. and Neufeld, T. P. (2006) 'Thinking globally and acting locally with TOR', *Current Opinion in Cell Biology*, 18(6), pp. 589–597. doi: https://doi.org/10.1016/j.ceb.2006.09.005.

Barber, F., Amir, A. and Murray, A. W. (2020) 'Cell-size regulation in budding yeast does not depend on linear accumulation of Whi5', *Proceedings of the National Academy of Sciences*, 117(25), p. 14243 LP-14250. doi: 10.1073/pnas.2001255117.

Barow, M. and Meister, A. (2003) 'Endopolyploidy in seed plants is differently correlated to systematics, organ, life strategy and genome size', *Plant, Cell & Environment*. John Wiley & Sons, Ltd, 26(4), pp. 571–584. doi: https://doi.org/10.1046/j.1365-3040.2003.00988.x.

Barrada, A. *et al.* (2019) 'A TOR-YAK1 signaling axis controls cell cycle, meristem activity and plant growth in Arabidopsis', *Development*, 146(3). doi: 10.1242/dev.171298.

Bassel, G. W. *et al.* (2014) 'Mechanical constraints imposed by 3D cellular geometry and arrangement modulate growth patterns in the Arabidopsis embryo', *Proceedings of the National Academy of Sciences*, 111(23), p. 8685 LP-8690. doi: 10.1073/pnas.1404616111.

Bateman, R. M. and DiMichelle, W. A. (1994) 'Heterospory: the most iterative key innovation in the evolutionary history of the plant kingdom', *Biological Reviews*. John Wiley & Sons, Ltd, 69(3), pp. 345–417. doi: https://doi.org/10.1111/j.1469-185X.1994.tb01276.x.

Baumgärtner, S. and Tolić-Nørrelykke, I. M. (2009) 'Growth pattern of single fission yeast cells is bilinear and depends on temperature and DNA synthesis', *Biophysical journal*. The Biophysical Society, 96(10), pp. 4336–4347. doi: 10.1016/j.bpj.2009.02.051.

Benton, M. J., Wilf, P. and Sauquet, H. (2021) 'The Angiosperm Terrestrial Revolution and the origins of modern biodiversity', *New Phytologist*. John Wiley & Sons, Ltd, n/a(n/a). doi: https://doi.org/10.1111/nph.17822.

Bird, D. A. *et al.* (2007) 'Arabidopsis cyclin-dependent kinase inhibitors are nuclear-localized and show different localization patterns within the nucleoplasm', *Plant Cell Reports*, 26(7), pp. 861–872. doi: 10.1007/s00299-006-0294-3.

Bomblies, K. (2020) 'When everything changes at once: finding a new normal after genome duplication', *Proceedings of the Royal Society B: Biological Sciences*. Royal Society, 287(1939), p. 20202154. doi: 10.1098/rspb.2020.2154.

Bonacorsi, N. K. *et al.* (2020) 'A novel reproductive strategy in an Early Devonian plant.', *Current biology*. England, pp. R388–R389. doi: 10.1016/j.cub.2020.03.040.

Bonacorsi, N. K. *et al.* (2021) 'Omniastrobus gen. nov., an Emsian Plant with Implications for the Evolution of Heterospory in the Early Devonian', *International Journal of Plant Sciences*. The University of Chicago Press, 182(3), pp. 198–209. doi: 10.1086/712356.

Boudolf, V. *et al.* (2004) 'B1-Type Cyclin-Dependent Kinases Are Essential for the Formation of Stomatal Complexes in Arabidopsis thaliana', *The Plant Cell*, 16(4), pp. 945–955. doi: 10.1105/tpc.021774.

Boudolf, V. *et al.* (2009) 'CDKB1;1 forms a functional complex with CYCA2;3 to suppress endocycle onset', *Plant physiology*. 2009/05/20. American Society of Plant Biologists, 150(3), pp. 1482–1493. doi: 10.1104/pp.109.140269.

Boudon, F. *et al.* (2015) 'A Computational Framework for 3D Mechanical Modeling of Plant Morphogenesis with Cellular Resolution', *PLOS Computational Biology*. Public Library of Science, 11(1), p. e1003950. Available at:

https://doi.org/10.1371/journal.pcbi.1003950.

Boveri, T. (1902) *Das Problem der Befruchtung*. G. Fischer.

Bramsiepe, J. *et al.* (2010) 'Endoreplication Controls Cell Fate Maintenance', *PLOS Genetics*. Public Library of Science, 6(6), p. e1000996. Available at: https://doi.org/10.1371/journal.pgen.1000996.

Butterfass, T. (1987) 'Cell Volume Ratios of Natural and of Induced Tetraploid and Diploid Flowering Plants', *CYTOLOGIA*, 52(2), pp. 309–316. doi: 10.1508/cytologia.52.309.

Cadart, C. *et al.* (2018) 'Size control in mammalian cells involves modulation of both growth rate and cell cycle duration', *Nature Communications*, 9(1), p. 3275. doi: 10.1038/s41467-018-05393-0.

Chaloner, W. G. (1967) 'Spores and land-plant evolution', *Review of Palaeobotany and Palynology*, 1(1), pp. 83–93. doi: https://doi.org/10.1016/0034-6667(67)90112-1.

Chung, J. *et al.* (1992) 'Rapamycin-FKBP specifically blocks growth-dependent activation of and signaling by the 70 kd S6 protein kinases', *Cell*, 69(7), pp. 1227–1236. doi: https://doi.org/10.1016/0092-8674(92)90643-Q.

Churchman, M. L. *et al.* (2006) 'SIAMESE, a plant-specific cell cycle regulator, controls endoreplication onset in Arabidopsis thaliana', *The Plant cell*. 2006/11/10. American Society of Plant Biologists, 18(11), pp. 3145–3157. doi: 10.1105/tpc.106.044834.

Cooper, S. (2006) 'Distinguishing between linear and exponential cell growth during the division cycle: single-cell studies, cell-culture studies, and the object of cell-cycle research', *Theoretical biology & medical modelling*. BioMed Central, 3, p. 10. doi: 10.1186/1742-4682-3-10.

Cooper, S. (2013) 'Schizosaccharomyces pombe grows exponentially during the division cycle with no rate change points.', *FEMS yeast research*. England, 13(7), pp. 650–658. doi: 10.1111/1567-1364.12072.

Cruz-Ramírez, A. *et al.* (2012) 'A bistable circuit involving SCARECROW-RETINOBLASTOMA integrates cues to inform asymmetric stem cell division', *Cell*, 150(5), pp. 1002–1015. doi: 10.1016/j.cell.2012.07.017.

D'Ario, M. *et al.* (2021) 'Cell size controlled in plants using DNA content as an internal scale', *Science*, 372(6547), p. 1176 LP-1181. doi: 10.1126/science.abb4348.

Dahl, M. *et al.* (1995) 'The D-type alfalfa cyclin gene cycMs4 complements G1 cyclin-deficient yeast and is induced in the G1 phase of the cell cycle', *The Plant cell*, 7(11), pp. 1847–1857. doi: 10.1105/tpc.7.11.1847.

Deprost, D. *et al.* (2007) 'The Arabidopsis TOR kinase links plant growth, yield, stress

resistance and mRNA translation', *EMBO reports*. John Wiley & Sons, Ltd, 8(9), pp. 864–870. doi: https://doi.org/10.1038/sj.embor.7401043.

Desvoyes, B. *et al.* (2019) 'FBL17 targets CDT1a for degradation in early S-phase to prevent Arabidopsis genome instability', *bioRxiv*, p. 774109. doi: 10.1101/774109.

DiMichele, W. A., Davis, J. I. and Olmstead, R. G. (1989) 'Origins of heterospory and the seed habit: the role of heterochrony', *TAXON*. John Wiley & Sons, Ltd, 38(1), pp. 1–11. doi: https://doi.org/10.2307/1220881.

Dutta, A. and Bell, S. P. (1997) 'INITIATION OF DNA REPLICATION IN EUKARYOTIC CELLS', *Annual Review of Cell and Developmental Biology*. Annual Reviews, 13(1), pp. 293–332. doi: 10.1146/annurev.cellbio.13.1.293.

Etchells, J. P. and Turner, S. R. (2010) 'The PXY-CLE41 receptor ligand pair defines a multifunctional pathway that controls the rate and orientation of vascular cell division', *Development*, 137(5), pp. 767–774. doi: 10.1242/dev.044941.

Evans, T. *et al.* (1983) 'Cyclin: A protein specified by maternal mRNA in sea urchin eggs that is destroyed at each cleavage division', *Cell*, 33(2), pp. 389–396. doi: https://doi.org/10.1016/0092-8674(83)90420-8.

Facchetti, G., Knapp, B., Chang, F., *et al.* (2019) 'Reassessment of the basis of cell size control based on analysis of cell-to-cell variability', *Biophysical Journal*, 117(9), pp. 1728–1738. doi: https://doi.org/10.1016/j.bpj.2019.09.031.

Facchetti, G., Knapp, B., Flor-Parra, I., *et al.* (2019) 'Reprogramming Cdr2-Dependent Geometry-Based Cell Size Control in Fission Yeast', *Current Biology*, 29(2), p. 350–358.e4. doi: https://doi.org/10.1016/j.cub.2018.12.017.

Facchetti, G., Chang, F. and Howard, M. (2017) 'Controlling cell size through sizer mechanisms', *Current Opinion in Systems Biology*. Elsevier Ltd, pp. 86–92. doi: 10.1016/j.coisb.2017.08.010.

Fankhauser, G. (1945) 'Maintenance of normal structure in heteroploid salamander larvae, through compensation of changes in cell size by adjustment of cell number and cell shape', *Journal of Experimental Zoology*. John Wiley & Sons, Ltd, 100(3), pp. 445–455. doi: https://doi.org/10.1002/jez.1401000310.

Fantes, P. A. *et al.* (1975) 'The regulation of cell size and the control of mitosis', *Journal of Theoretical Biology*, 50(1), pp. 213–244. doi: https://doi.org/10.1016/0022-5193(75)90034-X.

Fantes, P. and Nurse, P. (1977) 'Control of cell size at division in fission yeast by a growth-modulated size control over nuclear division', *Experimental Cell Research*, 107(2), pp.

377–386. doi: https://doi.org/10.1016/0014-4827(77)90359-7.

Franks, P. J. and Beerling, D. J. (2009) 'Maximum leaf conductance driven by CO2 effects on stomatal size and density over geologic time', *Proceedings of the National Academy of Sciences*, 106(25), p. 10343 LP-10347. doi: 10.1073/pnas.0904209106.

Franks, P. J., Drake, P. L. and Beerling, D. J. (2009) 'Plasticity in maximum stomatal conductance constrained by negative correlation between stomatal size and density: an analysis using Eucalyptus globulus', *Plant, Cell & Environment*. John Wiley & Sons, Ltd, 32(12), pp. 1737–1748. doi: https://doi.org/10.1111/j.1365-3040.2009.002031.x.

Franks, P. J. and Farquhar, G. D. (2007) 'The Mechanical Diversity of Stomata and Its Significance in Gas-Exchange Control', *Plant Physiology*, 143(1), pp. 78–87. doi: 10.1104/pp.106.089367.

Gallet, R. *et al.* (2017) 'The evolution of bacterial cell size: the internal diffusion-constraint hypothesis', *The ISME Journal*, 11(7), pp. 1559–1568. doi: 10.1038/ismej.2017.35.

Haig, D. and Westoby, M. (1988) 'A model for the origin of heterospory', *Journal of Theoretical Biology*, 134(2), pp. 257–272. doi: https://doi.org/10.1016/S0022-5193(88)80203-0.

Han, S.-K. *et al.* (2018) 'MUTE Directly Orchestrates Cell-State Switch and the Single Symmetric Division to Create Stomata', *Developmental Cell*, 45(3), p. 303–315.e5. doi: https://doi.org/10.1016/j.devcel.2018.04.010.

Heitman, J., Movva, N. R. and Hall, M. N. (1991) 'Targets for Cell Cycle Arrest by the Immunosuppressant Rapamycin in Yeast', *Science*. American Association for the Advancement of Science, 253(5022), pp. 905–909. doi: 10.1126/science.1715094.

Heldt, F. S. *et al.* (2018) 'Dilution and titration of cell-cycle regulators may control cell size in budding yeast', *PLOS Computational Biology*. Public Library of Science, 14(10), p. e1006548. Available at: https://doi.org/10.1371/journal.pcbi.1006548.

Hemsley, A. R., Scott, A. C. and Collinson, M. E. (1999) 'The architecture and functional biology of freely dispersed megaspores.', in Hemsley, A. R. and Kurmann, M. (eds) *Plant architecture*. London: Kew Gardens, pp. 253–277.

Henriques, R. *et al.* (2010) 'Arabidopsis S6 kinase mutants display chromosome instability and altered RBR1-E2F pathway activity', *The EMBO journal*. 2010/08/03. Nature Publishing Group, 29(17), pp. 2979–2993. doi: 10.1038/emboj.2010.164.

Henry, I. M. *et al.* (2010) 'Phenotypic consequences of aneuploidy in Arabidopsis thaliana', *Genetics*, 186(4), pp. 1231–1245. doi: 10.1534/genetics.110.121079.

Hervieux, N. *et al.* (2017) 'Mechanical Shielding of Rapidly Growing Cells Buffers Growth

Heterogeneity and Contributes to Organ Shape Reproducibility.', *Current Biology*. England, 27(22), p. 3468–3479.e4. doi: 10.1016/j.cub.2017.10.033.

Hirano, H. *et al.* (2008) 'Arabidopsis Retinoblastoma-Related Protein 1 is involved in G1 phase cell cycle arrest caused by sucrose starvation', *Plant Molecular Biology*, 66(3), pp. 259–275. doi: 10.1007/s11103-007-9268-2.

Hola, M. and Riley, P. A. (1987) 'The relative significance of growth rate and interdivision time in the size control of cultured mammalian epithelial cells', *Journal of Cell Science*, 88(1), pp. 73–80. doi: 10.1242/jcs.88.1.73.

Hong, L. *et al.* (2016) 'Variable Cell Growth Yields Reproducible Organ Development through Spatiotemporal Averaging', *Developmental Cell*, 38(1), pp. 15–32. doi: https://doi.org/10.1016/j.devcel.2016.06.016.

Hughes, A. L. and Hughes, M. K. (1995) 'Small genomes for better flyers', *Nature*, 377(6548), p. 391. doi: 10.1038/377391a0.

Janssens, V. and Goris, J. (2001) 'Protein phosphatase 2A: a highly regulated family of serine/threonine phosphatases implicated in cell growth and signalling', *The Biochemical journal*, 353(Pt 3), pp. 417–439. doi: 10.1042/0264-6021:3530417.

Jasinski, S. *et al.* (2002) 'The CDK inhibitor NtKIS1a is involved in plant development,endoreduplication and restores normal development of cyclin D3;1-overexpressing plants', *Journal of Cell Science*, 115(5), pp. 973–982. doi: 10.1242/jcs.115.5.973.

Jones, A. R. *et al.* (2017) 'Cell-size dependent progression of the cell cycle creates homeostasis and flexibility of plant cell size', *Nature Communications*. Nature Publishing Group, 8, p. 15060. doi: 10.1038/ncomms15060.

Jones, H. G. (1998) 'Stomatal control of photosynthesis and transpiration', *Journal of Experimental Botany*, 49(Special_Issue), pp. 387–398. doi: 10.1093/jxb/49.Special_Issue.387.

Killander, D. and Zetterberg, A. (1965a) 'A quantitative cytochemical investigation of the relationship between cell mass and initiation of DNA synthesis in mouse fibroblasts in vitro', *Experimental Cell Research*, 40(1), pp. 12–20. doi: https://doi.org/10.1016/0014-4827(65)90285-5.

Killander, D. and Zetterberg, A. (1965b) 'Quantitative cytochemical studies on interphase growth: I. Determination of DNA, RNA and mass content of age determined mouse fibroblasts in vitro and of intercellular variation in generation time', *Experimental Cell Research*, 38(2), pp. 272–284. doi: https://doi.org/10.1016/0014-4827(65)90403-9.

Kim, H. J. *et al.* (2008) 'Control of plant germline proliferation by SCFFBL17 degradation of cell cycle inhibitors', *Nature*, 455(7216), pp. 1134–1137. doi: 10.1038/nature07289.

Kleiber, M. (1932) 'Body size and metabolism', *Hilgardia*, 6(11), pp. 315–353. doi: 10.3733/hilg.v06n11p315.

Kozłowski, J., Konarzewski, M. and Gawelczyk, A. T. (2003) 'Cell size as a link between noncoding DNA and metabolic rate scaling', *Proceedings of the National Academy of Sciences*, 100(24), p. 14080 LP-14085. doi: 10.1073/pnas.2334605100.

Kubitschek, H. E. and Clay, K. B. (1986) 'A second growth state for Schizosaccharomyces pombe', *Experimental Cell Research*, 165(1), pp. 243–254. doi: https://doi.org/10.1016/0014-4827(86)90548-3.

Kumar, N. *et al.* (2015) 'Functional Conservation in the SIAMESE-RELATED Family of Cyclin-Dependent Kinase Inhibitors in Land Plants', *The Plant Cell*, 27(11), pp. 3065–3080. doi: 10.1105/tpc.15.00489.

Van Leene, J. *et al.* (2019) 'Capturing the phosphorylation and protein interaction landscape of the plant TOR kinase', *Nature Plants*, 5(3), pp. 316–327. doi: 10.1038/s41477-019-0378-z.

Leslie, A. B. and Bonacorsi, N. K. (2021) 'Understanding the appearance of heterospory and derived plant reproductive strategies in the Devonian', *Paleobiology*, In press.

Li, X. *et al.* (2017) 'Differential TOR activation and cell proliferation in Arabidopsis root and shoot apexes', *Proceedings of the National Academy of Sciences of the United States of America*. 2017/02/21. National Academy of Sciences, 114(10), pp. 2765–2770. doi: 10.1073/pnas.1618782114.

Li, Y. *et al.* (2016) 'A new class of cyclin dependent kinase in Chlamydomonas is required for coupling cell size to cell division', *eLife*. eLife Sciences Publications, Ltd, 5, pp. e10767–e10767. doi: 10.7554/eLife.10767.

Lin, J. and Amir, A. (2018) 'Homeostasis of protein and mRNA concentrations in growing cells', *Nature Communications*, 9(1), p. 4496. doi: 10.1038/s41467-018-06714-z.

Lockhart, J. A. (1965) 'An analysis of irreversible plant cell elongation', *Journal of Theoretical Biology*, 8(2), pp. 264–275. doi: https://doi.org/10.1016/0022-5193(65)90077-9.

Louveaux, M. *et al.* (2016) 'Cell division plane orientation based on tensile stress in Arabidopsis thaliana', *Proceedings of the National Academy of Sciences*, 113(30), p. E4294 LP-E4303. doi: 10.1073/pnas.1600677113.

Lui, H. *et al.* (2000) 'The Arabidopsis Cdc2a-interacting protein ICK2 is structurally related

to ICK1 and is a potent inhibitor of cyclin-dependent kinase activity in vitro', *The Plant Journal*. John Wiley & Sons, Ltd, 21(4), pp. 379–385. doi: https://doi.org/10.1046/j.1365-313x.2000.00688.x.

Mahfouz, M. M. *et al.* (2006) 'Arabidopsis TARGET OF RAPAMYCIN interacts with RAPTOR, which regulates the activity of S6 kinase in response to osmotic stress signals', *The Plant cell*. 2005/12/23. American Society of Plant Biologists, 18(2), pp. 477–490. doi: 10.1105/tpc.105.035931.

Martin, S. G. and Berthelot-Grosjean, M. (2009) 'Polar gradients of the DYRK-family kinase Pom1 couple cell length with the cell cycle', *Nature*, 459(7248), pp. 852–856. doi: 10.1038/nature08054.

Marty, F. (1999) 'Plant vacuoles', *The Plant cell*, 11(4), pp. 587–600. doi: 10.1105/tpc.11.4.587.

Matsuda, H. and Abrams, P. A. (1999) 'Why are equally sized gametes so rare? The instability of isogamy and the cost of anisogamyUnopened XML element'f'closed', *Evolutionary Ecology Research*. Evolutionary Ecology, Ltd., 1(7), pp. 769–784.

McCready, K., Spencer, V. and Kim, M. (2020) 'The Importance of TOR Kinase in Plant Development', *Frontiers in plant science*. Frontiers Media S.A., 11, p. 16. doi: 10.3389/fpls.2020.00016.

Melaragno, J. E., Mehrotra, B. and Coleman, A. W. (1993) 'Relationship between Endopolyploidy and Cell Size in Epidermal Tissue of Arabidopsis.', *The Plant Cell*, 5(11), pp. 1661–1668. doi: 10.1105/tpc.5.11.1661.

Menand, B. *et al.* (2002) 'Expression and disruption of the Arabidopsis TOR (target of rapamycin) gene', *Proceedings of the National Academy of Sciences of the United States of America*. The National Academy of Sciences, 99(9), pp. 6422–6427. doi: 10.1073/pnas.092141899.

Menges, M. *et al.* (2006) 'The D-Type Cyclin CYCD3;1 Is Limiting for the G1-to-S-Phase Transition in Arabidopsis', *the Plant Cell Online*, 18(4), pp. 893–906. doi: 10.1105/tpc.105.039636.

Meyer, H. M. *et al.* (2017) 'Fluctuations of the transcription factor ATML1 generate the pattern of giant cells in the Arabidopsis sepal', *eLife*. Edited by D. C. Bergmann. eLife Sciences Publications, Ltd, 6, p. e19131. doi: 10.7554/eLife.19131.

Miettinen, T. P. and Björklund, M. (2016) 'Cellular Allometry of Mitochondrial Functionality Establishes the Optimal Cell Size', *Developmental cell*. Cell Press, 39(3), pp. 370–382. doi: 10.1016/j.devcel.2016.09.004.

Mitchison, J. M. (1957) 'The growth of single cells: I. Schizosaccharomyces pombe', *Experimental Cell Research*, 13(2), pp. 244–262. doi: https://doi.org/10.1016/0014-4827(57)90005-8.

Moreau, M. *et al.* (2012) 'Mutations in the Arabidopsis homolog of LST8/GβL, a partner of the target of Rapamycin kinase, impair plant growth, flowering, and metabolic adaptation to long days', *The Plant cell*. 2012/02/03. American Society of Plant Biologists, 24(2), pp. 463–481. doi: 10.1105/tpc.111.091306.

Murray, A. W. and Kirschner, M. W. (1989) 'Cyclin synthesis drives the early embryonic cell cycle', *Nature*, 339(6222), pp. 275–280. doi: 10.1038/339275a0.

Nagar, S. *et al.* (1995) 'A geminivirus induces expression of a host DNA synthesis protein in terminally differentiated plant cells.', *The Plant Cell*, 7(6), pp. 705–719. doi: 10.1105/tpc.7.6.705.

Neurohr, G. E. *et al.* (2019) 'Excessive Cell Growth Causes Cytoplasm Dilution And Contributes to Senescence', *Cell*. Cell Press, 176(5), p. 1083–1097.e18. doi: 10.1016/j.cell.2019.01.018.

Noir, S. *et al.* (2015) 'The Control of *Arabidopsis thaliana* Growth by Cell Proliferation and Endoreplication Requires the F-Box Protein FBL17', *The Plant Cell*, 27(5), pp. 1461–1476. doi: 10.1105/tpc.114.135301.

Nowack, M. K. *et al.* (2012) 'Genetic Framework of Cyclin-Dependent Kinase Function in Arabidopsis', *Developmental Cell*. Elsevier Inc., 22(5), pp. 1030–1040. doi: 10.1016/j.devcel.2012.02.015.

Nurse, P. (1975) 'Genetic control of cell size at cell division in yeast', *Nature*, 256(5518), pp. 547–551. doi: 10.1038/256547a0.

Olson, B. J. S. C. *et al.* (2010) 'Regulation of the Chlamydomonas cell cycle by a stable, chromatin-associated retinoblastoma tumor suppressor complex', *The Plant cell*. 2010/10/26. American Society of Plant Biologists, 22(10), pp. 3331–3347. doi: 10.1105/tpc.110.076067.

Organ, C. L. *et al.* (2007) 'Origin of avian genome size and structure in non-avian dinosaurs', *Nature*. Nature Publishing Group, 446, p. 180. Available at: https://doi.org/10.1038/nature05621.

Pan, K. Z. *et al.* (2014) 'Cortical regulation of cell size by a sizer cdr2p', *eLife*, 2014(3), pp. 1–24. doi: 10.7554/eLife.02040.

Pérez-Hidalgo, L. and Moreno, S. (2017) 'Coupling TOR to the Cell Cycle by the Greatwall-Endosulfine-PP2A-B55 Pathway', *Biomolecules*. MDPI, 7(3), p. 59. doi:

10.3390/biom7030059.

Planchais, S., Samland, A. K. and Murray, J. A. H. (2004) 'Differential stability of Arabidopsis D-type cyclins: CYCD3;1 is a highly unstable protein degraded by a proteasome-dependent mechanism', *Plant Journal*, 38(4), pp. 616–625. doi: 10.1111/j.0960-7412.2004.02071.x.

Polymenis, M. and Schmidt, E. V (1997) 'Coupling of cell division to cell growth by translational control of the G1 cyclin CLN3 in yeast', *Genes & Development* , 11(19), pp. 2522–2531. Available at: http://genesdev.cshlp.org/content/11/19/2522.abstract.

Priestley, J. H. (1929) 'Cell Growth and Cell Division in the Shoot of the Flowering Plant', *The New Phytologist*. [Wiley, New Phytologist Trust], 28(1), pp. 54–81. Available at: http://www.jstor.org/stable/2428042.

Ramirez-Parra, E., Fründt, C. and Gutierrez, C. (2003) 'A genome-wide identification of E2F-regulated genes in Arabidopsis', *The Plant Journal*. John Wiley & Sons, Ltd, 33(4), pp. 801–811. doi: https://doi.org/10.1046/j.1365-313X.2003.01662.x.

Reiser, L., Sanchez-Baracaldo, P. and Hake, S. (2000) 'Knots in the family tree: evolutionary relationships and functions of knox homeobox genes', *Plant Mol Biol*. 2000/02/25, 42(1), pp. 151–166.

Robinson, D. O. *et al.* (2018) 'Ploidy and Size at Multiple Scales in the Arabidopsis Sepal', *The Plant cell*. 2018/08/24. American Society of Plant Biologists, 30(10), pp. 2308–2329. doi: 10.1105/tpc.18.00344.

Roeder, A. H. K. *et al.* (2010) 'Variability in the Control of Cell Division Underlies Sepal Epidermal Patterning in Arabidopsis thaliana', *PLOS Biology*. Public Library of Science, 8(5), p. e1000367. Available at: https://doi.org/10.1371/journal.pbio.1000367.

Sabers, C. J. *et al.* (1995) 'Isolation of a Protein Target of the FKBP12-Rapamycin Complex in Mammalian Cells (∗)', *Journal of Biological Chemistry*, 270(2), pp. 815–822. doi: https://doi.org/10.1074/jbc.270.2.815.

Salem, M. A. *et al.* (2017) 'Regulatory-associated protein of TOR (RAPTOR) alters the hormonal and metabolic composition of Arabidopsis seeds, controlling seed morphology, viability and germination potential', *The Plant Journal*. John Wiley & Sons, Ltd, 92(4), pp. 525–545. doi: https://doi.org/10.1111/tpj.13667.

Sapala, A. *et al.* (2018) 'Why plants make puzzle cells, and how their shape emerges', *eLife*. Edited by S. McCormick. eLife Sciences Publications, Ltd, 7, p. e32794. doi: 10.7554/eLife.32794.

Schaechter, M. *et al.* (1962) 'Growth, cell and nuclear divisions in some bacteria',

Microbiology. Microbiology Society, 29(3), pp. 421–434.

Schaechter, M., Maaloe, O. and Kjeldgaard, N. O. (1958) 'Dependency on Medium and Temperature of Cell Size and Chemical Composition during Balanced Growth of Salmonella typhimurium', *Microbiology*, 19(3), pp. 592–606. doi: 10.1099/00221287-19-3-592.

Schiessl, K. *et al.* (2012) 'JAGGED controls growth anisotropy and coordination between cell size and cell cycle during plant organogenesis', *Current Biology*. Elsevier Ltd, 22(19), pp. 1739–1746. doi: 10.1016/j.cub.2012.07.020.

Schiessl, K. (2014) *The role of the transcription factor JAGGED in early floral organogenesis*. University of East Anglia. Available at: https://ueaeprints.uea.ac.uk/id/eprint/49812/%5C.

Schiessl, K., Muino, J. M. and Sablowski, R. (2014) 'Arabidopsis JAGGED links floral organ patterning to tissue growth by repressing Kip-related cell cycle inhibitors', *Proceedings of the National Academy of Sciences*, 111(7), pp. 2830–2835. doi: 10.1073/pnas.1320457111.

Schmoller, K. M. *et al.* (2015) 'Dilution of the cell cycle inhibitor Whi5 controls budding-yeast cell size', *Nature*, 526(7572), pp. 268–272. doi: 10.1038/nature14908.

Schnittger, A. *et al.* (2002) 'Ectopic B-type cyclin expression induces mitotic cycles in endoreduplicating Arabidopsis trichomes', *Current Biology*, 12(5), pp. 415–420. doi: 10.1016/S0960-9822(02)00693-0.

Schnittger, A. *et al.* (2003) 'Misexpression of the cyclin-dependent kinase inhibitor ICK1/KRP1 in single-celled Arabidopsis trichomes reduces endoreduplication and cell size and induces cell death', *The Plant cell*. American Society of Plant Biologists, 15(2), pp. 303–315. doi: 10.1105/tpc.008342.

Schwarz, E. M. and Roeder, A. H. K. (2016) 'Transcriptomic Effects of the Cell Cycle Regulator LGO in Arabidopsis Sepals', *Frontiers in plant science*. Frontiers Media S.A., 7, p. 1744. doi: 10.3389/fpls.2016.01744.

Scotchman, E. *et al.* (2021) 'Identification of mutants with increased variation in cell size at onset of mitosis in fission yeast', *Journal of Cell Science*, 134(3). doi: 10.1242/jcs.251769.

Serrano-Mislata, A. *et al.* (2017) 'DELLA genes restrict inflorescence meristem function independently of plant height', *Nature Plants*. Springer US, 3(9), pp. 749–754. doi: 10.1038/s41477-017-0003-y.

Serrano-Mislata, A., Schiessl, K. and Sablowski, R. (2015) 'Active Control of Cell Size

Generates Spatial Detail during Plant Organogenesis', *Current Biology*. The Authors, 25(22), pp. 2991–2996. doi: 10.1016/j.cub.2015.10.008.

Shattuck, C. H. (1910) 'The Origin of Heterospory in Marsilia', *Botanical Gazette*. The University of Chicago Press, 49(1), pp. 19–40. doi: 10.1086/330087.

Shimotohno, A. *et al.* (2021) 'Regulation of the Plant Cell Cycle in Response to Hormones and the Environment', *Annual Review of Plant Biology*. Annual Reviews, 72(1), pp. 273–296. doi: 10.1146/annurev-arplant-080720-103739.

Simonin, K. A. and Roddy, A. B. (2018) 'Genome downsizing, physiological novelty, and the global dominance of flowering plants', *PLOS Biology*. Public Library of Science, 16(1), p. e2003706. Available at: https://doi.org/10.1371/journal.pbio.2003706.

Simpson, M. G. (2019) *Plant Embryology*. Third Edit, *Plant Systematics*. Third Edit. Edited by M. G. B. T.-P. S. (Third E. Simpson. Academic Press. doi: https://doi.org/10.1016/B978-0-12-812628-8.50011-0.

Smith, H. H. (1943) 'Studies on Induced Heteroploids of Nicotiana', *American Journal of Botany*. Botanical Society of America, 30(2), pp. 121–130. doi: 10.2307/2437254.

Soni, R. *et al.* (1995) 'A family of cyclin D homologs from plants differentially controlled by growth regulators and containing the conserved retinoblastoma protein interaction motif', *The Plant cell*, 7(1), pp. 85–103. doi: 10.1105/tpc.7.1.85.

Streiblová, E. and Wolf, A. (1972) 'Cell wall growth during the cell cycle of Schizosaccharomyces pombe', *Zeitschrift für allgemeine Mikrobiologie*. Wiley Online Library, 12(8), pp. 673–684.

Swaffer, M. P. *et al.* (2021) 'Transcriptional and chromatin-based partitioning mechanisms uncouple protein scaling from cell size', *Molecular Cell*. doi: https://doi.org/10.1016/j.molcel.2021.10.007.

Szarski, H. (1983) 'Cell size and the concept of wasteful and frugal evolutionary strategies.', *Journal of theoretical biology*. England, 105(2), pp. 201–209.

Tanaka, Y. *et al.* (2007) 'Intra-Vacuolar Reserves of Membranes During Stomatal Closure: The Possible Role of Guard Cell Vacuoles Estimated by 3-D Reconstruction', *Plant and Cell Physiology*, 48(8), pp. 1159–1169. doi: 10.1093/pcp/pcm085.

Togashi, T. *et al.* (2012) 'Evolutionary trajectories explain the diversified evolution of isogamy and anisogamy in marine green algae', *Proceedings of the National Academy of Sciences*, 109(34), p. 13692 LP-13697. doi: 10.1073/pnas.1203495109.

Tolmsoff, W. J. (1983) 'Heteroploidy as a Mechanism of Variability Among Fungi', *Annual Review of Phytopathology*. Annual Reviews, 21(1), pp. 317–340. doi:

10.1146/annurev.py.21.090183.001533.

Torres-Acosta, J. A., Fowke, L. C. and Wang, H. (2011) 'Analyses of phylogeny, evolution, conserved sequences and genome-wide expression of the ICK/KRP family of plant CDK inhibitors', *Annals of Botany*, 107(7), pp. 1141–1157. doi: 10.1093/aob/mcr034.

Turner, J. J., Ewald, J. C. and Skotheim, J. M. (2012) 'Cell size control in yeast', *Current Biology*. Elsevier Ltd, 22(9), pp. R350–R359. doi: 10.1016/j.cub.2012.02.041.

Tyson, C. B., Lord, P. G. and Wheals, A. E. (1979) 'Dependency of size of Saccharomyces cerevisiae cells on growth rate', *Journal of Bacteriology*. American Society for Microbiology, 138(1), pp. 92–98. doi: 10.1128/jb.138.1.92-98.1979.

Umen, J. G. and Goodenough, U. W. (2001) 'Control of cell division by a retinoblastoma protein homolog in Chlamydomonas', *Genes and Development*, 15(13), pp. 1652–1661. doi: 10.1101/gad.892101.

Verkest, A. *et al.* (2005) 'Switching the cell cycle. Kip-related proteins in plant cell cycle control', *Plant physiology*. American Society of Plant Biologists, 139(3), pp. 1099–1106. doi: 10.1104/pp.105.069906.

De Veylder, L. *et al.* (2001) 'Functional Analysis of Cyclin-Dependent Kinase Inhibitors of Arabidopsis', *The Plant Cell*, 13(7), pp. 1653–1668. doi: 10.1105/TPC.010087.

De Veylder, L., Beeckman, T. and Inzé, D. (2007) 'The ins and outs of the plant cell cycle', *Nature Reviews Molecular Cell Biology*, 8(8), pp. 655–665. doi: 10.1038/nrm2227.

Virchow, R. (1858) 'Die Cellularpathologie in ihrer Begründung auf physiologische und pathologische Gewebelehre: 20 Vorlesungen...' Hirschwald.

Walker, J. D. *et al.* (2000) 'SIAMESE, a gene controlling the endoreduplication cell cycle in Arabidopsis thaliana trichomes', *Development*, 127(18), pp. 3931–3940. doi: 10.1242/dev.127.18.3931.

Wang, H. *et al.* (2009) 'Recruitment of Cln3 cyclin to promoters controls cell cycle entry via histone deacetylase and other targets', *PLoS Biology*, 7(9). doi: 10.1371/journal.pbio.1000189.

Wang, H., Fowke, L. C. and Crosby, W. L. (1997) 'A plant cyclin-dependent kinase inhibitor gene', *Nature*, 386(6624), pp. 451–452. doi: 10.1038/386451a0.

Williamson, W. C. and Scott, D. H. (1894) 'Further Observations on the Organisation of the Fossil Plants of the Coal-Measures', *Phitos. Trans.* The Royal Society, 185(863). doi: https://doi.org/10.1098/rspl.1894.0124.

Willis, L. *et al.* (2016) 'Cell size and growth regulation in the *Arabidopsis thaliana* apical stem cell niche', *Proceedings of the National Academy of Sciences*, 113(51), pp. E8238–

E8246. doi: 10.1073/pnas.1616768113.

Wood, E. and Nurse, P. (2013) 'Pom1 and cell size homeostasis in fission yeast', *Cell cycle (Georgetown, Tex.)*. 2013/09/12. Landes Bioscience, 12(19), pp. 3228–3236. doi: 10.4161/cc.26462.

Xie, Q. *et al.* (1996) 'Plant cells contain a novel member of the retinoblastoma family of growth regulatory proteins', *The EMBO journal*, 15(18), pp. 4900–4908. Available at: https://pubmed.ncbi.nlm.nih.gov/8890163.

Xie, Q., Suárez-López, P. and Gutiérrez, C. (1995) 'Identification and analysis of a retinoblastoma binding motif in the replication protein of a plant DNA virus: requirement for efficient viral DNA replication', *The EMBO journal*, 14(16), pp. 4073–4082. Available at: https://pubmed.ncbi.nlm.nih.gov/7664747.

Xiong, Y. *et al.* (2013) 'Glucose-TOR signalling reprograms the transcriptome and activates meristems', *Nature*. 2013/03/31, 496(7444), pp. 181–186. doi: 10.1038/nature12030.

Yang, W., Wightman, R. and Meyerowitz, E. M. (2017) 'Cell Cycle Control by Nuclear Sequestration of CDC20 and CDH1 mRNA in Plant Stem Cells', *Molecular Cell*. Elsevier Inc., 68(6), p. 1108–1119.e3. doi: 10.1016/j.molcel.2017.11.008.

Yi, D. *et al.* (2014) 'The Arabidopsis SIAMESE-RELATED cyclin-dependent kinase inhibitors SMR5 and SMR7 regulate the DNA damage checkpoint in response to reactive oxygen species', *The Plant cell*. 2014/01/07. American Society of Plant Biologists, 26(1), pp. 296–309. doi: 10.1105/tpc.113.118943.

Zatulovskiy, E. *et al.* (2020) 'Cell growth dilutes the cell cycle inhibitor Rb to trigger cell division', *Science*, 471(July), pp. 466–471.

Zetterberg, A. and Killander, D. (1965) 'Quantitative cytophotometric and autoradiographic studies on the rate of protein synthesis during interphase in mouse fibroblasts in vitro', *Experimental Cell Research*, 40(1), pp. 1–11. doi: https://doi.org/10.1016/0014-4827(65)90284-3.

Zhao, F. *et al.* (2020) 'Microtubule-Mediated Wall Anisotropy Contributes to Leaf Blade Flattening', *Current Biology*, 30(20), p. 3972–3985.e6. doi: https://doi.org/10.1016/j.cub.2020.07.076.

Zimmermann, U., Hüsken, D. and Schulze, E.-D. (1980) 'Direct turgor pressure measurements in individual leaf cells of Tradescantia virginiana', *Planta*, 149(5), pp. 445–453. doi: 10.1007/BF00385746.

Chapter 2: Evidence for size control at the G1/S transition

2.1 Introduction

Before diving into the search and characterisation of molecular mechanisms for cell size control, it is important to study the cellular behaviours of growth and division, and how cell size and cell cycle are interconnected. This information will help us to formulate hypotheses on the possible components for this mechanism, as well as giving us the opportunity to understand more profoundly the results obtained in the totality of this project.

The major goal of this chapter is to address the question of when during the cell cycle is cell size variability corrected. The importance of this question is highlighted by previous studies conducted in *Saccharomyces cerevisiae* that identified entry in S-phase as a major cell size checkpoint (Schmoller *et al.*, 2015). These studies contrasted with work showing that in *Schizosaccharomyces pombe*, cell size regulation occurs primarily at the commitment to mitotic division (Pan *et al.*, 2014). Other studies in plants have suggested that cell size regulation might arise from the integration of regulations that act on CDKa during the whole cell cycle, with possible mechanisms feeding into each other (Jones *et al.*, 2017), whilst other have even suggested that growth rates might play a role in reducing cell size variability (Willis *et al.*, 2016). Although the latter phenomenon is known to occur in mammalian cells (Kafri *et al.*, 2013), it seems unlikely to be a major driver for size regulation in plants, whose tissues made of tightly connected cells would deform under forces generated by heterogeneous growth (D'Ario and Sablowski, 2019). Therefore, understanding how cell size and growth connect to cell cycle progression is paramount to identifying the molecular mechanism for cell size homeostasis.

Hypotheses on cell size control are strongly dependent on how cells grow over time. Growth rate has been a highly debated topic, especially between the 90s and early 2000s (Kubitschek and Clay, 1986; Cooper, 2006; Baumgärtner and Tolić-Nørrelykke, 2009), a debate that eventually culminated with the consensus that cells grow, or strive to grow, exponentially (Cooper, 2013). Whilst this debate is beyond the focus of this text, it highlighted important features of growth rate: it is experimentally hard to measure and focusing on data that solely rely on growth rate might lead to erroneous conclusions. However, the non-linear nature of growth is an important feature of cell growth and impacts the way we try to understand cell size regulation – size variability accumulated by

rounds of division during linear growth does not scale as it does in exponential growth (see Chapter 5). A time mechanism for division, in which cells divided at fixed amount of times, would be enough to reduce this variability if growth was linear (D'Ario and Sablowski, 2019). Therefore, any suggested molecular mechanism for size homeostasis should account for the levels of size variability experimentally observed and be able to theoretically reduce variability while assuming exponential growth.

Work that supported size-dependent cell cycle progression in plants (Serrano-Mislata, Schiessl and Sablowski, 2015; Willis *et al.*, 2016; Jones *et al.*, 2017) took advantage of the meristem tissue to address this question. The advantages of this system are manyfold. First of all, cells preserve their topology whilst growing, making them easily trackable via imaging software (Serrano-Mislata, Schiessl and Sablowski, 2015). Secondly, they can be grown *in vitro* for several days, allowing for extended time courses to be carried out. However, difficulties related to the survival of apexes originally limited the frequency of imaging, which was brought to a maximum of 8h per time point (Jones *et al.*, 2017). The apex needed to be stained with a cell membrane marker at each time point, a step that reduced cell survival. After a new plasma membrane marker line was implemented (Willis *et al.*, 2016), imaging frequency could be taken down to 2h intervals. This higher temporal resolution was necessary to study the relationship between size and specific cell cycle phases, considering that individual cell cycle stages can last as little as 15h (Jones *et al.*, 2017). The last missing technical piece was the lack of a reliable cell cycle marker, able to sharply discriminate between cells in different phases (Desvoyes *et al.*, 2020). Thanks to these materials and technical improvements, we could study the relationships between cell size and cell cycle, and answer the question whether cell size variability is corrected as the G1/S transition.

2.2 The long-time course – optimisation

To address the question on how cell cycle progression is linked to cell size, I implemented a time course protocol using the cell cycle reporter kindly provided by our collaborators (Desvoyes *et al.*, 2020) (Fig. 2.1). This reporter contained a CFP tagged version of CDT1, which marks the transition to S-phase, and a RFP tagged H3.1, a histone variant mainly produced during G2 (Desvoyes *et al.*, 2020). The next step in developing a protocol for long time imaging is to image meristem cells at highest possible frequency, to observe changes in cell size related to cell cycle progression. To image the apex for such an extended period,

it is critical to minimise cell damage and stress. Previous attempts have utilised auxin inhibitors to prevent bud formation, removing the requirement for dissection of the shoot apex (Willis *et al.*, 2016). This obviously made it impossible to image developing flower buds and removed any effect that auxin might have on the cell autonomous signal we are trying to analyse.

In order to reduce the stress caused by live imaging whilst preserving bud emergence and auxin flow, we opted for a different approach. I used a novel imaging system developed by Zeiss: the Airyscan (Huff, 2015). This system is much more sensitive to light, allowing for less laser intensity to be used during imaging (Huff, 2015). Additionally, Airyscan removes the need for the same confocal slices to be imaged multiple times, further decreasing stress by reducing imaging time. For a comparison, a full Z-stack using normal confocal technology would take 15-20min, whilst Airyscan protocols optimised for fast image acquisition can take as little as 2-3min for the same samples.
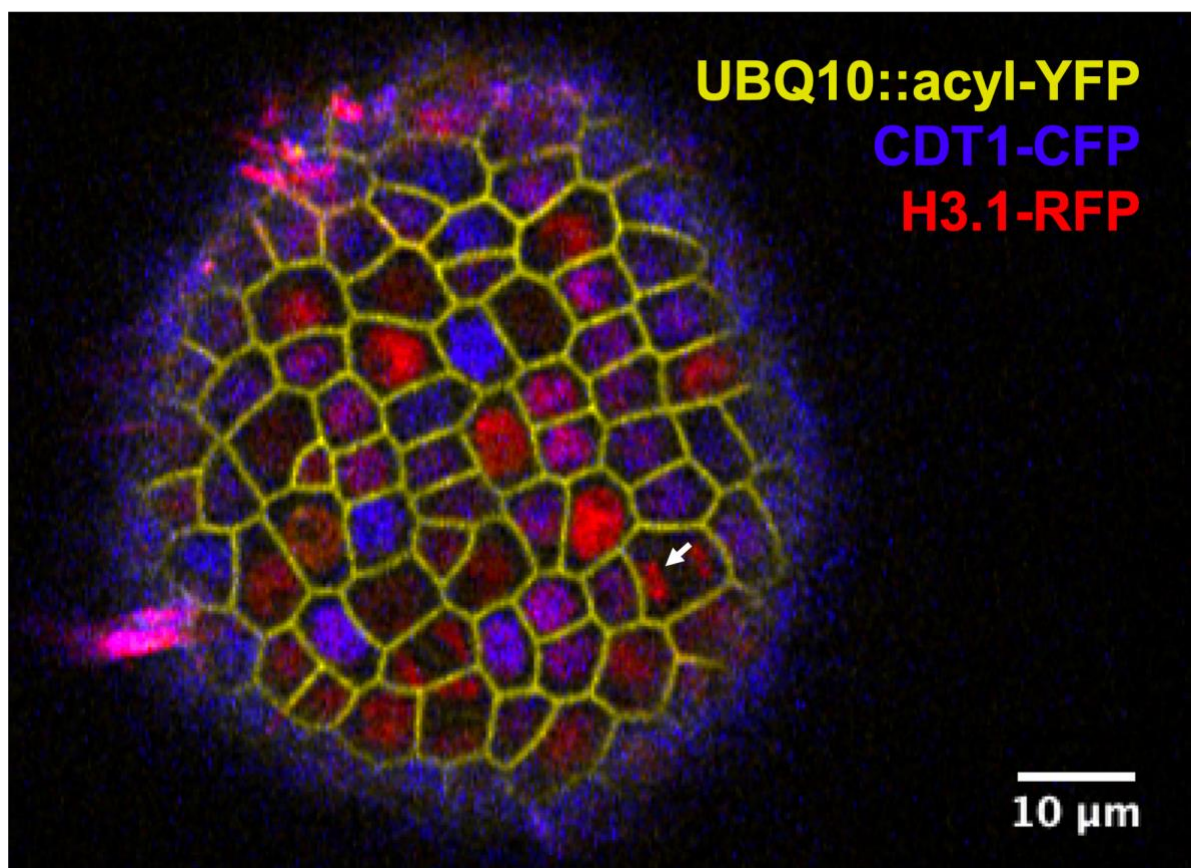
Figure 2.1: The triple reporter line. Confocal micrograph of the line used in this experiment. The line is a F1 cross between a line expressing acylated-YFP (UBQ10::acyl-YFP, yellow), and a cell cycle line expressing CDT1 fused to CFP (CDT1-CFP, blue) and Histone H3.1 fused to RFP (H3.1-RFP, red) under their native promoters. Magenta nuclei are nuclei where both CDT1 and H3.1 are present. Arrows indicate segregating chromosomes, visible thanks to H3.1-RFP.

Another factor critical to reduce stress was the implementation of a system that does not use dyes to visualise cells outlines. Staining cell membranes multiple times cause stress to the cells, and endocytosis leads to accumulation of dye in intracellular vesicles, which interfere with cell segmentation and tracking. For these reasons I crossed the cell cycle reporter line with a line expressing an acylated version of the YFP under the ubiquitously expressed UBIQUITIN10 promoter (UBQ10::acyl-YFP or acyl-YFP) (Willis *et al.*, 2016). Using F1 crosses of these lines (Fig. 2.1) I made various attempts (data not shown) to estimate what could be the highest possible frequency of imaging to reduce the experimental noise in measuring cell cycle transitions. I tested 1h and 1.5h but the apexes imaged in this way frequently did not survive beyond 6h of imaging, as visible from the highly vesiculated cells. Cell stress was not visible when apexes where imaged every 2h hours instead, a similar timing employed by previous studies (Willis *et al.*, 2016). It is hard to know why apexes do not survive such high frequency in imaging, especially given that the laser stress and imaging timing are reduced to a minimum thanks to Airyscan technology.

Finally, a known phenomenon related to live imaging sees an increased average cell size during *in vitro* growth (Landrein *et al.*, 2018). In previous studies that implemented long time imaging as described here, this phenomenon was clearly noted, and cell size was normalised in each time point, in an attempt to correct this bias (Willis *et al.*, 2016). However, it was later shown that the increase in average cell size was a response to decreasing levels of cytokinin, normally supplied by the root, which in turn, switch off *WUSCHEL* expression (Landrein *et al.*, 2018). For this reason, we opted to supply cytokin in the medium, aiming to produce a time course that more closely recapitulates *in vivo* growth.

The role of cytokinin in cell division is further underlined by its role in connecting cell cycle progression to the time of the day via the carcadian rhythm (Fung-Uceda *et al.*, 2018). Therefore, any effect of the carcadian rhythm on cell division could mask the relationship between cell size and cell cycle progression. To overcome this problem, all the apexes where grown under continuous light, making sure that the biological replicates were very unlikely synchronised. With a set up to unsure minimum stress of the samples and maximum relatability to *in vivo growth*, the relationship between cell size and cell cycle progression was investigated in new detail.

2.3 Validation of the system

T1 crosses between the cell cycle reporter and acyl-YFP were imaged at 2h intervals for 48h, collecting 24 time points each of 6 apexes, for a total of 144 confocal stacks. 4 of those apexes were selected based on visual impression on how healthy they looked at the end of the time course. Before moving to the analysis of the cell cycle reporters, it was important to evaluate the validity of this experiment by understanding how the data related to the normal behaviour of cells.
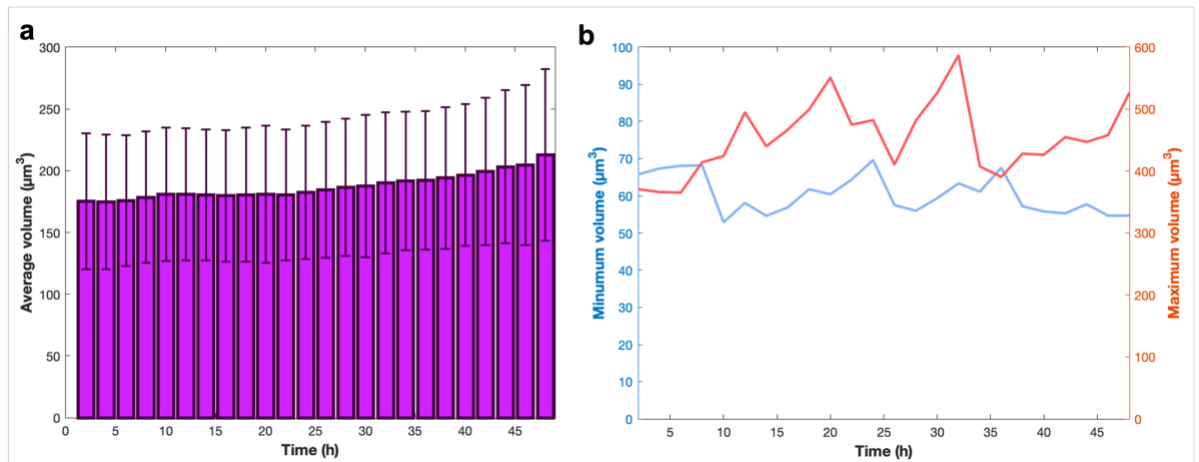
Figure 2.2: Volume changes during the time course. a) Average cell volume over the time course. Volume at 0h equals $175.6 \pm 55.1\mu m^3$, at 36h equals $192.3 \pm 56.1\mu m^3$ and at the end equals $213.0 \pm 63.3\mu m^3$. Error bars represent standard deviation. b) Graphs showing the minimum (blue) and maximum (red) detectable volumes. Note how the minimum remains roughly constant during the duration of the experiment.

Figure 2.2a shows how the average size of meristematic cells changed for each time point of the experiment. The volumes averaged $175.6 \pm 55.1\mu m^3$ (standard deviation is used throughout unless differently stated) at the start of the experiment and roughly remained constant, although with a slight increase (Fig. 2.2a). Note that the relatively high standard deviation, approx. 30%, is expected since those cells are doubling and dividing, therefore there is a high degree of variability among the whole cell population. Within the first 36h of the experiment, the average cell size increased to $192.3 \pm 56.1\mu m^3$, only approx. 9% higher than the starting average volume (Fig. 2.2a). Compared with previous studies with similar frequency of imaging, where average increase during this time reached 20% (Willis *et al.*, 2016), our experimental set up might more closely represent what happens in apexes that are not abscised from the stem. At the end of the experiments, average cell size reached its maximum at $213.0 \pm 63.3\mu m^3$, approx. 20% larger than the starting point (Fig. 2.2a). Therefore, the measured cells in this experiments seemed to reach the same enlargement as in previous studies (Willis *et al.*, 2016), but appeared to take much longer

to do so, with more than half of their increase occurring in the last quarter of the experiment. Considering the known role of cytokinin in setting average cell size (Landrein *et al.*, 2018), I speculate that reduction of exogenous cytokinin is behind this behaviour. When imaging, a small amount of water, approximately 5ml or a quarter of the volume of the growing medium (see material and method), was added between the lens and the sample. It is conceivable that this process slowly "washed" cytokinin from the medium and caused the increase in cell size. Interestingly, the minimum cell volume in the experiment seems not to be affected as much as the average cell size is (Fig. 2.2b), suggesting that the minimum size at birth is not impacted by the slow removal of cytokinin.
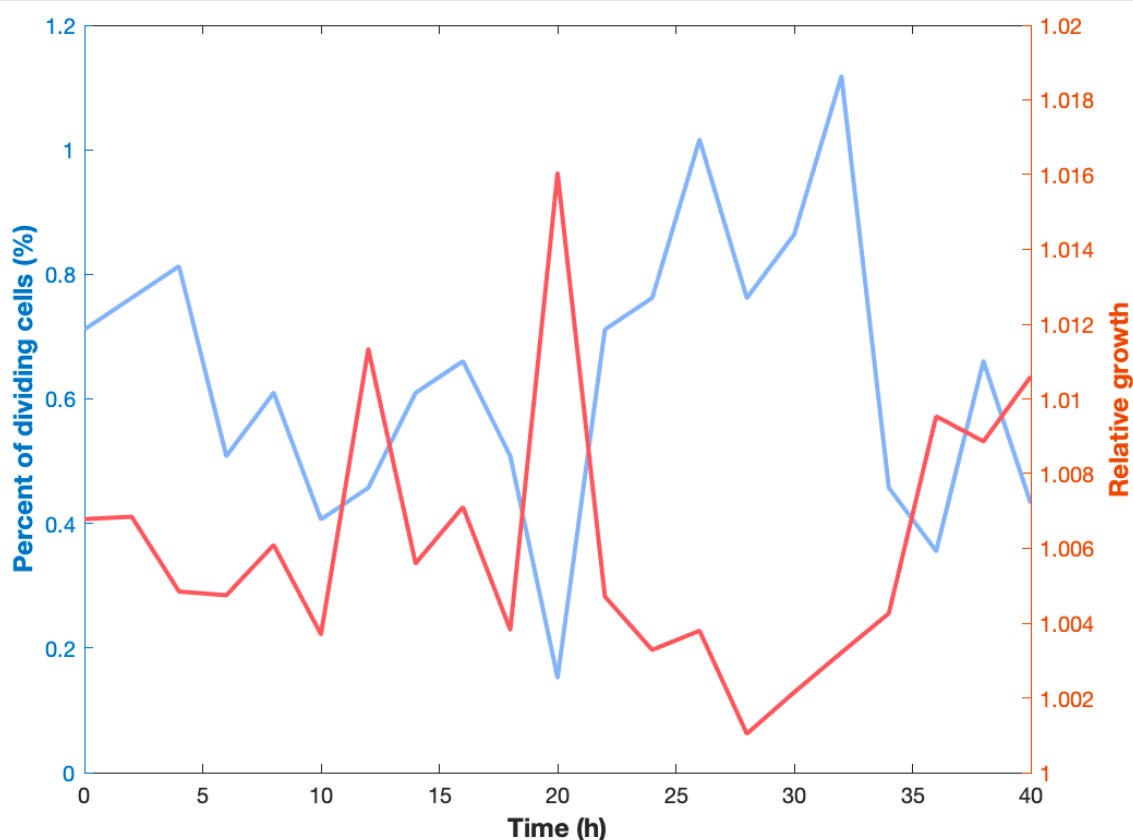
Figure 2.3: Rates changing during the time course. Changing of division rate (blue) expressed as percent of detected cells that divided at each tome point. 13.3% of detected cells divided by the end of the experiment. Changing of relative growth (red) expressed as $(V_1/V_0)^{1/t}$ where V_0 and V_1 are starting and ending volume respectively and t is 2h.

To further confirm that the cellular behaviour observed in the experiment was not part of a change in growth trend, I wanted to observe how growth and division rates changed during the duration of the experiment (Fig. 2.3). The number of detected divisions per time point did not follow any apparent trend, with approximately 0.5% of detected cells dividing every 2 hours (Fig. 2.3, blue), with 13.3% of detected cells having divided by the end of the experiment. Similarly, the relative growth (see Figure 2.3 legend for calculation) seemed to

oscillate randomly and not to follow a trend over time. Therefore, with the data on volume increase, absolute growth, and cell division, we can conclude that there were not strong trends that related to experiment progression that could mask the natural progression in the cell cycle and its dependency on cell size. However, it is worth noticing that the average volume increased toward the end of the experiments, so any relationship that only applies to this part should be discarded. For this reason, detected cell lineages were aligned based on cell cycle stage, rather than by volume or time point of the experiment, so any effect related to the latter should be averaged across the time course.

2.4 CDT1 concentration as a marker for S-phase

With the intent of assigning growing cells to specific cell cycle phases, the behaviour of CDT1-CFP and H3.1-RFP are discussed next. Individual cells were tracked for the duration of the experiment and Figure 2.4 shows some examples of the changing concentration of the two fluorophores. A very common occurrence is shown in Figure 2.4 (red panels), where CDT1 concentration increased rapidly, before sharply decreasing by 2 to 3 fold. This behaviour is associated with the entry in S-phase, with CDT1 licensing DNA replication before being proteolyzed by FBl17 (Yin *et al.*, 2014; Desvoyes *et al.*, 2019, 2020). This behaviour will be used to determine whether cells are in G1 or G2. Note that, in order to diminish the likelihood of artifacts, cells are considered entering S-phase only when an increase of CDT1 concentration, followed by a sharp decrease of it, is observed. Another common types of cell lineages are those that divided early in the time course and did not have the time to transition to S-phase (Fig. 2.4, blue panels). Those cells are in early G1 and slowly accumulate CDT1. In some rare cases we were able to observe cells dividing during the time course, with both daughter cells entering S-phase at similar time (Fig. 2.4, purple panels). It is interesting to see how similar CDT1 concentration was in distinct cells, suggesting a tight regulation of this pathway. Therefore, CDT1 behaviour during this experiment was consistent with previous reports (Yin *et al.*, 2014; Desvoyes *et al.*, 2020), allowing us to use the information related to its change in concentration to detect cells transitioning to S-phase. Additionally, accumulation of CDT1 appeared to be size dependent, as shown by its concentration being the highest in cells around 150µm^3 (Fig. 2.5a), the expected volume for S-phase transition (Jones *et al.*, 2017). This observation was further confirmed in sister cells, where CDT1 concentration was higher in the larger cell, suggesting that cell cycle progression is linked to cell size via a mechanism that is upstream of CDT1 (Fig. 2.5b).
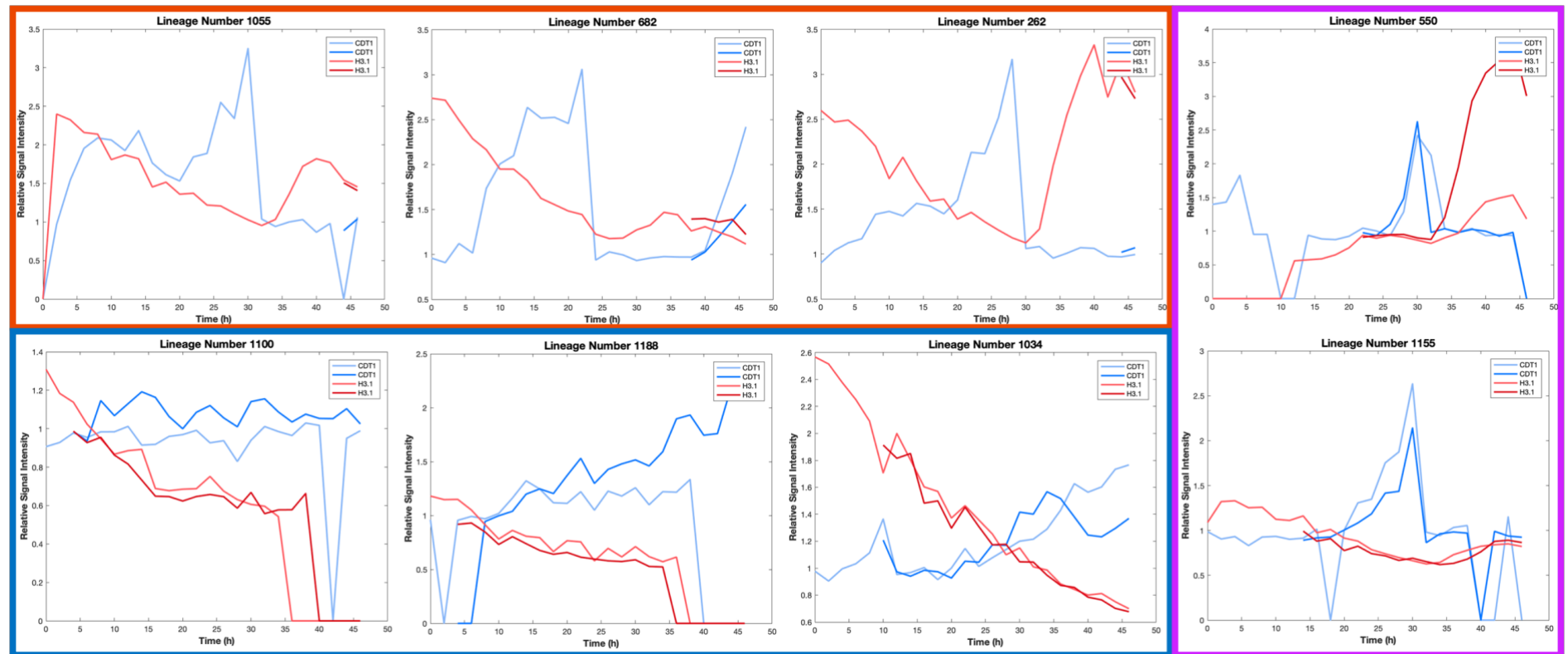
Figure 2.4: Single cell data on CDT1 and H3.1 expression. CDT1 (blue) and H3.1 (red) relative concentration changes during cell cycle progression. When the detected cell divided, relative concentration was followed in daughter cells (darker colours). Red panels: S-phase transition is marked by increase of CDT1 followed by sharp decrease in its concentration. After this, H3.1 concentration slowly increases. Blue panels: early G1 sister cells, showing howCDT1 slowly accumulates at birth, whilst H3.1 concentration slowly decreases. Purple panes: rare events where cells go through S-phase shortly after birth.
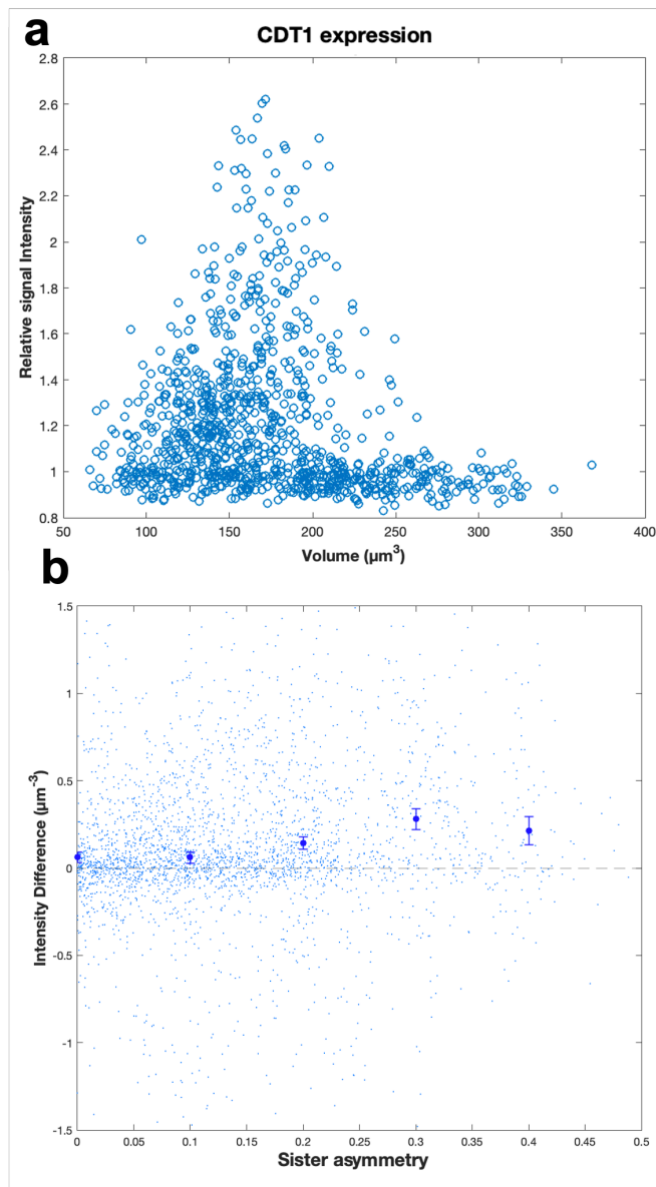
Figure 2.5: CDT1 concentration is cell size dependent. a) CDT1 concentration and cell volume. Note how CDT1 concentration increases for small volumes, and how it peaks at around 150μm, highlighting how cell cycle progression related to cell size. b) CDT1 signal intensity difference among sisters (V_l-V_s), against sister asymmetry ((V_l-V_s)/(V_l+V_s)) with V_l and V_s equal to the volume of larger and small sister respectively. In other words, the x axis represents the degree of asymmetry of sister cells, with zero representing cells identical in size – the y axis represents in which sisters CDT1 is more concentrated, with negative numbers representing higher concentration in the smaller sister and positive numbers representing higher concentration in the bigger sister. Dark blue points represent the mean population of points that spans across 0.1 asymmetry (0.05 before and after) and the error bars represent the 95% confidence interval in this area. Note how the mean of the difference increases with increasing sister asymmetry.

The H3.1-RFP fluorophore was introduced into the cell cycle marker line in order to discriminate cells that are in G2, in the case that S-phase was not observed. In fact, in Figure 2.4 (red panels) we can see how the concentration of H3.1 sharply increases during G2, almost mimicking CDT1 increase before S-phase transition. However, H3.1 behaviour is not as regular as CDT1, because its concentration often does not increase consistently after S-phase transition (compare Figure 2.4 top and bottom purple panels) and importantly, does not sharply decrease at G1 entry, but rather does so slowly during the duration of G1 (Fig. 2.4, blue panels). This behaviour appears different to the one reported for H3.1 in the root meristem, where its concentration seems to decrease more sharply after division (Otero *et al.*, 2016). According to this study, the concentration difference between H3 variants, H3.1 and H3.3, is part of a mechanism that connects proliferation and entering into the

45

endocycle, but their accumulation shows different behaviours depending on the tissues (Otero *et al.*, 2016). Therefore, the inconsistent behaviour we observed for H3.1 might relate to differences between root and shoot meristems. This observation is further highlighted in Figure 2.1 (arrow) where association between H3.1 and chromosomes is observed, a behaviour reported in roots for H3.3 but not H3.1 (Otero *et al.*, 2016). Nevertheless, we opted for not using H3.1 as a marker for G2, and rather only use CDT1 concentration change and cell division as markers for cell cycle progression.
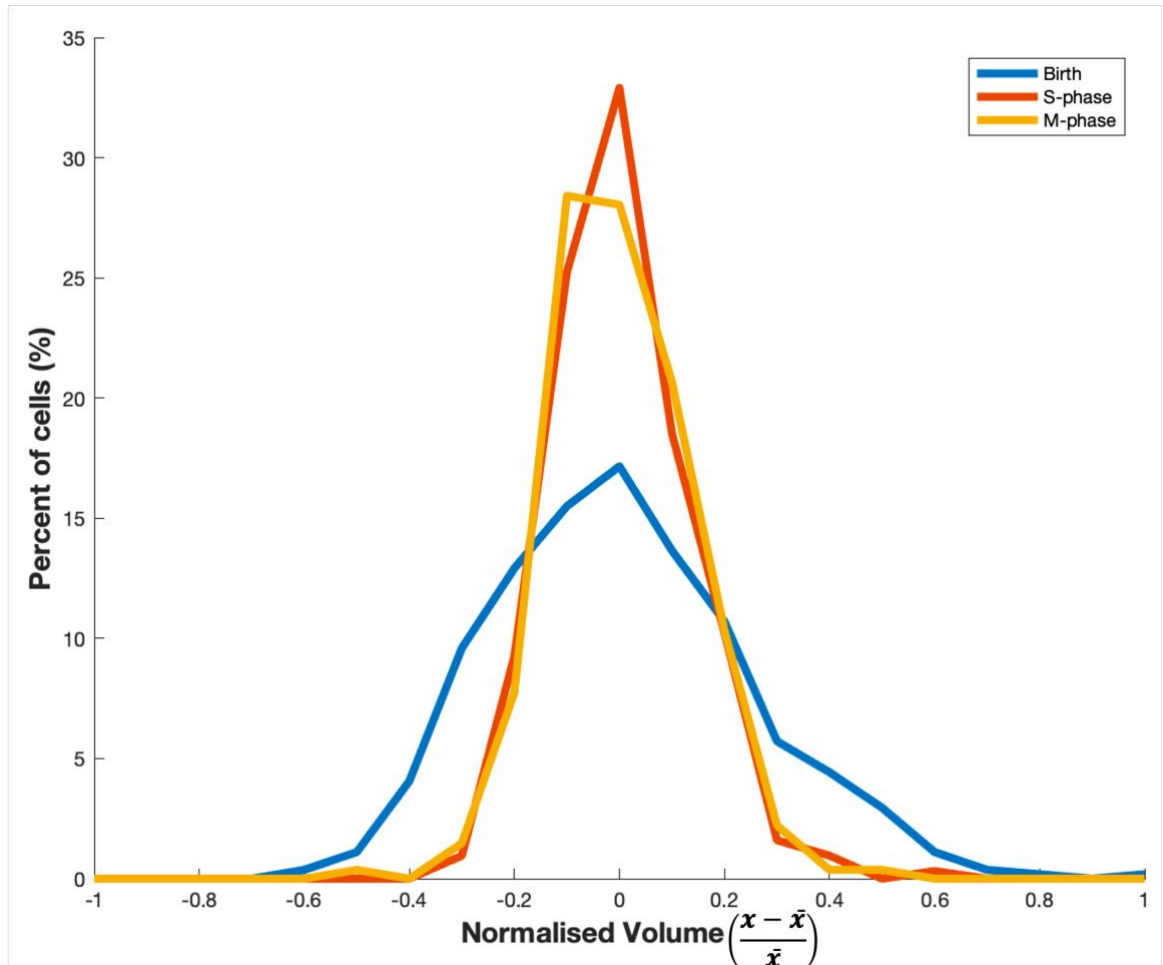
Figure 2.6: Variability in cell volume is highest at birth. Probability distributions showing size variability at birth (blue, CV = 0.24), during S-phase (red, CV = 0.13) and at division (yellow, CV = 0.13). Volume was normalised as $(x-\bar{x})/(\bar{x})$, where x is the individual value and $\bar{x}$ the mean value. Notice how high the size variability generated as result of division is restored at S-phase and preserved through division.

2.5 Cell size variability is reduced at S-Phase

With the means for correlating cell size at various cell cycle stages, I could finally answer the question whether the size variability seen at cell birth is corrected during the subsequent progression through the cell cycle. Figure 2.6 shows the normalised

distribution of cell size at birth, S-phase and division. The coefficients of variation (CV) at S and at division are virtually identical (0.127 and 0.129 respectively), halved when compared to the CV at birth (0.245). This information alone showed that cells actively reduce the variability accumulated at birth before entering S-phase.

One of the suggested mechanisms for reduced size variability involves linking growth rate to cell size, allowing smaller cells to grow faster that larger ones. This was reported for mammalian cells (Kafri *et al.*, 2013) and suggested for plant cells (Willis *et al.*, 2016). Figure 2.8, however, shows that there is no correlation between cell volume at birth and growth in the first 4h of G1 ($R^2 = 0.003$), suggesting that meristem cells might behave differently than mammalian cells in this regard.
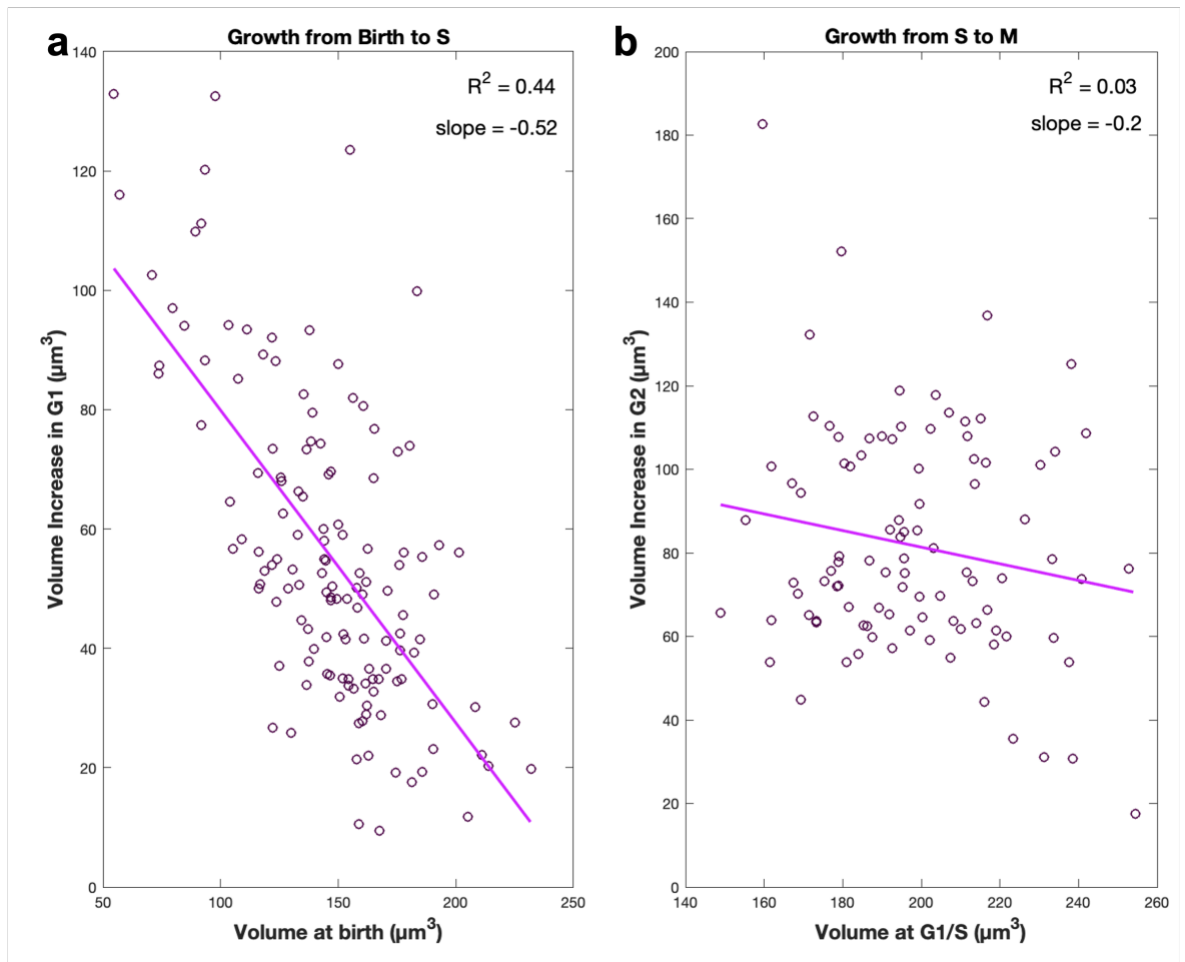
Figure 2.7: Difference in volume increase in G1 and G2. Relationship between volume at the start of the phase (birth for G1 and S-phase for G2) and volume increase in that phase, calculated as $V_1 - V_0$, with V_0 and V_1 = volumes at birth and S-phase for G1 (a) and volumes at S and division for G2 (b). (a) The negative correlation ($R^2 = 0.44$) at G1 with a slope of -0.5 shows how larger cells grow less than smaller cells to counteract size variability. (b) The lack of correlation at G2 ($R^2 = 0.03$) suggests that cells at G2 maintain low variability by adding a similar volume quantity per each cycle.

Another mechanism for reduced cell size variability at S-phase would be to link cell size to cell cycle progression, with smaller cells adding more size than larger ones before division. To support this idea, Figure 2.7a shows a negative correlation between volume at birth and volume at the G1/S transition. This suggests that the mechanism used by meristem cells to reduce variability most likely operates by acting on cell cycle progression in response of difference in cell size, rather than operating through a growth rate mechanism as previously suggested (Willis *et al.*, 2016).
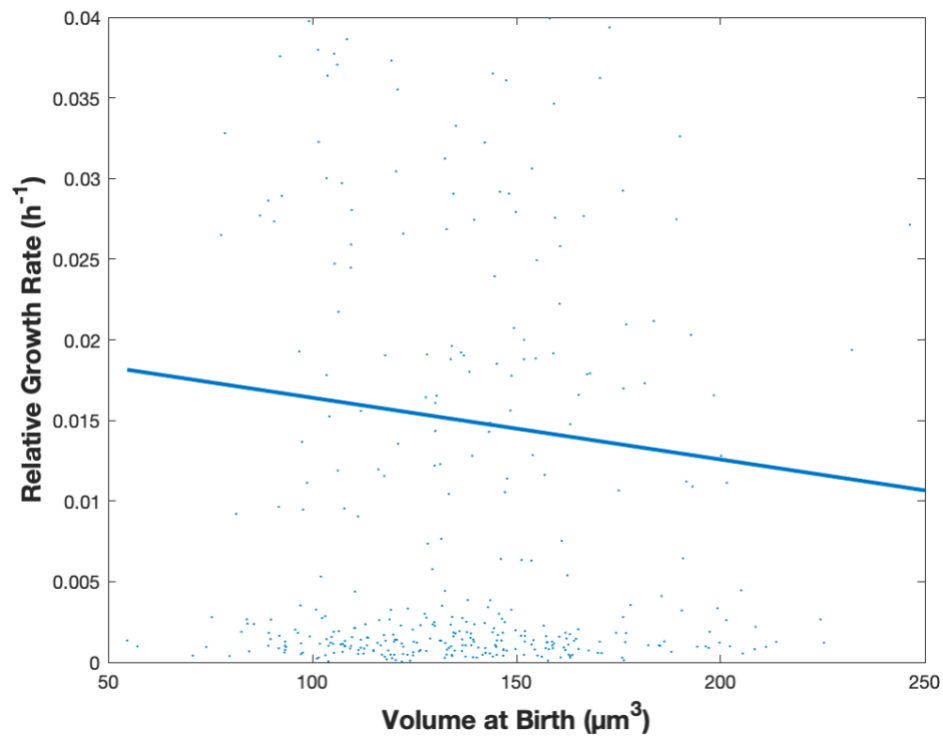
Figure 2.8: Change in growth rate in new-born cells. Relationship between new-born cells and their relative growth rate in the first 4h of their life. Relative growth rate was calculated as $\ln(V_1/V_0)/t$, where V_0 and V_1 are the volume at birth and the volume after 4h, respectively, and t is the time of the interval = 4h. In case of perfect exponential growth, the relative growth rate is a constant. There is no correlation between volume and growth rate ($R^2 = 0.003$).

Moreover, is important to notice that the CV at S-phase entry and division are virtually identical (0.127 and 0.129 respectively) (Fig. 2.6). Combined with the information that G2 length is 21 ± 5h (Fig. 2.10), it suggests that either cells are able to grow during this period of time without accumulating any variability, or a mechanism must be in place to ensure that any further accumulated variability is reduced before division. To corroborate this observation, the lack of correlation between volume increase at G2 and cell size at S (Fig. 2.7b), suggests that cells are able to always add a fixed amount of volume at G2, regardless of their size at the G1/S transition, in a mechanism able to ensure reduction of variability

(Facchetti, Chang and Howard, 2017). Therefore, although the majority of cell size variability accumulated after division is restored at S-phase entry, a further mechanism is in place to ensure that this variability is kept low before division.
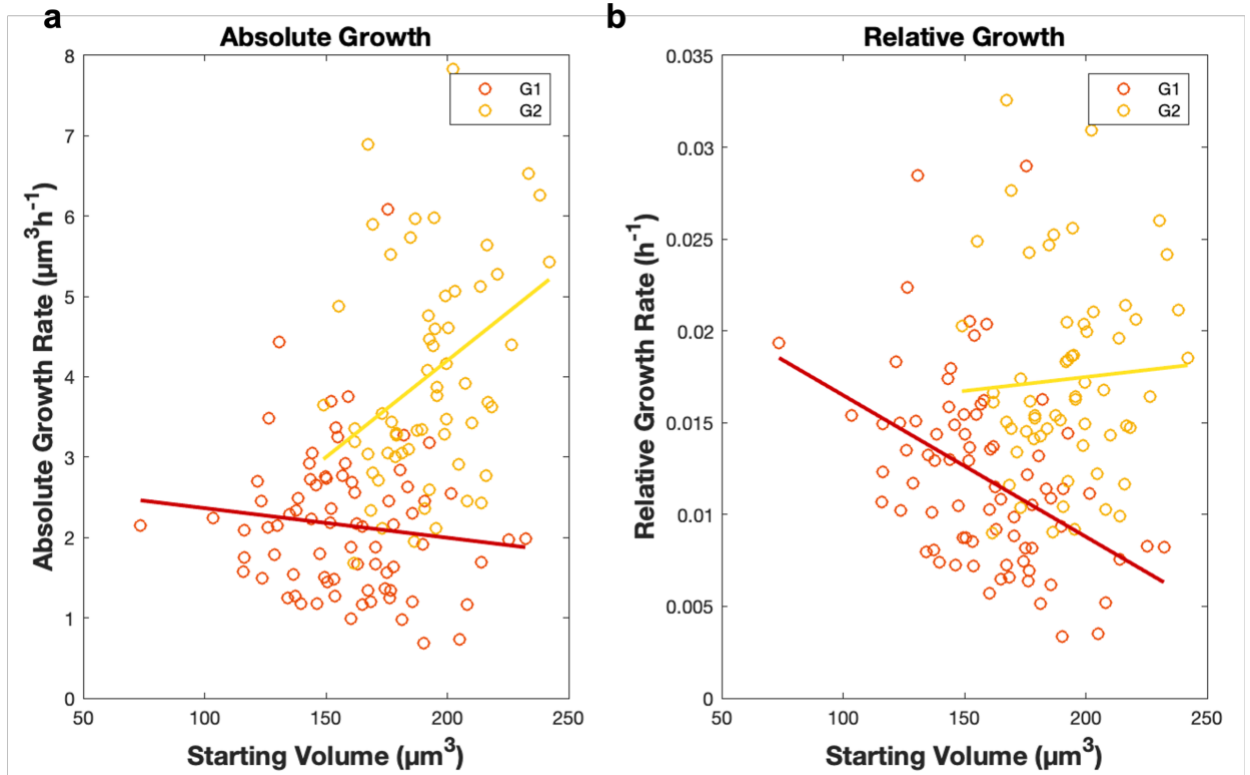
Figure 2.9: Difference in growth rate in G1 and G2. Relationship between absolute (a) and relative (b) growth in G1 and G2. Growth here is measured over the duration of the whole interval as follows: absolute growth = $(V_1 - V_0)/t$ and relative growth = $\ln(V_1/V_0)/t$; where V_0 and V_1 are the volume at the beginning and the end of the transition, respectively, and t is the time of the growth phase. Linear regressions for absolute growth (a) have R^2 = 0.013 for G1 and R^2 = 0.123 for G2. Linear regressions for relative growth (b) have R^2 = 0.183 for G1 and R^2 = 0.004 for G2.

2.6 Cell growth behaviour

The absence of a correlation between cell size and relative growth rate in the first 4h of the experiment strongly supports the idea of the exponential nature of cell growth (Fig. 2.8). To further investigate this possibility, Figure 2.9 shows how cell size and growth rate changes in G1 and G2. Before diving into these data, it is important to underline that growth rate in this case was calculated from the start to the end of a cell cycle phase. So, in contrast to the data shown in Figure 2.8, these represent growth for a longer period. Absolute growth in G1 and G2 appear very different, both in trend and in their average, which almost doubles in G2 compared to G1 (2.2 and 4.0 $\mu m^3 h^{-1}$, respectively) (Fig. 2.9a). Interestingly, whilst the lack of correlation between relative growth and volume in the first 4h would

support exponential growth (Fig. 2.8), the lack of correlation between absolute growth and volume at G1 would indicate linear growth for this period (Fig. 2.9a). So, growth in new-born cells could approximate to exponential, then move to linear later, whilst reaching S-phase. This behaviour it is very similar to the one suggested on the theoretical model that predicts linear growth as consequence of the limitation imposed by DNA concentration (Lin and Amir, 2018), although the question of when this limitation becomes physiologically significant remains open (see discussion). In contrast to G1 cells, the weak positive correlation between the volume at the start of G2 and the absolute growth rate during this period ($R^2 = 0.13$), combined with lack of correlation with relative growth rate in G2 ($R^2 < 0.01$), would best be explained by exponential growth in this period (Fig. 2.9b). In the case of relative growth, even if the trends in G1 and G2 differ, their average is very similar (0.0120 and $0.0174h^{-1}$, respectively), Indicating that, exponential or not, cells in G1 grow at a similar speed compared to those in G2 (Fig. 2.9b).
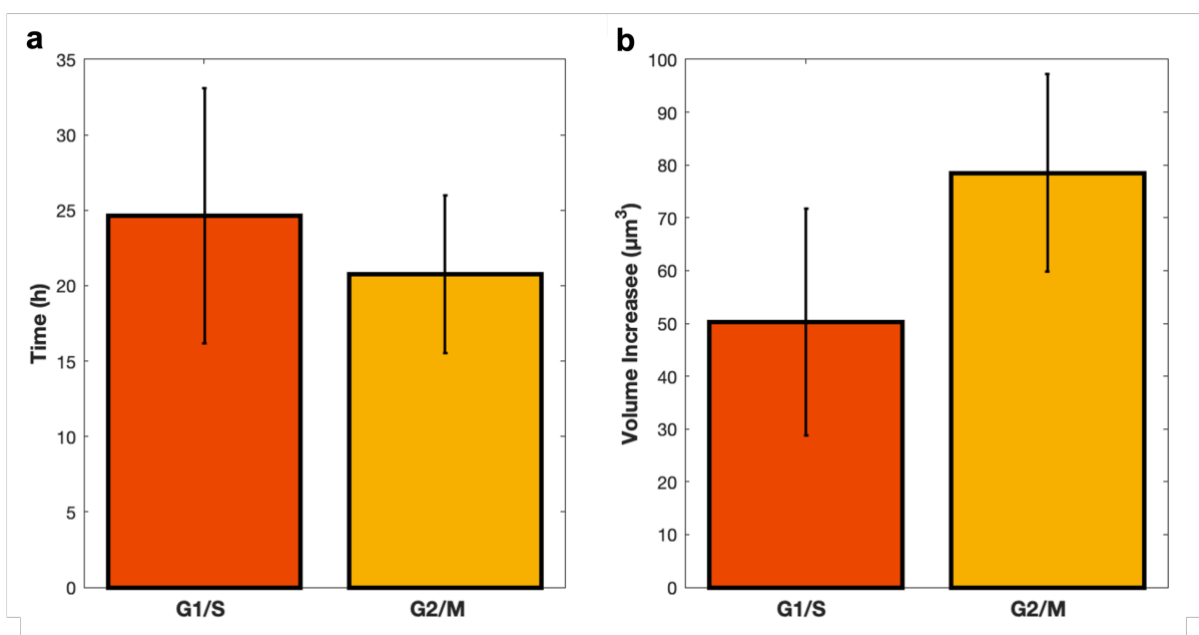
Figure 2.10: Difference in volume increase and phase length in G1 and G2. a) Cell cycle phases length in detected cells. G1 to S averaged 24.7 ± 8.4h and G2 to M 20.8 ± 5.2h (significant difference via t-test p = 0.001). b) Volume increase difference in detected cells, calculated as volume at the end of the transition minus volume at the end. G1 to S averaged 50.4 ± $21.5\mu m^3$ and G2 to M 78.6 ± $18.7\mu m^3$ (significant difference via t-test p < 0.0001). Error bars represents standard deviation.

However, it is important to emphasise the caveats of these observations and with studying growth rates in general. Critically, cells do not grow in a vacuum and must integrate various developmental signals – therefore often pause and their growth rate is not constant over their life span. This observation has been reported multiple times (Serrano-Mislata, Schiessl and Sablowski, 2015; Willis *et al.*, 2016; Jones *et al.*, 2017; D'Ario *et al.*, 2021) and it is

apparent from noticing how variable growth rate was during the course of this experiment (Fig. 2.3). This phenomenon is incompatible with the way growth rate is measured, where the inherent assumption of continuous growth is essential for the measurement.

Another important observation is that the expansion of plant cells occurs against the surrounding cell wall, with an internal pressure higher than 1MPa (Fricke, 1997; Beauzamy *et al.*, 2015). Therefore, more or less growth can be achieved depending on the thickness of the surrounding walls, which can vary depending on the age of the wall. Finally, since four distinct measurements are required to calculate growth rate, the starting and ending volumes and times, the obtained error is relatively large. In yeast, this error was shown to favour an erroneous conclusion of linear growth, which was later shown to be exponential (Cooper, 2013). However, other than the data observed so far, the simple observation that the volume increase at G2 was higher than in G1 ($78 \pm 19\mu m$ and $50 \pm 21\mu m$, respectively; $p < 0.0001$), even if it G2 is shorter than G1 ($21 \pm 5h$ and $24 \pm 8h$ respectively; $p = 0.001$) (Fig. 2.10) suggest that growth is overall higher than linear, and support the view that cell growth approaches exponential behaviour.

2.7 Discussion

The novel protocol of performing long-term imaging at high frequency of imaging, which heavily leveraged Airyscan technology (Huff, 2015), and use of reliable cell-cycle (Desvoyes *et al.*, 2020) and plasma membrane (Willis *et al.*, 2016) reporters, was long awaited by the plant cell community. This allowed us to address questions regarding cell size variability and cell cycle progression. Both the imaging technology and the marker lines will be central in answering cell-centric questions using plants as a model system. The dataset generated here helped us to better understand how meristem cells grows and how their cell cycle progresses in a novel way, but most importantly, helped me to answer an important question on size homeostasis. Here I showed that the cell size variability produced as birth is reduced at the G1/S transition. Or in other words, cell size is perceived by cells at some point during G1 and this information is integrated to decide whether the cell should progress through S-phase, or not. This information is critical because it informs us that the molecular mechanism responsible for sensing cell size must act during G1 and be upstream of CDT1a. As we will see in the next chapters, this information was critical in creating a hypothesis-driven experimental framework to address this question.

Beyond cell size sensing during G1, this experiment suggested that a mechanism that links cell size to G2/M entry could also be present. Unlike the G1/S mechanism, which ensures halving of the variability accumulated at birth, the role of this putative G2/M mechanism would be to preserve this state, counteracting the effect of growth on variability. Confirming this different role, the slope of the linear regression on Figure 2.7b, which represents the impact on variability, is higher than the one calculated for G1/S. As better explained in Chapter 5, the closer this slope is to -1, the higher the reduction of variability, with the slope being close to 0 for G2/M and -0.5 for G1/S (an $R^2 = 0.03$ for the linear regression at G2/M indicates no correlation between volume at S and volume increase, effectively suggesting that the volume increase is the same, regardless of the volume at S. For this reason, I interpret the slope at G2/M to be approximately 0, rather than assigning to it the value of -0.2 shown on the graph). Interestingly, if indeed a mechanism is in place during G2, to ensure that the same volume is added before division, any effect that perturbs G1/S size sensing, would still be visible at division, effectively making any effect on the G1/S mechanism epistatic to the mechanism at G2/M. Such behaviour would explain how mutants that shorten G1 time still produce small cells, effectively transmitting any size defect at the G1/S transition to division (Jones *et al.*, 2017).

A very interesting question in cell biology is about the growth rate of cells, simplified by whether they grow linearly or exponentially. Although this seems a problem of semantic, it hides a more fundamental question on what the limits of growth are and what cells do to overcome them. Another way to pose this question is to ask what the biological maximum for growth is and what is there to limit it. Exponential growth seems to be both the theoretical limit of growth and what likely occurs in live cells (Cooper, 2013), despite the various arguments in favour of different growth types (Mitchison, 2003). Exponential growth is found everywhere in biology and is the simple consequence of a positive feedback loop between what causes growth and what it is growing. In the case of cell size, volume increases as proteins and ribosomes are synthesised, which in turn are responsible for making more proteins and ribosomes, increasing the rate at which volume grows (Lin and Amir, 2018). For this reason, the transcription and translation machineries are the limiting factor for maximum growth.

However, theoretical work has suggested that upon reaching a certain size, DNA concentration becomes the limiting factor for growth, which in turn turns into linear as

opposed to exponential (Lin and Amir, 2018; Neurohr *et al.*, 2019). This opens the question of what the physiological relevance of this phenomenon could be in plants. In the case of organs like leaves and sepals, the phenomenon of polyploidisation followed by cell size increase is well recorded (Robinson *et al.*, 2018) and speculation can be made on the role of increasing genomic copies to ensure that the optimal concentration of DNA in kept in these giant cells. This observation is different than speculating that proliferating cells live at the edge of growth capacity, so the minimum size that disrupts optimal growth might be well off the recorded one for meristem cells. To confirm this view, experiments where average cell size was enlarged by three-fold, cells grew at comparable rates as wild type cells (Serrano-Mislata, Schiessl and Sablowski, 2015), suggesting that the physiological limit to exponential growth in meristematic tissue is not reached due to DNA dilution. Unfortunately, regardless of the importance of this question, addressing it is a complicated issue due to limitations in measuring growth rates with sufficient precision and due to the behaviour of the cells themselves, whose growth oscillates rather than progressing unimpeded (Serrano-Mislata, Schiessl and Sablowski, 2015; Willis *et al.*, 2016; Jones *et al.*, 2017; D'Ario *et al.*, 2021).

This chapter presented important information that guided us in the hunt for the mechanism of cell size homeostasis. First of all, I showed that a mechanism for size control is present prior to S-phase progression, and that this mechanism must be upstream to CDT1, because CDT1 accumulation was shown to be size dependent. The known role of G1/S inhibitors in size control in yeast (Schmoller *et al.*, 2015) and Chlamydomonas (Umen and Goodenough, 2001), their suggested role in mammalian cells (Zatulovskiy *et al.*, 2020) and their well-established function upstream of CDT1 (Sablowski and Gutierrez, 2021), makes these type of proteins ideal candidates for this purpose and they will be the main focus of this work. Unfortunately, information on the G2/M transition is more scarce. The only known mechanism that directly links cell size to commitment to division has been described in *Schizosaccharomyces pombe* (Pan *et al.*, 2014; Facchetti *et al.*, 2019) and involves proteins which have no obvious homologues in plants. Additionally, the phenomenological nature of these two mechanisms appears very different, with *S. pombe* dividing at the same size every time, and meristem cells adding a similar amount of volume each G2. Nevertheless, an attempt will be made to set the stage for possible future studies in that direction.

2.8 References

Baumgärtner, S. and Tolić-Nørrelykke, I. M. (2009) 'Growth pattern of single fission yeast cells is bilinear and depends on temperature and DNA synthesis', *Biophysical journal*. The Biophysical Society, 96(10), pp. 4336–4347. doi: 10.1016/j.bpj.2009.02.051.

Beauzamy, L. *et al.* (2015) 'Mechanically, the Shoot Apical Meristem of Arabidopsis Behaves like a Shell Inflated by a Pressure of About 1 MPa ', *Frontiers in Plant Science* , p. 1038. Available at: https://www.frontiersin.org/article/10.3389/fpls.2015.01038.

Cooper, S. (2006) 'Distinguishing between linear and exponential cell growth during the division cycle: single-cell studies, cell-culture studies, and the object of cell-cycle research', *Theoretical biology & medical modelling*. BioMed Central, 3, p. 10. doi: 10.1186/1742-4682-3-10.

Cooper, S. (2013) 'Schizosaccharomyces pombe grows exponentially during the division cycle with no rate change points.', *FEMS yeast research*. England, 13(7), pp. 650–658. doi: 10.1111/1567-1364.12072.

D'Ario, M. *et al.* (2021) 'Cell size controlled in plants using DNA content as an internal scale', *Science*, 372(6547), p. 1176 LP-1181. doi: 10.1126/science.abb4348.

D'Ario, M. and Sablowski, R. (2019) 'Cell Size Control in Plants', *Annual Review of Genetics*. Annual Reviews, 53(1), pp. 45–65. doi: 10.1146/annurev-genet-112618-043602.

Desvoyes, B. *et al.* (2019) 'FBL17 targets CDT1a for degradation in early S-phase to prevent Arabidopsis genome instability', *bioRxiv*, p. 774109. doi: 10.1101/774109.

Desvoyes, B. *et al.* (2020) 'A comprehensive fluorescent sensor for spatiotemporal cell cycle analysis in Arabidopsis', *Nature Plants*, 6(11), pp. 1330–1334. doi: 10.1038/s41477-020-00770-4.

Facchetti, G. *et al.* (2019) 'Reprogramming Cdr2-Dependent Geometry-Based Cell Size Control in Fission Yeast', *Current Biology*, 29(2), p. 350–358.e4. doi: https://doi.org/10.1016/j.cub.2018.12.017.

Facchetti, G., Chang, F. and Howard, M. (2017) 'Controlling cell size through sizer mechanisms', *Current Opinion in Systems Biology*. Elsevier Ltd, pp. 86–92. doi: 10.1016/j.coisb.2017.08.010.

Fricke, W. (1997) 'Cell turgor, osmotic pressure and water potential in the upper epidermis of barley leaves in relation to cell location and in response to NaCl and air humidity', *Journal of Experimental Botany*, 48(1), pp. 45–58. doi: 10.1093/jxb/48.1.45.

Fung-Uceda, J. *et al.* (2018) 'The Circadian Clock Sets the Time of DNA Replication Licensing to Regulate Growth in Arabidopsis', *Developmental Cell*. Elsevier,

45(1), p. 101–113.e4. doi: 10.1016/j.devcel.2018.02.022.

Huff, J. (2015) 'The Airyscan detector from ZEISS: confocal imaging with improved signal-to-noise ratio and super-resolution', *Nature Methods*, 12(12), pp. i–ii. doi: 10.1038/nmeth.f.388.

Jones, A. R. *et al.* (2017) 'Cell-size dependent progression of the cell cycle creates homeostasis and flexibility of plant cell size', *Nature Communications*. Nature Publishing Group, 8, p. 15060. doi: 10.1038/ncomms15060.

Kafri, R. *et al.* (2013) 'Dynamics extracted from fixed cells reveal feedback linking cell growth to cell cycle', *Nature*. Nature Publishing Group, 494(7438), pp. 480–483. doi: 10.1038/nature11897.

Kubitschek, H. E. and Clay, K. B. (1986) 'A second growth state for Schizosaccharomyces pombe', *Experimental Cell Research*, 165(1), pp. 243–254. doi: https://doi.org/10.1016/0014-4827(86)90548-3.

Landrein, B. *et al.* (2018) 'Nitrate modulates stem cell dynamics in *Arabidopsis* shoot meristems through cytokinins', *Proceedings of the National Academy of Sciences*, 0, p. 201718670. doi: 10.1073/pnas.1718670115.

Lin, J. and Amir, A. (2018) 'Homeostasis of protein and mRNA concentrations in growing cells', *Nature Communications*, 9(1), p. 4496. doi: 10.1038/s41467-018-06714-z.

Mitchison, J. M. B. T.-I. R. of C. (2003) 'Growth During the Cell Cycle', in. Academic Press, pp. 165–258. doi: https://doi.org/10.1016/S0074-7696(03)01004-0.

Neurohr, G. E. *et al.* (2019) 'Excessive Cell Growth Causes Cytoplasm Dilution And Contributes to Senescence', *Cell*. Cell Press, 176(5), p. 1083–1097.e18. doi: 10.1016/j.cell.2019.01.018.

Otero, S. *et al.* (2016) 'Histone H3 Dynamics Reveal Domains with Distinct Proliferation Potential in the Arabidopsis Root', *The Plant cell*. 2016/05/20. American Society of Plant Biologists, 28(6), pp. 1361–1371. doi: 10.1105/tpc.15.01003.

Pan, K. Z. *et al.* (2014) 'Cortical regulation of cell size by a sizer cdr2p', *eLife*, 2014(3), pp. 1–24. doi: 10.7554/eLife.02040.

Robinson, D. O. *et al.* (2018) 'Ploidy and Size at Multiple Scales in the Arabidopsis Sepal', *The Plant cell*. 2018/08/24. American Society of Plant Biologists, 30(10), pp. 2308–2329. doi: 10.1105/tpc.18.00344.

Sablowski, R. and Gutierrez, C. (2021) 'Cycling in a crowd: coordination of plant cell division, growth, and cell fate', *The Plant Cell*. doi: 10.1093/plcell/koab222.

Schmoller, K. M. *et al.* (2015) 'Dilution of the cell cycle inhibitor Whi5 controls budding-

yeast cell size', *Nature*, 526(7572), pp. 268–272. doi: 10.1038/nature14908.

Serrano-Mislata, A., Schiessl, K. and Sablowski, R. (2015) 'Active Control of Cell Size Generates Spatial Detail during Plant Organogenesis', *Current Biology*. The Authors, 25(22), pp. 2991–2996. doi: 10.1016/j.cub.2015.10.008.

Umen, J. G. and Goodenough, U. W. (2001) 'Control of cell division by a retinoblastoma protein homolog in Chlamydomonas', *Genes and Development*, 15(13), pp. 1652–1661. doi: 10.1101/gad.892101.

Willis, L. *et al.* (2016) 'Cell size and growth regulation in the *Arabidopsis thaliana* apical stem cell niche', *Proceedings of the National Academy of Sciences*, 113(51), pp. E8238–E8246. doi: 10.1073/pnas.1616768113.

Yin, K. *et al.* (2014) 'A dual-color marker system for in vivo visualization of cell cycle progression in Arabidopsis.', *The Plant journal : for cell and molecular biology*. England, 80(3), pp. 541–552. doi: 10.1111/tpj.12652.

Zatulovskiy, E. *et al.* (2020) 'Cell growth dilutes the cell cycle inhibitor Rb to trigger cell division', *Science*, 471(July), pp. 466–471.

Chapter 3: G1-S size control using KRPs as proxy for chromatin content

3.1 Introduction

In the previous chapter we showed that the variability in cell size that accumulates at birth is reduced at S-phase. Here I move my attention to finding a mechanism for cell size sensing, which integrates cell size to cell cycle progression. Multiple studies in other organisms identified protein homologues or analogues of plant RETINOBLASTOMA RELATED (RBR) to be responsible for size-dependent S-phase transition. Here I will refer to this class of proteins, including all the homologous and functional analogues of the Arabidopsis AtRBR1, as RBRs.

RBRs have been shown to control cell size directly in fungi, with the RBR functional analog Whi5 (Schmoller *et al.*, 2015), and mammalian cells, by Rb (Zatulovskiy *et al.*, 2020) and indirectly in *Chlamydomonas reinhardtii*, where the RBR homologue MAT3 is responsible for setting the number of divisions that occurs at night (Umen and Goodenough, 2001). These mechanisms rely on the role of RBRs as inhibitors of S-phase transition and involve some form of growth-driven dilution of this molecule. This is commonly known as the "dilution of inhibitor model" which, in order to result in size homeostasis, requires three attributes: i) the inhibitor molecule has to remain constant in the period before S-phase entry, so its concentration drops as the result of the growth-driven volume increase; ii) the inhibitor needs to be produced at some point when it is involved in measuring size, in order to return to its original state; iii) the amount of the molecule when dilution starts needs to be independent of cell volume, or the volume at S-phase will not be constant.

In addition, in order for dilution to impact cell cycle progression, the compartment in which this molecule signals, i.e. the nucleus, has to grow proportionally to the rest of the cell. If that were not the case and nuclear volume were constant, the concentration of all nuclear proteins would increase as the cell grew, therefore any promoter of the cell cycle would act in a size-dependent manner. That has been shown not to be the case, and nuclear volume was reported to be proportional to cell size in multiple organisms (Wilson, 1925; Neumann and Nurse, 2007; Webster, Witkin and Cohen-Fix, 2009). A caveat of the study in Arabidopsis (Willis *et al.*, 2016), however, was the use of a nuclear localised protein under the expression of the CLAVATA3 promoter, which could create artifacts due to the way apparent volume scales with fluorophore intensity – the higher the intensity the bigger the

object appears. To complicate this, proteins expressed under CLAVATA3 promoter have different concentration in different cells, increasing possible technical complications. Thus the correlation between nuclear and cellular growth needed to be revisited in Arabidopsis.

Due to their involvement in size sensing in mammalian, algal and yeast cells, RBRs were the initial candidates in the present study. These inhibitors of the S-phase transition are essential proteins, which act as hubs to coordinate multiple inputs (Desvoyes and Gutierrez, 2020) (Fig. 3.1). In the green lineage, other than inhibiting S-phase transition, RBR proteins acquired a plethora of specialised roles, ranging from sex gene expression in the alga *Volvox carteri* (Kianianmomeni, Nematollahi and Hallmann, 2008) to meristem cell maintenance (Borghi *et al.*, 2010). Other roles of the plant RBR are reviewed in (Desvoyes and Gutierrez, 2020).

In Chlamydomonas, as discussed in Chapter 1, MAT3 indirectly regulates cell size acting downstream of CDKG, a CYCLIN DEPENDENT KINASE only found in algae (Li *et al.*, 2016). The unique way that *Chlamydomonas* senses its size might relate to its peculiar life cycle: *Chlamydomonas* grows during the day whilst photosynthesising and accumulating CDKG molecules in a size dependent manner (Li *et al.*, 2016). The alga does not divide during this period and only does so at night, when photosynthesis cannot be carried out. At night, *Chlamydomonas* undergoes a number of divisions proportional to CDKG amount, hence to size (Li *et al.*, 2016). MAT3 sets the proportion between number of divisions and CDKG amount, therefore it is responsible for determining cell size but not cell size homeostasis per se (Umen and Goodenough, 2001).

Spermatophytes seem to have adapted RBR role in setting rounds of division in a context different that the one showed by *Chlamydomonas*. The female gametophyte of Arabidopsis undergoes three rounds of nuclear division before cellularisation and RBR is responsible for ensuring this number (Ebel, Mariconti and Gruissem, 2004) (for a review on female gametophyte development see (Yang, Shi and Chen, 2010)). Therefore, given the role as size sensors of Opisthokonts (animal and fungi) RBRs and the role of RBRs in setting division rounds in the green lineage, AtRBR1 is a reasonable candidate as size sensor of the G1/S transition in meristem cells.

Other than RBR, plants have a unique family of S-phase inhibitors, called the KIP-RELATED PROTEINs (KRPs), which act upstream of RBR by inhibiting the kinase activity of CDKa (Verkest *et al.*, 2005) (Fig. 3.1). In Arabidopsis, the KRP family is composed of 7 distinct members with diverse expression patterns (Yang, Wightman and Meyerowitz, 2017) and subcellular localisation (Bird *et al.*, 2007). In the rest of the thesis, I will discuss this family and its phylogeny in more details, but here I will introduce KRP4, which we used as the representative family member expressed in the shoot meristem. The role of *KRP4* in delaying S-phase has been shown to be critical during plant development, because it is one of the genes targeted by the transcription factor JAGGED (Schiessl, Muino and Sablowski, 2014). During sepal emergence, JAGGED promotes organ growth and is responsible for uncoupling progression through S-phase from cell size (Schiessl *et al.*, 2012). The stimulatory effect on growth is caused by repression of *KRP4*, whilst it remains to be determined whether regulation of *KRP4* is also important for role of JAG in the coordination between cell growth and cell cycle (Schiessl, Muino and Sablowski, 2014). These studies, combined with KRP4 expression in the meristem (Yang, Wightman and Meyerowitz, 2017), made KRP4 a good candidate to participate in size-dependent cell cycle progression.

Therefore, the first aim of this chapter was to show that meristem cells satisfy the physical properties for accommodating a dilution of inhibitor model, by testing how protein and nuclear volume scale with meristem cell size. The second major aim was to test whether RBR or KRP4 behave as required by the dilution of inhibitor model.
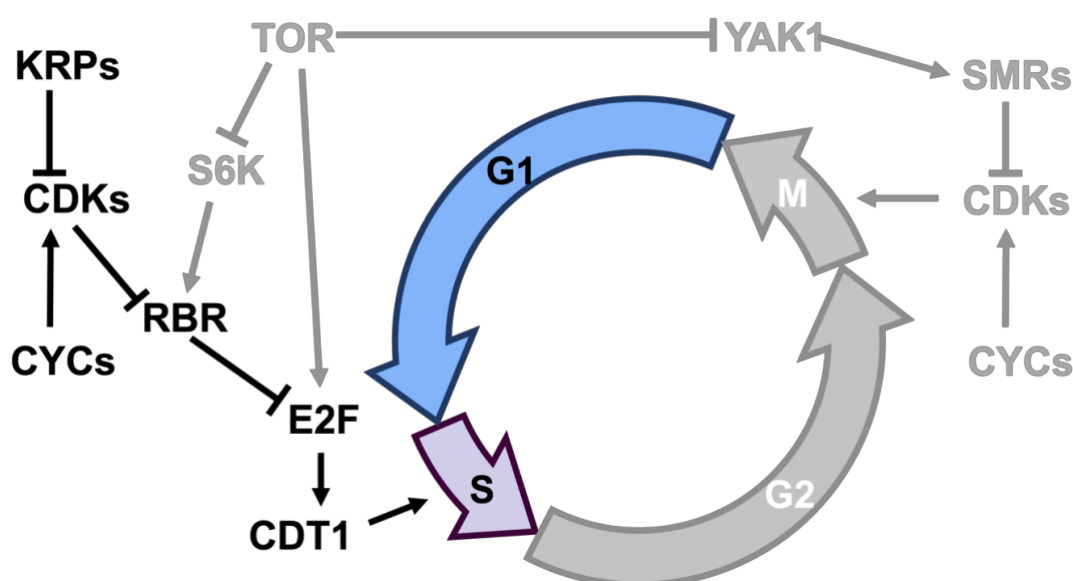
Figure 3.1: Interactions between genes involved in the control of the G1/S phase transition. This simplified diagram shows inhibitory (flatheaded arrows) and activating (arrows) interactions. Recall this diagram for Chapter 1 where the entirety of the pathway is explained in more details. Here the components which are not mentioned are greyed out.

3.2 Protein scaling

Before beginning the hunt for components of a G1/S size sensing mechanism, I needed to confirm that essential components of the cell scale with volume. Critically, if protein amount were constant over volume, any protein would carry information on cell size, trivialising the mechanism for cell size regulation. Since a cell grows by gradual, proportional accumulation of its components, it seems intuitive that protein amounts should indeed be proportional to volume. To confirm this expectation, I labelled proteins in meristem cells using Alexa-Ester (Alexa Fluor™ 488 NHS Ester, Succinimidyl Ester) (Fig. 3.2a). During the labelling process, the ester group on the Alexa molecule reacts with free lysine in the proteins, resulting in a stoichiometric labelling of the cellular protein content (Kendall *et al.*, 2015) (see material and methods for more details).

As expected, protein content scaled linearly ($R^2 = 0.42$) with cell volume, such that there was no correlation between protein concentration and volume ($R^2 = 0.02$) (Fig. 3.2b). This indicated that protein concentration is constant throughout the cell cycle and independent of cell size, or, in other words, protein concentration remains the same as each meristem cell grows and divides.
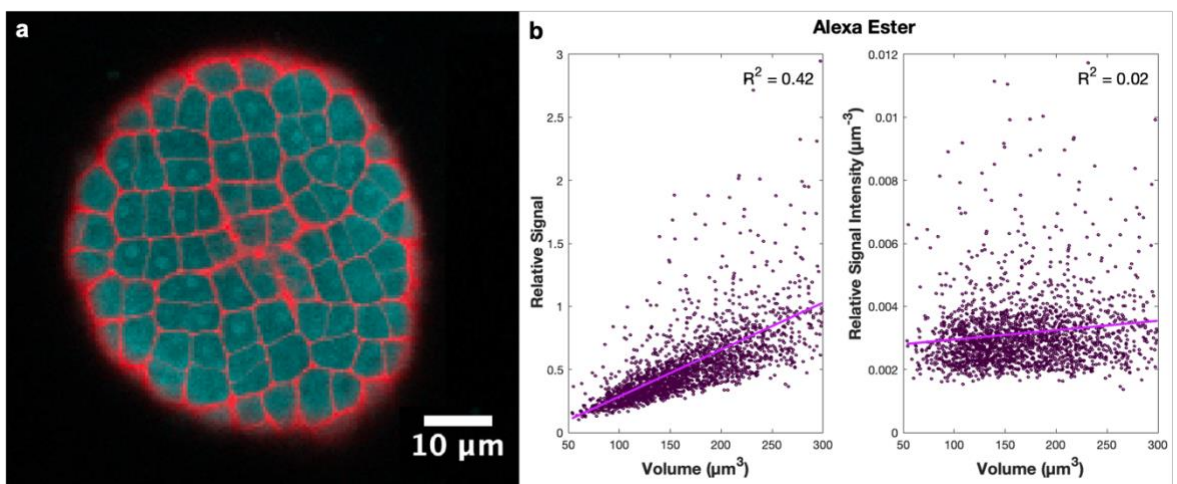
Figure 3.2: Protein content scaling. a) Confocal slice of shoot meristem stained with Alexa Fluor™ 488 NHS Ester (cyan) and Propidium iodide (red). Note how the signal does not chance in relation to cell size. The brighter spots are likely nucleoli. b) Quantification of the signal (left) and signal intensity (right) relative to the respective medians. Note the strong correlation between signal and volume, compared with the lack of corelation between concentration and cell size.

3.3 Nuclear volume scaling

If protein concentration is constant in the cell, it should also be constant in the nucleus, assuming that the nuclear volume scales linearly with cell. To test this hypothesis, I imaged two separate marker lines for the nuclear envelope: Nup136 (Tamura, 2017) and ACE-R11 (Liao and Weijers, 2018). Nup136 is localised at the nuclear membrane, interacts with the nuclear pore complex, and acts redundantly with Nup82 during immune signalling (Tamura, 2017). The line used here expressed a GFP tagged NUP136 under the CaMV35s promoter (Nakagawa *et al.*, 2007) (Fig. 3.3a). ACE-R11 corresponds to a GFP- tagged version of Nup54 (Tamura *et al.*, 2010), which is part of the nuclear pore complex instead (Fig. 3.3b). ACE-R11 is part of the "Arabidopsis cellular markers for embryogenesis" (ACE), a set of cellular markers driven either by WUS (ACE-W) or by pRPS5A (ACE-R), like the one used here (Liao and Weijers, 2018)**.**
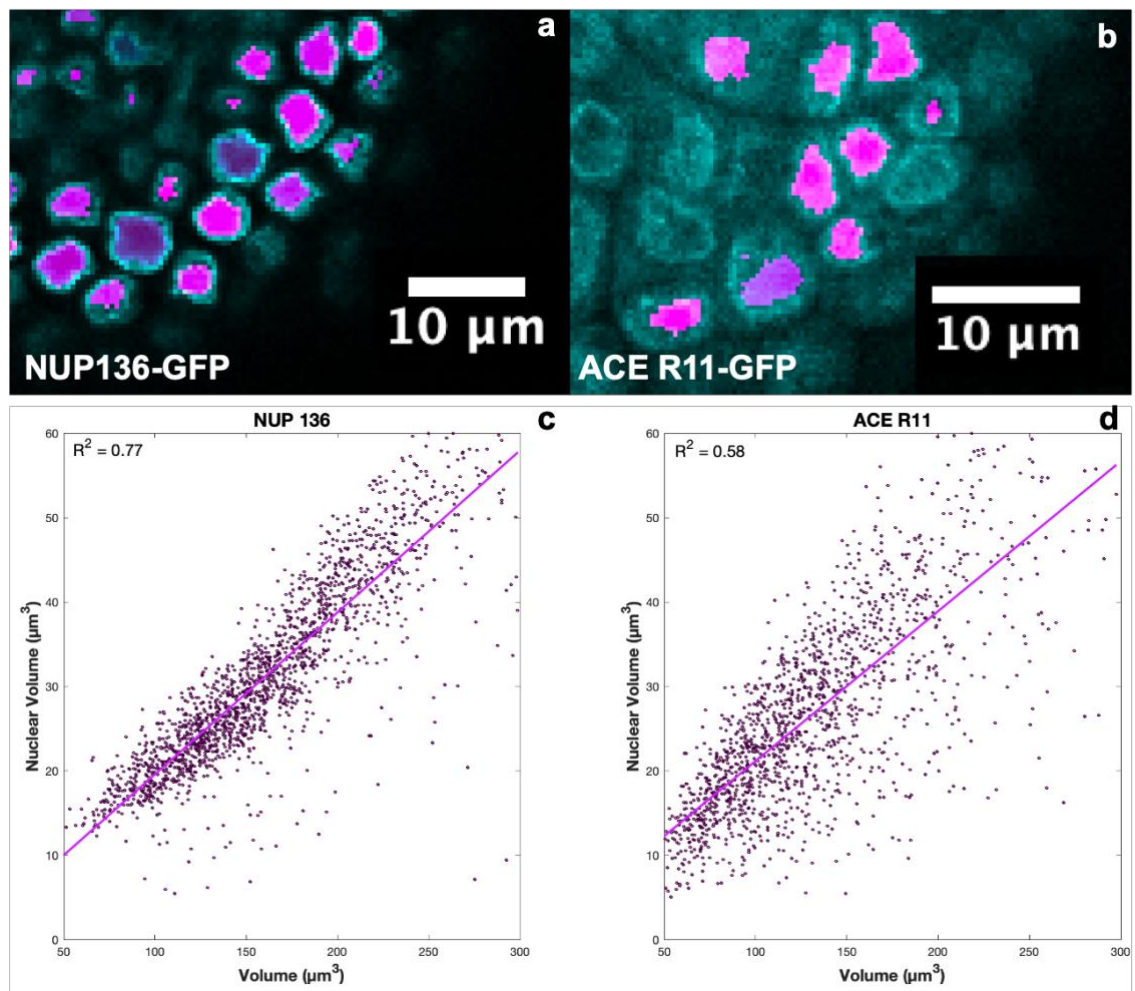
Figure 3.3: Scaling of nuclear volume with meristem cell volume. a,b) Confocal slices of a shoot meristem showing two distinct markers for the nuclear envelope (cyan) overlapped with the automated segmentation (magenta). Notice the sharper signal for NUP136, compared to ACE-R11. (c,d) Quantification of nuclear volume versus cell volume. Notice the strong correlation between these two measurements, with NUP136 having a stronger correlation possible due more precise segmentation.

As shown in Figure 3.3c and d, there was a strong correlation between cellular and nuclear volume, both in the case of Nup136 and ACE-R11. The stronger correlation given by Nup136 (R^2 = 0.77) compared to ACE R11 (R^2 = 0.58) is most likely due to the amount of segmentation errors, which are more prominent in the latter. This is due to the lower specificity of ACR R11 as a nuclear envelope marker (notice the cytoplasmatic noise in Figure 3.3b), making NUP136 the preferred choice for future experiments. This disparity could be the result of the different role played by the proteins, with ACE-R11 being part of a complex and possibly needing to be associated with other proteins to maintain its localisation. Folding defects and promoter related issues could also be the cause of ACE-R11 lower specificity. Regardless the differences in correlation, the results confirmed that the nucleus grows proportionally to the cell volume from birth to division, as previously suggested (Willis *et al.*, 2016). This information, combined with the experiment on protein amount, indicates that protein concentration within the nucleus is constant; therefore, proteins that localise in the nucleoplasm cannot carry information related to size. They can only do so if their concentration is not constant or, in other words, if their amount does not scale linearly with cellular volume and, therefore, nuclear volume.

3.4 RBR1 accumulation is not compatible with an inhibitor dilution model

Given the involvement of RBR proteins in other systems, we sought to test whether AtRBR1 could function as a size-dependent inhibitor of the G1/S transition. To do so, we imaged apical meristems expressing RBR1-GFP under its native promoter (Magyar *et al.*, 2012) and stained with FM4-64 (Fig. 3.4a). As visible in Figure 3.4a, RBR1 appeared homogeneously distributed in the nucleus but excluded from the nucleolus. The homogeneous appearance of RBR1 indicated that the protein does not associates with any specific sub-nuclear structure, although I could not exclude weak associations or associations with components with a size below the image resolution, or those overwhelmed by the concentration of the nucleosolic RBR1. To understand how RBR1 scales with cell size, I analysed the data and tested how RBR1 relative amount and concentration correlated with cell volume (Fig. 3.4b). After linear regression, both showed a correlation, with RBR1 amount being strongly correlated to volume (R^2=0.53) compared to RBR1 concentration (R^2=0.22). Surprisingly, RBR1 concentration showed a positive correlation with volume, which did not remain constant during growth, unlike the bulk of proteins. When observing the qualitative data in Figure 3.4a, it appeared that RBR1 increased in concentration in a digital manner, as if RBR1 concentration were different at different stages of the cell cycle, but the same at

same stages. Unfortunately, this cannot be quantified with the experimental set up I employed here, but requires a finer time course analysis. Regardless, these data show that RBR1 is unlikely used by meristem cells as size-dependent inhibitor, and it was discarded from the list of candidates.
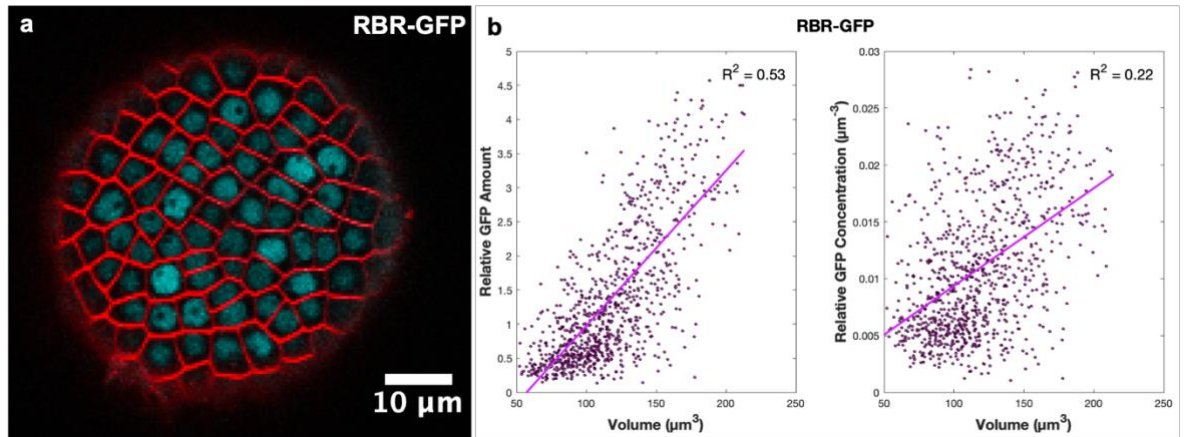
Figure 3.4: RBR1-GFP expression in the shoot meristem. a) Confocal slice of a shoot meristem expressing RBR1-GFP (cyan) under its own promoter. FM4-64 (red) was used to stain membranes. b) Quantification of RBR amount (left) and RBR concentration (right) relative to the median. Note how both quantities are positively correlated with volume, even concentration, which for most proteins would be expected to be constant.

3.5 KRP4 is inherited in proportion to DNA content

With RBR1 excluded from the list of candies for G1/S size regulation, I moved my attention to the only other known other family of inhibitors of the G1/S transition: the KRP family. Figure 3.5a shows a confocal image of pKRP4::KRP4-GFP which, unlike RBR1, appeared localised in puncta within the nucleus. A close examination revealed that KRP4 associated with chromosomes during mitosis, as shown in the panels in Figure 3.5a. Indeed, previous reports have highlighted that the KRP4 colocalises with chromatin (Bird *et al.*, 2007), suggesting that KRP4 interaction with genomic content not only occurs at division, but also during interphase. When investigating the relationship between KRP4 amount and cell volume, I found no correlation ($R^2 < 0.01$), suggesting that KRP4 amount remains unchanged during cell growth and is independent of cell volume (Fig. 3.5b). To corroborate this idea, comparing KRP4 concentration to cell volume revealed a negative correlation ($R^2 = 0.26$), indicative of a dilution of the protein as a result of cell enlargement (Fig. 3.5b). Critically, association of KRP4 with chromatin hinted to a mechanism for equal inheritance of KRP4 in sister cells, which would be in line with a role in size-sensing. To confirm this observation, Figure 3.6a shows how sister cells, indicated by the segmented line, shared

similar amount of KRP4 (panel above) – meanwhile, the concentration of KRP4 in these same cells was highly asymmetric, with smaller cells having the highest concentration of KRP4 (lower panel). To quantify this phenomenon in Figure 3.6b, signal and concentration difference against sister asymmetry are shown (see Figure 3.6 legend for detail). The lack of correlation between KRP4 amount and sister asymmetry ($R^2 < 0.01$) confirmed that KRP4 is inherited equally in sister cells. To corroborate this observation, the strong correlation found between KRP4 concentration and sister asymmetry highlighted that KRP4 is highly concentrated in the small sister of the pairs (Fig. 3.6b). However, these correlations were obtained from population data and do not necessarily represent what happens in each growing cell. Therefore, I decide to investigate the relationship with KRP4 and cell cycle progression on finer spatial and temporal scale.
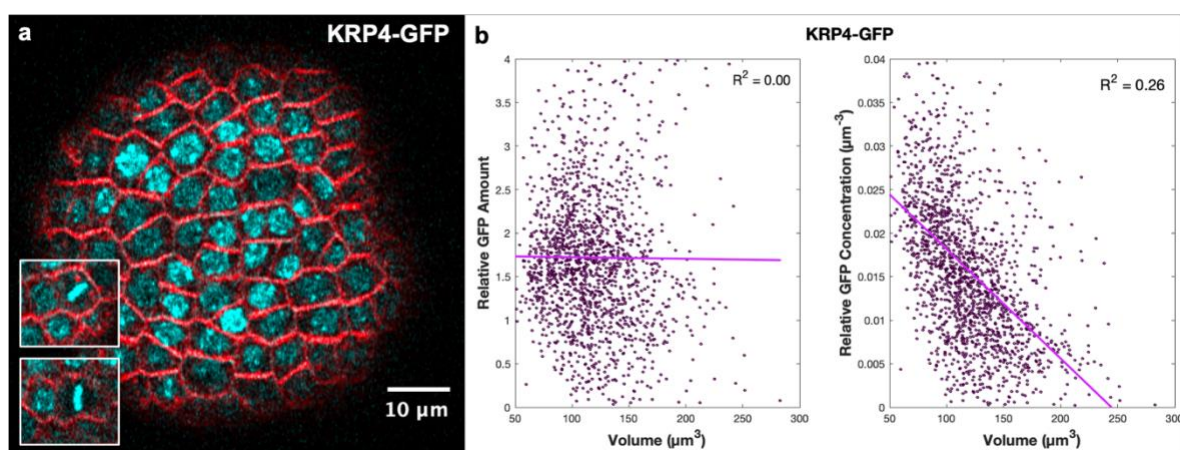
Figure 3.5: KRP4 expression in the meristem. a) Confocal slice of shoot meristem expressing KRP4-GFP (cyan) under its own promoter. FM4-64 (red) was used to stain membranes. The inner panels show KRP4 associated with metaphase chromosomes in two different cells. b) Quantification of KRP4 amount (left) and KRP4 concentration (right) relative to the median. Note how there is no correlation between KRP4 amount and volume ($R^2 < 0.01$), whilst concentration and volume are negatively correlated.

3.6 KRP4 accumulation during the cell cycle is compatible with a dilution inhibitor model

To study the behaviour of KRP4 during growth I used a F1 cross between pKRP4::KRP4-mCherry (made by Dr Katharina Schiessl, (D'Ario *et al.*, 2021)) and UB10::acyl-YFP (Willis *et al.*, 2016). I monitored the shoot apical meristem of this genotype for 36h, during which I could observe KRP4 going through clear qualitative changes (Fig. 3.7). In particular, it was noticeable how much the concentration of KRP4 decreased in 4h, and how KRP4 appeared bound to chromatin throughout the cell cycle (Fig. 3.7 top panels). In the time lapse, it was also possible to appreciate how KRP4 concentration increased again hours before division (Fig. 3.7 third panel). I had already observed KRP4 bound to chromatin during metaphase (Fig. 3.5a) and here I could observe KRP4 being segregated into the sister cells during

telophase (Fig. 3.7 last panel). Using image analysis tools, I was able to track a total of 531 cells and observed the changes in KRP4 in each individual cell.
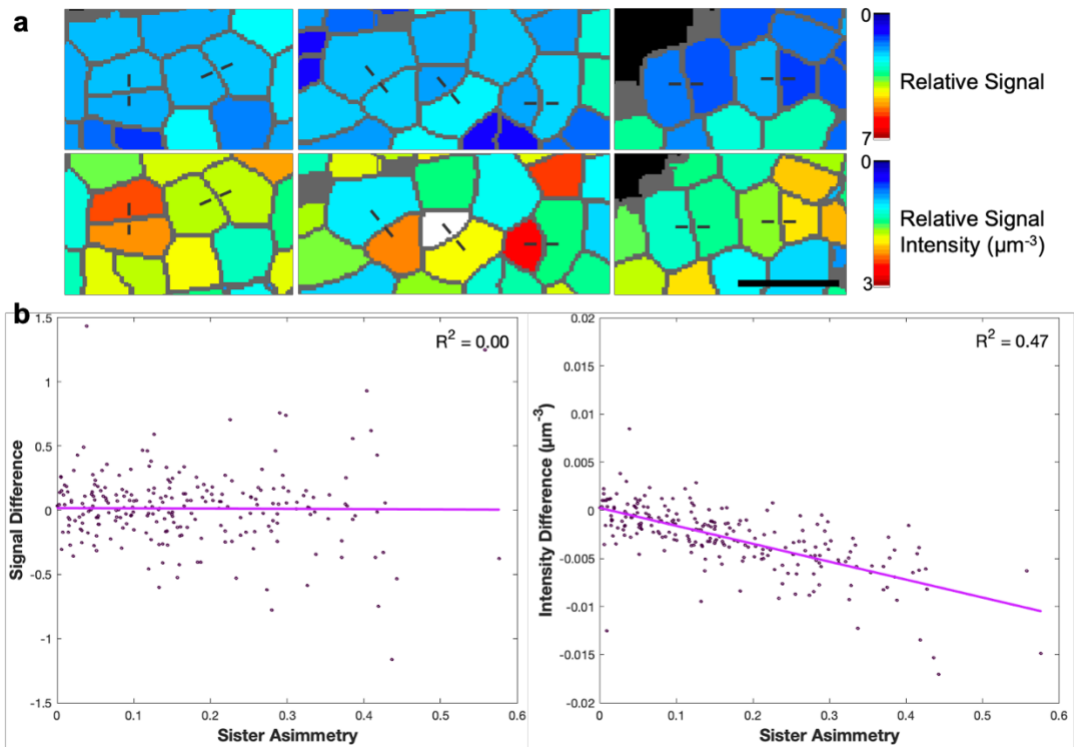
Figure 3.6: Comparison of KRP4 amount in sister cells. a) Segmented cells of shoot meristems showing the total amount of KRP4-mCherry (top) and its concentration (bottom) relative to the median in the same cells. Sister cells are indicated by a dashed blacked line. Scale bar = 10μm. Note how sister cells shared similar amounts of KRP4, whilst the same cells had a very different range of KRP4 concentration. The concentration of KRP4 in the white cell in the middle panel was even higher than the scale used (bigger that $3μm^{-3}$). b) Comparison of KRP4 signal and intensity difference among sisters (V_l-V_s), against sister asymmetry ((V_l-V_s)/(V_l+V_s)) with V_l and V_s equal to the volume of larger and small sister, respectively. In other words, the x axis represents the degree of asymmetry of sister cells, with zero representing cells identical in size – the y axis represents which siters contains more KRP4, with negative numbers representing more signal in the smaller sister and positive numbers representing more signal in the bigger sister.

The individual examples shown in Figure 3.9 highlighted some important features of KRP4. In the figure, the mother cell is represented by the dark colour and the information of each individual cell follows division. In the blue panels, notice how KRP4 amount increased sharply just before division (Fig. 3.9), feature that was also visible in the confocal images (Fig. 3.7). In these same panels, it is also evident that KRP4 amount increased again at birth, an interesting feature that will discussed more throughout this thesis. However, it is interesting to notice how the amount of KRP4 in each sister cells shows an almost identical behaviour, fluctuating to similar extent in each sister cell (Fig. 3.9, blue panels). Another important feature of KRP4 is highlighted by the green panels in Figure 3.8, which shows

that the KRP4 amount remained relatively constant for long growing periods, in cells that were supposedly in G1, based on their cell size. It is interesting to notice that KRP4 seemed to oscillate, although slightly, during this period. However, I cannot exclude that this oscillation was an artifact of technical issues, like the way that total signal is normalised in each time point, as signal relative to the median. Finally, in the red panels in Figure 3.9, some abnormal cells are shown, highlighting an unexpected behaviour for KRP4. The most obvious feature of this cells is a huge spike, representing a sudden change in KRP4 in one time point, which is restored in the following time point. It seems likely that this is an artifact, possibly due to imaging or segmentation error at 14h, since these cases seems to have occurred at that time.
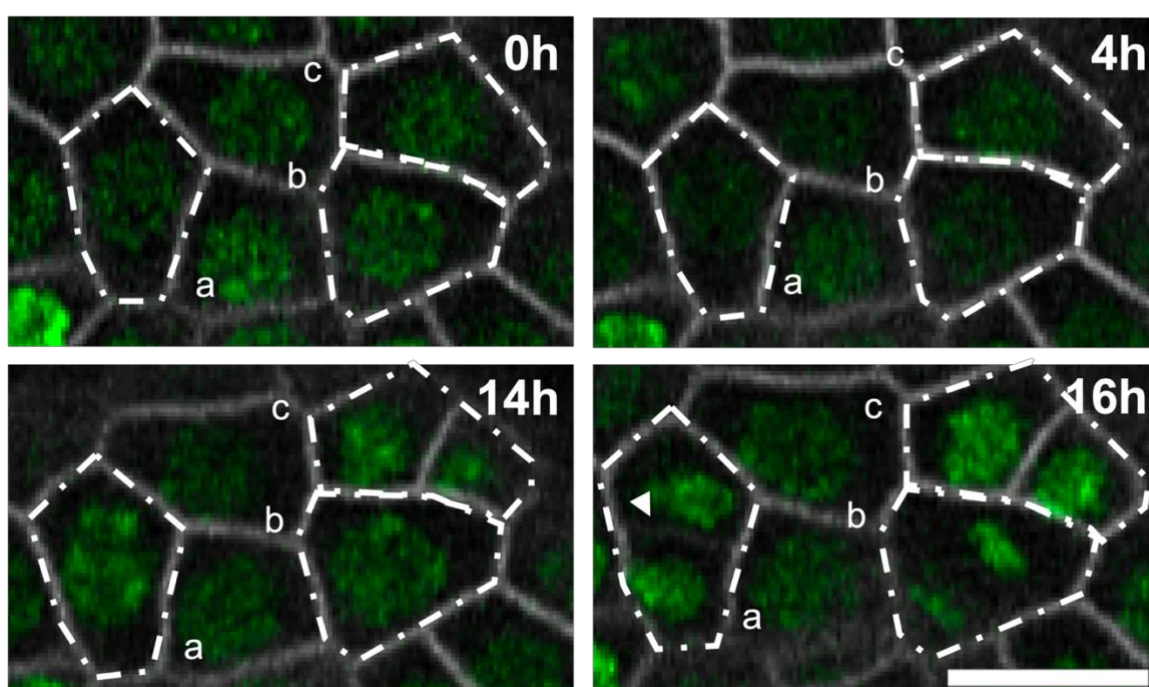
Figure 3.7: Details of representative cells in the KRP4-mCherry time course. Confocal images of cells in a shoot meristem expressing KRP4-mCherry (green) under its own promoter and acyl-YFP (grey) under the *UB10* promoter. Only 4 time points are shown here, at varying intervals. Scale bar = 10μm. Three cells, a, b and c, are highlighted with a white dash line. Note how KRP4 concentration decreased in the first 4h and increased again before division at 14h for cell c, and 16h for cells a and b. The last panel shows cell a after completing division, note the forming phragmoplast in the middle (arrowhead), and cell b undergoing telophase. Cell c undergoes division at least 2h before a and b, indicating that it reaches its size threshold earlier.

The differences in KRP4 amount observed in these cells may be mainly due to the differences in the cell cycle stage they were at. Therefore, to appreciate how KRP4 amount changes throughout the cell cycle, I aligned the time course of each cell to mitosis, so that I could average the KRP4 amount during cell cycle progression (Fig. 3.10). When plotted this way, the KRP4 amount summarises well what was seen in the individual cells, as well as complying with the behaviour expected form a molecule that acts as size dependent

inhibitor of G1/S progression – KRP4 amount increases steadily during the last 12h before division (Fig. 3.10), consistent with the expected length of G2 in meristem cells, as shown in Chapter 2 of this thesis and reported in previous studies (Jones *et al.*, 2017). This is highlighted in Figure 3.8a where the last 12h are magnified and the linear regression shows that this increase is most likely non-linear, and follows the rate of volume increase, as expected for protein production (Lin and Amir, 2018). After division, KRP4 amount increases for 6h, before settling to a constant amount. The increase in early G1 is highlighted in Figure 3.8b and it appears to be linear or sublinear, although the resolution is too low to speculate further. Note that since we align the time points at M-phase, we could not include cells that did not divide during the 24h of the experiment, like those shown in the green panel of Figure 3.9. However, we can assume that most of those cells were in G1, because we were able to image multiple cells going from G2 to M. This suggests that KRP4 amount remains constant during growth in G1, resulting in its concentration to be the highest at birth (Fig. 3.8b) ready to be diluted by growth.
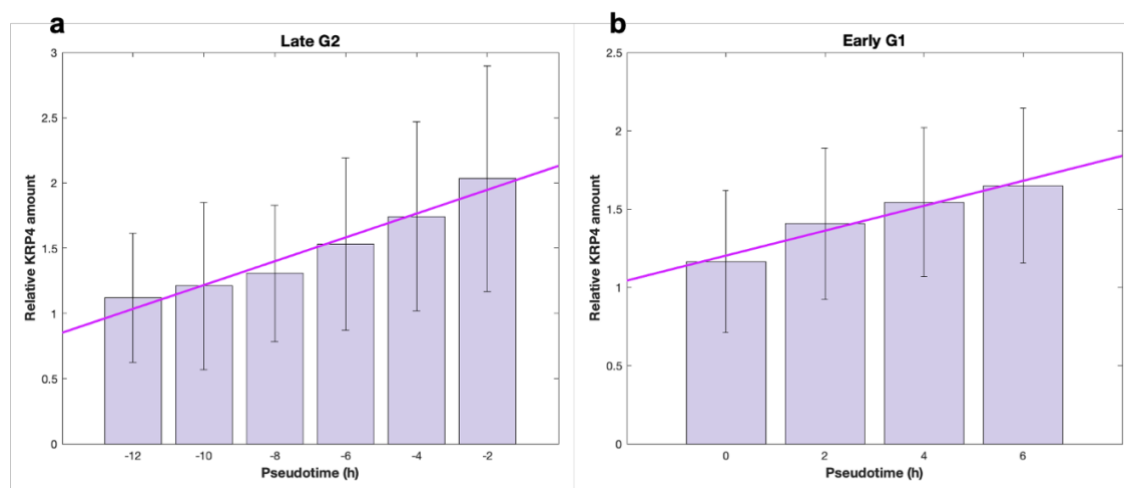
Figure 3.8: Detail of KRP4 aligned data. KRP4 amount relative to the mean of the early moments before and after division, enlarged for better readability. a) KRP4 amount 12h before division. Note how rapidly it doubles from 1 to 2. b) KRP4 amount after division. Note the unexpected production of the protein during the first 6h. Error bars represent standard deviation.

Figure 3.9, on next page: Examples of individual cells expressing KRP4. If the cell divided during the experiment, one daughter cell is coloured the same as the mother (dark purple) and the other cell is coloured pink. Total KRP4 amount is expressed as relative to the median. Blue panel: cells showing a behaviour characteristic of many other cells in the experiment. KRP4 is expressed at the end of the cell cycle and during the first 6h after division. This latter production is almost identical in sister cells. KRP4 amount stays constant after this. Green panel: cells that did not go through M or S-phase and are supposedly in G1 (see text). Note how KRP4 remains relatively constant but oscillates differently in different cells. Red panel: cells that exhibit abnormal behaviour, with abrupt changes in KRP4 amount. Only a few cells showed this behaviour and are possibly due to segmentation artifacts. Time point 7 was particularly odd for one of the samples.
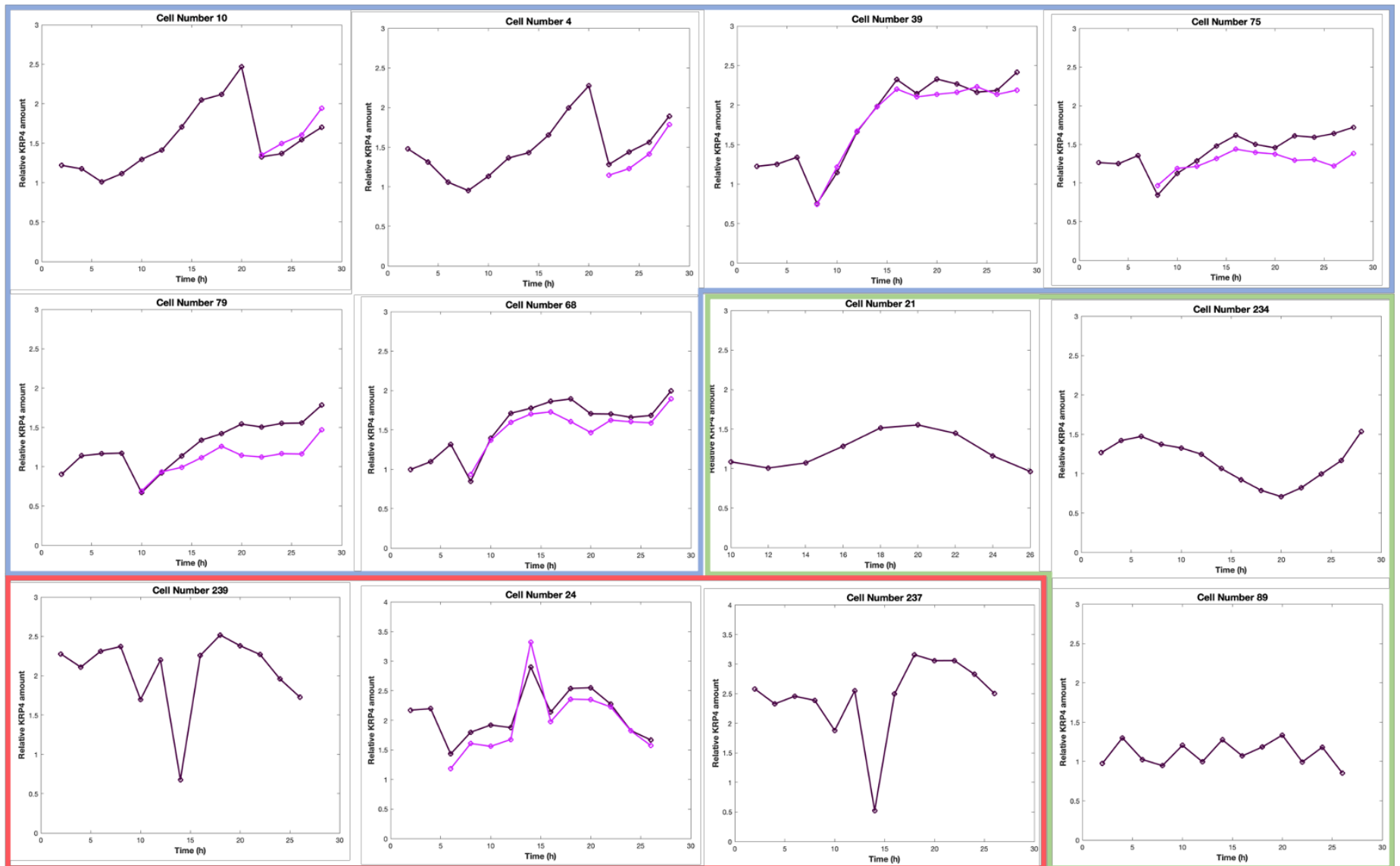
3.7 KRP4 and CDT1a concentrations change at the G1/S transition

Once KRP4 behaviour was analysed, I wanted to test whether the decreasing concentration of KPR4 correlated with entry in S-phase. To do so, I crossed the KRP4-mCherry; acyl-YFP double marker, used in the previous experiment, with a line expressing CDT1a-CFP provided by Professor Crisanto Gutierrez (CSIC, Madrid) (Desvoyes *et al.*, 2019). Robert Sablowski used plants from the F1 cross that resulted positive for each of the fluorophores and imaged them every 2h for 8h. Figure 3.11 shows examples for individual cells of the behaviour of KRP4 and CDT1a concentration during this time. Detection of S-phase transition was automated by comparing CDT1a levels (normalised to the median value in each time point) for successive time points and selecting the first pair in which the CDT1a concentration decreased by at least one unit. Overall, this strategy was accurate in detecting S-phase – in the majority of cells in Figure 3.11, CDT1a concentration remained low after decreasing, a hallmark of successful S-phase entry (Castellano *et al.*, 2004). However, a few cells showed an increase in CDT1a concentration after the initial drop (Fig. 3.11 red panels), which suggested an unsuccessful attempt made by the cell to enter S-phase. Nevertheless, KRP4 concentration appeared consistent with a size sensor for S-phase entry, as shown by its concentration decreasing as result of dilution (Fig. 3.11 blue panels), followed by an increase due to production in G2 (Fig. 3.11 green panels). Even in the cases where S-phase entry failed, KRP4 behaviour was consistent with this observation, as its concentration does not increase, symptomatic of a cell that did not enter in G2 (Fig. 3.11 red panels). To observe the general behaviour of meristem cells, the data were aligned at S-phase and averaged (Fig. 3.12). The combined data were again consistent with the dilution of inhibitor model, showing that as CDT1a concentration at G1 increased, KRP4 concentration decreased until S-phase was reached. During G2, CDT1a oscillated, possibly due to noise, and KRP4 was produced (Fig. 3.12). Finally, this experiment highlighted the exact timing of KRP4 production that we could only infer from the previous time course: KRP4 production initiates almost instantly after S-phase transition. However, it remains unclear how KRP4 can be produced during G2 to match exactly the DNA content in the cell. One possibility is that KRP4 would be produced in excess and that only the population that remains unbound from chromatin would be degraded.
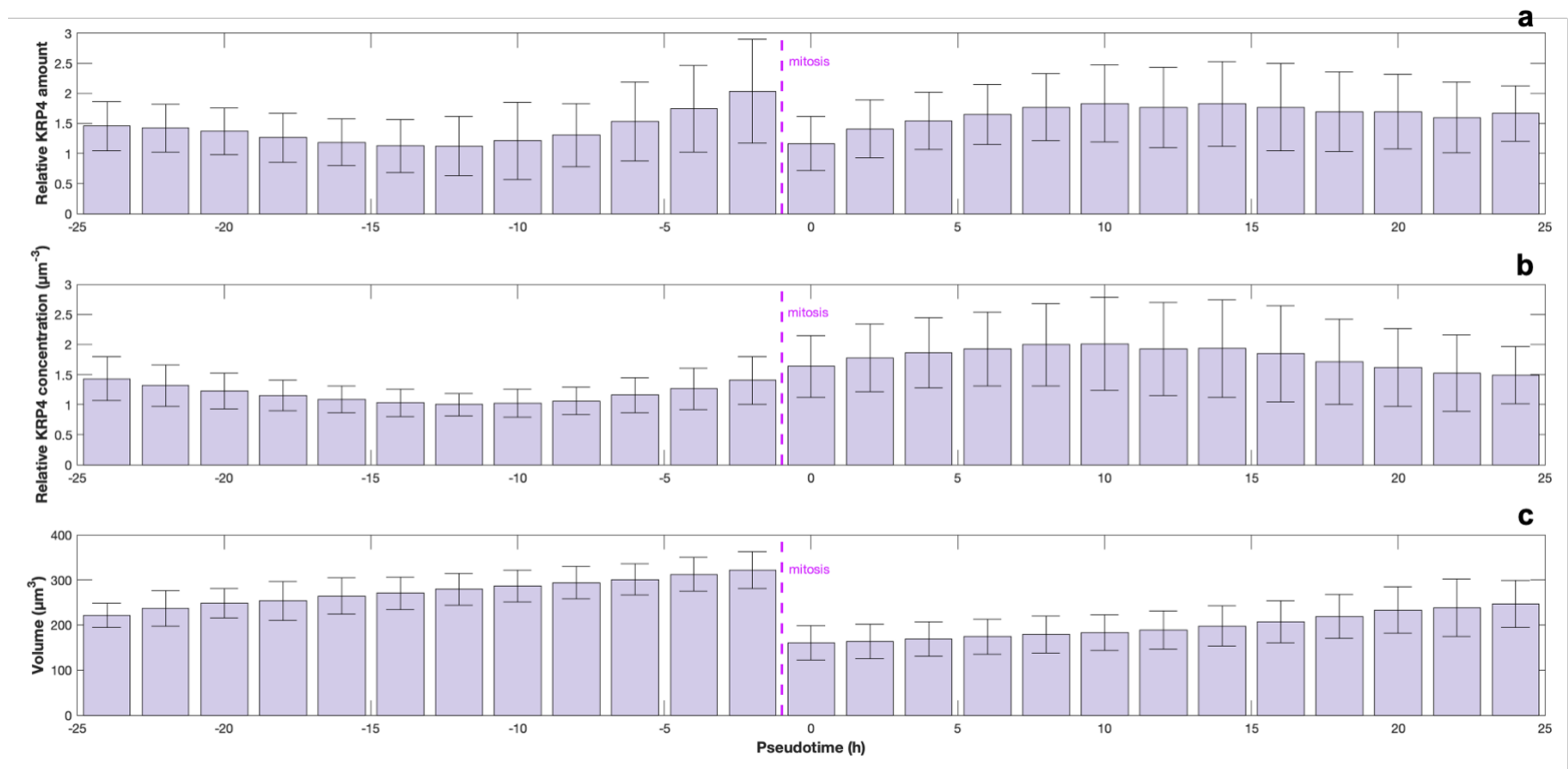
Figure 3.10: KRP4 data aligned at division. Data for individual cells aligned at birth (pseudotime = 0h) and averaged. Error bars represents stand deviation. Note that the pseudotime is aligned to match the tree quantities measured here: KRP4 amount (a) and concentration (b) relative to the mean, as well as cell volume.

3.8 Discussion

The correlations between total protein, nuclear size and cell volume, confirmed in this chapter, was expected from theoretical models of growth and previous experiments (Willis *et al.*, 2016; Lin and Amir, 2018). The implications of these results are very clear: nuclear protein concentration is expected to be constant, so nuclear cell cycle factors whose synthesis rate is expected to be proportional to cell size, as proposed for CDKa, cannot carry information on cell size. This observation contrasts with a previous model produced for cell size homeostasis, in which nuclear volume was hypothesised to remain constant, and consequently nuclear CDKa concentration and activity would increase as the cell cycle progressed (Jones *et al.*, 2017).

In this chapter, I considered two other cell cycle regulators as candidates for cell size sensing: KRP4, which regulates CDKa activity, and RBR1, which functions downstream of CDKA (Fig. 3.1). My results supported KRP4 as a plausible candidate, but not RBR1. A role of KRP4 in size sensing, but not RBR1, would still be in line with the hypothesis that CDKa activity plays a key role in cell size homeostasis (Jones *et al.*, 2017). This observation might encourage further studies in the hunt for a G2/M size sensor, which might also signal through CDKs activity.

Other than KRPs, CDKa is controlled by cyclins (CYCs) (Fig. 3.1), which take their name from their cyclic patterns of accumulation. This feature results in increased cyclin concentration near cell cycle transitions, as seen for CYCD3s specifically in the case of the S-phase transition (Menges *et al.*, 2006). Considering the results shown in Chapter 2, it appears likely that, as seen for CDT1a, the concentration of G1/S cyclins would initially increase, then drop at the transition to S-phase. Therefore, as KRP4 concentration drives G1/S transition, one would expect the CDKa/RBR cascade to activate G1/S cyclins expression in a positive feedback loop to trigger S-phase transition, as suggested by the presence of a E2F binding motif on the CYCD3;1 promoter (de Jager *et al.*, 2009). In this way, KRP4 concentration would be the major driver of cyclin expression, whose role would be to finalise the commitment to S-phase entry, instead of initiating it. This behaviour would be consistent with CYCD3;1 having a dosage-dependent effect on the G1/S transition (Menges *et al.*, 2006).
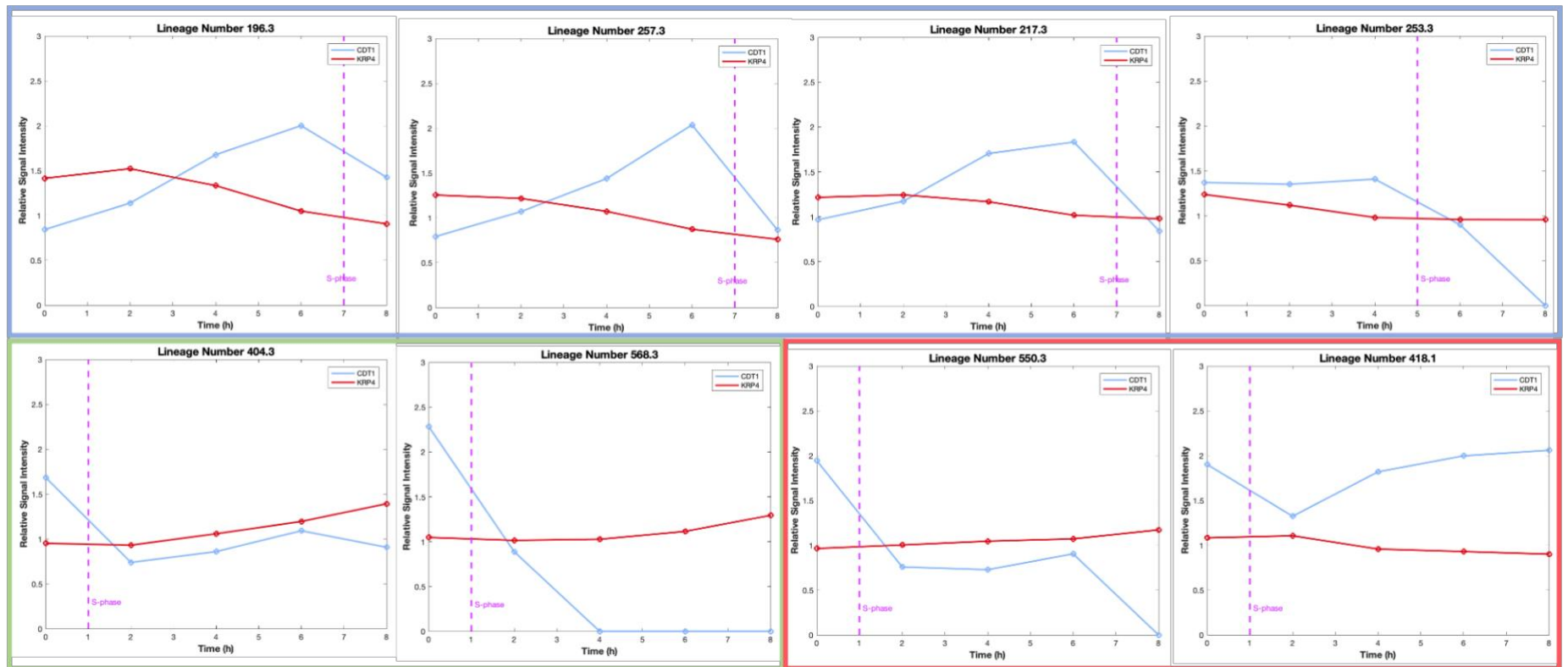
Figure 3.11: Examples of individual cells expressing KRP4 and CDT1. Data for individual cells expressing KRP4-mCherry (red) and CDT1-CFP (cyan) both expressed as signal relative to the median. The time of S-phase transition was calculated based on decreasing CDT1 level and it is indicated by the pink dashed line. Blue panel: these cells show a common behaviour and enter in S-phase towards the end of the experiment. Note how CDT1 concentration increased whilst KRP4 concentration decreased. Green panel: these cells entered in S-phase at an early time during the experiment and showed a lower level of CDT1. Notice how KRP4 concentration increased almost immediately after S-phase transition. Red panel: few cells showed an odd behaviour of CDT1, which increased after the calculated S-phase transition. In these cases however, KRP4 did not increase, indicating that the cell had not transitioned to G2.

The data presented here show that KRP4 is very unlike other proteins in term of its expression during the cell cycle. At a population level, there is no correlation with KRP4 and cell size, indicating that these two are uncoupled. This characteristic, fundamental for size sensing, relates to how KRP4 oscillates during the cell cycle. For the majority of G1, until S-phase is reached, KRP4 amount remains constant, or fluctuates around a specific amount. When KRP4 concentration reaches a certain toehold, S-phase is triggered, evident by the opposing behaviour of KRP4 and CDT1. KRP4 amount is set at birth, directly or indirectly, and is identical in sister cells. This is possible thanks to the ability of KRP4 to bind chromatin, particularly at division during chromosome segregation. This allows sister cell to inherit equal amount of KRP4, in proportion to the genetic content. This might explain the long-known correlation between ploidy and cell size (Jovtchev *et al.*, 2006), and also clarifies how endoreduplication in cells of determined organs, like leaves or sepals, leads to increase in cell size without any additional apparent mechanisms .
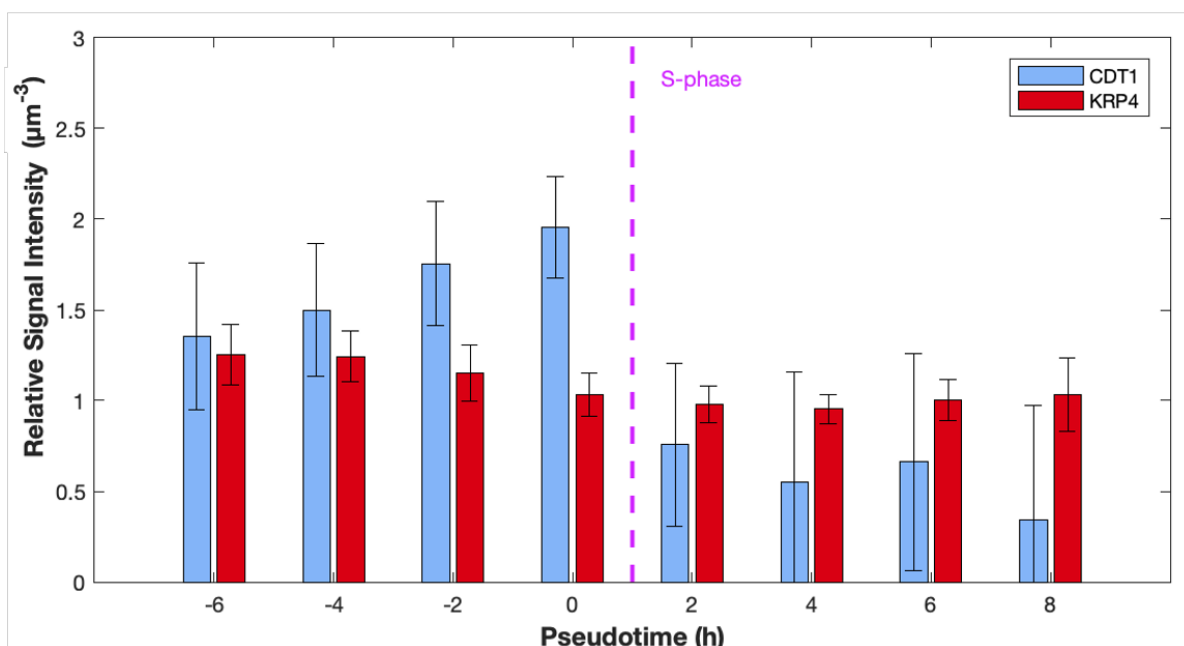
Figure 3.12: KRP4 and CDT1 data aligned at S-phase. Data for individual cells aligned at S-phase (pseudotime = 0h) and averaged. Error bars represents stand deviation. S-phase transition was inferred as CDT1 drops. Note how KRP4 concentration decreases during G1 and increases again at G2. The high variability of CDT1 at G2 is likely due to artefacts created by misassigned cells (see red panels in Figure 3.11).

Nevertheless, KRP4 is still produced in the first 6h of G1, in a way that seem to be identical in each sister. In Chapter 5 I will go into this feature in much more detail, when I will combine this data with a mathematical discussion to speculate on the mechanism and impact of this phenomenon. In later G1, KRP4 levels remained constant, then its production seemed to re-start as the cells exited S-phase (Fig. 3.11 and 3.12). This production in G2

would be essential to allow KRP4 amount to double before being distributed in the daughter cells. However, models for protein production suggest that total protein scales to reach a maximum concentration (Lin and Amir, 2018), as also suggested by the experiment presented here (Fig. 3.1). Therefore, a mechanism must be in place to allow KRP4 to be produced to match chromatin content rather than a set concentration. A solution to this conundrum was suggested for Whi5, where it was proposed that the protein is produced for a fixed amount of time at G2 (Schmoller *et al.*, 2015). In this case, the maximum possible concentration of Whi5 is far from the one used by the cell, so a fixed production time results in a production of a determined amount, regardless of volume. However, this mechanism is not self-contained and any oscillations in the length of G2 or in Whi5 amount at S-phase would accumulate and eventually destabilise size homeostasis. To add to this controversy, a recent study showed that disruption in Whi5 expression causes cell size average to change, but homeostasis is preserved (Barber, Amir and Murray, 2020), re-opening the question of size regulation in budding yeast.

If Whi5 will be confirmed as size sensor, a robust system to ensure correct Whi5 amount before division will need to be unveiled. A possible mechanism for accurate production could be to produce the inhibitor protein in a larger amount than needed, and to remove the excess to match the requirement. In the case of KRP4, a physical means of achieving this is hinted by its close association with chromatin – by removing excess nucleosolic free KRP4, the chromatin bound portion would be the only one left and would be the same amount every time. I will explore this possibility in the next chapter, where a protein that targets KRP4 for degradation will be introduced.

3.9 Reference

Barber, F., Amir, A. and Murray, A. W. (2020) 'Cell-size regulation in budding yeast does not depend on linear accumulation of Whi5', *Proceedings of the National Academy of Sciences*, 117(25), p. 14243 LP-14250. doi: 10.1073/pnas.2001255117.

Bird, D. A. *et al.* (2007) 'Arabidopsis cyclin-dependent kinase inhibitors are nuclear-localized and show different localization patterns within the nucleoplasm', *Plant Cell Reports*, 26(7), pp. 861–872. doi: 10.1007/s00299-006-0294-3.

Borghi, L. *et al.* (2010) '*Arabidopsis* RETINOBLASTOMA-RELATED Is Required for Stem Cell Maintenance, Cell Differentiation, and Lateral Organ Production', *The Plant Cell*, 22(6), pp. 1792–1811. doi: 10.1105/tpc.110.074591.

Castellano, M. del M. *et al.* (2004) 'DNA Replication Licensing Affects Cell Proliferation or Endoreplication in a Cell Type–Specific Manner', *The Plant Cell*, 16(9), pp. 2380–2393. doi: 10.1105/tpc.104.022400.

D'Ario, M. *et al.* (2021) 'Cell size controlled in plants using DNA content as an internal scale', *Science*, 372(6547), p. 1176 LP-1181. doi: 10.1126/science.abb4348.

Desvoyes, B. *et al.* (2019) 'FBL17 targets CDT1a for degradation in early S-phase to prevent Arabidopsis genome instability', *bioRxiv*, p. 774109. doi: 10.1101/774109.

Desvoyes, B. and Gutierrez, C. (2020) 'Roles of plant retinoblastoma protein: cell cycle and beyond', *The EMBO Journal*. John Wiley & Sons, Ltd, 39(19), p. e105802. doi: https://doi.org/10.15252/embj.2020105802.

Ebel, C., Mariconti, L. and Gruissem, W. (2004) 'Plant retinoblastoma homologues control nuclear proliferation in the female gametophyte', *Nature*, 429(6993), pp. 776–780. doi: 10.1038/nature02637.

de Jager, S. M. *et al.* (2009) 'Dissecting regulatory pathways of G1/S control in Arabidopsis: common and distinct targets of CYCD3;1, E2Fa and E2Fc.', *Plant molecular biology*. Netherlands, 71(4–5), pp. 345–365. doi: 10.1007/s11103-009-9527-5.

Jones, A. R. *et al.* (2017) 'Cell-size dependent progression of the cell cycle creates homeostasis and flexibility of plant cell size', *Nature Communications*. Nature Publishing Group, 8, p. 15060. doi: 10.1038/ncomms15060.

Jovtchev, G. *et al.* (2006) 'Nuclear DNA content and nuclear and cell volume are positively correlated in angiosperms', *Cytogenetic and Genome Research*, 114(1), pp. 77–82. doi: 10.1159/000091932.

Kendall, C. G. *et al.* (2015) 'Amine Analysis Using AlexaFluor 488 Succinimidyl Ester and Capillary Electrophoresis with Laser-Induced Fluorescence', *Journal of Analytical Methods*

in Chemistry. Edited by C.-C. Huang. Hindawi Publishing Corporation, 2015, p. 368362. doi: 10.1155/2015/368362.

Kianianmomeni, A., Nematollahi, G. and Hallmann, A. (2008) 'A gender-specific retinoblastoma-related protein in Volvox carteri implies a role for the retinoblastoma protein family in sexual development', *The Plant cell*. 2008/09/12. American Society of Plant Biologists, 20(9), pp. 2399–2419. doi: 10.1105/tpc.107.057836.

Li, Y. *et al.* (2016) 'A new class of cyclin dependent kinase in Chlamydomonas is required for coupling cell size to cell division', *eLife*. eLife Sciences Publications, Ltd, 5, pp. e10767–e10767. doi: 10.7554/eLife.10767.

Liao, C. and Weijers, D. (2018) 'A toolkit for studying cellular reorganization during early embryogenesis in Arabidopsis thaliana', *The Plant Journal*, pp. 1–14. doi: 10.1111/tpj.13841.

Lin, J. and Amir, A. (2018) 'Homeostasis of protein and mRNA concentrations in growing cells', *Nature Communications*, 9(1), p. 4496. doi: 10.1038/s41467-018-06714-z.

Magyar, Z. *et al.* (2012) 'Arabidopsis E2FA stimulates proliferation and endocycle separately through RBR-bound and RBR-free complexes', *The EMBO Journal*, 31(6), pp. 1480–1493. doi: 10.1038/emboj.2012.13.

Menges, M. *et al.* (2006) 'The D-Type Cyclin CYCD3;1 Is Limiting for the G1-to-S-Phase Transition in Arabidopsis', *the Plant Cell Online*, 18(4), pp. 893–906. doi: 10.1105/tpc.105.039636.

Nakagawa, T. *et al.* (2007) 'Development of series of gateway binary vectors, pGWBs, for realizing efficient construction of fusion genes for plant transformation', *Journal of Bioscience and Bioengineering*, 104(1), pp. 34–41. doi: https://doi.org/10.1263/jbb.104.34.

Neumann, F. R. and Nurse, P. (2007) 'Nuclear size control in fission yeast', *The Journal of cell biology*. 2007/11/12. The Rockefeller University Press, 179(4), pp. 593–600. doi: 10.1083/jcb.200708054.

Schiessl, K. *et al.* (2012) 'JAGGED controls growth anisotropy and coordination between cell size and cell cycle during plant organogenesis', *Current Biology*. Elsevier Ltd, 22(19), pp. 1739–1746. doi: 10.1016/j.cub.2012.07.020.

Schiessl, K., Muino, J. M. and Sablowski, R. (2014) 'Arabidopsis JAGGED links floral organ patterning to tissue growth by repressing Kip-related cell cycle inhibitors', *Proceedings of the National Academy of Sciences*, 111(7), pp. 2830–2835. doi: 10.1073/pnas.1320457111.

Schmoller, K. M. *et al.* (2015) 'Dilution of the cell cycle inhibitor Whi5 controls budding-yeast cell size', *Nature*, 526(7572), pp. 268–272. doi: 10.1038/nature14908.

Tamura, K. *et al.* (2010) 'Identification and Characterization of Nuclear Pore Complex Components in Arabidopsis thaliana   ', *The Plant Cell*, 22(12), pp. 4084–4097. doi: 10.1105/tpc.110.079947.

Tamura, K. (2017) 'Nup82 functions redundantly with Nup136 in a salicylic acid-dependent defense response of Arabidopsis thaliana', *Nucleus*. Taylor & Francis, 8(3), pp. 301–311. doi: 10.1080/19491034.2017.1279774.

Umen, J. G. and Goodenough, U. W. (2001) 'Control of cell division by a retinoblastoma protein homolog in Chlamydomonas', *Genes and Development*, 15(13), pp. 1652–1661. doi: 10.1101/gad.892101.

Verkest, A. *et al.* (2005) 'Switching the cell cycle. Kip-related proteins in plant cell cycle control', *Plant physiology*. American Society of Plant Biologists, 139(3), pp. 1099–1106. doi: 10.1104/pp.105.069906.

Webster, M., Witkin, K. L. and Cohen-Fix, O. (2009) 'Sizing up the nucleus: nuclear shape, size and nuclear-envelope assembly', *Journal of cell science*. Company of Biologists, 122(Pt 10), pp. 1477–1486. doi: 10.1242/jcs.037333.

Willis, L. *et al.* (2016) 'Cell size and growth regulation in the *Arabidopsis thaliana* apical stem cell niche', *Proceedings of the National Academy of Sciences*, 113(51), pp. E8238–E8246. doi: 10.1073/pnas.1616768113.

Wilson, E. B. (1925) 'The karyoplasmic ratio', *The cell in development and heredity*. The Macmillan Company New York, pp. 727–733.

Yang, W.-C., Shi, D.-Q. and Chen, Y.-H. (2010) 'Female Gametophyte Development in Flowering Plants', *Annual Review of Plant Biology*. Annual Reviews, 61(1), pp. 89–108. doi: 10.1146/annurev-arplant-042809-112203.

Yang, W., Wightman, R. and Meyerowitz, E. M. (2017) 'Cell Cycle Control by Nuclear Sequestration of CDC20 and CDH1 mRNA in Plant Stem Cells', *Molecular Cell*. Elsevier Inc., 68(6), p. 1108–1119.e3. doi: 10.1016/j.molcel.2017.11.008.

Zatulovskiy, E. *et al.* (2020) 'Cell growth dilutes the cell cycle inhibitor Rb to trigger cell division', *Science*, 471(July), pp. 466–471.

Chapter 4: Ensuring scaling of KRP with DNA

4.1 Introduction

In the previous chapter, I showed that KRP4 is inherited equally in sister cells, and that its amount remained constant during the majority of G1. The mechanism that allows KRP4 to be equally inherited in sister cells involves binding of KRP4 to chromatin, which is used as a means for equal partitioning. However, for this mechanism to work, the amount of KRP4 at the end of G2 needs to be proportional to DNA content, otherwise inheritance would not be equal. This is not an easy feat, because proteins tend to accumulate in the cell to a constant concentration, and consequently to an amount that varies with cell volume (Lin and Amir, 2018). A simple way to overcome this constraint would be to produce KRP4 in excess and remove the fraction which is not bound to chromatin. This would leave the mother cell with KRP4-saturated DNA, ready to be equally partitioned into the daughter cells.

The idea of protein turnover being a major component for KRP4 regulation is supported by multiple studies that have shown how degradation of KRPs is a major control point for this family (Kim *et al.*, 2008; Liu *et al.*, 2008; Ren *et al.*, 2008; Li *et al.*, 2020). A common feature of KRP degradation is the involvement of E3 ligases (Kim *et al.*, 2008; Liu *et al.*, 2008; Ren *et al.*, 2008; Li *et al.*, 2020), ubiquitinating proteins that target specific proteins for degradation (Chen and Hellmann, 2013). Among the known E3 ligases, FBL17 has been shown to play a critical role in the degradation of KPRs during pollen development (Kim *et al.*, 2008), and has also been shown to interact with multiple members of the KRP family, albeit with different affinities (Zhao *et al.*, 2012). In addition, FBL17 is required for degradation of CDT1, which is required for the G1/S transition as an essential component of the mechanism that licenses chromatin for replication (Desvoyes *et al.*, 2019). The role in CDT1a degradation suggests a role for FBL17 as a regulator of cell cycle proteins after DNA synthesis.

FBL17 characteristics make it a good candidate to ensure KRP4 scaling with DNA, leading to the following hypothesis: once a KPR4 concentration threshold has been reached at the end of G1 and S-phase is triggered, FBL17 is expressed. FBL17 is required to be present exclusively in G2 to ensure that it does not interfere with KRP4 dilution during G1. This behaviour would be consisted with the role of FBL17 in CDT1 degradation (Desvoyes *et al.*,

2019). In G2, FBL17 would target KRP4 for degradation, specifically interacting with a portion of KRP4 that is not bound to chromatin. This means that, if FBL17 levels are compromised and its expression is reduced, KRP4 would accumulate during G2, specifically in the nucleoplasm, whilst the KRP4 amount on chromatin would remain the same.

If the cellular behaviour described above were confirmed, it would be interesting to understand the biochemical basis of the interaction between KRP4 and FBL17 and try to unveil a mechanism that allows KRP4 to be immune to FBL17 when bound on chromatin. The aim of this chapter is to test these predictions on FBL17 behaviour and to test its interaction with KRP4. Additionally, an argument will be made on KRP4 evolution regarding homology of domains that might be important for regulation by FBL17.
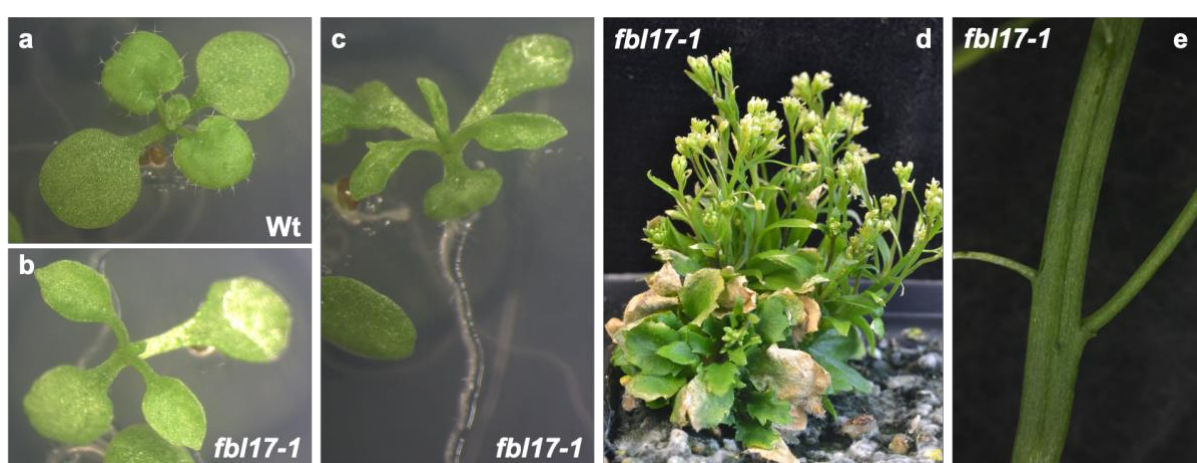
Figure 4.1: *fbl17-1* mutant phenotype. a) 3 weeks old wild type (Wt) Col-0 for comparison. b-e) Mutant in *fbl17* at various stages of development. b) 2 weeks old. c) 3 weeks old. d) 2 months old. e) Stem detail, showing splitting phenotype.

4.2 Gross phenotype of the *fbl17* mutant

Before moving to test the hypothesis of FBL17 interaction with KRP4 to control size regulation, I will describe the gross morphological phenotype of the *fbl17* mutants. This will highlight the pleiotropic effects of the mutation and the critical role of FBL17 in multiple processes, as well as bringing up the difficulties associated with designing experiments using this mutant.

Given the requirement of FBL17 in sperm development, it was originally reported that *fbl17* homozygous mutants could not be recovered from the available knock out lines (Gusti *et al.*, 2009). However, successive studies reported that these mutants can be recovered at rate of ~1% (Noir *et al.*, 2015). When trying to recover *fbl17 -/-* mutants (see material and methods) I found that roughly 1 every 300 seedlings could be identified from 2-3 weeks old

plates (Fig. 4.1b and c) and of these only ~1/8 would survive to adulthood (Fig. 4.1d). Effectively, only 1 meristem could be recovered and analysed from every 2400 planted seeds (0.04%).

After 2 weeks of growth, *fbl17* mutants looked distinctively different from their *fbl17/FBL17* and *FBL17* siblings (Fig. 4.1). The cotyledons did not show any striking phenotype, but the first leaves were less round and showed a less textured surface, a feature partially related to the inconspicuous mid vein. Additionally, the smooth surface of the leaf was related to a much reduced number of trichomes (Fig. 4.1b-c), which appeared unbranched when present (Noir *et al.*, 2015). Interestingly, the mature leaf shape (Fig. 4.1d) resembled that of plants overexpressing KRP2 (Noir *et al.*, 2015), corroborating the role of FBL17 in counteracting the accumulation of KRPs. Perhaps the most interesting phenotype of *fbl17* could be observed in mature plants, which had a very "bushy" appearance (Fig. 4.1d) due to the way their stems split (Fig. 4.1e), forming multiple branches.
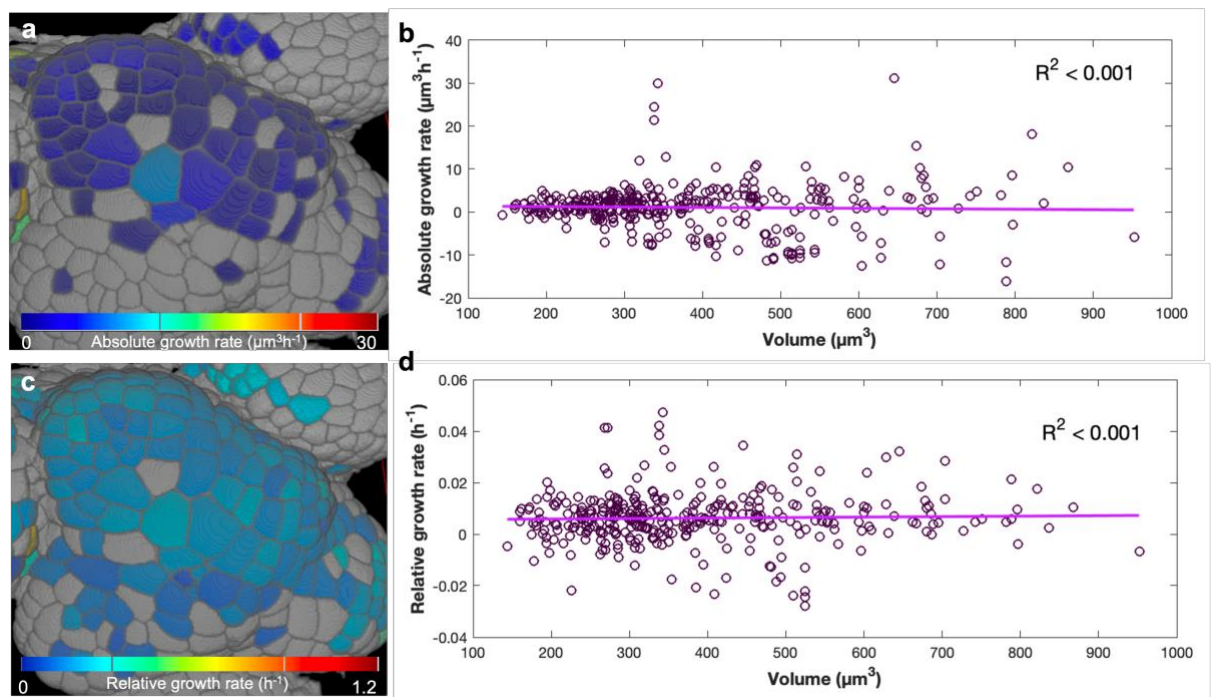
Figure 4.2: Cell growth in the *fbl17-1* mutant. a and c) 3D reconstruction of the same *fbl17* apical meristem coloured for absolute growth rate in a) (measured as $(V_{t1}-V_{t0})/(t1-t0)$) and relative growth rate in b) (expressed as $\ln(V_{t1}/V_{t0})/(t1-t0)$). V_{t1} and V_{t0} represents volumes at time t=24h and t=0h respectively. b and d) Scatter plots of growth versus cell volume. Note that there is no correlation between cell volume and growth and that the cells in the first layer grows very slowly. This experiment was only conducted on one meristem.

In order to connect the branching phenotype of the *fbl17* mutant with meristem development, meristems of *fbl17* mutants were imaged twice at 24h interval using confocal microscopy (Fig. 4.2a and c). When observed through confocal microscopy, cells in *fbl17* mutant meristems were of different sizes and showed clusters of giant cells. This was the first reported example of a mutant suggesting loss of size homeostasis, a phenotype that will be analysed in more detail in the next chapter. Here, I focus on the question whether the split stem showed by the mature *fbl17* (Fig. 4.1e) could be the result of defects in meristem structure and function. One hypothesis was that inequality of cell size could be associated with inequality of cellular growth, which could deform the meristem to the point of fasciation. To test this, the time course images were analysed to measure the absolute and relative growth rates of individual cells (Fig. 4.2 a-b and c-d, respectively). There was no correlation between cell size and growth rate ($R^2 < 0.001$ for either growth rates) suggesting that meristem splitting in the *fbl17* was not caused by heterogenous growth rates. A caveat with this experiment however, is that I could only analyse one meristem, due to the low recoverability of the mutants.

The lack of correlation between cell size and growth rate was also found in the meristems analysed in Chapter 2, suggesting that changes in cell size in the meristem do not contribute significantly to growth. However, the cell growth of the *fbl17* mutant was much reduced, averaging to 6.2×10^{-3} h^{-1}, almost a third of the expected growth rate of a meristem cell (17×10^{-3} h^{-1} as reported in (Serrano-Mislata, Schiessl and Sablowski, 2015; Jones *et al.*, 2017)), suggesting that either these cells might have not have grown properly in this experiment or that *fbl17* cells struggled growing in the conditions required for imaging. Nevertheless, in some cases cell division was observed, even for the largest cells (Fig. 4.3), suggesting that development was not arrested and that cells were progressing normally through the cell cycle. In the next chapter I will focus on the cells size phenotype of *fbl17* mutants with a more quantitative approach, using mathematical modelling. However, to inform development of the model, the role of FBL17 in the meristem and its relation to KRP4 needed to be investigated further.

4.3 FBL17 expression pattern in the SAM

Based on the assumptions of the model developed so far, FBL17 would need to be expressed only during G2 or KRP4 could be destabilised in G1, when it is expected to measure size. To test this hypothesis, shoot apexes expressing FBL17-GFP (Noir *et al.*, 2015)
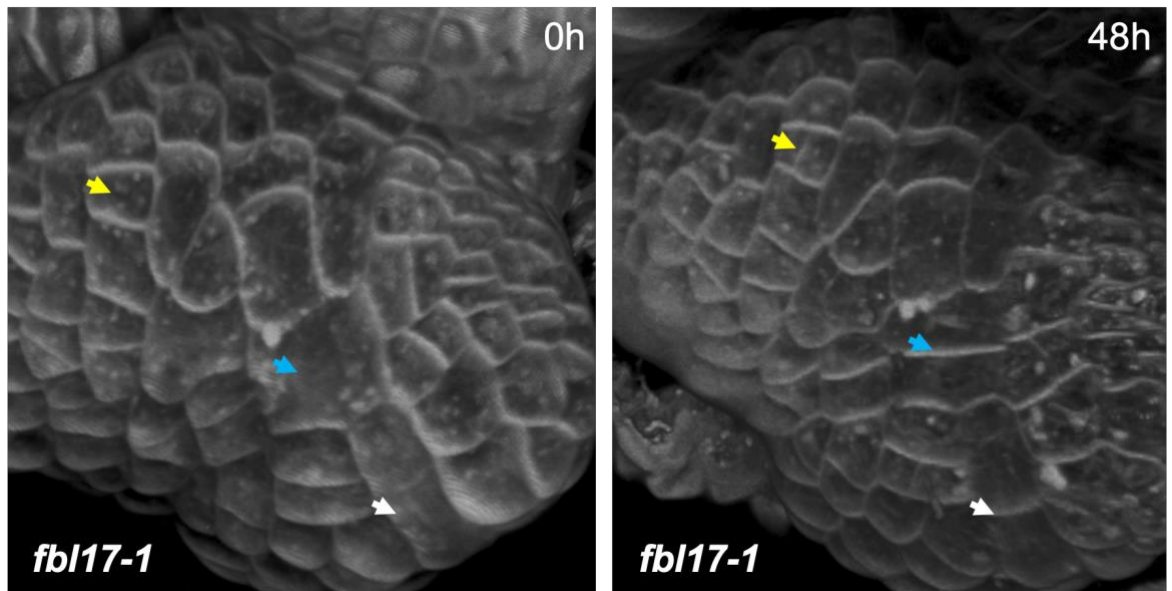
Figure 4.3: Cells in *fbl17-1* mutant are able to divide. 3D confocal reconstruction of the same meristem 48h apart, showing cells (arrows) in the *fbl17* mutant dividing at different sizes.

were imaged using FM4-64 for membrane staining (Fig. 4.4a). The confocal slice in Figure 4.4a shows that FBL17 is only expressed in cells larger than approximately 150µm (Fig. 4.4c), the size at which cells exit the G1 phase, as shown by our previous experiments. This suggested that FBL17 expression in the meristem occurs at G2, as previously reported in roots (Desvoyes *et al.*, 2019). This hypothesis was also corroborated by comparing cell size in relation to expression of FBL17-GFP and of CDT1-CFP (Fig. 4.4b), the latter from a previous experiment was overlapped to this data and show that the cells in which FBL17 is expressed are complementary to CDT1 expression (Fig. 4.4d).

4.4 Testing the effect of loss of FBL17 function on KRP4 levels

The first step in testing the functional relationship between KRP4 and FBL17 was to show that in the *fbl17* mutant the known correlation between cell size and DNA content was lost. This might be apparent from the aberrant cell sizes shown in Figure 4.2a, but given the role of FBL17 in regulating the DNA damage response (Gentric *et al.*, 2020) and avoid supernumerary rounds of DNA duplication (Desvoyes *et al.*, 2019), I could not exclude that the abnormal cell sizes were related to abnormalities in DNA content. To investigate this, apexes were stained for membranes, using the fixable stain FM4-64 FX, and DNA, using DAPI (see material and methods) (Fig. 4.5). As expected, wild type apexes showed a bimodal relationship between DAPI signal, which should be stoichiometric to DNA, and nuclear size (Fig. 4.5b), which is proportional to cell volume (Willis *et al.*, 2016; D'Ario *et al.*, 2021). DNA concentration decreased in proportion to cell size, until the nuclear volume

reached ~50μm³, when the concentration of DNA approximately doubled (Fig. 4.5b), presumably as result of entering S-phase, consistent with ~150μm³ of cell volume during this transition. This behaviour was reflected in the DNA amount, which was bimodally distributed between, presumably, G1 and G2 cells (Fig. 4.5b). In contrast, these relationships were blurred or lost in the *fbl17* mutants (Fig. 4.5b, lower panels), corroborating the idea that FBL17 is required to link DNA content to cell size via KRP4. Additionally, this experiment confirmed that the cells of *fbl17* mutants were not bigger due to an increase in DNA content, as shown by the giant cells in the confocal image, which had a highly diluted DAPI signal (Fig. 4.5c-d). Finally, it was interesting to notice mitotic figures in some of the large cells of the mutant (Fig. 4.5d), indicating that these cells were still able to divide. As shown in Figure 4.3, cells in the *fbl17* mutants apex were able to divide at a range of volumes, indicating that not only S-phase entry, but also commitment to division was uncoupled from cell size and DNA concentration.
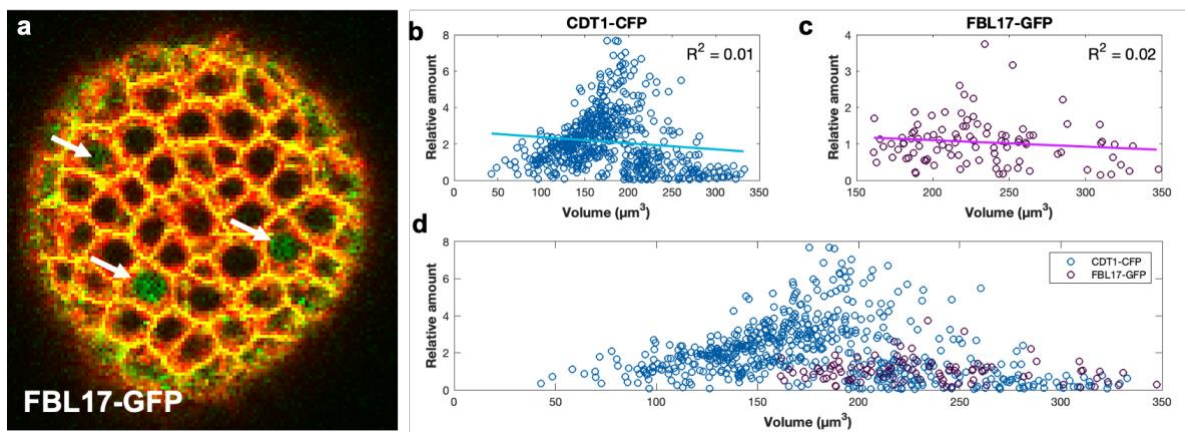
Figure 4.4: FBL17 expression is specific to cells in G2. a) Confocal slice of a meristem expressing FBL17-GFP. Arrows show cells with the GFP signal. b) Scatter plot showing CDT1 amount against volume. c) Scatter plot showing FBL17 amount versus volume. Note that neither CDT1 nor FBL17 show a correlation with volume, due to their cell cycle dependent expression. d) Combined data for CDT1 and FBL17, showing complementary expression. This suggests that FBL17 expression occurs after S-phase transition.

4.4.1 KRP4-GFP in *fbl17* background

Once the effect of the *fbl17* mutation on the correlation between size and DNA content was established, I was eager to study the relationship between FBL17 and KRP4. To do so, the heterozygous *fbl17/FBL17* was crossed to a line expressing KRP4-GFP (Schiessl, Muino and Sablowski, 2014), using *fbl17/FBL17* as the female parent, because of very low transmission of *fbl17* through the male gametophyte (Gusti *et al.*, 2009). The segregating F1 generation was selected on sulfadiazine, the antibiotic marker of the *fbl17* mutation, and the subsequent population was screened for *fbl17* homozygous plants, as described in

material and methods. Multiple attempts were performed, some of which yielded no *fbl17-/-* and others where 1 to 2 mutants were found, at a rate worst that 1 in 3000, more than ten times lower that the normal recovery of 1 in 300. Due to the even lower recovery of adult mutants after sowing, the expected frequency of *fbl17 x* KRP4-GFP meristems for imaging was 1 in 32000 (considering 1/8 recovery on soil and 3/4 for KRP4-GFP segregation). There could be various reasons for the low frequency of fbl17 mutants in these crosses, particularly the putative genetic interaction between *KRP4* and *FBL17.* If FBL17 were indeed responsible for counteracting KRP4 accumulation, the transgene containing KRP4-GFP might add to the effect of the *fbl17* mutation, reducing the lethality of the male gametophyte. In practice, it became very difficult to test the effect of the *fbl17* mutation on KRP4-GFP expression in the shoot meristem.

Due to the low chances of imaging meristematic cells of *fbl17* KRP4-GFP, one experiment was conducted by imaging the root meristem (Fig. 4.6). F2 seedlings were screened based on the *fbl17* qualitative phenotype and those that did not show it were used as controls.
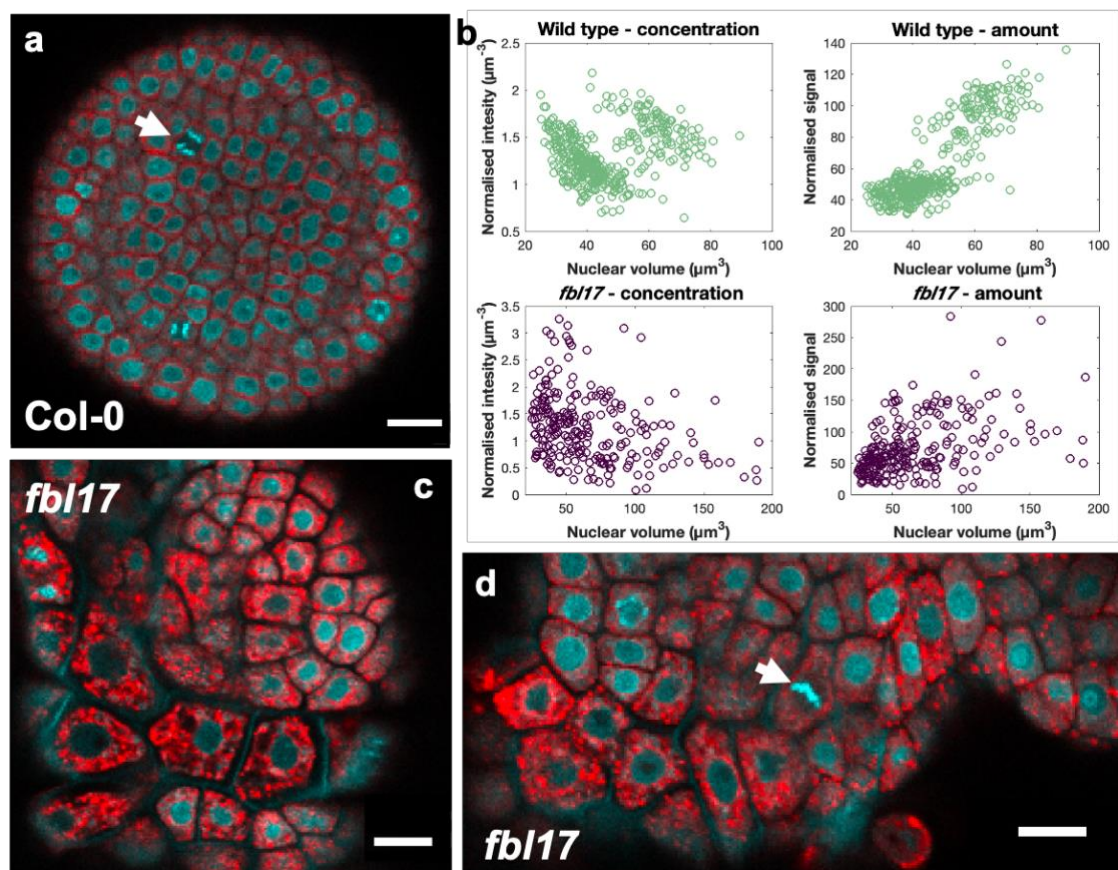
Figure 4.5: Relationship between DNA and cells size in the *fbl17* mutants. a, c and d) Confocal slices of a meristems treated with DAPI to visualise DNA in Col-o (a) and *fbl17* mutants (c and d). Scale bars=10µm. Note cells in M-phase indicated by arrows. Telophase (a) and metaphase (d). b) Scatter plots showing relationship between DNA concentration (left panels) or amount (right panels) against nuclear volume. Note how two distinct groups are present in Col-0 (top panels) and no distinction is visible in the *fbl17* mutants (bottom panels).

Using roots for this experiment also allowed me to use high resolution imaging to investigate KRP4 localisation. In the control root meristems, KRP4-GFP localised in puncta inside the nuclei (Fig. 4.6a-c), as observed in the shoot meristem and previously reported (Bird *et al.*, 2007), suggesting that KRP4 associates with chromatin in roots as it does in shoots. The number of puncta seemed to be up to 10, suggesting these might correspond to the centromeres of the 2x5 Arabidopsis chromosomes, supporting the idea of preferential interaction of KRP4 with heterochromatin. In contrast, KRP4-GFP in the *fbl17* mutant appeared homogeneously distributed across the nucleus in many cells, and partially excluded from the nucleolus (Fig. 4.6b). However, some cells showed KRP4-GFP puncta, like the one observed in the wild type, as well as diffuse nucleosolic signal (Fig. 4.6d). This appearance was likely due to excess of KRP4, which accumulated in the nucleosol after chromatin has been saturated. In the cases where puncta were not visible, the concentration of KRP4 on chromatin may have been lower or equal to KRP4 concentration in the nucleoplasm, with the later overwhelming the signal of the former and resulting in a homogeneous appearance (Fig. 4.6b). However, KRP4 might be more diluted when the puncta are visible, presumably as the result of cell growth (Fig. 4.6d).
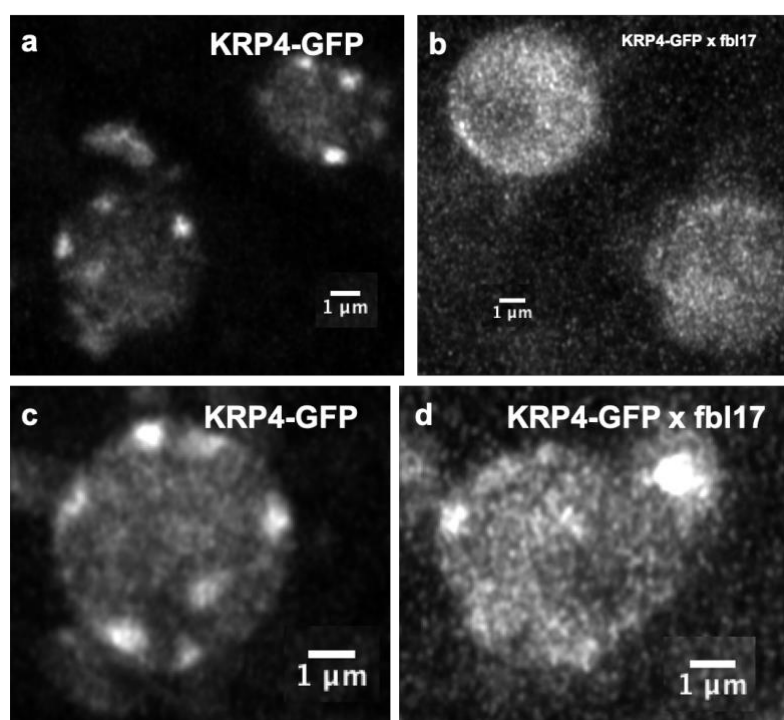
Figure 4.6: Effect of FBL17 on KRP4-GFP localisation. High resolution microscopy on root cells of KRP4-GFP in *fbl17-/-* mutants (b and d) and presumed *fbl17-/+* controls (a and c). Note how KRP localised to puncta inside the nucleus in the control plants and how nucleoplasmic KRP4-GFP potentially obscured the chromatin-bound KRP4-GFP in the mutant. Presumably, the puncta in the nuclei are visible again due to low concentration of KRP4 .

The results in roots were indicative of an interaction between KRP4 and FBL17, but I still wanted to focus on this relationship in the shoot meristem. To do so, roughly 70000 seeds of the F2 cross explained above, were sown on plates and individually screened for the *fbl17* phenotype. Of these, 3 individuals were selected and moved to soil, where 2 survived

to adulthood. One of these individuals did not express KRP4-GFP, while the other was the only individual where I could ever image KRP4-GFP in *fbl17* meristems (Fig. 4.7). Note that, thanks to the meristem splitting feature of *fbl17*, multiple meristems could be recovered for imaging, but all belonged to this individual plant. Surprisingly, KRP4 expression was heterogenous and cells often lacked KRP4-GFP signal. This feature was even more evident in large cells, where the nuclear space was visible as a black region in the cell (Fig. 4.7c and d). While carrying a similar screening, Professor Robert Sablowski reported *fbl17* individuals containing KRP4-GFP at the seedling stage, and losing it at maturity, suggesting that silencing of KRP4-GFP might occur in *fbl17* background. This might explain the sporadic lack of KRP4-GFP in cells of the apexes shown in Figure 4.7. Unfortunately, only one biological replicate was not enough to support any conclusion or to perform quantitative investigation. Therefore, to further investigate the effect of FBL17 on the accumulation of KRP4 in the shoot meristem, a different approach was required.
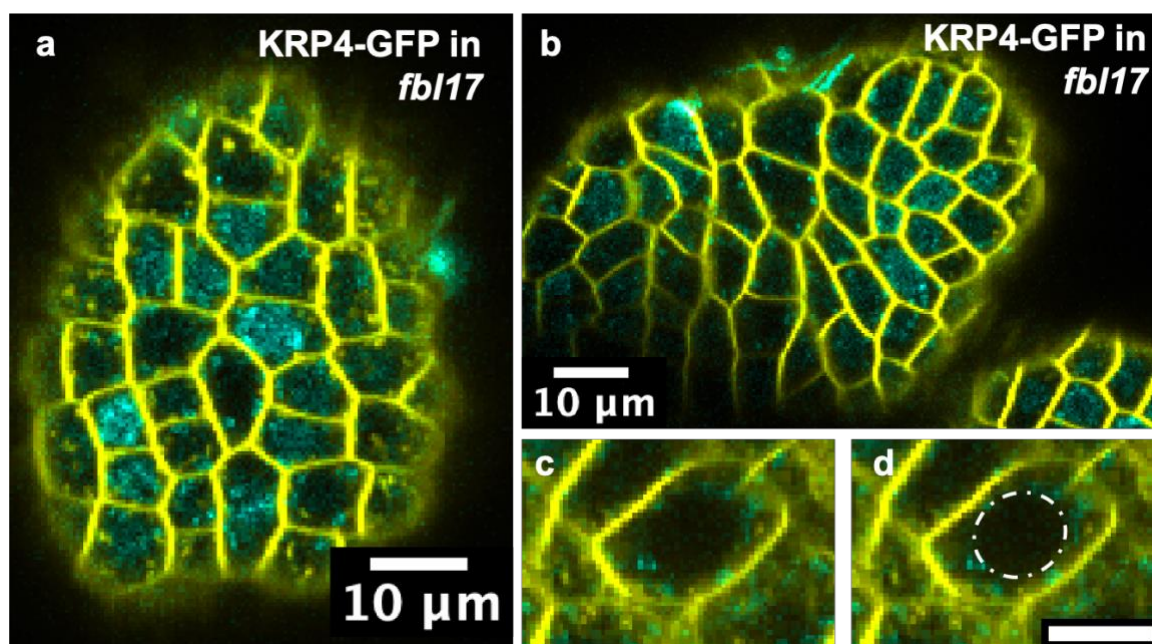
Figure 4.7: KRP4 expression in *fbl17* mutant meristems. a,b) Confocal slices of *fbl17* mutant meristem expressing KRP4-GFP. c,d) Detail of a giant cell that shows lack of KRP4. The nucleus seems so empty that that is possible to see its outline (dotted line in d). All scale bars are 10µm. Note how heterogenous KRP4 expression is, as this is visible in some of the giant cells. While missing in others.

4.4.2 Inhibition of FBL17 using artificial micro RNAs (amiRNAs)

While I was dedicated to finding *fbl17* mutants expressing KRP4-GFP, to overcome the difficulties of working with it, Dr Rafael Tavares and Prof Robert Sablowski developed an alternative system. Dr Rafael Tavares produced a β-estradiol inducible amiRNA construct, targeting the 3' end of the *FBL17* mRNA (D'Ario *et al.*, 2021). This construct was

transformed into a line expressing KRP4-GFP and Prof. Robert Sablowski imaged independent lines with and without induction. The results showed that KRP4-GFP accumulated upon miRNA induction, particularly in large cells, those expected to be in G2, as hypothesised by our model (D'Ario *et al.*, 2021). Additionally, within 24h of induction, KRP4 was also seen in higher levels in new-born cells, confirming that excess of KRP4 during G2 could be carried over through division and inherited in daughter cells. To confirm that overaccumulation of KRP4 occurred in the nucleosol rather than on chromatin, they were able to compare the amount of KRP4 on mitotic chromosomes and show that this was comparable between induced and not induced samples, despite total KRP4 level being higher in the induced samples. These observations confirmed that FBL17 is required for clearing nucleosolic KRP4 excess in G2, which saturate chromatin prior to division (D'Ario *et al.*, 2021).

4.5 Search for KRP sequences that mediate interactions with chromatin and FBL17

To find possible motifs in KRP4 that could be involved in its regulation and interaction with FBL17, I first looked for correlations between conserved motifs and subcellular behaviour across the KRP family. Localisation of KRPs and interaction with chromatin was previously reported (Bird *et al.*, 2007; Boruc *et al.*, 2010), but was not done in the meristem. A phylogenetic study had also been conducted previously (Torres-Acosta, Fowke and Wang, 2011), but this was done in the context of monocots versus eudicots, whereas I aim to contextualise KRP phylogeny in term of the evolution of size regulation and divergent functionality within Arabidopsis. To this end, a phylogenetic tree of the KRP family in Arabidopsis is shown in Figure 4.8. Note that all seven proteins share high similarity in the two C-terminus motifs called Motif 1 and Motif 2 (Fig. 4.9a and b). These are the motifs required for interaction with CDKa and CYCD, respectively (Torres-Acosta, Fowke and Wang, 2011), and define the KRP family – by definition, a protein containing sequences
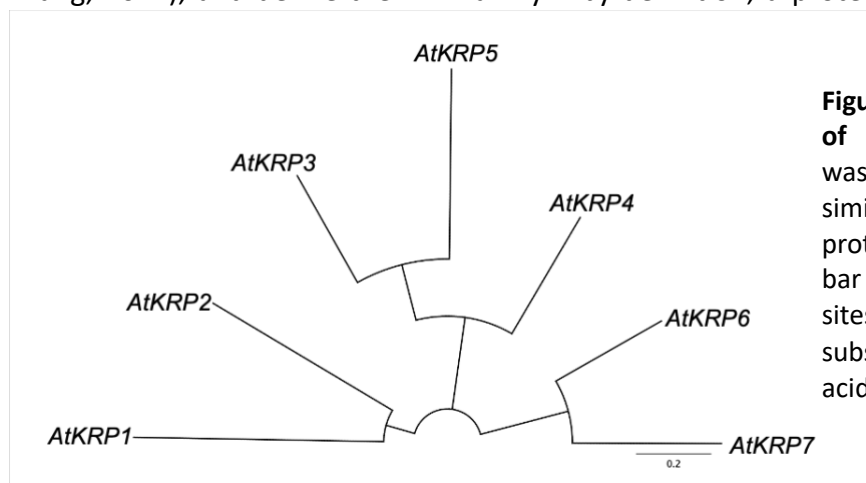
Figure 4.8: Phylogenetic tree of KRP proteins. Blosum62 was used to score sequence similarity between KRP protein sequences. The scale bar is 0.2 substitution per sites, calculated as number substitution per 100 amino acids.

homologues to these motifs is considered a KRP. Based on sequence similarity, three distinct classes of KPRs can be identified in Arabidopsis (Fig. 4.8), with KRP4 belonging to the KRP3,4,5 subfamily. To test the involvement of each KRP in size sensing, their subcellular localisation needed to be investigated.

4.5.1 Confirmation that other KRPs interact with chromatin

Confocal images were taken of each of the seven Arabidopsis KRPs fused with a GFP tag, (kindly provided by Yuling Jiao, IGDB, China). None of the KRP outside the KRP3,4,5 subfamily showed nuclear puncta, suggesting that none of them associates with chromatin (Fig. 4.10). KRP1 expression seemed to be relegated to the very centre of the SAM and it was very faint – it seemed to preferentially accumulate in large cells, so perhaps it was expressed in G2 (Fig. 4.10a). KRP2, the KRP most similar in sequence to KRP1, was faintly expressed in the rib meristem as previously reported (Serrano-Mislata *et al.*, 2017), and no association with chromatin could be detected (Fig. 4.10b). KRP6 expression was the most heterogenous, only appearing in large cells, where its apparent concentration drastically changed from cell to cell (Fig. 4.10c). Surprisingly, even if KRP7 is redundant with KRP6 in pollen development (Gusti *et al.*, 2009) and they group together by sequence similarity (Fig.
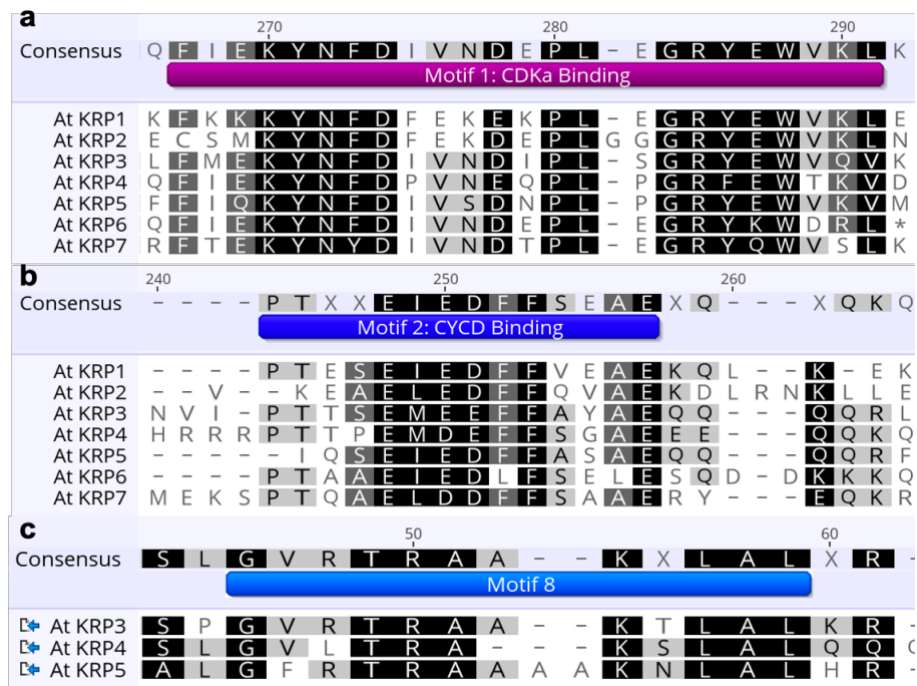
Figure 4.9: Similarities between KRP proteins. Alignment of KRP protein sequences showing similarity of Motif 1 and 2 (a and b respectively) among all KRPs and Motif 8 (c) for the class of KRP3,4,5. Blosum62 score matrix was used for alignment and consensus, which is coloured by Bosum62 similarity as follows: black = 100%, dark grey = 80 to 100%, light grey = 60 to 80%, no colour less than 60%. Note that KRP4's K52 (c) appear in the consensus as 100% similarity.

4.8), they showed a very different expression in the SAM (Fig. 4.10c and d). KRP7 expression was very faint and only seemed to be present in small cells, perhaps those that recently divided. In fact, KRP7 seemed to be present in each sister cell of a recent division (Fig. 4.10d), contrasting with KRP6 expression in larger cells. The behaviour of these KRPs was unlike the one required in our model for performing size sensing, so they were not investigated further in this study. Nevertheless, it is important not to forget that these are also cell cycle inhibitors, which might perform a role in establishing size thresholds in certain conditions, without necessarily contributing to cell size homeostasis.
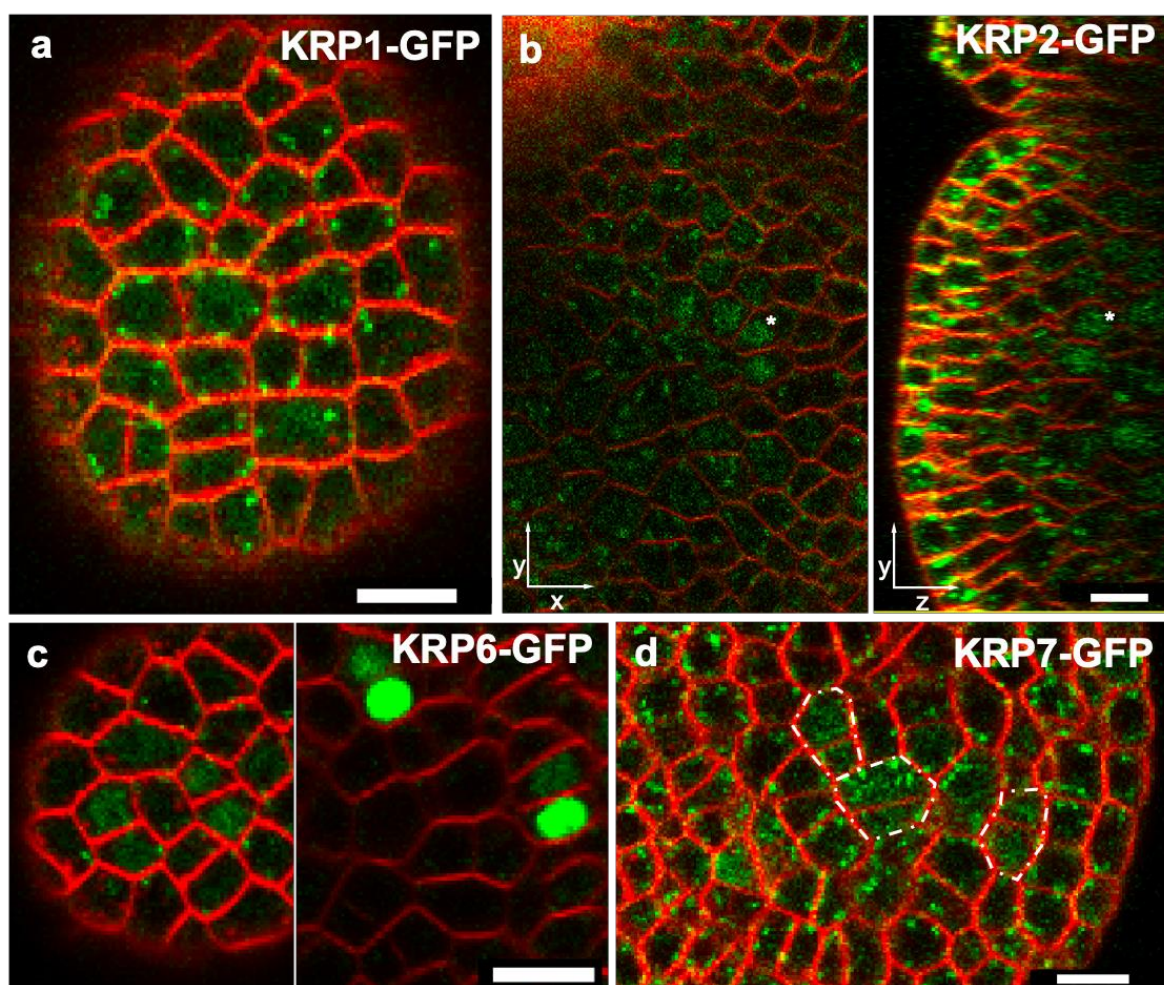
Figure 4.10: Expression and localisation of KRP1,2,6 and 7. Confocal slices of shoot meristems expressing the various KRP proteins tagged with GFP. a) KRP1-GFP appeared to localise faintly in the nucleus but not the nucleolus. b) KRP2-GFP mainly localised in the rib meristem, deep within the shoot apex. The asterisk used in the two panes indicates the same cell, in an attempt to simplify the orthogonal view. c) KRP6-GFP expression was very heterogenous, and sometimes appeared very concentrated (second panel). d) KRP7-GFP was also heterogenous, localised in small cells that seemed to have just divided, as highlighted by their shape, characteristic of newly born sister cells (dotter line). Scale bar = 10 μm.

4.5.2 Understanding the KRP3,4,5 subfamily

Based on images of GFP fusions, in contrast to the rest of the family, both KRP3 and KRP5 appeared as puncta in the nucleus (Fig. 4.11), very similar to KRP4. Unlike KRP4 however, KRP3 expression was heterogenous across the meristem and much stronger at the boundaries than it was in the centre of the SAM (Fig. 4.11a). KRP5 expression is even more restricted to the boundaries and was basically absent from the central zone (Fig. 4.11b). It was possible to see KRP3 associated with metaphase chromosomes (Fig. 4.11a small panel), but the same behaviour was not visible for KRP5. However, KRP5 was expressed in much fewer cells, so it is possible that there were no dividing cells during the experiment. These data show that KRP3 and KRP5 can associate with chromatin, like KRP4, and at least KRP3 does so during division. Additionally, the data suggest that KRP3 and KRP5 could be partially redundant with KRP4 in size sensing at G1/S. It has been suggested that the interaction of KRP3,4,5 with chromatin by is mediated by Motifs 7,8 and 9, or a combination of these motifs (Bird *et al.*, 2007). In addition to this information, when using multiple online resources for prediction of ubiquitinated lysines (Du *et al.*, 2009; Nguyen *et al.*, 2016; Yadav, Gupta and Bist, 2018), K52 of KRP4 was one of the hits. Note that these website are now deprecated, possible due to the advent of artificial intelligent based approaches (Fu *et al.*, 2019), which are making many obsolete algorithm-driven approaches. As shown in Figure 4.9c, lysine 52 is conserved in both KRP3 and KRP5 and resides in Motif 8. Together,
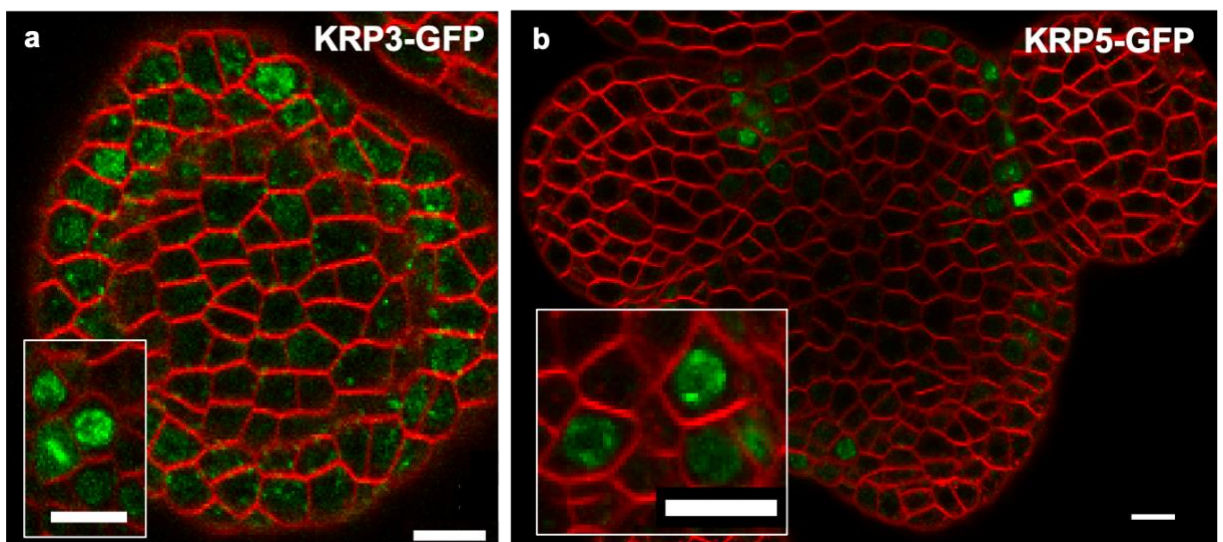
Figure 4.11: Expression and localisation of KRP3 and 5. Confocal slices of shoot meristems expressing KRP3 and 5 tagged with GFP. Both proteins appeared as puncta in the nucleus, like KRP4 (inner panels for better resolution). a) KRP3-GFP localised at the periphery of the meristem more sharply than in the centre. The inner panels show a mitotic figure with KPR3 associated to it. b) KRP5-GFP seemed to only localise at the organ boundaries and no association with mitotic chromosomes could be observed, although this association could not be excluded. Scale bars = 10μm.

these observations led to the hypothesis that FBL17 targets KRP3,4,5 to degradation via ubiquitination of K52, but this amino acid could be hidden when KRP3,4 or 5 interact with chromatin. An assumption of this hypothesis would be that Motif 8 is the one required for this interaction. To test this hypothesis, protein variants were designed.

4.5.3 Testing predictions for chromatin interaction and ubiquitination of KRP4

β-estradiol-inducible lines were produced to express wild type KRP4 protein, KRP4 lacking Motif 8 (Δ8KRP4) and a KRP4 variant where K52 was replaced with an arginine (K52RKRP4). These protein variants were tagged with GFP (Fig. 4.12). Unfortunately, the plasmid used for these constructs was the pER8, designed to contain a β-estradiol-inducible expression cassette (Schlücking *et al.*, 2013) with the XVE protein for β-estradiol detection designed under a multimerised G-box motif (GCCACGTGCC) fused to a minimal 35s promoter (Ishige *et al.*, 1999). This promoter is now being overtaken by other over expressing sequences, one reason being that the promoter used in pER8 does not drive expression in all organs and appears to be weakly active in the meristem. Therefore, the tests carried out on these
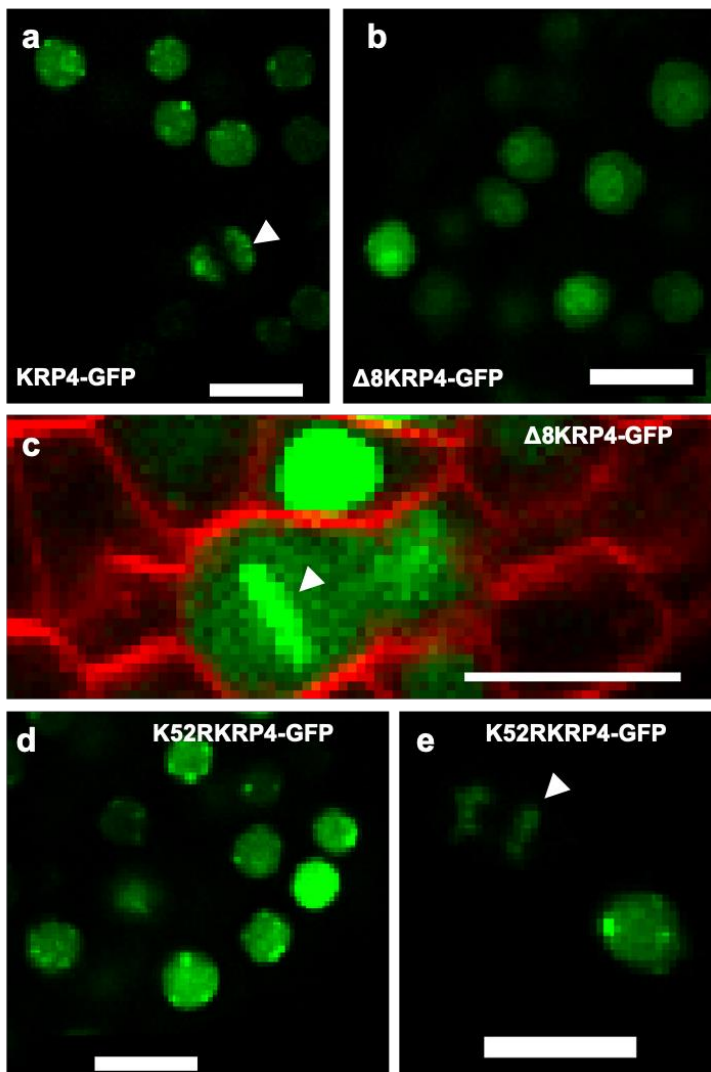
Figure 4.12: subcellular localisation of different KRP4 variants. a) Confocal image showing induced Wt KRP4 protein. The white arrowhead indicates telophase chromosomes. b-c) Confocal image of Δ8KRP4. Note how it resembles KRP4 in *fbl17* mutants. The white arrowhead indicates a metaphase chromosome, showing that interaction with chromatin was preserved, at least during division. d) Confocal image of K52RKRP4. Note how similar the protein is to the Wt. The arrowhead indicates telophase chromosomes. Scale bars = 10µm.

protein fusions (Fig. 4.12) were mainly in emerging sepals and boundary regions, where the reporter proteins could be detected clearly.

Nevertheless, the subcellular behaviour of these protein fusion could be observed. The wild type protein behaved similarly to what was seen previously: the protein was localised in puncta into the nucleus, suggesting chromatin binding, and associated with chromosomes during division (Fig. 4.12a). However, unlike genomic KRP4, the induced protein was much more visible in the nucleoplasm and somewhat more concentrated in the nucleolus than in the rest of the nucleus (Fig. 4.12b). When Motif 8 was absent, no puncta were visible, suggesting that during the cell cycle the Δ8KRP4 variant does not bind chromatin (Fig. 4.12b) and corroborating the idea of Motif 8 being responsible for association with chromatin. Intriguingly, a metaphase chromosome was detectable in a dividing cell expressing the Δ8KRP4 variant (Fig. 4.12c), suggesting that chromatin binding during division is mediated by a motif other than Motif 8. Alternatively, it is possible that Domain 8 is responsible for KRP4 stability and the smooth appearance of Δ8KRP4 is the result of it accumulating in the nucleus and overwhelming the signal corresponding to the puncta, as seen in the root meristem (Fig. 4.6). However, in the root some cells showed puncta because some of the excess KRP4 may have been diluted, presumably during growth, revealing the reporter bound to chromatin. Thus, since no puncta were observed in Δ8KRP4, the latter hypothesis is unlikely.

Finally, K52RKRP4 localised similarly to the wild type variant (Fig. 4.12d and e), disproving the hypothesis of ubiquitination by FBl17 on K52. Overall, these experiments suggested that Motif 8 is one of the motifs required for KRP4 binding on chromatin but is not required for binding at mitosis. Note that one could conclude that lack of Motif 8 causes accumulation of KRP4 in the nucleoplasm in the presence of FBL17, suggesting that Motif 8 is required for this interaction. However, the overaccumulation may be due to the promoter used and the time of induction, since the wild type of protein also over-accumulates when compared with KRP4 genomic constructs.

It was surprising to find that K52 did not seem to be the ubiquitination target of FBL17, despite being conserved in the KRP3,4,5 subfamily. To better understand the relevance conservation of this lysine, of Motif 8 and of this protein subfamily in general, a more in depth analysis is required.

4.6 Wider evolutionary relationship of KRPs and FBL17

In an attempt to better understand the evolutionary history of the functional module formed by KRP-FBL17, protein sequences were used to identify possible candidates in other plant species. Before focusing the attention on the KRPs, I will just mention that no clear orthologues of FBL17 were found in distantly related plant taxa. This is likely due to the FBL17 identity as a F-BOX protein, defined by the highly conserved F-BOX motif, which may lead to other F-BOX proteins being the best match when searching for homology (Xu *et al.*, 2009). Additionally, little is known about other FBL17 domains, so shorter sequences cannot be used for this purpose. Therefore, the attention was focused on the KRPs and KPR4 protein sequence was used on the Phytozome database (Goodstein *et al.*, 2012), to identify members of the family in other land plants.

The blast algorithm identified KRPs of the KRP3,4,5 subfamily in all vascular plants, suggesting that cell size regulation using KRP4 evolved before the split between lycophytes and other vascular plants. Figure 4.13a shows the alignment of Motif 8, of the Arabidopsis KRPs and putative homologues in *Selaginella moellendorffii*, remarkably conserved in this distantly related plant. Notably, K52, which appeared very conserved when comparing Arabidopsis proteins, is not part of the consensus in this alignment, supporting the observation of K52RKRP4 mutants did not behave differently from the wild type. The wide conservation of Motif 8 suggests an ancient role of KRP3,4,5 class of proteins as size sensors in vascular plants. Interestingly, *S. moellendorffii* has a unique KRP, annotated as SmCDKI3, which only shares homology to Motif 1, making it a KRP by definition, but with no similarities with any of the other Arabidopsis KRPs. Perhaps a unique function of this protein evolved in the Lycophytes.
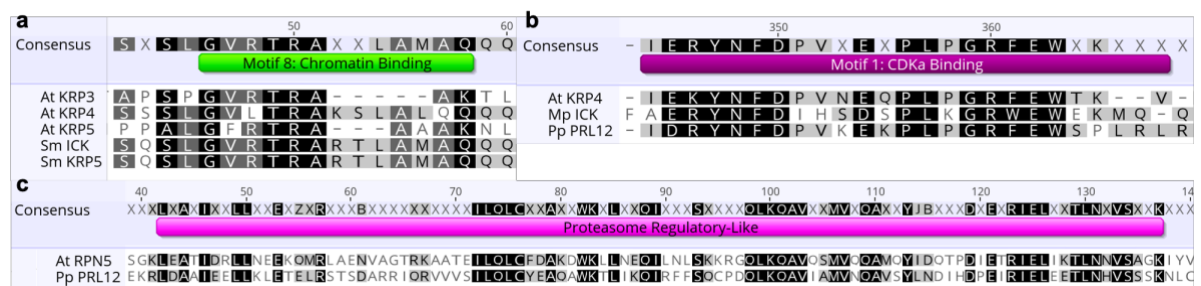
Figure 4.13: Alignment of various KRPs and putative KRP homologues. a) Alignment of KRP3,4,5 class with putative KRP proteins form *Selaginella moellendorffii*. Note how Motif 8 seems to be present in lycophytes and how KRP4's K52 now does not appear in the consensus. b) Motif 1 alignment between Arabidopsis KRP4, *Marchantia polymorpha* putative ICK and *Physcomitrium patens* PRL12. c) Alignment between Arabidopsis RPN5 and *P. patens* 12. Blosum62 score matrix was used for alignment and consensus, which is coloured by Bosum62 similarity as follows: black = 100%, dark grey = 80 to 100%, light grey = 60 to 80%, no colour less than 60%.

It was interesting to find that no KRPs were detected by Phytozome in bryophytes. To further investigate this, I blasted the CDKa binding domain, Motif 1, alone against the bryophyte database using NCBI blast (Coordinators, 2018). Two proteins shared similarities to KRP4 Motif 1: an unannotated protein belonging to *Marchantia polymorpha*, which I will refer to as MpICK, and a protein in the *Physcomitrium patens* genome, annotated as PROTEOSOME REGULATORY-Like (PpPRL12) (Fig. 4.13b). Unsurprisingly, reversed blast of MpICK against Arabidopsis genome yielded KPRs, but no other proteins. Additionally, MpICK seems not to have any sequence homologous to Motif 8 or any other domains, suggesting that MpICK might perform a unique function in liverworts. However, when reverse blasting PpPRL12, the origin of its annotation name was revealed, as, other than KRPs, the blast yielded similarities to the Arabidopsis RPN5 protein, a proteosome regulatory subunit (Book *et al.*, 2009). The gross morphology of the *rpn5a* mutant in Arabidopsis resembles the *fbl17* mutants, with split meristems and similar leaf morphology (Book *et al.*, 2009). It is reasonable to assume that these similarities are connected to the role of FBL17 as E3 ligase, responsible for directing proteins to the proteosome, a process upstream to RPN5, responsible for the correct functioning of the proteosome. As shown in Figure 4.13c, PpPRL12 shares sequence similarities with both, the KRPs and RPN5. This interesting feature suggests the intriguing speculation that PpPRL12 can function both as inhibitor of S-phase transition and as its own repressor via self-degradation, in a system homologous to KRP4-FBL17. I hope that future studies will address this possibility.

4.7 Discussion

In this chapter, the role of FBL17 in size sensing was tested. FBL17 is critical for the success of the proposed role of KRP4 as size sensor, required for ensuring linear scaling of KRP4 with regard to DNA. Any mechanism for dilution that does not rely on a robust mechanism that ensures equal inheritance of the inhibitor molecule, will eventually succumb to the accumulation of errors, built over cell generations. Therefore, the role covered by FBL17 is critical in the model proposed. Here, I showed that FBL17 localisation and genetic interaction with KRP4 matched the model predictions.

First of all, FBL17 expression was complementary to CDT1, indicating that the E3 ligase is expressed during G2. The importance of FBL17 as core genetic component was highlighted by the pleiotropic effects of the *fbl17* mutation, which also hindered part of the study. Nevertheless, I showed that the correlation between DNA concentration and cell cycle

progression was lost in the mutant, and that KRP4 accumulated in roots, consistent with the proposed role of FBL17. Direct evidence for KRP4 accumulation during G2, as a consequence of low FBL17 expression, could not be obtained using this mutant and instead an amiRNA approach had to be used (D'Ario *et al.*, 2021). Overall, these experiments confirmed the proposed role of FBL17 as repressor of KRP4. It would have been interesting to test the hypothesis that overexpression of FBL17 would result in the removal of KRP4 and its homologues during G1, causing the cell to enter S-phase prematurely, eventually leading to abnormally small cells. Unfortunately however, previous studies have revealed that FBL17 stability is regulated via proteosome-dependent proteolysis, hindering overexpression approaches (Noir *et al.*, 2015).

The dilution mechanism proposed here not only requires FBL17 to remove excess KRP4 in G2, but also requires the E3 ligase to specifically target nucleosolic KRP4, leaving the chromatin-bound molecules untouched. A simple mechanism for this interaction would be the interaction of KRP4 with chromatin shielding either the FBL17 interacting domain or the ubiquitination site (Fig. 4.14). This could be accomplished by a dual function domain, that is able to interact with chromatin and FBL17 at the same time. Similarly, a dual function domain might conceal KRP4's ubiquitination site. In the absence of interaction with chromatin, i.e. when KRP4 would be cytosolic, FBL17 would be free to degrade KRP4 (Fig. 4.14 left). I will refer to this as the domain hypothesis.

Alternatively, the shielding of FBL17 could occur due to conformational changes in the KRP4 protein, as a result of interaction with chromatin (Fig. 4.14 right). In this scenario, the domain for chromatin interaction could be far apart from the domain for interaction with FBL17. I will call this the conformation hypothesis. This latter hypothesis can only be tested via a structural approach, in which free KRP4 and chromatin-bound KRP4 are crystallised to solve their structure. If this approach were not difficult already, there are multiple candidates for chromatin interactors with KRP4, the identity of which ranges from histones to other cell cycle proteins, to DNA itself. Therefore, until *in vitro* protocols for stable expression of KRP4 are established and until KRP4 interactors are discovered, testing the conformation hypothesis will not be possible.

Therefore, I focused my attention on testing the domain hypothesis by mutating the K52 residue, part of the chromatin binding domain, Motif8, and showed that this KRP4 variant

accumulates similarly to the wild type protein (Fig. 4.12d and e). However, I could not exclude that Motif 8 directs the interaction with both chromatin and FBL17, hence the domain hypothesis cannot be fully dismissed. An interesting observation is that multiple KRPs are reported to interact with FBL17 (Zhao *et al.*, 2012), but the only shared motifs among these proteins are Motif 1 and 2, required for the interaction with CDKa and CYCD, respectively (Torres-Acosta, Fowke and Wang, 2011). CDKa has been reported to interact with chromatin, in particular during metaphase, even if it does not appear in puncta as KRP4 (Vanstraelen *et al.*, 2004; Boruc *et al.*, 2010). This observation might suggest that interaction with FBL17 by the KRPs is mediated by the same domain that mediates CDKa interaction, making the C-terminus of KRPs a putative protein interaction site. However, this would imply that other KRPs are able to associate with chromatin and there is no evidence that KRP2,6 and 7 do so, even if KRP1 was observed to associate with metaphase chromosomes in BY2 cells, despite its smooth appearance in the nucleus (Boruc *et al.*, 2010). Developing *in vitro* assays for interaction of KRP4 and FBL17 might be a critical requirement to properly reveal the domains required for the interaction between these two proteins and test the domain hypothesis.
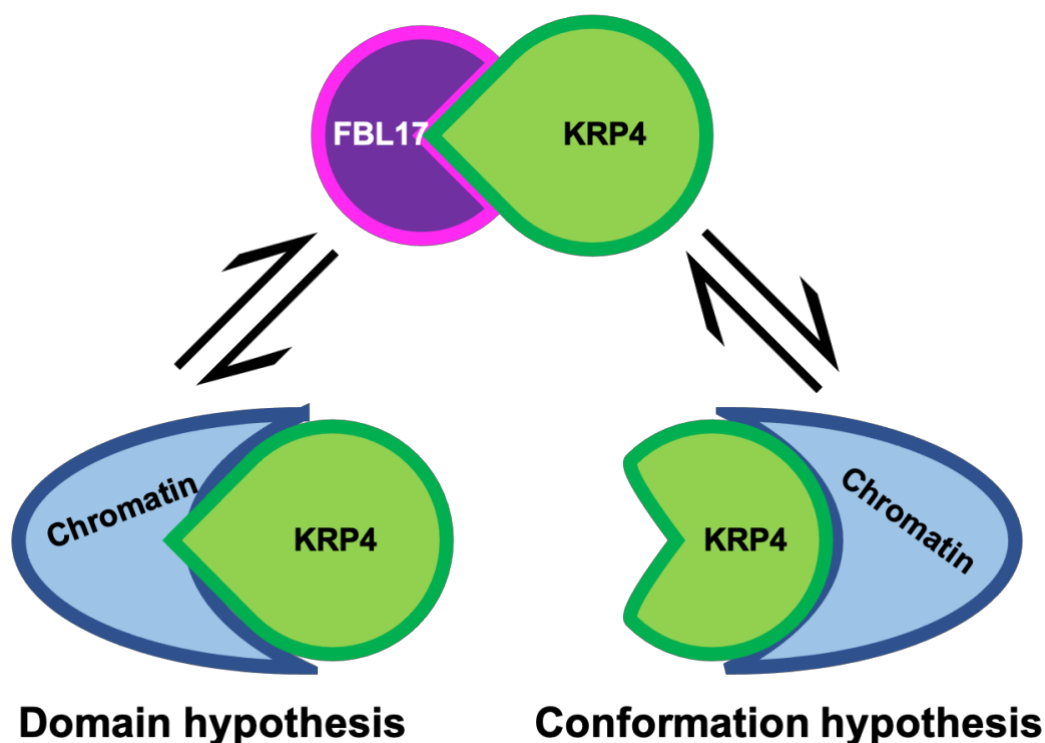
Figure 4.14: Cartoon for different FBL17 and KRP4 interaction. FBL17 interacts with KRP4 in the cytoplasm, resulting in its degradation. Chromatin can prevent this interaction either by shielding the interactor domain (domain hypothesis on the left) or by causing a conformational change of KRP4 that prevents interaction with FBL17 (conformation hypothesis on the right). Equilibrium arrows indicate that binding is reversible.

The KRP4 variant lacking Motif 8, Δ8KRP4, showed nuclear localisation, likely resulting from lack of interaction with chromatin. However, metaphase chromosomes were visible in these lines, suggesting that at least this type of interaction with chromatin is not performed by Motif 8 and perhaps is the result of interaction with CDKa. An interesting possibility is that Motif 8 is indeed the domain that interacts with FBL17 and the smooth appearance of Δ8KRP4 is the result of KRP4 accumulation due to lack of degradation as suggested in the roots. More data on this line needs to be collected to understand the role of Motif 8.

Two other domains are shared among KRP3,4 and 5, which have not been explored in this study: Motif 9 and Motif 7. Interestingly, Motif 7 has been previously reported to be partly necessary for chromatin association, as removal of Motif 7 and Motif 8 resulted in homogeneous nuclear localisation of KRP3,4 and 5 (Bird *et al.*, 2007). Our data suggest that deletion of Motif 8 alone is sufficient for loss of interaction with chromatin, so the role of Motif 7 might need rethinking. It is possible that Motif 7 is required for chromatin interaction as suggested (Bird *et al.*, 2007), but performs a role during division and its responsible for the association with metaphase chromosomes, an interaction that I showed to be independent of Motif 8. An important observation is that Motif 7 is also present in KRP1 and studies have shown that this motif is required for proteolysis of KPR1 via a pathway independent of FBL17 (Li *et al.*, 2016). It is reasonable to assume that also KRP3,4 and 5 proteins are controlled by this pathway, although there is no evidence to suggest that Motif 7 plays a role in cell size homeostasis. An intriguing, albeit speculative, hypothesis is that FBL17-independent degradation is responsible for correct scaling of KRPs in early G1, when our data show that the total amount of KRP4 increases independently of cell size, in the absence of FBL17. Undoubtably, there is much more to uncover regarding the role of these different domains.

The possibility of redundancy between KRP3, 4 and 5 was evident from the subcellular localisation of these proteins (Fig. 4.11). However, it was interesting to notice that, unlike KRP4, KRP3 and 5 are not homogenously distributed across the meristem. Perhaps, this is a system that ensures homeostasis across the meristem, whilst setting a different size threshold for cells with different identity. Heterogeneity in size and growth rate across the meristem has long been observed (Serrano-Mislata, Schiessl and Sablowski, 2015; Jones *et al.*, 2017), and it is easy to envision a mechanism that involves KRPs to accomplish this. Interestingly, other KRPs are also expressed in the meristem, and these might perform a

size-independent role for cell cycle progression. For example, it has been shown that KRP2 is under the control of GA, which impacts cell size in specific regions of the meristem (Serrano-Mislata *et al.*, 2017). Therefore, there are mechanisms that can be used by the plant to change the average cell size of specific tissues without affecting size homeostasis, by adjusting the expression of KRPs other than KRP3,4 and 5. Given the existence of these non-size sensing KRPs, it is natural to ask questions regarding the ancestral state of KRPs: did these originally evolved as size-independent inhibitors of cell cycle progression, or as size sensors, perhaps replacing RBR for the size-sensing function in the sporophyte, as RBR role in establishing cell identity become critical (see Chapter 7 for the full discussion on the possible evolution history of KRPs and RBR).

The data presented in this chapter allowed me to confirm the involvement of FBL17 in KRP4 regulation. The phenotype of *fbl17* added to this idea and it is, to my knowledge, the only reported phenotype that shows a lack of size homeostasis. Due to the importance of FBL17 in reproduction (Gusti *et al.*, 2009) and general DNA maintenance (Gentric *et al.*, 2020), as well as size homeostasis, it is not surprising that similar mutants have not been described in other systems. The loss of homeostasis in *fbl17* mutants might also be connected to other phenotypes, like the meristem spit, which gives *fbl17* its bushy appearance. While my data rejected the idea of differential growth rate being the cause behind this, other physical phenomena could be the cause. For example, mechanical stress could be the reason behind the spitting of meristems as cell division acts to release mechanical stress (Alim, Hamant and Boudaoud, 2012; Michels *et al.*, 2020; Robinson, 2021), implying that homeostasis in cell size also results in homogeneous stress in the shoot apical meristem. I tried to collect data to test this hypothesis by crossing a microtubule marker line with *fbl17-1* mutants, but this experiment could not be performed due to the difficulties of working with the *fbl17* mutant. I hope that resources will be developed, similar to the miRNA of FBL17 (D'Ario *et al.*, 2021), to further characterise this interesting mutant.

Until now, I have presented and quantified the behaviour of KRP4 and FBL17, but could only produce a qualitative hypothesis for their role in cell size homeostasis. To deepen the quantitative understanding of this mechanism, I sought to produce a mathematical framework, that would allow quantitative predictions on this system. The production and study of the mathematical model is the focus of the next chapter.

4.8 References

Alim, K., Hamant, O. and Boudaoud, A. (2012) 'Regulatory role of cell division rules on tissue growth heterogeneity', *Frontiers in plant science*. Frontiers Research Foundation, 3, p. 174. doi: 10.3389/fpls.2012.00174.

Bird, D. A. *et al.* (2007) 'Arabidopsis cyclin-dependent kinase inhibitors are nuclear-localized and show different localization patterns within the nucleoplasm', *Plant Cell Reports*, 26(7), pp. 861–872. doi: 10.1007/s00299-006-0294-3.

Book, A. J. *et al.* (2009) 'The RPN5 subunit of the 26s proteasome is essential for gametogenesis, sporophyte development, and complex assembly in Arabidopsis', *The Plant cell*. 2009/02/27. American Society of Plant Biologists, 21(2), pp. 460–478. doi: 10.1105/tpc.108.064444.

Boruc, J. *et al.* (2010) 'Systematic Localization of the Arabidopsis Core Cell Cycle Proteins Reveals Novel Cell Division Complexes', *Plant Physiology*, 152(2), pp. 553–565. doi: 10.1104/pp.109.148643.

Chen, L. and Hellmann, H. (2013) 'Plant E3 Ligases: Flexible Enzymes in a Sessile World', *Molecular Plant*, 6(5), pp. 1388–1404. doi: https://doi.org/10.1093/mp/sst005.

Coordinators, N. R. (2018) 'Database resources of the National Center for Biotechnology Information', *Nucleic acids research*. Oxford University Press, 46(D1), pp. D8–D13. doi: 10.1093/nar/gkx1095.

D'Ario, M. *et al.* (2021) 'Cell size controlled in plants using DNA content as an internal scale', *Science*, 372(6547), p. 1176 LP-1181. doi: 10.1126/science.abb4348.

Desvoyes, B. *et al.* (2019) 'FBL17 targets CDT1a for degradation in early S-phase to prevent Arabidopsis genome instability', *bioRxiv*, p. 774109. doi: 10.1101/774109.

Du, Z. *et al.* (2009) 'plantsUPS: a database of plants' Ubiquitin Proteasome System', *BMC genomics*. BioMed Central, 10, p. 227. doi: 10.1186/1471-2164-10-227.

Fu, H. *et al.* (2019) 'DeepUbi: a deep learning framework for prediction of ubiquitination sites in proteins', *BMC Bioinformatics*, 20(1), p. 86. doi: 10.1186/s12859-019-2677-9.

Gentric, N. *et al.* (2020) 'The F-Box-Like Protein FBL17 Is a Regulator of DNA-Damage Response and Colocalizes with RETINOBLASTOMA RELATED1 at DNA Lesion Sites1 [OPEN]', *Plant Physiology*, 183(3), pp. 1295–1305. doi: 10.1104/pp.20.00188.

Goodstein, D. M. *et al.* (2012) 'Phytozome: a comparative platform for green plant genomics', *Nucleic acids research*. 2011/11/22. Oxford University Press, 40(Database issue), pp. D1178–D1186. doi: 10.1093/nar/gkr944.

Gusti, A. *et al.* (2009) 'The Arabidopsis thaliana F-box protein FBL17 is essential for

progression through the second mitosis during pollen development', *PloS one*. 2009/03/11. Public Library of Science, 4(3), pp. e4780–e4780. doi: 10.1371/journal.pone.0004780.

Harris, B. J. *et al.* (2020) 'Phylogenomic Evidence for the Monophyly of Bryophytes and the Reductive Evolution of Stomata', *Current Biology*. Elsevier, 30(11), p. 2001–2012.e2. doi: 10.1016/j.cub.2020.03.048.

Harrison, C. J. and Morris, J. L. (2018) 'The origin and early evolution of vascular plant shoots and leaves', *Philosophical Transactions of the Royal Society B: Biological Sciences*. Royal Society, 373(1739), p. 20160496. doi: 10.1098/rstb.2016.0496.

Ishige, F. *et al.* (1999) 'A G-box motif (GCCACGTGCC) tetramer confers high-level constitutive expression in dicot and monocot plants', *The Plant Journal*. John Wiley & Sons, Ltd, 18(4), pp. 443–448. doi: 10.1046/j.1365-313X.1999.00456.x.

Jones, A. R. *et al.* (2017) 'Cell-size dependent progression of the cell cycle creates homeostasis and flexibility of plant cell size', *Nature Communications*. Nature Publishing Group, 8, p. 15060. doi: 10.1038/ncomms15060.

Kim, H. J. *et al.* (2008) 'Control of plant germline proliferation by SCFFBL17 degradation of cell cycle inhibitors', *Nature*, 455(7216), pp. 1134–1137. doi: 10.1038/nature07289.

Li, L. *et al.* (2020) 'Arabidopsis RAD23B regulates pollen development by mediating degradation of KRP1', *Journal of Experimental Botany*, 71(14), pp. 4010–4019. doi: 10.1093/jxb/eraa167.

Li, Q. *et al.* (2016) 'A short motif in Arabidopsis CDK inhibitor ICK1 decreases the protein level, probably through a ubiquitin-independent mechanism', *The Plant Journal*. John Wiley & Sons, Ltd (10.1111), 87(6), pp. 617–628. doi: 10.1111/tpj.13223.

Lin, J. and Amir, A. (2018) 'Homeostasis of protein and mRNA concentrations in growing cells', *Nature Communications*, 9(1), p. 4496. doi: 10.1038/s41467-018-06714-z.

Liu, J. *et al.* (2008) 'Targeted degradation of the cyclin-dependent kinase inhibitor ICK4/KRP6 by RING-type E3 ligases is essential for mitotic cell cycle progression during Arabidopsis gametogenesis', *The Plant cell*. 2008/06/13. American Society of Plant Biologists, 20(6), pp. 1538–1554. doi: 10.1105/tpc.108.059741.

Michels, L. *et al.* (2020) 'Complete microviscosity maps of living plant cells and tissues with a toolbox of targeting mechanoprobes', *Proceedings of the National Academy of Sciences*, 117(30), p. 18110 LP-18118. doi: 10.1073/pnas.1921374117.

Nguyen, V.-N. *et al.* (2016) 'UbiNet: an online resource for exploring the functional associations and regulatory networks of protein ubiquitylation', *Database : the journal of*

biological databases and curation. Oxford University Press, 2016, p. baw054. doi: 10.1093/database/baw054.

Noir, S. *et al.* (2015) 'The Control of *Arabidopsis thaliana* Growth by Cell Proliferation and Endoreplication Requires the F-Box Protein FBL17', *The Plant Cell*, 27(5), pp. 1461–1476. doi: 10.1105/tpc.114.135301.

Puttick, M. N. *et al.* (2018) 'The Interrelationships of Land Plants and the Nature of the Ancestral Embryophyte', *Current Biology*. Elsevier, 28(5), p. 733–745.e2. doi: 10.1016/j.cub.2018.01.063.

Ren, H. *et al.* (2008) 'Degradation of the cyclin-dependent kinase inhibitor KRP1 is regulated by two different ubiquitin E3 ligases', *The Plant Journal*. John Wiley & Sons, Ltd, 53(5), pp. 705–716. doi: https://doi.org/10.1111/j.1365-313X.2007.03370.x.

Robinson, S. (2021) 'Mechanobiology of cell division in plant growth', *New Phytologist*. John Wiley & Sons, Ltd, 231(2), pp. 559–564. doi: https://doi.org/10.1111/nph.17369.

Schiessl, K., Muino, J. M. and Sablowski, R. (2014) 'Arabidopsis JAGGED links floral organ patterning to tissue growth by repressing Kip-related cell cycle inhibitors', *Proceedings of the National Academy of Sciences*, 111(7), pp. 2830–2835. doi: 10.1073/pnas.1320457111.

Schlücking, K. *et al.* (2013) 'A New β-Estradiol-Inducible Vector Set that Facilitates Easy Construction and Efficient Expression of Transgenes Reveals CBL3-Dependent Cytoplasm to Tonoplast Translocation of CIPK5', *Molecular Plant*, 6(6), pp. 1814–1829. doi: https://doi.org/10.1093/mp/sst065.

Serrano-Mislata, A. *et al.* (2017) 'DELLA genes restrict inflorescence meristem function independently of plant height', *Nature Plants*. Springer US, 3(9), pp. 749–754. doi: 10.1038/s41477-017-0003-y.

Serrano-Mislata, A., Schiessl, K. and Sablowski, R. (2015) 'Active Control of Cell Size Generates Spatial Detail during Plant Organogenesis', *Current Biology*. The Authors, 25(22), pp. 2991–2996. doi: 10.1016/j.cub.2015.10.008.

de Sousa, F. *et al.* (2019) 'Nuclear protein phylogenies support the monophyly of the three bryophyte groups (Bryophyta Schimp.)', *New Phytologist*. John Wiley & Sons, Ltd, 222(1), pp. 565–575. doi: https://doi.org/10.1111/nph.15587.

Torres-Acosta, J. A., Fowke, L. C. and Wang, H. (2011) 'Analyses of phylogeny, evolution, conserved sequences and genome-wide expression of the ICK/KRP family of plant CDK inhibitors', *Annals of Botany*, 107(7), pp. 1141–1157. doi: 10.1093/aob/mcr034.

Vanstraelen, M. *et al.* (2004) 'A plant-specific subclass of C-terminal kinesins contains a

conserved a-type cyclin-dependent kinase site implicated in folding and dimerization', *Plant physiology*. 2004/07/09. American Society of Plant Biologists, 135(3), pp. 1417–1429. doi: 10.1104/pp.104.044818.

Willis, L. *et al.* (2016) 'Cell size and growth regulation in the *Arabidopsis thaliana* apical stem cell niche', *Proceedings of the National Academy of Sciences*, 113(51), pp. E8238–E8246. doi: 10.1073/pnas.1616768113.

Xu, G. *et al.* (2009) 'Evolution of F-box genes in plants: Different modes of sequence divergence and their relationships with functional diversification', *Proceedings of the National Academy of Sciences*, 106(3), p. 835 LP-840. doi: 10.1073/pnas.0812043106.

Yadav, S., Gupta, M. and Bist, A. S. (2018) 'Prediction of Ubiquitination Sites Using UbiNets', *Advances in Fuzzy Systems*. Edited by M. O. Efe. Hindawi, 2018, p. 5125103. doi: 10.1155/2018/5125103.

Zhao, X. *et al.* (2012) 'A general G1/S-phase cell-cycle control module in the flowering plant Arabidopsis thaliana', *PLoS genetics*. 2012/08/02. Public Library of Science, 8(8), pp. e1002847–e1002847. doi: 10.1371/journal.pgen.1002847.

Chapter 5: A mathematical model for cell size homeostasis

5.1 Introduction

Reflecting the fact that size is a quantitative phenotype, mathematical modelling has played a prominent role in studies of how cells maintain size homeostasis (Turner, Ewald and Skotheim, 2012; Pan *et al.*, 2014; Schmoller *et al.*, 2015; Willis *et al.*, 2016; Facchetti, Chang and Howard, 2017; Jones *et al.*, 2017; Facchetti, Knapp, Flor-Parra, *et al.*, 2019). Modelling gives the opportunity to study cell size homeostasis in details that could not be addressed otherwise and highlights the limitations of a system. For example, it was through the understanding generated by modelling that Cdr2, the area sensor in *Schizosaccharomyces pombe* (Pan *et al.*, 2014), was subsequently engineered to sense length (Facchetti, Knapp, Flor-Parra, *et al.*, 2019), changing our understanding of what geometric quantity can be sensed by the cell. It is however important to understand that any proposed mathematical framework is only one of myriads of possible mechanisms employed by nature and needs to be challenged by experimental tests before being accepted. The field of cell size homeostasis offers unique examples in which suggested mechanism for homeostasis (Martin and Berthelot-Grosjean, 2009) did not survive experimental scrutiny (Wood and Nurse, 2013). Nevertheless, mathematical frameworks are particularly good at delineating the boundaries of a system and identifying what cannot
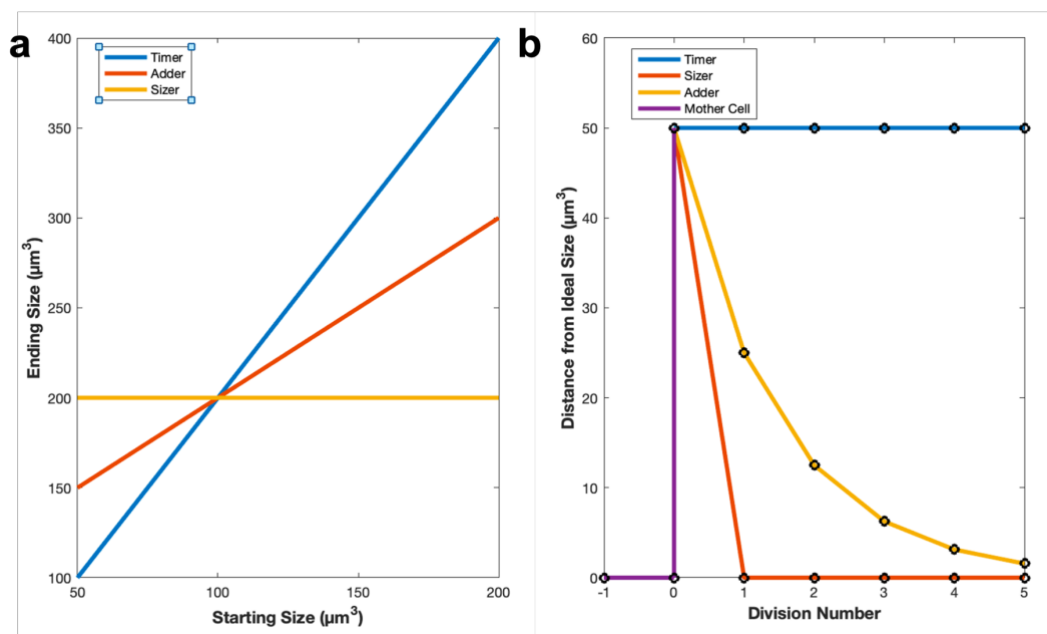
Figure 5.1: Phenomenological models of cell size homeostasis. a) Plots showing various possible relationships between starting and ending sizes (e.g. between birth and S-phase) and how those are identifiable as sizers, adders or timers. b) Plots showing how variability, represented as distance from the ideal size, is recovered by different models. At division number = 0, variability is introduced, and never introduced again, to show how this variability can be theoretically dissipated.

work, much more easily than uniquely identifying what can (Antoniou Kourounioti *et al.*, 2013; Antoniou-Kourounioti *et al.*, 2018; Ripoll *et al.*, 2019). With this sentiment, I took a mathematical approach to understand the limitations of the KRP4/FBl17 system in achieving cell size homeostasis and what features of the system still remain to be addressed.
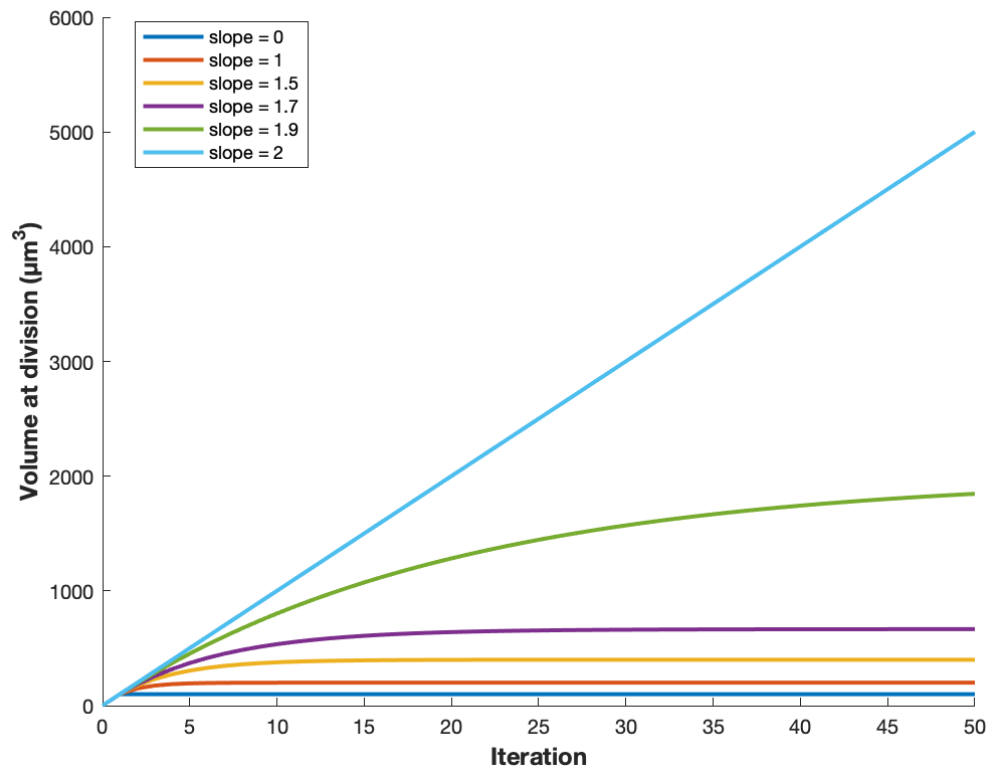
Figure 5.2: Effect of various slope values on target division volume. Simulation shows how slope values that are smaller than 2 converge to finite volume, thus can recapitulate homeostasis. In contrast, if the slope is higher or equal than 2 the target size is infinite (see text for more details).

As defined in the introductory Chapter 1, a cell population is said to be in size homeostasis if it is able to recover average cell size and lower cell size variability when perturbations in size occurs, for example as the result of asymmetric division for example. Thus, for a molecular mechanism to contribute to size homeostasis, it needs to act against the accumulated variability. In doing so, one can plot the starting and ending size (birth and S-phase for example) for each individual cell and measure the slope of the linear regression between those two. A slope zero would indicate that, regardless of the starting volume, the ending size is constant (Fig. 5.1a). This is called a sizer and it is the best most effective theoretical mechanism at counteracting variability, because it cell size variability to zero in just one round of division (Fig. 5.1b). A slope of one indicates that at the end of the cycle a

constant size is added to the starting one (Fig. 5.1a). This is called an adder and this system would halve the variability at each round of division (Fig. 5.1b). When a cell cycle phase has a constant time, the model is called a timer and the slope of the relationship between birth and division size is equal to two (Fig. 5.1a), assuming that the system is in homeostasis and the growth is exponential. However, these two assumptions are in fact incompatible for a timer, because this mechanism does not reduce variability, but it amplifies it, depending on the type of growth (Fig. 5.1b) (see also below).

Sizers, adders and timers are called phenomenological models and have been described in more detail elsewhere (Facchetti, Chang and Howard, 2017; D'Ario and Sablowski, 2019). Assuming that actual mechanisms for size regulation fit into these categories can be misleading for many reasons, one of which being that experimental errors often results in the misidentification between sizers and adders (Facchetti, Knapp, Chang, *et al.*, 2019). Additionally, molecular mechanism might not behave as simply, since non-integer slopes have been described (Willis *et al.*, 2016) (also recall a slope of -0.5 in Chapter 2) and even not behave linearly. However, these are useful starting ideas when discussing possible mechanism for size regulation.

Importantly, we can show that if the slope between size at birth and size at division is equal or higher than two homeostasis is broken, and cell size is bound to increase. To do so, let $V_d(n)$ be the volume at division after n iterations, s be the slope of the curve in the graph in question (Fig. 5.1a) and q the intercept of such curve. Let also assume that cells divide perfectly into two, we can therefore calculate $V_d(n+1)$ the volume at the $n+1$ iteration as:

$$(1) \qquad V_d(n+1) = s\frac{V_d(n)}{2} + q$$

The volume of convergence $\dot{V}$, the volume which the population would tend to, can be found observing that, after enough iterations, $\dot{V}(n) = \dot{V}(n+1)$ for every n, as long as n is large enough. Thus:

$$(2) \qquad \dot{V}(n) = \dot{V}(n+1) = s\frac{\dot{v}(n)}{2} + q \implies \dot{V}(n) = \frac{q}{\left(1-\frac{s}{2}\right)} = \frac{2q}{(2-s)}$$

From this equation it is clear that for $s > 2$ the volume at convergence would be negative and tend to infinity when s tends to 2. In other words, homeostasis can only be established for value smaller than 2. Figure 5.2 summaries this idea graphically, where simulations were carried out for various values of s, showing how each of these plateaus, except for $s = 2$. Values higher than 2 are not shown, but those tend to infinity even faster than for $s = 2$. With these considerations in mind, let us now dive into a mathematical treatment of how KRP4, FBL17 and DNA interact to reduce cell size variability.

5.2 Cell cycle length, growth rate and variability

Before moving into the details of the mathematical model it is important to establish some definitions related to growth. As discussed plentifully, I will assume that cells grow exponentially here for two main reasons: firstly, we have experimental data to support that it occurs in the shoot meristem (Chapter 2), and secondly, mechanisms to maintain size homeostasis are required particularly to deal with the error accumulated by exponential growth (Cooper, 2006, 2013; Lin and Amir, 2018). Furthermore, exponential growth is a simple consequence of the idea that any produced volume, in the form of cytoplasm, contributes to the production of more volume, in the form of cytoplasm (Cooper, 2013). In other words, the rate at which volume changes over time is proportional to the volume itself with some factor λ:

$$(3) \qquad \frac{\mathrm{d}V}{\mathrm{d}t} = \lambda V$$

λ is equivalent to the relative growth rate (see Chapter 2). Solving analytically this equation results in volume being expressed by an exponential relationship, explaining exponential increase as the expected mode of cellular growth (Miettinen and Björklund, 2016; Lin and Amir, 2018; Neurohr *et al.*, 2019):

$$(4) \qquad V_{\mathrm{exponential}}(t) = V_0 e^{\lambda t}$$

where V_0 is the volume at time zero.

An interesting consequence of exponential growth is that, assuming that a cell population is in homeostasis, the average cell cycle time T is constant and independent of cell volume

or the type of cell size homeostasis mechanism. The only parameter that affects average cell cycle time T is the relative growth rate λ. This is a consequence of the following:

$$(5) \qquad V_d = 2V_b \implies V_b e^{\lambda T} = 2V_b \implies e^{\lambda T} = 2 \implies \mathbf{T} = \frac{\ln 2}{\lambda}$$

This phenomenon has been reported experimentally in Arabidopsis meristem cells (Jones *et al.*, 2017), where it was observed that in certain cell cycle mutants, the average cell cycle time is comparable with wild-type controls, whilst the average cell size and the average length of individual cell cycle phases (i.e. G1 and G2) change dramatically (Jones *et al.*, 2017). To corroborate this observation, using the average relative growth rate from the data shown in Chapter 2 (0.0144h[-1]), Equation 3 would predict a cell cycle length of 48.1h, close to the experimentally observed average cell cycle time of 45.4h.

When considering cell size homeostasis, perhaps the most important consequence of exponential growth is its impact on accumulated variability. Variability resultant from growth can be calculated by using the experimentally calculated standard deviations (SDs) in time (δ) and starting volume (V_ε). As discussed in the introductory Chapter 1, fluctuations in growth rates can be attributed to molecular mechanism and tissue mechanics which can interact with cell cycle progression in non-trivial ways. Thus for simplicity, I decided to only consider fluctuations in time and starting volume for this section. For comparison, I will also consider linear growth, defined as:

$$(6) \qquad V_{\text{linear}}(t) = \lambda_l t + V_0$$

where λ_l is the equivalent to the absolute growth rate. When considering variability, the SD associated with time and volume are added to the respective values as follows:

$$(7) \qquad V_{\text{linear}}(t + \delta) = \lambda_l(t + \delta) + V_0 + V_\varepsilon = \lambda_l t + V_0 + \mathbf{V_\varepsilon} + \boldsymbol{\lambda_l \delta}$$

Again, δ is the SD associated with time t and V_ε is the SD associated with the starting volume V_0. In bold, I highlighted the calculated SD, for linear growth in this case. Note how the SD in this case does not depend on the time or volume themselves, but only on the inherent variability. In other words, the term $V_\varepsilon + \lambda_l \delta$ only has an additive effect on variability, not a multiplying one. This contrast with the calculated variability for exponential growth:

107

$$(8) \qquad V_{exponential}(t + \delta) = (V_0 + V_\varepsilon)e^{\lambda(t+\delta)} = V_0 e^{\lambda t} e^{\lambda \delta} + V_\varepsilon e^{\lambda t} e^{\lambda \delta} =$$

$$= V_0 e^{\lambda t} \left(e^{\lambda \delta} + \frac{V_\varepsilon}{V_0} e^{\lambda \delta} \right) = V_0 e^{\lambda t} + \mathbf{V_0 e^{\lambda t} \left(e^{\lambda \delta} + \frac{V_\varepsilon}{V_0} e^{\lambda \delta} - 1 \right)}$$

In this case the SD, highlighted in bold, is dependent on both starting volume V_0 and time t, therefore any starting variation is multiplied. To compare this with experimental data, in Table 5.1 I summarised data from Chapter 2 on growth during G2. Notice that in this case, the starting volume V_0 is the volume at the G1/S transition. Note how starting the coefficient of variation (CV = 0.13) is partially preserved assuming linear growth (CV = 0.16), but it almost doubles assuming exponential growth (CV = 0.23). In contrast, the experimentally observed variability is much smaller than the one predicted (CV = 0.13), corroborating the idea that a mechanism is in place to ensure suppression of the accumulated variability during growth in G2.

Variables	SDs		CVs	
λ (relative growth)	$0.017h^{-1}$			
λ_l (absolute growth)	$4\mu m^3 h^{-1}$			
V_0 (Volume at S)	$201.7\mu m^3$ SD (V_ε)	$25.8\mu m^3$ CV	0.13	
t (G2 length)	20.8h SD (δ)	5.2h		
V_d (experimental)	$272.3\mu m^3$ SD	$35.3\mu m^3$ CV	0.13	
V_d (exponential)	$289.7\mu m^3$ SD	$68.0\mu m^3$ CV	0.23	
V_d (linear)	$284.9\mu m^3$ SD	$46.6\mu m^3$ CV	0.16	

Table 5.1: Variables used to calculate accumulated variability during growth. SD = Standard Deviation. CV = coefficient of variation (calculated as standard deviation divided by the mean).

A further advantage of assuming exponential growth for mathematical modelling follows from the accumulated variability during growth: any mathematical model for size homeostasis should be able to suppress any amplifying variability.

5.3 The model

With the information gained in the previous chapters, we can now develop a model for the role of KRP4 in size homeostasis. Before describing the dynamic model, an idealised description of the pattern of KRP4 accumulation during cell cycle is given (Fig. 5.3). As seen in Chapter 3, the nuclear volume of meristem cells is in a linear relationship with the cell volume, with the former always measuring approximately a third of the latter. Therefore, there will be no discrimination between cellular and nuclear volume in this model, with term "volume" representing the general growth output of the cell (Fig. 5.3). Daughter cells

are born with equal amounts of KRP4 bound to DNA (referred to as C for complex) and equal concentration of nucleosolic KRP4 (referred to as F for free KRP) (Fig. 5.3a). Note that I will use the term DNA and chromatin here interchangeably, as these simply represents the "molecule" to which KRP4 is bound to. Cells then grow and dilute KRP4 during G1, until S-phase is triggered, when KRP4 concentration reaches a certain threshold (see below for mathematical definition of the threshold) (Fig. 5.3b). DNA is replicated during S-phase, which for simplicity is considered instantaneous in this model, and KRP4 production is activated (Fig. 5.3c). At the same time, FBL17 production is also activated. As we will see later, FBL17 production can occur at any time in G2, because the equilibrium between produced and degraded KRP4 is not dependent on the exact timing of FBL17 production. Therefore, for simplicity FBL17 production is also activated simultaneously to KRP4 production and considered instantaneous. In this model the length of G2 is considered constant, even though there is strong evidence for size regulation at G2. A timer was chosen for G2 because any conclusion on homeostasis should be linked to the KRP4 system and not be masked by any assumed additional mechanism during G2. Of course, there are mechanism that would increase variability even more than a timer, but a timer is an easy mechanism to understand, implement and study, while still contributing to variability. So, once enough time in G2 has passed, the cell divides asymmetrically, and the cycle starts again (Fig. 5.3a).
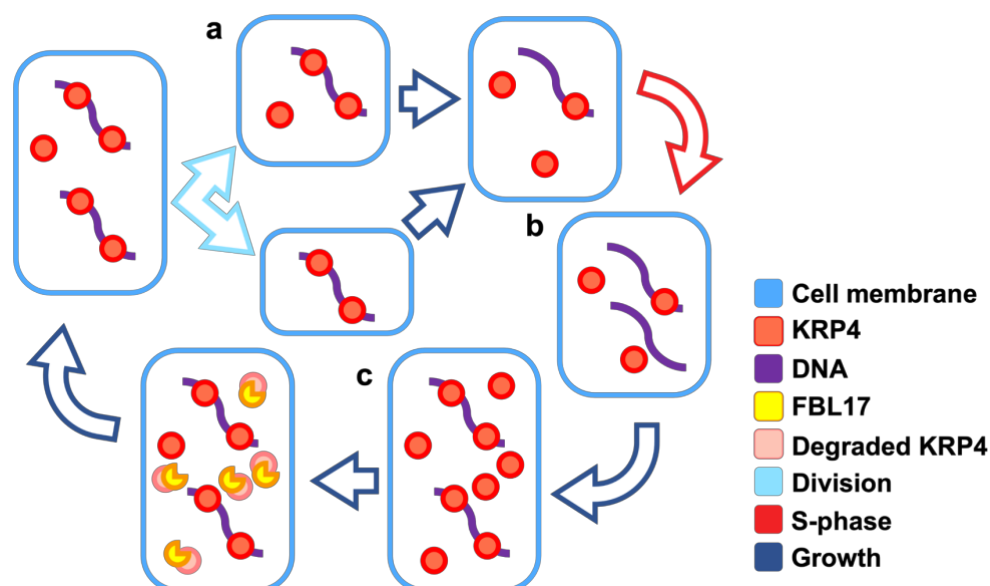
Figure 5.3: Conceptualised model for cell cycle progression and KRP4 accumulation. a) Two cells are born, inheriting equal amount of DNA-bound KRP4 and free KRP4 proportional to the volume. b) They dilute KRP4 until a certain threshold is reached and the cells enter S-phase, duplicating DNA. c) KRP4 production is activated and FBL17 is also produced, removing KRP4 that is not bound to DNA. Finally, the cell reaches the end of G2, which is assumed to be on a timer (see text), and divides, ready for another round.

To this conceptualised cell cycle progression, a mathematical model is added, which describes the dynamics of binding, unbinding, production, and degradation of KRP4 during growth. Before moving to the formalisation of such dynamics, let me introduce some of the notations that I will use in this chapter. When referring to the amount of a molecule, i.e. the absolute number of those molecules, I will use the notation N with a subscript representing a certain molecule (e.g. N_m, number of molecules M), whilst when referring to a concentration of a certain molecule I will use a capital letter (e.g. M, concentration of molecule M). From the definition, it is clear that, for any volume V:

$$(9) \qquad\qquad M = \frac{N_m}{V}$$

The concentration of a molecule is equal to its amount divided by the volume. There will be three events that change how the system behaves: cell birth, S-phase and division. Given the importance of these events, I will use the subscripts b, S and d to represent these transitions. So, for example, the volume at birth will be V_b and the number of molecules M at S-phase is N_{m_S}. Finally, I will use the subscripts 1 and 2 to represents constants and variables during G1 and during G2, respectively.
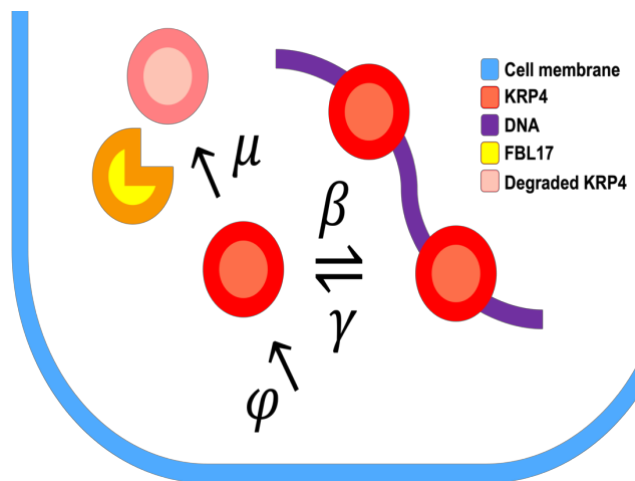
Figure 5.4: Conceptualised model for KRP4 dynamics. KRP4 exists in 2 populations, one bound to DNA and the other free in the nucleoplasm. KRP4 binds to DNA with a binding rate β and it enters the nucleoplasm with a rate of γ. In G2, its production φ is activated and FBL17 targets KRP4 for degradation with a rate of μ.

With this set of notations, Figure 5.4 shows a cartoon of a magnified cell nucleus, showing the dynamics I aim to describe. This cartoon can be formalised as follows

$$(10) \qquad\qquad \begin{array}{cc} \uparrow_\mu & \beta \\ F + D & \rightleftharpoons C \\ \uparrow_\varphi & \gamma \end{array}$$

Where F represents free nucleosolic KRP4, represented in Figure 5.4 as a free-floating red circle; D is free chromatin, i.e. chromatin which is unoccupied by KRP4, purple line in Figure 5.4; and C is the complex formed by KRP4 and chromatin. β and γ are constants representing the rate of chromatin-binding and unbinding by KRP4, respectively, φ is the rate of KRP4 production and μ represents the rate of KRP4 degradation by FBL17. Note that KRP4 can only be produced in its nucleosolic form, representing the fact that KRP4 is not synthesised on chromatin. Similarly, degradation of KRP4 by FBL17 only occurs in its nucleosolic form, representing the mechanism proposed in Chapter 4, where KRP4 interaction with chromatin prevents its ubiquitination by FBL17. The KRP4 amount only changes during G2, so I used a Boolean multiplier (g_2) to effectively set to zero the production and degradation dynamics during G1 ($g_2 = 0$) and switch this on during G2 ($g_2 = 1$). Equation (10) can be written in its differential form as follows:

$$
(11) \quad
\begin{cases}
\dfrac{dN_f}{dt} = \gamma N_c - \beta \dfrac{N_f N_d}{V} + (\varphi V - \mu N_f)g_2 \\
\dfrac{dN_d}{dt} = \gamma N_c - \beta \dfrac{N_f N_d}{V} \\
\dfrac{dN_c}{dt} = \beta \dfrac{N_f N_d}{V} - \gamma N_c
\end{cases}
$$

Note how the rate of complex formation $\beta \dfrac{N_f N_d}{V}$ is inversely proportional to the volume, representing that the bigger the cell, the harder it is for a KRP4 molecule to encounter chromatin. The total amount of DNA (θ) is constant and only doubles at G2. So total DNA at G1 is equivalent to the amount of free DNA, plus the amount of DNA-KRP4 complexes:

$$
(12) \quad N_{d_1} + N_{c_1} = \theta
$$

Note that in G2, the total amount of DNA is simply 2θ. Similarly, the total amount of KRP4 molecule at G1 (κ) is constant and can be calculated by adding the number of free KRP4 to the number of KRP4-DNA complexes:

$$
(13) \quad N_{f_1} + N_{c_1} = \kappa
$$

Unlike DNA, the total amount of KRP4 is not constant in G2 and we will see shortly how it changes through time.

Finally, the number of KRP4 molecules that decorate DNA will be fewer as the cell grows and total KRP4 is diluted. Once a certain minimum number of KRP4-DNA complexes (N_{c_s}) is reached, the S-phase transition is triggered. I will define a proportionality factor α (such that $\alpha > 1$) to represent the minimum amount of KRP4-coated DNA required for S-phase transition, in proportion to the total DNA as follows:

$$\alpha N_{c_s} = \theta \tag{14}$$

In this way, DNA and DNA-KRP4 complexes required for S transition can be written as a function of each other. It is important to define S-phase transition as a function of either the amount of KRP4 on chromatin or the concentration of KRP4 in the nucleoplasm, because any machinery that acts downstream of KRP4, most likely directly through CDKa, would either interact with one form or the other, in a distinct manner, but not as if they both were diluted in the nucleus together. As we will see later, the S-phase transition can be defined using either form of KRP4, interchangeably.

Variable	Value	Description
β	$1\mu m^3 min^{-1}$	DNA binding rate
γ_2	$0.1 min^{-1}$	DNA unbinding rate
φ	$0.1\mu m^{-3} min^{-1}$	Production rate
μ	$0.5 min^{-1}$	Degradation rate
θ	2	DNA copies
λ	$0.017 h^{-1}$	Relative growth
V	$200\mu m^3$	Volume

Table 5.2: Variables used for the phase plane plot. These variables were used for the plot shown in Figure 5.5.

5.4 KRP4 behaviour in G2

We will now try to answer the question on whether KRP4 can fully decorate DNA by the end of a G2 cycle, and how efficient is FBL17 required to be in order to accomplish this feat. In doing so, we will need to calculate the KRP4 amount before division and will be able to describe some interesting properties of protein production. First of all, let us start by analysing how KRP4 accumulates during G2 and what is the effect of FBL17 on it. To do so, Table 5.2 summarises the rates that will be used in this section, to describe the dynamics in G2. Note that the binding and unbinding of KRP4 happens relatively faster than production and degradation, with binding (β) occurring 10 time faster than production (φ) and unbinding twice as fast than degradation (μ). To visualise this, phase plane method can

be implemented. To do so, two variables, in this case the amount of DNA-bound KRP4 molecules (N_c) and the concentration of free KRP4 (F) are plot against each other (Fig. 5.5). Then, for each point, a vector is plotted on the graph to represent the rate of change of each variable. In this way, each vector represents the velocity at which the system moves towards the steady state. The steady state of each variables is represented on this graph by the solid curves (Fig. 5.5, red for F and purple for N_c). The intercept between those curves is the convergence point, i.e. the steady state, of the whole system.
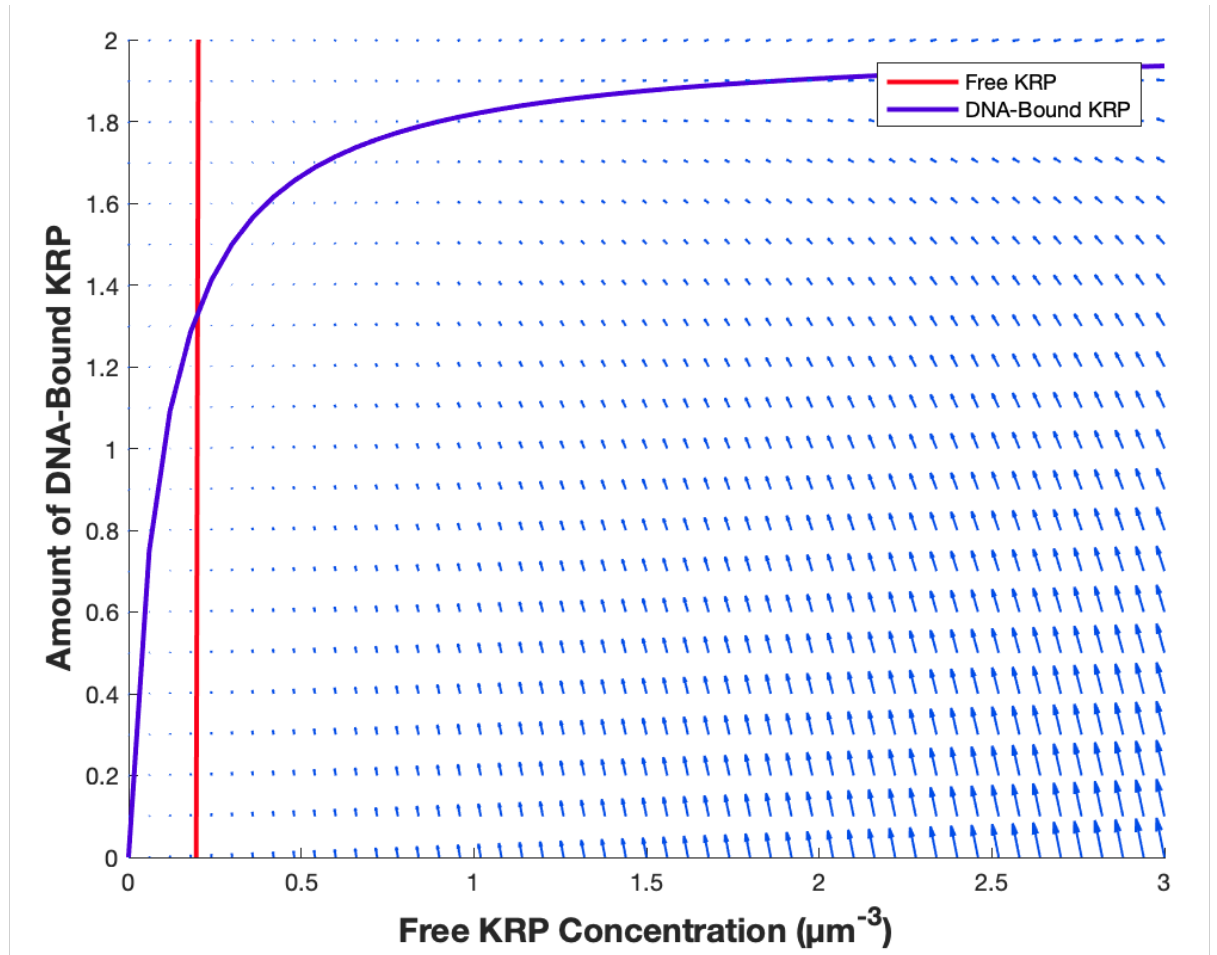
Figure 5.5: Phase plane plot of KRP4 Dynamics in G2. The arrows are calculated by solving the derivative of the equation in that point and represents how each pair of values moves towards equilibrium. The solid lines represent the quasi-steady-state of free nucleosolic KRP4 (F, red) and DNA-bound KRP4 (N_c, purple). Notice how the arrows point more prominently towards DNA-bound KRP4, because binding is much faster than production. Table 2 contains the values used in this plot.

The equation of the steady states of N_c and F can be calculated using (11) as follows:

(15) $$\frac{dN_d}{dt} = 0 = \gamma N_c - \beta \frac{N_f N_d}{V} \Longrightarrow \gamma N_c = \beta F(2\theta - N_c) \Longrightarrow$$

$$N_c(\gamma + \beta F) = \beta 2\theta F \Longrightarrow \mathbf{N_c} = \frac{2\beta\theta F}{\gamma + \beta F}$$

113

and for the concentration of free KRP4 (F):

(16) $\quad \frac{dN_f}{dt} = 0 = \gamma N_c - \beta \frac{N_f N_d}{V} + \varphi V - \mu N_f \Longrightarrow -\gamma N_c = -\beta F(2\theta - N_c) + \varphi V -$

$\mu N_f \Longrightarrow -\gamma N_c = F(-\beta 2\theta + \beta N_c - \mu V) + \varphi V \Longrightarrow F(-\beta 2\theta + \beta N_c - \mu V) = -\gamma N_c -$

$\varphi V \Longrightarrow$

$$\mathbf{F} = \frac{-\gamma N_c - \varphi V}{-\beta 2\theta + \beta N_c - \mu V} = \frac{\boldsymbol{\gamma N_c + \varphi V}}{\mathbf{2\beta\theta - \beta N_c + \mu V}}$$

Note that 2θ is used here instead of θ to represent double of DNA amount during G2. The phase plane plots show how the system reaches steady state much faster for DNA binding than it does for KRP4 production (Fig. 5.5). In other words, given any total amount of KRP4 in G2 and a random partitioning of KRP4 between nucleosol and chromatin, the system will quickly tend to resolve the binding dynamics of KRP4. Therefore, we can assume that:

(17) $$\gamma N_c - \beta \frac{N_f N_d}{V} \ll \varphi V - \mu N_f$$

And solve the following:

(18) $$\frac{dN_f}{dt} = \varphi V - \mu N_f$$

Assuming that the system is in quasi-steady-state, we can calculate the final concentration as follows:

(19) $$\frac{dN_f}{dt} = 0 = \varphi V - \mu N_f \Longrightarrow \mu N_f = \varphi V \Longrightarrow F = \frac{\varphi}{\mu}$$

Interestingly, we can show that this upper limit is never reached as long as the cell is growing, which will be important later when the effect of FBL17 is discussed. To show that (19) is never reached in a growing cell, let us consider (18) not at quasi-steady-state and let us solve this differential equation. I will use the notion of exponential growth as defined in (3) and (4):

(20) $$\frac{dN_f}{dt} = \varphi V - \mu N_f \Longrightarrow \frac{dN_f}{dt} + \mu N_f = \varphi V$$

114

To solve this linear differential equation, let the function $h(t)$ be defined as follows:

$$(21) \qquad h(t) = e^{\int \mu \, dt} = e^{\mu t}$$

By multiplying both sides of (18) by $h(t)$ we obtain:

$$(22) \qquad h(t)\left(\frac{dN_f}{dt} + \mu N_f\right) = h(t)\varphi V \Longrightarrow \frac{dN_f}{dt}e^{\mu t} + \mu N_f e^{\mu t} = \varphi V e^{\mu t}$$

The factor on the left is the result of the derivate of a product, therefore:

$$(23) \qquad \frac{d}{dt}(N_f e^{\mu t}) = \varphi V e^{\mu t}$$

Finally, by integration:

$$(24) \qquad N_f e^{\mu t} = \int \varphi V e^{\mu t} dt$$

Here we will use the exponential growth to our advantage. Using the definition of exponential growth (4), (24) can be solved as follows:

$$(25) \qquad N_f e^{\mu t} = \varphi \int V e^{\mu t} dt = \varphi \int V_0 e^{\lambda t} e^{\mu t} dt = \varphi V_0 \int e^{(\lambda+\mu)t} dt =$$

$$\frac{\varphi}{\lambda+\mu} V_0 e^{(\lambda+\mu)t} + c \Longrightarrow N_f = \frac{\frac{\varphi}{\lambda+\mu} V_0 e^{(\lambda+\mu)t} + c}{e^{\mu t}} = \frac{\varphi}{\lambda+\mu} V_0 e^{\lambda t} + \frac{c}{e^{\mu t}} = \frac{\varphi}{\lambda+\mu} V + \frac{c}{e^{\mu t}}$$

Then by dividing by the volume we have:

$$(26) \qquad \frac{N_f}{V} = \frac{\frac{\varphi}{\lambda+\mu} V + \frac{c}{e^{\mu t}}}{V} \Longrightarrow F = \frac{\varphi}{\lambda+\mu} + \frac{c}{V e^{\mu t}}$$

To solve for c, let us set $F_0 = 0$. This is the case that would take the longest for producing KRP4 to saturation. At $t_0 = 0$ we have:

$$(27) \qquad 0 = \frac{\varphi}{\lambda+\mu} + \frac{c}{V_0} \Longrightarrow c = -\frac{\varphi}{\lambda+\mu} V_0$$

Finally, F be written as follows:

$$(28) \qquad F = \frac{\varphi}{\lambda+\mu}\left[1 - e^{-(\mu+\lambda)t}\right]$$

The maximum concentration reached by F can be easily calculated by sending t to infinity:

$$(29) \qquad \lim_{t\to\infty} F = \frac{\varphi}{\lambda+\mu}$$

This relationship shows two important feature of protein production: firstly, the effect of growth in protein production is numerically the same as the effect of degradation. In fact, increasing or decreasing either the growth rate λ or degradation rate μ would have the same effect on the maximum concentration. Secondly, as long as a cell grows the quasi-steady-state for protein production calculated in (19) can never be reached. This is important because without degradation (i.e. for $\mu = 0$) the steady state predicts an infinite concentration of the protein, clearly impossible, whilst we have now shown that in this case the concentration of protein would tend to $\frac{\varphi}{\lambda}$. Therefore, when considering the rate of degradation, the growth rate must be taken in consideration too. To corroborate this observation, let us now estimate how fast production of KRP4 and degradation by FBL17 has to be, in order for DNA to be fully coated by the end of G2. To do so, Equation (28) can be interpreted as follows: the limit shown in (29), represents the maximum concentration of free KRP4 protein, and the term $e^{-(\mu+\lambda)t}$ represents the missing concentration of free KRP4 at t to reach this limit, expressed as a percentage. For example, if F has reached 95% of its maximum concentration, $e^{-(\mu+\lambda)t} = 100\% - 95\% = 5\%$. Let us denotate this missing percentage as η, so we can calculate the time required to produce $100\% - \eta$ of F as follows:

$$(30) \qquad e^{-(\mu+\lambda)t} = \eta \Rightarrow -(\mu + \lambda)t = \ln\eta \Rightarrow \mathbf{t} = -\frac{\ln\eta}{\mu+\lambda}$$

Interestingly, if there is no degradation ($\mu = 0$) the time required to reach 50% of F is:

$$(31) \qquad t = -\frac{\ln\eta}{\mu+\lambda} = -\frac{\ln\frac{1}{2}}{\lambda} = \frac{\ln 2}{\lambda}$$

As seen in Equation (5), this is the average length of the cell cycle, indicating that degradation is required for allowing sufficient production of KRP4. In other words, considering protein production dynamics, FBL17 is required for allowing cycling cells to produce the right amount of KRP4 in time for division. Surprisingly, the rate of protein production φ does not appear in (30). Thus, protein production has no impact on the time required to reach maximum concentration, rather it only plays a role in setting its limit. Therefore, the impact of FBL17 degradation goes beyond its role in ensuring that the right amount of KRP4 is produced, but it is required to ensure that this is achieved in time for division.

We can now calculate how fast the degradation rate needs be to ensure that this limit is reached. Let us assume that G2 length T_2 is shorter than ½ of the cell cycle (in our case it was ~ 46%), so I will use ¼, to be excessive. Therefore, if $T = 4T_2$ and we have:

$$(32) \qquad\qquad T = \frac{\ln 2}{\lambda} = 4T_2 \Longrightarrow T_2 = \frac{\ln 2}{4\lambda}$$

We can now calculate the FBL17 degradation rate μ as function of the growth rate λ and KRP4 missing percentage η. We have:

$$(33) \qquad T_2 = \frac{\ln 2}{4\lambda} > -\frac{\ln \eta}{\mu+\lambda} \Longrightarrow \frac{\mu+\lambda}{4\lambda} > \frac{\ln \eta^{-1}}{\ln 2} \Longrightarrow \mu + \lambda > \frac{\ln \eta^{-1}}{\ln 2}4\lambda \Longrightarrow$$

$$\mu > \left(\frac{\ln \eta^{-1}}{\ln 2}4 - 1\right)\lambda$$

For a requirement of 99% (i.e. $\eta = 1\%$) there is enough time in G2 as long as $\mu > 26\lambda$. For a requirement of 99.9% (i.e. $\eta = 0.1\%$) $\mu > 39\lambda$ and for 99.99% (i.e. $\eta = 0.01\%$) $\mu > 52\lambda$. Since the timescale for μ is on the magnitude of minutes (Table 5.2) and λ on the magnitude of hours (Table 5.2), cells are expected to easily complete this task. In the case of my simulation (see below), $\mu \cong 1750\lambda$, so the condition would also hold for much shorter G2 lengths. Interestingly, simulations (see below) showed that disruption of homeostasis is only reached for values of μ that are well away from this range, suggesting that the time required to fully decorate DNA is never a limiting factor in the particular case that we are studying. Nevertheless, it highlights a non-trivial relationship between degradation and growth, which is intrinsic for these two variables, and does not require other variables, like

protein production. Additionally, this observation has consequences on the possible way that the system has evolved, as discussed in more details in the discussion section.

With this result we can finally calculate the total amount of KRP4 molecules at division κ_d. Thanks to (33), we can approximate the concentration of free KRP4 with its limit shown in (29) ($F = \frac{\varphi}{\lambda + \mu}$) and we can use this information to calculate the amount of DNA-bound KRP4 N_{c_d} using (15), as follows:

$$(34) \qquad N_{c_d} = \frac{2\beta\theta F}{\gamma + \beta F} = \left(\frac{\gamma + \beta F}{2\beta\theta F}\right)^{-1} = \left(\frac{1}{2\theta} + \frac{\gamma}{2\beta\theta F}\right)^{-1} = 2\theta \left(1 + \frac{\gamma(\lambda + \mu)}{\beta\varphi}\right)^{-1}$$

Indicating that at division, the amount of DNA-bound KRP4 N_{c_d} is a constant, proportional to DNA content θ. Therefore, the total amount of KRP4 molecules at division κ_d can be calculated as follows:

$$(35) \qquad \kappa_d = N_{c_d} + N_{f_d} = N_{c_d} + F_d V_d = 2\theta \left(1 + \frac{\gamma(\lambda + \mu)}{\beta\varphi}\right)^{-1} + \frac{\varphi}{\lambda + \mu} V_d$$

We can finally calculate the total amount of KRP4 at birth, considering that the part associated with chromatin will halve precisely (i.e. 2θ will become θ) and the volume at division will now be the volume at birth:

$$(36) \qquad \kappa_b = \theta \left(1 + \frac{\gamma(\lambda + \mu)}{\beta\varphi}\right)^{-1} + \frac{\varphi}{\lambda + \mu} V_b$$

Note how the total amount of KRP4 is dependent on volume, even if the association with DNA should push it toward volume independency. To further this observation, I want to ask the following question: given that the system ultimately needs to produce an amount of KRP4 independent from cell size, does its rate of accumulation need to be size independent? Using total KRP4 is a convenient parameter since this is the only one that can be realistically measured experimentally. To do so let first see how the binding dynamics affects the rate of production of KRP4, and whether binding to DNA would result in KRP4 accumulating in a size independent manner. In other words, I want to find $\frac{dN_{\kappa_2}}{dt}$ where N_{κ_2} is the total amount of KRP4 in G2, or:

(37)
$$N_{f_2} + N_{c_2} = N_{\kappa_2}$$

By calculating the derivative of (37) and substituting using (11), we have:

(38)
$$\frac{dN_{\kappa_2}}{dt} = \frac{d(N_c + N_f)}{dt} = \frac{dN_c}{dt} + \frac{dN_f}{dt} = \varphi V - \mu N_f$$

which is the same rate of production of a protein if no binding/unbinding dynamics were present. In other words, binding/unbinding to DNA does not affect the rate of accumulation of KRP4 in G2. Let us now study the rate of change of total KRP4 over the volume:

(39)
$$\frac{dN_{\kappa_2}}{dt} \frac{dt}{dV} = \frac{dN_{\kappa_2}}{dV}$$

Therefore, assuming exponential growth we can calculate $\frac{dN_{\kappa_2}}{dV}$:

(40)
$$\frac{dN_{\kappa_2}}{dV} = \frac{\varphi V - \mu N_f}{\lambda V} = \frac{\varphi}{\lambda} - \frac{\mu}{\lambda} F$$

Therefore, whilst KRP4 is being produced and the free KRP4 concentration (F) has not reached its maximum, the rate of change of total KRP over the volume is never zero, so KRP4 accumulation always will be dependent on volume. Note that this result in not dependent on exponential growth and a similar conclusion can be achieved in the case of linear growth:

(41)
$$\frac{dN_{\kappa_2}}{dV_{linear}} = \frac{\varphi V - \mu N_f}{\lambda_l} = \frac{V}{\lambda_l}(\varphi - \mu F)$$

Similarly, this relationship is always bigger than zero. This observation is important because other proposed mechanisms for size homeostasis, require a cell size-independent production step (Schmoller *et al.*, 2015; Zatulovskiy *et al.*, 2020). This would require the coordination of various cell processes to occur, like a precise length of G2 (Schmoller *et al.*, 2015), therefore demanding high precision to achieve an accurate system. The system we present here, instead, is more robust because it does not rely on precise events, rather on a series of imprecise events that produce a highly accurate system. To prove this statement, we will need to study the behaviour of the system in G1.

5.5 KRP4 in G1 and volume prediction at S-phase

With the information on G2 set, let us now study the system in G1 and find a way to determine the volume at S-phase (V_S) as a function of the various system parameters. This will be important to understand the impact of the different components of this system on cell size homeostasis. Recall from (14) the definition of the proportionality factor α (such that $\alpha > 1$) representing the minimum amount of KRP4-coated DNA required for the S-phase transition, in proportion to the total DNA. Using (12) and (14), with N_{d_S} the number of free DNA-binding sites at S and N_{c_S} the number of KRP4 molecules bound to DNA at S, we have:

$$(42) \qquad N_{d_S} + N_{c_S} = \theta = \alpha N_{c_S} \Rightarrow \mathbf{N_{d_S}} = \alpha N_{c_S} - N_{c_S} = \mathbf{(\alpha - 1)N_{c_S}}$$

Let us consider the system at quasi-steady-state during the transition at S. Using (11) we have:

$$(43) \qquad \frac{dN_d}{dt} = \gamma N_c - \beta \frac{N_f N_d}{V} = 0 \Rightarrow \gamma N_{c_S} = \beta \frac{N_{f_S} N_{d_S}}{V_S} \Rightarrow V_S = \frac{\beta}{\gamma} \frac{N_{f_S} N_{d_S}}{N_{c_S}} =$$

$$\frac{\beta}{\gamma} \frac{N_{f_S} N_{c_S}(\alpha - 1)}{N_{c_S}} \Rightarrow \mathbf{V_S} = \frac{\beta}{\gamma}(\alpha - 1)\mathbf{N_{f_S}}$$

Note that whilst α, β and γ are constants, by definition, the number of free KRP4 molecules at S (N_{f_S}) is not. However, when considering the concentration of free KRP4 molecules at S (F_S) by dividing the number of these molecule by the volume:

$$(44) \qquad V_S = \frac{\beta}{\gamma}(\alpha - 1)N_{f_S} \Rightarrow \frac{V_S}{N_{f_S}} = \frac{\beta}{\gamma}(\alpha - 1) \Rightarrow \mathbf{F_S} = \frac{\gamma}{\beta(\alpha - 1)}$$

In addition, for the DNA-bound KRP4, we have:

$$(45) \qquad \frac{dN_d}{dt} = \gamma N_c - \beta \frac{N_f N_d}{V} = 0 \Rightarrow \gamma N_{c_S} = \beta \frac{N_{f_S}(\theta - N_{c_S})}{V_S} = \beta F_S(\theta - N_{c_S}) \Rightarrow$$

$$\mathbf{N_{c_S}} = \frac{\beta F_S \theta}{\gamma + \beta F_S}$$

Together, these results mean that during S-phase transition, there is a fixed amount of KRP4 molecules decorating chromatin (N_{c_S}) and a fixed concentration of free KRP4 in the

nucleoplasm (F_s), highlighting how interconnected these two KRP4 populations are, one in amount and the other in concentration. This also implies that either the amount on DNA or the concentration in the nucleoplasm can be used by the cell, interchangeably, as a means to decide whether to trigger the S-phase transition.

Equation (45) is equivalent to equation (15) but during G1, so total DNA is θ instead of 2θ. Since the total number of KRP4 molecules is constant during G1, we have:

$$(46) \qquad \kappa_b = N_f + N_c = FV + \frac{\beta F \theta}{\beta F + \gamma} \Rightarrow \kappa_b - FV = \frac{\beta F \theta}{\beta F + \gamma} \Rightarrow V = \frac{\kappa_b}{F} - \frac{\beta \theta}{\beta F + \gamma}$$

So, at S:

$$(47) \qquad V_S = \frac{\kappa_b}{F_S} - \frac{\beta_1 \theta}{\beta_1 F_S + \gamma_1}$$

So, as longs as the cell starts with a constant amount of KRP4 molecules, the volume at S will be the same, suggesting this system can produce cell size homeostasis, as long as κ_b allows for it. Note I used the subscript 1 in (47) to denotate those variables during G1, as this will help with the next step. We can now combine the information on the KRP4 amount at birth obtained in (36) to find:

$$(48) \qquad V_S = \frac{\varphi}{F_S(\lambda+\mu)} V_b + \frac{\theta}{F_S}\left(1 + \frac{\gamma_2(\lambda+\mu)}{\beta_2 \varphi}\right)^{-1} - \frac{\beta_1 \theta}{\beta_1 F_S + \gamma_1}$$

With some more substitution, this becomes:

$$(49) \qquad V_S = \frac{\varphi}{(\lambda+\mu)}\frac{\beta_1(\alpha-1)}{\gamma_1} V_b + \frac{\beta_1(\alpha-1)}{\gamma_1}\frac{\theta\beta_2\frac{\varphi}{(\lambda+\mu)}}{\beta_2\frac{\varphi}{(\lambda+\mu)}+\gamma_2} - \frac{\theta\beta_1}{\frac{\gamma_1}{(\alpha-1)}+\gamma_1}$$

Note that, in spite of the multiple variables, each component is still recognisable. The concentration of inherited free KRP4 ($F_b = \frac{\varphi}{(\lambda+\mu)}$), which is the same at birth and the end of G2. $F_S = \left(\frac{\beta_1(\alpha-1)}{\gamma_1}\right)^{-1}$ is the concentration of KRP4 during the S-phase transition. $N_{c_b} = \frac{\theta\beta_2\frac{\varphi}{(\lambda+\mu)}}{\beta_2\frac{\varphi}{(\lambda+\mu)}+\gamma_2}$ is the number of inherited KRP4 molecules bound to chromatin at birth (multiply

by 2 to have the molecular number before division). $\frac{N_{c_S}}{F_S} = \frac{\theta\beta_1}{\frac{\gamma_1}{(\alpha-1)}+\gamma_1}$ is the ratio between thresholds of DNA-bound KRP4 and free KRP4 that triggers S-phase. Note that all of these quantities are constant during S-phase, except for the volume at birth V_b, and can be easily used to compute the volume at S-phase.

We can finally use this equation to see whether this dynamic system can recapitulate size homeostasis. This equation has the same form used experimentally to determine what type of phenomenological model this system is (see introduction and the notion of sizer, adder and timer). The term multiplying V_b is the term determining the type of phenomenological mode, and it is necessary that this term is smaller than 2 for homeostasis to be achieved, as explained in (2) and Figure 5.2. As seen in Chapter 2, this was measured to be equal to 0.5 experimentally. Furthermore, if $\frac{\varphi}{(\lambda+\mu)}\frac{\beta_1(\alpha-1)}{\gamma_1} = 1$ (adder behaviour) the remaining term

$(\frac{\beta_1(\alpha-1)}{\gamma_1}\frac{\theta\beta_2\frac{\varphi}{(\lambda+\mu)}}{\beta_2\frac{\varphi}{(\lambda+\mu)}+\gamma_2} - \frac{\theta\beta_1}{\frac{\gamma_1}{(\alpha-1)}+\gamma_1})$ represents added volume. If $\frac{\varphi}{(\lambda+\mu)}\frac{\beta_1(\alpha-1)}{\gamma_1} = 0$ (sizer behaviour) the remaining term $(\frac{\beta_1(\alpha-1)}{\gamma_1}\frac{\theta\beta_2\frac{\varphi}{(\lambda+\mu)}}{\beta_2\frac{\varphi}{(\lambda+\mu)}+\gamma_2} - \frac{\theta\beta_1}{\frac{\gamma_1}{(\alpha-1)}+\gamma_1})$ represents the target volume.

Of course, intermediate behaviours are also possible. For simplicity I will refer to the term

$\frac{\beta_1(\alpha-1)}{\gamma_1}\frac{\theta\beta_2\frac{\varphi}{(\lambda+\mu)}}{\beta_2\frac{\varphi}{(\lambda+\mu)}+\gamma_2} - \frac{\theta\beta_1}{\frac{\gamma_1}{(\alpha-1)}+\gamma_1}$ as the target volume.

I will now show that this system cannot preserve homeostasis unless a further assumption is made. Conceptually, for the system to converge $\frac{\varphi}{(\lambda+\mu)}\frac{\beta_1(\alpha-1)}{\gamma_1}$ has to be relatively small. For this to be true, either the red term (inherited free KRP4) or the yellow term (free KRP4 at S) has to be very small. If either of these is very small, the term $\frac{\beta_1(\alpha-1)}{\gamma_1}\frac{\theta\beta_2\frac{\varphi}{(\lambda+\mu)}}{\beta_2\frac{\varphi}{(\lambda+\mu)}+\gamma_2}$ would be very small (note how that both red and yellow terms appear here too), therefore making the target volume negative. So far, we assumed that the binding constant γ in G1 has the same value in G2, but I allowed a notation to distinguish them mathematically. As a matter of fact, if we allow the unbinding rate in G1 (γ_1) to be relatively large compared to the unbinding rate in G2 (γ_2), it is possible to render the terms that multiplies V_b very small, whilst allowing the target volume to remain positive allowing for relatively large N_{c_b} (notice γ_2 in the light blue term) and relatively small N_{c_S} (notice γ_1 in the dark blue term). As a matter of fact, I was never able to run a numerical simulation to recapitulate homeostasis,

unless I had different γ in G1 and G2. The alternative way to obtain a similar result would be to change the binding rate β.

This information tells us something critical about this system and what are its limitations: the speed of the KRP4 dynamics in G2 must be different from the dynamics in G1, or cell size homeostasis cannot be achieved. This is reasonably intuitive because KRP4 in G1 and in G2 is performing two distinct functions. In G1, KRP4 measures cell volume against DNA concentration: it therefore needs to be mobile and readily pass information on size from chromatin to the nucleosol – its unbinding rate γ_1 has to therefore be big. In contrast, in G2 the role of KRP4 is to coat DNA, tightly, and ensure full saturation before division – its unbinding rate γ_2 has to therefore be close to zero.
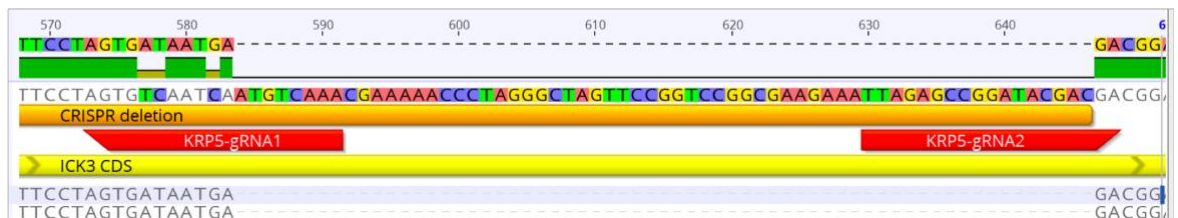
Figure 5.6: Sequencing of KRP CRISPR Mutants. (a) Deletion in the *KRP3* gene in the *krp3-11* mutant line. Deletion of 49bp in the first exon resulted in a premature stop codon (back asterisks) (b). (c) Deletion of 63bp preserved the frame of the protein. The red arrows represent the guide RNA (gRNA) used in designing the CRIPSR constructs. The yellow bar represents the CDS of the protein as reported on NCBI (note that the ICK notation is used instead).

Equation (49) is a useful tool to predict various phenotypes and explain how certain characteristics might arise. For this reason, I will simplify the equation to a more accessible form, removing some of the constants that define S-phase entry. Since the following section mainly focus on mutants that affects the G2 dynamics and not threshold, I will only preserve the information related to the former. Note that the removed terms (N_{c_S} and F_S) are constants. So, the equation can be summarised as:

$$(50) \qquad V_S \propto \frac{\varphi}{\lambda+\mu} V_b + \frac{\theta \beta_2 \frac{\varphi}{(\lambda+\mu)}}{\beta_2 \frac{\varphi}{(\lambda+\mu)}+\gamma_2} \Rightarrow \mathbf{V_S} \propto \mathbf{F_b V_b} + \boldsymbol{\theta}$$

5.6 Mutants in the KRP family

We can now use the Equation (50) to predict the behaviour of various mutants in the KRP family. Most specifically, I will discuss KRP3,4 and 5, which share very similar subcellular behaviours (see Chapter 4). There are two possibilities when considering KRPs binding chromatin – either they have unique binding sites, and share some to none binding sites amongst each other, or they share all of the binding sites. In the latter case, any DNA binding site would accept any KRP3,4 or 5 and mutants in any of these would be unaffected, as the remaining KRPs would act redundantly for the missing ones. In the other scenario, if each KRP have their specific binding sites on chromatin, the effect of knocking one out is equivalent to reducing the total chromatin binding sites (θ). From equation (50) is clear that in this scenario, the average volume would decrease, but homeostasis would be unaltered. This phenomenon clarifies why it is so difficult to find size homeostasis mutants: even if we knock out KRP4, one of the major components of this system, no alteration of homeostasis is expected. To confirm this prediction, I used CRISPR technology aiming to produce KRP3 and 5 mutants, using the already available *krp4-2* as a mutant background (Schiessl *et al.*, 2012; Schiessl, Muino and Sablowski, 2014). Figure 5.6 shows the deletion I was able to obtain for these two genes. *krp3-11* is a deletion of 49bp in the first exons, exactly on the guide RNA (gRNA) site designed (Fig. 5.6a). The deletion causes a frame shift in the protein sequence and a premature STOP codon, resulting in a protein product of 20 amino acids (Fig. 5.6b). In contrast, despite the numerous attempts, I could never obtain a similar mutant for KRP5, and all the mutations I obtained were on frame, even if the gRNAs were designed not to be (Fig. 5c). In the example given, 63bp were deleted from the genomic sequence, but in other cases deletions of 6bp were also observed. It is possible that KRP5 mutants are lethal and future experiments should use miRNA technology to test this hypothesis.
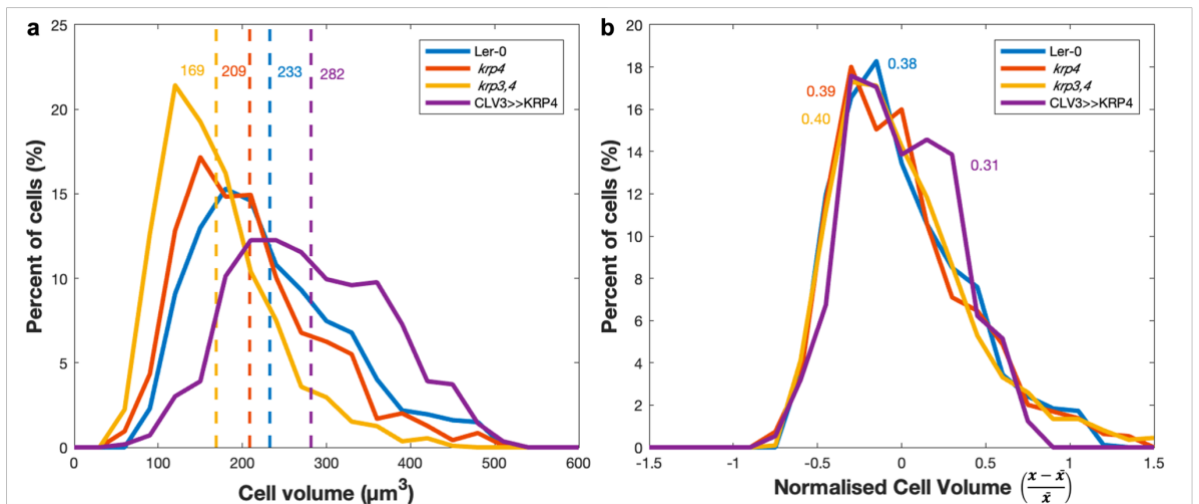
Figure 5.7: Phenotype of various *krp* mutants and KRP4 expression lines. (a) Cell size distribution comparison between Ler-0 (blue), *krp4-2* mutants (red), *krp3-11* in *krp4-2* background (yellow) and overexpressor CVL3>>KRP4 (purple). Dashed lines represent the mean of each distribution. All the distributions were found to be different statistically using ANOVA test (p < 10^{-15}). Tukey test for CLV4>>KRP4 vs Ler-0 was p = 2.5×10^{-3}, and p<10^{-8} for all other pairs. (b) Probability distributions for normalised volume from (a), normalised as $(x - \bar{x})/\bar{x}$, where $\bar{x}$ is the mean and x are the individual values. On the graph, CV are represented, calculated as SD divided by the mean. Tukey test revealed that Ler-0, *krp4 and krp3,4* are statistically identical (Ler-0 vs *krp4* p = 0.09, Ler-0 vs *krp3,4* p = 0.98, *krp4* vs *krp3,4* p = 0.14), but CLV3>>KRP4 was found statistically to be different from the other genotypes (CLV3>>KRP4 vs Ler-0 p = 0.007, CLV3>>KRP4 vs *krp4* p < 10^{-6}, CLV3>>KRP4 vs *krp3,4* p = 0.001).

Using the *krp4-2* mutants and the *krp3-11* mutant in a *krp4-2* background, I could test the prediction produced by equation (50). Figure 5.7a shows the cell size distribution of shoot meristems of various genotypes, showing that, not only do *krp* mutants have lower average volume, but that their effect is cumulative (different with a p < 10^{-15}). In addition, when normalising cell size to compare variation, the cell size distribution overlapped almost perfectly and their coefficient of variation were very close (identical with a p > 0.09) (Fig. 5.7b). Data for a line overexpressing KRP4 in the meristem, were also added to this experiment. In this line, KRP4 is under the expression of CLAVATA3 (CLV3) a classical genetic component of meristem maintenance (Serrano-Mislata, Schiessl and Sablowski, 2015). The effect of the CLV3>>KRP4 construct is equivalent to increasing the production of KRP4 (φ), so from Equation (50) the increase in the slope of the relationship between volume at S and volume at birth would predict an increase in cell size variability, as well as in increase in cell size. Interestingly, CLV3>>KRP4 have bigger cells sizes (p < 10^{-15}) as expected, but a lower CV (p < 0.007) (Fig. 5.7). So CLV3>>KRP4 variability is significantly different from the other variabilities, an effect that seem to be caused by those cells closer to the cell size mean (Fig. 5.7b). It seems that the cells larger than the mean are more likely

to be close to it, as indicated by the peculiar shape of this distribution. However, it is very likely that this is an artefact of the CLV3 promoter, which is not homogeneous in the area studied (Serrano-Mislata, Schiessl and Sablowski, 2015). In fact, there was a correlation between average size and CLV3 expression in this experiment (Serrano-Mislata, Schiessl and Sablowski, 2015), suggesting that this phenotype is harder to interpret. In this case, cells would also leave the CLV3 domain and recover their initial size, suggesting that the aberrant cells detected in this experiment might not have been part of a cycling population; instead, they might have grown to increase their size, left the CLV3 domain and re-entered normal size regulation.
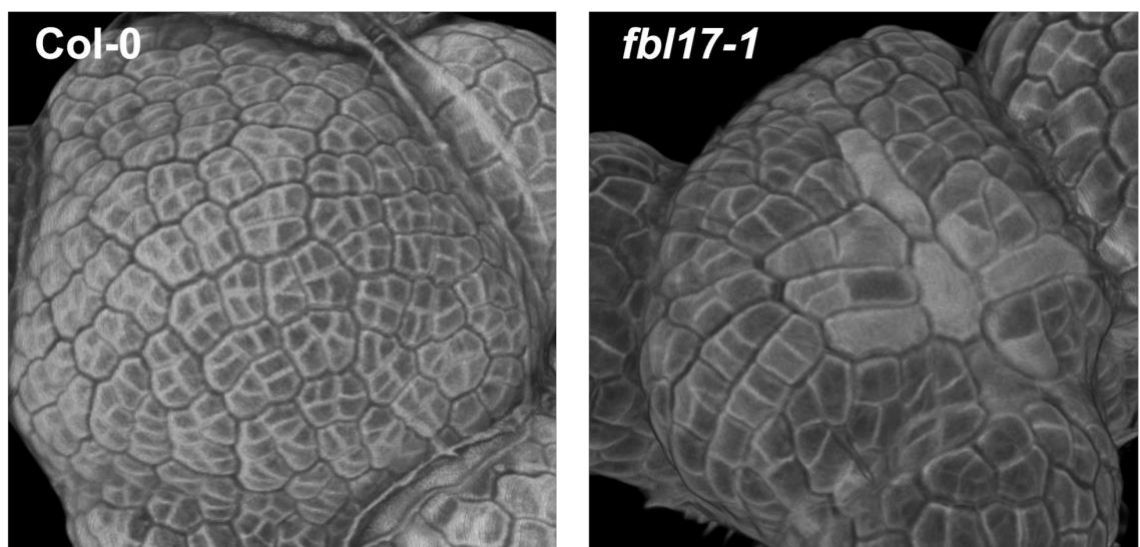
Figure 5.8: Cell size phenotype of the *fbl17-1* mutant. 3D reconstruction of shoot apical meristem of Col-0 and *fbl17-1* mutant. Notice the giant cells in the *fbl17-1* mutant that spread from the centre to the periphery of the apex. The surrounding smaller cells seems to preserve homeostasis.

5.7 FBL17 mutants

The result for the *krp* mutants in light of equation (50) highlights that, in order to observe loss of size homeostasis, a mutant affecting the term $\frac{\varphi}{\lambda+\mu}$ is required. *fbl17-1* should be such a mutant and should represent a decrease of μ, which would move the homeostasis away from a sizer/adder towards a system that does not reduce variability (like at timer or worse). To test this hypothesis, Figure 5.8 shows a 3D reconstruction of a Col-0 apex compared to *fbl17-1*. The enormous cells in the mutant were already observed in Chapter 4 but notice how a population of small cells surrounding the giant ones still appear to preserve homeostasis (Fig. 5.8). This can be explained using equation (50) – notice how the non-constant part of the equation, $F_b V_b$, depends on both the inherited free KRP4 concentration and volume at birth. In fact, for smaller birth volumes the constant part of

equation (50), the amount DNA-bound KRP4 (θ), would overwhelm the number of free KRP4 molecules at birth ($F_b V_b$) and preserve homeostasis. On the other hand, large volumes amplify even further the error carried by free KRP4 and are more likely to brake homeostasis. A way to write this observation is as follows:

$$\text{(51)} \qquad \text{If } F_b V_b \ll \theta \Rightarrow \mathbf{V_S \propto \theta}$$

Hence the system tends to a perfect sizer, that ensures proportionality between volume at S and DNA content. This is a situation similar to the one observed in the Wild type. Otherwise, if the free amount of inherited KRP4 ($F_b V_b$) is more than the chromatin bound population:

$$\text{(52)} \qquad \text{If } F_b V_b \gg \theta \Rightarrow \mathbf{V_S \propto F_b V_b}$$

In the case of exponential growth, if the time spent in G1 = T_1, the equation can be further reduced to:

$$\text{(53)} \qquad V_S = V_b e^{\lambda T_1} \propto F_b V_b \Rightarrow \lambda T_1 \propto \ln F_b \Rightarrow \mathbf{T_1} \propto \frac{\ln F_b}{\lambda}$$

Or in other words, G1 length is constant for large volumes in the *fbl17* mutant, i.e., the system behaves like a timer. So, in a way, the *fbl17* mutant can interpolate between a perfect sizer and timer, with the tip of the balance being moved by the volume at birth.

Variable	Value	Description
β	$1.2\mu m^3 min^{-1}$	DNA binding rate
γ_1	$1 min^{-1}$	DNA unbinding rate
γ_2	$10^{-3} min^{-1}$	DNA unbinding rate
φ	$0.2\mu m^{-3} min^{-1}$	Production rate
μ	$0.4 min^{-1}$	Degradation rate
μ_{fbl17}	$0.25 min^{-1}$	Degradation rate in *fbl17-1*
θ	200	DNA binding sites
λ	$0.017 h^{-1}$	Relative growth
α	50%	Proportionality factor
σ	0.17	SD for division symmetry

Table 5.3: Variables used for simulation of the *fbl17* mutant behaviour. Recall Equation (14) for the definition of the proportionality factor α. σ is the SD of division symmetry calculated from experimental data, representing the deviation from perfect volume symmetry such that $\frac{V_M}{V_{Do}} = 2 + \sigma$, where V_M and V_{Do} are the volumes of the mother and daughter cell, respectively.

To further understand the model, simulations were carried out using the values in Table 5.3 in an attempt to recapitulate the experimental data. Figure 5.9 shows the comparison of such simulations with the experimental data, showing that the system can easily predict both Col-0 and *fbl17-1* size distributions. The only difference between the simulated wild type and mutant is the value of μ (0.4min^{-1} and 0.25min^{-1}, respectively), values that reflect FBL17 proteolysis. Using the same parameters, I was able to recapitulate the phenomenon of loss of homeostasis for larger cells only (Fig. 5.10). In this simulation, only the smaller and the bigger cells were followed, showing how wild type cells are able to maintain homeostasis in the extreme cases, whilst in the *fbl17* mutant the larger cells grow uncontrollably (Fig. 5.10). Interestingly, the discrepancy between these two phenotypes can be attributed to a rather minimal change in the rate of degradation of ~60%, which seemingly contradicts the result obtained in (33), which suggested that a decrease of μ by a factor of 1000 would have been necessary to perturb homeostasis. However, (33) only took in consideration the time required to fully decorate DNA, which is still accomplished in the *fbl17* mutants, and does not consider the impact of changing the degradation rate on homeostasis. Once again, equation (50) can easily explain this behaviour – assuming that μ ≫ λ (Table 5.3) a decrease of μ by 60%, results in an increase of the slope in Equation (50) by 160%, a change that would be enough to push an adder away from homeostasis, explaining how a little change in degradation at G2 might have such large effect on size homeostasis.
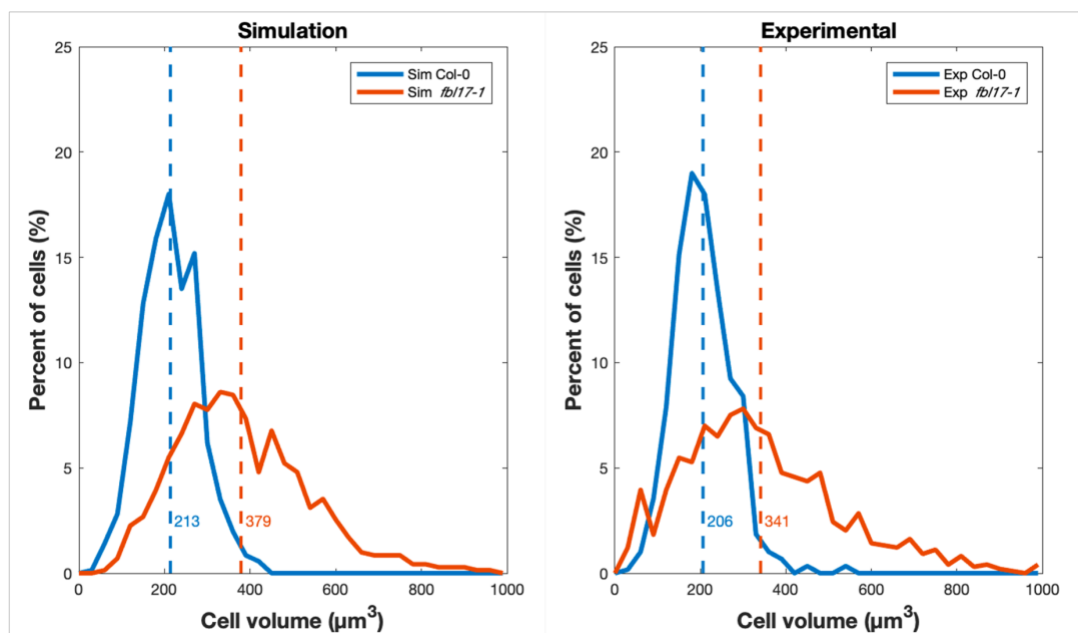
Figure 5.9: Mathematical simulations can recapitulate the experimental data. Probability density of simulated cell population (left), compared to experimental data (right). Dotted lines represent population means. Note the asymmetry of the distributions of the *fbl17* mutants, that are skewed towards the right, indicating the presence of a few giant cells. Values in Table 5.3 were used to produce these simulations.

5.8 KRP4 production in early G1

We finally have the tools to discuss production of KRP4 during G1, observed in Chapter 3. Thanks to Equation (50), it is very easy to show that the observed production of KRP4 during this period cannot affect size homeostasis. To do so, let us consider two possible situations: either KRP4 during G1 is produced in a volume-independent manner, i.e. a fixed amount is added, or it is produced in a volume-dependent manner. In the former case, this is the equivalent of adding a constant to equation (50), and simply results in a higher target volume, with no impact on size homeostasis. As we saw, adding an amount of KRP4 in proportion to the volume, could destabilise homeostasis. However, the observed increase is ~30% (see Chapter 3) a far cry from the 160% required for loss of homeostasis. However, in this latter case the cell size variability at S would be higher than if no production of KRP4 in G1 was present, leaving open the speculation that the production of KRP4 in G1 might play a role in increasing cell size variability. Although controversial, size variability has been suggested to play an important role in developmental robustness of plant organs (Hong *et al.*, 2018), so this possibility should not be lightly discarded.
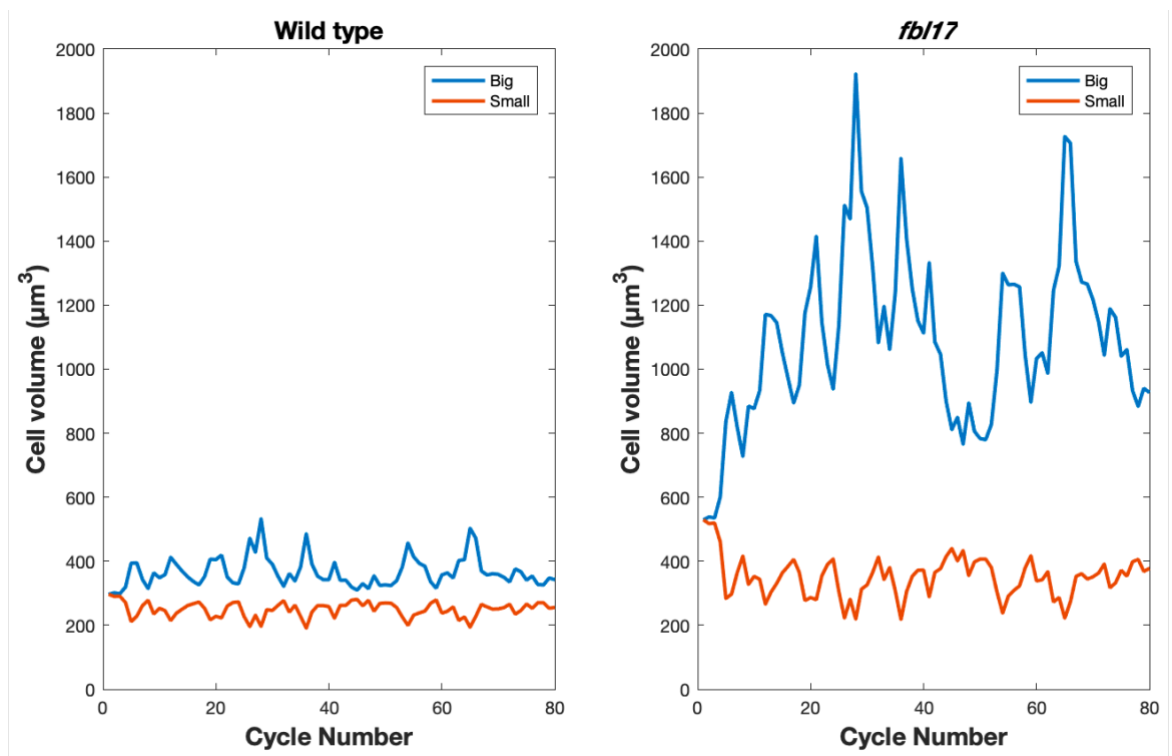
Figure 5.10: Only the larger cells in the *fbl17* mutants have lost size homeostasis. Cell volume at division for the smallest (red) and the largest (blue) cells of cycling populations of wild type (left) and *fbl17-1* mutants (right). Asymmetric division is introduced at cycle = 0, after 15 rounds of symmetric divisions, which are carried out to stabilise the volume at birth, explaining why the volumes of small and big cells are identical at the beginning of the simulation. Note how the larger cells in the *fbl17* mutant are unable to reduce variability, and only do so as a result of random division. Values in Table 5.3 were used to produce these simulations.

5.9 Discussion

After many discussions on growth rate, we finally saw the definition for exponential growth and we should agree that exponential growth appears to be the most reasonable way to grow: the default way to grow, so to speak. What is remarkable however, is that exponential growth comes with the price of inflated variability, which pushes cells away from their ideal size and applies an obvious pressure to evolve a mechanism for size homeostasis. It is interesting to consider that linear growth could function as such mechanism, making this type of growth advantageous in the absence of a different type of regulation. Obviously, any evidence for such occurrence would be lost in the eons of evolution, so it is worth considering other, more testable ways, for achieving homeostasis. Here I explored the mathematics of such a mechanism, and I was able to show that it preserves homeostasis and that predictions made by the model were able to recapitulate experimental results. At the same time, some observations could not be tested.

One such conclusion was the necessity of the unbinding (binding) rate of KRP4 to chromatin at G2 to be lower (higher) than the one at G1 ($\gamma_2 < \gamma_1$ or $\beta_2 > \beta_1$). I chose the unbinding rate for discussion and a possible mechanism for this change could involve FBL17 itself. Perhaps FBL17 binding to KRP4 results in a change in conformation, that decreases the likelihood of the latter to dissociate from chromatin. In this way, FBL17 would play a dual role in counteracting accumulation of nucleosolic KRP4, by also promoting chromatin saturation. Perhaps the change in dissociation rate is a passive one, not requiring specific factors to be accomplish and instead is part of the sequence of events that happens in G2. For example, condensing chromatin might act by trapping KRP4, decreasing the likelihood of entering the nucleosol. This phenomenon has been observed in human cells, where the protein Ki-67 coats condensed chromosomes preventing diffusion of chromatin components, and effectively acting as membraneless cellular compartment (Cuylen *et al.*, 2016). Regardless of the mechanism, testing this hypothesis is very challenging since it requires distinguishing between cells in G1 and in G2, whilst performing binding tests *in vivo*. In Chapter 2, I discussed the limitations of distinguishing cells at different stages, but cell size and chromatin morphology (like metaphase plane visible before division), could be used to discriminate between mitotic and interphase cells. I performed various attempts to measure this value using Fluorescence Recovery After Photobleaching (Meyvis *et al.*, 1999) assays, but the quick time between metaphase and division, combined with the low expression of KRP4, never allowed me to obtain such a result.

Hopefully in the future this will be addressed by different means. However, I argue that there is evidence for increased binding during G2, or at least at division: metaphase chromosomes always appear bright and decorated by KRP4 (see Chapter 3) even when the nuclear envelope has broken down. Effectively, this means that the "nuclear volume" equal to the cell volume during anaphase, increasing by three-fold the volume in which KRP4 can diffuse. This should result in the dispersion of KRP4 in the cytoplasm, similar to what is observed in cells entering S-phase (see Chapter 3). This information supports the idea of a change in the binding rate during G2, but further experiments will be required to test this idea. Biochemical characterisation of KRP4 and the way it interacts with FBL17 and chromatin, will prove critical in addressing this question.

A silent observation of this model involves the strength of the *fbl17-1* mutant. In the simulations shown in Figures 5.9 and 5.10, the degradation rate was not even halved, and this was enough to mimic the phenotypic effect of the mutants. Ideally, these mutants should be simulated by setting the degradation rate to $0min^{-1}$, or to a number small enough that is effectively zero. When doing so, the system simply becomes a timer, for reasons explained in equation (53). Therefore, cells would just grow and divide much later than any attempt at homeostasis would require, and exponentially grow towards infinite sizes. This phenomenon would happen regardless of their volume at birth, which is now too big to result in a situation similar to the one described in (51). Therefore, the partial loss of homeostasis observed in *fbl17-1* can be explained in various ways: a simple explanation is that *fbl17-1* is just a mild mutant, rather than a full knock out.

This is plausible since this allele has a T-DNA insertion towards the end of the gene (Kim *et al.*, 2008), so mRNA expression and some protein functionality might be preserved. Another possibility is that the putative mechanism for size regulation acting at G2 might partially mask the expected loss of homeostasis in *fbl17-1*, although the adder-like behaviour of size regulation at G2 should not be able to recover variability for large cells, so eventually those should just grow indefinitely. However, we observed that those cells are still able to divide (Chapter 4), suggesting that a mechanism other that the putative adder in G2 is preserving partial homeostasis. A final possibility is that KRP4 and its homologues are regulated by another pathway for degradation, responsible for keeping the degradation rate above zero. A hint of this possibility comes from a study on KRP1, in which the authors showed that this protein is targeted by a proteolytic pathway other than

the one involving FBL17 (Ren *et al.*, 2008). Interestingly, this unknown pathway targets KRP1 on Motif 7, a sequence shared with KRP3,4 and 5 (see Chapter 4) and so it presumably targets those, too. It would be interesting in the future to identify such a pathway and study its role in size homeostasis.

The role of FBL17 in preserving homeostasis should be obvious by now: it prevents accumulation of free KRP4, ensuring cell size homeostasis. However, we have also seen a further role of degradation in ensuring that KRP4 production reaches its equilibrium before the end of G2 (33). Reaching equilibrium is a feature ensuring consistent accumulation of KRP4 by the end of G2. If this did not happen, the system would fluctuate between a non-saturated chromatin and a saturated one but with random (i.e. non predictable) KRP4 excess. This would strongly impact homeostasis and the length of individual G2 phases would play a role in determining cell size in the following cell cycle. So in a way, degradation of KRP4 in G2 is also required for the consistency of production during this period. A consequence of this observation becomes clear when speculating on the possible evolutionary pathways that led to the evolution of the cell size homeostasis mechanism used by plant meristem cells.

We have seen so far that KRP4, FBL17 and DNA act in concert, to reduce the size variability accumulated during division. I have also discussed the evidence that another mechanism still remains to be characterised, one that acts to preserve variability at G2. In the next chapter, I will present my attempts in characterising the components of such a putative mechanism and discuss possible future avenues to be taken in this direction.

5.10 References

Antoniou-Kourounioti, R. L. *et al.* (2018) 'Temperature Sensing Is Distributed throughout the Regulatory Network that Controls FLC Epigenetic Silencing in Vernalization', *Cell Systems*. Elsevier, 7(6), p. 643–655.e9. doi: 10.1016/j.cels.2018.10.011.

Antoniou Kourounioti, R. *et al.* (2013) 'Buckling as an origin of ordered cuticular patterns in flower petals', *Journal of the Royal Society, Interface / the Royal Society*, 10, p. 20120847. doi: 10.1098/rsif.2012.0847.

Cooper, S. (2006) 'Distinguishing between linear and exponential cell growth during the division cycle: single-cell studies, cell-culture studies, and the object of cell-cycle research', *Theoretical biology & medical modelling*. BioMed Central, 3, p. 10. doi: 10.1186/1742-4682-3-10.

Cooper, S. (2013) 'Schizosaccharomyces pombe grows exponentially during the division cycle with no rate change points.', *FEMS yeast research*. England, 13(7), pp. 650–658. doi: 10.1111/1567-1364.12072.

Cuylen, S. *et al.* (2016) 'Ki-67 acts as a biological surfactant to disperse mitotic chromosomes', *Nature*, 535(7611), pp. 308–312. doi: 10.1038/nature18610.

D'Ario, M. and Sablowski, R. (2019) 'Cell Size Control in Plants', *Annual Review of Genetics*. Annual Reviews, 53(1), pp. 45–65. doi: 10.1146/annurev-genet-112618-043602.

Desvoyes, B. *et al.* (2019) 'FBL17 targets CDT1a for degradation in early S-phase to prevent Arabidopsis genome instability', *bioRxiv*, p. 774109. doi: 10.1101/774109.

Facchetti, G., Knapp, B., Chang, F., *et al.* (2019) 'Reassessment of the basis of cell size control based on analysis of cell-to-cell variability', *Biophysical Journal*, 117(9), pp. 1728–1738. doi: https://doi.org/10.1016/j.bpj.2019.09.031.

Facchetti, G., Knapp, B., Flor-Parra, I., *et al.* (2019) 'Reprogramming Cdr2-Dependent Geometry-Based Cell Size Control in Fission Yeast', *Current Biology*, 29(2), p. 350–358.e4. doi: https://doi.org/10.1016/j.cub.2018.12.017.

Facchetti, G., Chang, F. and Howard, M. (2017) 'Controlling cell size through sizer mechanisms', *Current Opinion in Systems Biology*. Elsevier Ltd, pp. 86–92. doi: 10.1016/j.coisb.2017.08.010.

Hong, L. *et al.* (2018) 'Heterogeneity and Robustness in Plant Morphogenesis: From Cells to Organs', *Annual Review of Plant Biology*. Annual Reviews, 69(1), pp. 469–495. doi: 10.1146/annurev-arplant-042817-040517.

Jones, A. R. *et al.* (2017) 'Cell-size dependent progression of the cell cycle creates homeostasis and flexibility of plant cell size', *Nature Communications*. Nature Publishing

Group, 8, p. 15060. doi: 10.1038/ncomms15060.

Kim, H. J. *et al.* (2008) 'Control of plant germline proliferation by SCFFBL17 degradation of cell cycle inhibitors', *Nature*, 455(7216), pp. 1134–1137. doi: 10.1038/nature07289.

Lin, J. and Amir, A. (2018) 'Homeostasis of protein and mRNA concentrations in growing cells', *Nature Communications*, 9(1), p. 4496. doi: 10.1038/s41467-018-06714-z.

Martin, S. G. and Berthelot-Grosjean, M. (2009) 'Polar gradients of the DYRK-family kinase Pom1 couple cell length with the cell cycle', *Nature*, 459(7248), pp. 852–856. doi: 10.1038/nature08054.

Meyvis, T. K. L. *et al.* (1999) 'Fluorescence Recovery After Photobleaching: A Versatile Tool for Mobility and Interaction Measurements in Pharmaceutical Research', *Pharmaceutical Research*, 16(8), pp. 1153–1162. doi: 10.1023/A:1011924909138.

Miettinen, T. P. and Björklund, M. (2016) 'Cellular Allometry of Mitochondrial Functionality Establishes the Optimal Cell Size', *Developmental cell*. Cell Press, 39(3), pp. 370–382. doi: 10.1016/j.devcel.2016.09.004.

Neurohr, G. E. *et al.* (2019) 'Excessive Cell Growth Causes Cytoplasm Dilution And Contributes to Senescence', *Cell*. Cell Press, 176(5), p. 1083–1097.e18. doi: 10.1016/j.cell.2019.01.018.

Pan, K. Z. *et al.* (2014) 'Cortical regulation of cell size by a sizer cdr2p', *eLife*, 2014(3), pp. 1–24. doi: 10.7554/eLife.02040.

Ren, H. *et al.* (2008) 'Degradation of the cyclin-dependent kinase inhibitor KRP1 is regulated by two different ubiquitin E3 ligases', *The Plant Journal*. John Wiley & Sons, Ltd, 53(5), pp. 705–716. doi: https://doi.org/10.1111/j.1365-313X.2007.03370.x.

Ripoll, J.-J. *et al.* (2019) 'Growth dynamics of the Arabidopsis fruit is mediated by cell expansion', *Proceedings of the National Academy of Sciences*, 116(50), p. 25333 LP-25342. doi: 10.1073/pnas.1914096116.

Schiessl, K. *et al.* (2012) 'JAGGED controls growth anisotropy and coordination between cell size and cell cycle during plant organogenesis', *Current Biology*. Elsevier Ltd, 22(19), pp. 1739–1746. doi: 10.1016/j.cub.2012.07.020.

Schiessl, K., Muino, J. M. and Sablowski, R. (2014) 'Arabidopsis JAGGED links floral organ patterning to tissue growth by repressing Kip-related cell cycle inhibitors', *Proceedings of the National Academy of Sciences*, 111(7), pp. 2830–2835. doi: 10.1073/pnas.1320457111.

Schmoller, K. M. *et al.* (2015) 'Dilution of the cell cycle inhibitor Whi5 controls budding-yeast cell size', *Nature*, 526(7572), pp. 268–272. doi: 10.1038/nature14908.

Serrano-Mislata, A. *et al.* (2017) 'DELLA genes restrict inflorescence meristem function independently of plant height', *Nature Plants*. Springer US, 3(9), pp. 749–754. doi: 10.1038/s41477-017-0003-y.

Serrano-Mislata, A., Schiessl, K. and Sablowski, R. (2015) 'Active Control of Cell Size Generates Spatial Detail during Plant Organogenesis', *Current Biology*. The Authors, 25(22), pp. 2991–2996. doi: 10.1016/j.cub.2015.10.008.

Turner, J. J., Ewald, J. C. and Skotheim, J. M. (2012) 'Cell size control in yeast', *Current Biology*. Elsevier Ltd, 22(9), pp. R350–R359. doi: 10.1016/j.cub.2012.02.041.

Willis, L. *et al.* (2016) 'Cell size and growth regulation in the *Arabidopsis thaliana* apical stem cell niche', *Proceedings of the National Academy of Sciences*, 113(51), pp. E8238–E8246. doi: 10.1073/pnas.1616768113.

Wood, E. and Nurse, P. (2013) 'Pom1 and cell size homeostasis in fission yeast', *Cell cycle (Georgetown, Tex.)*. 2013/09/12. Landes Bioscience, 12(19), pp. 3228–3236. doi: 10.4161/cc.26462.

Zatulovskiy, E. *et al.* (2020) 'Cell growth dilutes the cell cycle inhibitor Rb to trigger cell division', *Science*, 471(July), pp. 466–471.

Chapter 6: A plausible mechanism for size sensing at G2

6.1 Introduction

With a system in place to reduce variability at S-phase, any additional mechanism for cell size regulation would seem superfluous. Nevertheless, in budding yeast a cryptic mechanism for size regulation during G2 is visible when the G1/S size control is compromised (Garmendia-Torres *et al.*, 2018) and, in the plant meristem, regulation of CDK activity during G2 has been suggested to be part of the mechanism of cell size homeostasis (Jones *et al.*, 2017), the implied presence of which I also discussed in Chapters 2 and 5.

Whilst G2 size control remains elusive in almost all eukaryotes, in fission yeast size control is primarily performed in G2/M, using a mechanism that involves the cell cycle promoter Cdr2 (Pan *et al.*, 2014). Cdr2 shows a complicated dynamics, in binding equilibrium between the plasma membrane, the cytoplasm and the cortical band (Pan *et al.*, 2014). The cortical band is an area situated on the plasma membrane that surrounds the nucleus of *Schizosaccharomyces pombe* cells, the size of which remains constant during growth, and which predicts the position of the contractile ring responsible for cell fission (Nurse, Thuriaux and Nasmyth, 1976). As a consequence of its dynamics, Cdr2 concentration on the cortical band increases with cell size, proportionally to a geometric quantity referred to as pseudo-area, which is proportional to the ratio between cell volume and the size of the cortical band (Facchetti *et al.*, 2019).

Interestingly, although the biology of cell cycle progression greatly differs between bacteria and eukaryotes, a mechanism analogous to the *S. pombe* Cdr2 mechanism has been described in bacteria. It has been shown that the FtsZ protein forms a ring around the nucleoid and participates in the control of cell size of these organisms (Weart *et al.*, 2007). FtsZ is part of the mechanism that physically divides bacterial cells, contracting the plasma membrane and resulting in fission (Weiss, 2004). In this way, fission yeast and bacteria convergently evolved a system to use the area that surrounds the centre of the cell, as part of a mechanism to measure size and predict the position of the plane of division. Such pseudo-area sensing mechanisms so far have not been found in other taxa, so they are likely are derived traits. However, plants also possess a unique structure that surrounds the nucleus before division and functions as marker for positioning of the division plane: the preprophase band (PPB).

As the name suggests, the PPB appears in the cell before prophase, preceding chromosome condensation, and it is composed of microtubules (Pickett-Heaps and Northcote, 1966). PPB positioning is dependent on cell geometry and mechanical stress (Louveaux *et al.*, 2016) and its deposition occurs at the periphery of the cell, thus its length is a function of cell size and cell shape (Livanos and Müller, 2019). Before division, during metaphase, the PPB disassembles to form the spindle, a microtubule structure required for chromosome segregation (Walker *et al.*, 2007). The cell preserves a memory of the location of the PPB even after disassembly, and the phragmoplast deposits in the location previously occupied by the PPB (Walker *et al.*, 2007). Even if the ring formed by the PPB runs all the way along the cell perimeter, which in meristem cells is around 30 μm, its width is very narrow, between 2 to 3μm, and the variability in PPB width is very low (Yabuuchi *et al.*, 2015). The scaling with size at deposition and the low variability in width make the PPB an appealing structure for cell size control.

Any protein using the PPB as a proxy for cell size would have information on cell size at PPB deposition, which in turn relates to the size at the G1/S transition. This phenomenon must occur for size control at G2 because mutants in the G1/S transition, including *krp* mutants (see Chapter 5), show both, a reduction in cell size at division and at S-phase transition (Jones *et al.*, 2017). Therefore, a mechanism for cell size during G2 must maintain information on the size at the G1/S. Additionally, low variability in PPB width would contribute to the accuracy of the system, allowing for the length of the PPB to be the only variable factor in measuring size. Considering that some cell cycle regulators, including CDKs, are observed associating with this structure (Boruc *et al.*, 2010), the PPB could serve as a subcellular environment for connecting size to cell cycle progression during G2. Critically, if the PPB act as size sensor at G2, there must be a negative correlation between the size at the beginning of preprophase, i.e. when the PPB first appears, and the size at division, meaning that cells that enter preprophase larger will accumulate less volume before commitment to division. Testing this hypothesis would be the first step in recognising the PPB as a subcellular structure used for size sensing.

If a system like the one described for KRP4 and DNA holds for G2 progression and the PPB, it would require an inhibitor of cell cycle progression, which is produced in G1 and binds to the PPB when it appears. The presence of such an inhibitor during G1 should ideally not interfere with the G1/S progression and its localisation in G2 should coincide with the PPB.

SIAMESE is the only known family of inhibitors that exclusively acts during the G2/M progression (Churchman *et al.*, 2006). Although many of the members of these family seem to have a conserved function in preventing division in the trichomes (Kumar *et al.*, 2015) and in DNA damage response (Yi *et al.*, 2014), *in situ* experiments suggested that at least one member of the family, SMR11, is expressed in the shoot apical meristem (Yang, Wightman and Meyerowitz, 2017). Interestingly, principal component analysis of pairwise sequence distances of the members of the SMR family revealed a clustering of SMR11 and 16, which greatly differ from the rest of the family (Kumar *et al.*, 2015). For these reasons, I decided to study SMR11 further, with the hope of finding some connection with the PPB. For SMR11 to perform a function in a dilution-like mechanism at G2/M, it would require to be accumulated prior to preprophase and interact with the PPB afterwards.

In this chapter, I explored the possibility that pseudo-area sensing regulates the G2/M transition in the meristem, and that SIM11 might be involved in this mechanism.
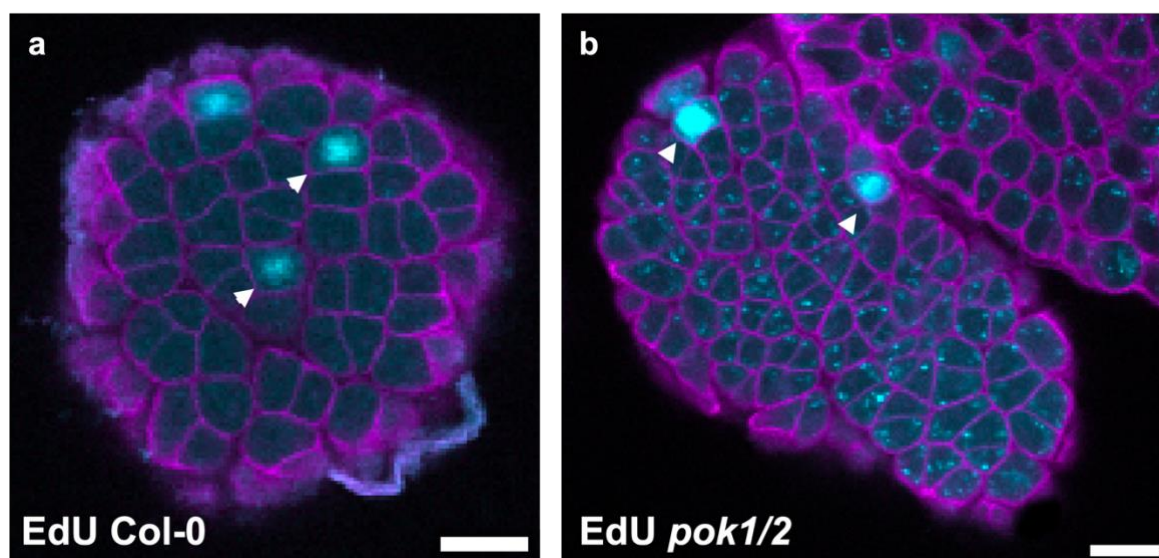
Figure 6.1: S-phase transition in mutants of the cell shape. Confocal slices of apexes stained for cell wall (magenta) using mPS-PI protocol and EdU for nascent DNA synthesis (cyan, arrowheads). Notice the difference in cell morphology between Wild type Col-0 (a) and *pok1/2* mutant (b), where some of the cells appear triangular in cross section. Scale bar = 10μm.

6.2 Surface area scaling

In order to understand what geometric quantity meristem cells use as information to commit to division, mutant lines in the protein PHRAGMOPLAST ORIENTING KINESINS1 and 2 (POK1/2) were used (Müller, Han and Smith, 2006). POK1/2 are kinesins essential for the maintenance of TANGLED in position, after PPB disassembly, until the phragmoplast is fully deposited (Rasmussen, Sun and Smith, 2011). This interaction is required for maintaining

the "memory" of PPB positioning during division and loss of POK1/2 causes uncoupling of phragmoplast deposition from the position at which the PPB first formed (Walker *et al.*, 2007). Note that in the *pok1/2* mutant the PPB still forms, the only information related to PPB lost in these mutants is the coupling between PPB positioning and division plane orientation. As result, in *pok1/2* mutants the geometry of the cells varies much more than it does in the wild type (Fig. 6.1). The high variability in cell shapes between wild type and *pok1/2* should allow me to compare between volume and surface areas, and test which geometric quantity is more similar at division in differently shaped cells.
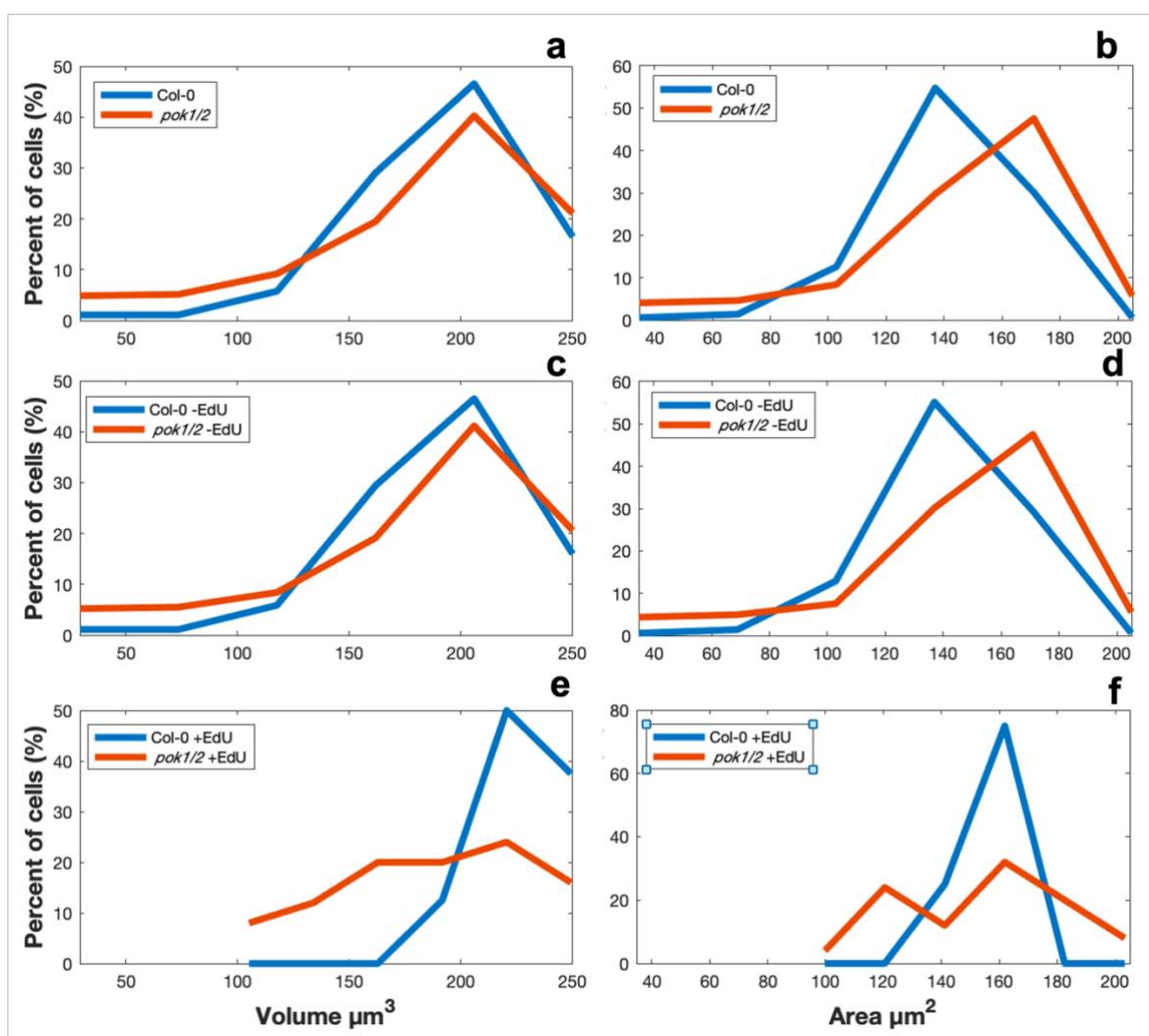
Figure 6.2: Comparison of different geometric quantities during different cell cycle stages. Probability distribution of cells *pok1/2* cells (orange) and Col-0 (blue), showing differences between volume and surface area. There is no statistical difference in volume (a) (p = 0.017), or surface area (b) (p < 10^{-10}) in the whole population. When subpopulations of cells are considered, EdU negative cells (-EdU) (c,d) also showed no difference (p = 0.023 for volumes and p < 10^{-10} for areas), but EdU positive *pok1/2* cells (EdU+) are statistically identical for both volume (e) (p = 0.089) and surface area (f) (p = 0.220). Statistical comparisons were done using two-sample Kolmogorov–Smirnov test.

Since recent divisions cannot be automatically detected due to the abnormal shapes of the cells, and that long term live imaging is unlikely to work due to the stunted growth of the *pok1/2* mutants, a different approach for detecting dividing cells needed to be taken. To focus the analysis on cells that had passed the G1/S transition, EdU staining (Salic and Mitchison, 2008), a chemical approach for labelling cells undergoing S-phase, was used for this purpose (Fig. 6.1) (see Material and Methods). Labelled cells had entered S-phase, therefore their cell cycle progression would no longer be subject to the KRP4-based mechanism. To confirm this view, in Figure 6.2 the size distribution of labelled cells can be compared to the size distribution of the whole population, showing that labelled cells are those corresponding with the largest sizes, consistent with S/G2 phases. A caveat of this way of considering cells at division, however, is that a portion of cells in G2 will not be labelled, as they would have finished S-phase before exposure to EdU. Perhaps more extensive imaging experiments should be carried out in the future to finalise this result, using a variety of cell shape mutants.

With this caveat considered, two-samples Kolmogorov-Smirnov test was carried out to test whether *pok1/2* and Col-0 cells belong to populations of similar distribution, depending on different geometric quantities. The whole population differed in both volume ($p = 0.017$) and surface area ($p < 10^{-10}$) (Figure 6.2a and b, respectively). The same observation holds for the subpopulation of EdU negative cells (-EdU), composed of mainly G1 cells, which also differed in both volume ($p = 0.023$) and surface area ($p < 10^{-10}$) (Figure 6.2c and d, respectively). Even if different statistically, it is interesting to notice how much lower the probability of difference in the surface area distributions is ($p < 10^{-10}$) when compared to volumes (whole population, $p = 0.017$ and -EdU population $p = 0.023$), leaving open the question of whether similar results would be obtained with smaller measuring errors. In contrast, there was no statistical difference between subpopulations of cells that were labelled with EdU (EdU+), not for volume ($p = 0.089$) nor for surface area ($p = 0.220$) (Figure 6.2e and f, respectively). Interestingly, in this case the probability for difference was reverse, with higher probability associated with surface area than volume. However, it is important to highlight that of the roughly 370 cells detected for each genotype, only 25 were labelled with Edu for the *pok1/2* mutants and only 8 in Col-0, suggesting that the high probability resulting from the two-samples Kolmogorov-Smirnov test in the EdU+ cells, could be linked to small population sizes. Overall, these results would argue against a
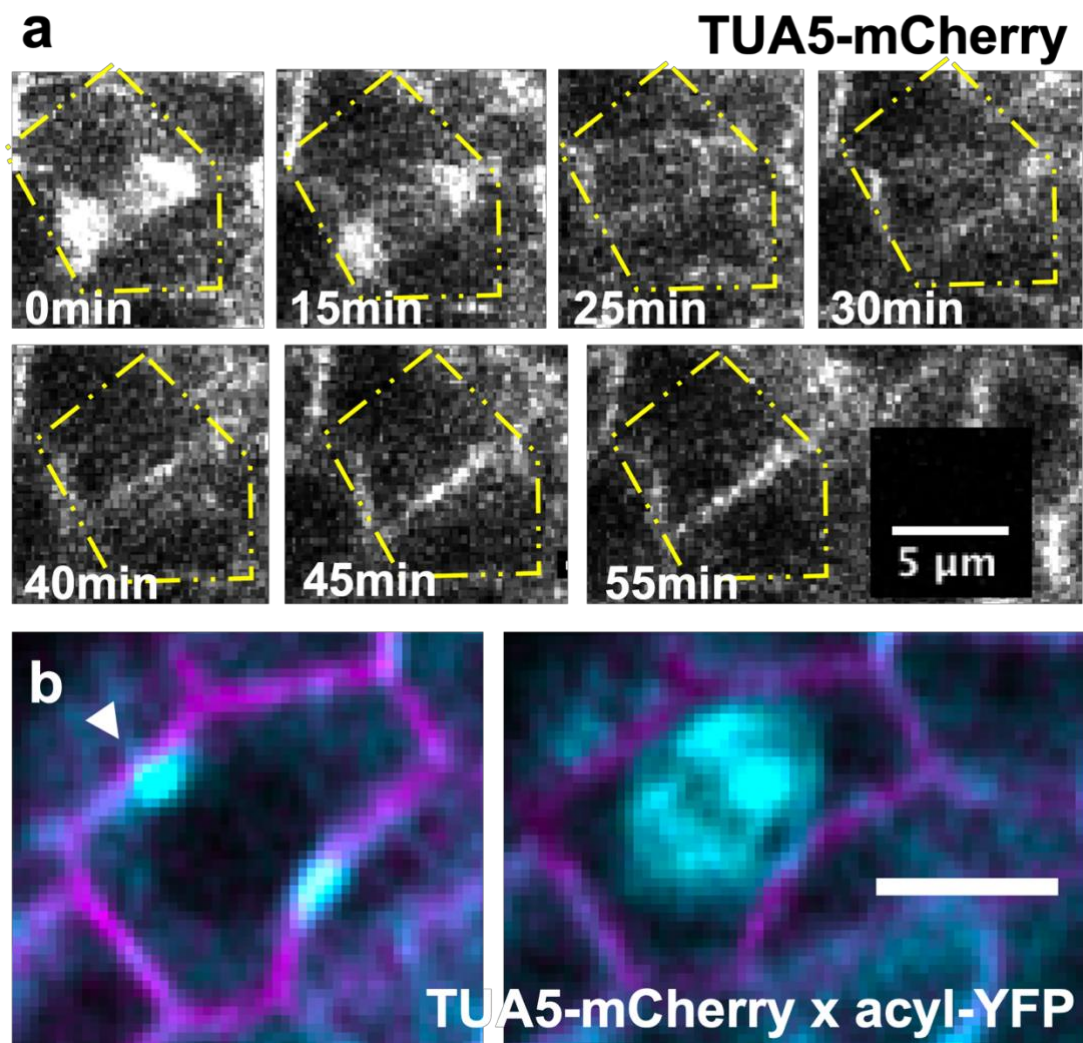
Figure 6.3: Preprophase last longer than M-phase. Confocal images of TUA5-mCherry used as microtubules marker lines. a) Confocal slices showing a cell (dashed yellow lines) progressing through division. The original video was taken with 10s for each frame, but here critical time points are shown. Note how the PPB is visible for the first 15min, but disappear afterwards. At 40min the phragmoplast become visible and it is fully deposited at the 55min mark. Scale bar = 10 μm b) Cross between TUA5-mCherry and acyl-YFP for the plasma membrane, showing a high resolution of one cell moving form preprophase (note the PPB in cyan on the left, arrowhead) to metaphase, recognisable thanks to the spindle (cyan). Scale bar = 10 μm.

simple area sensing mechanism, and suggesting that measuring of more complicated geometric quantity is in place during these phase transitions. In fact, the surface area sensing observed in *S. pombe* is a consequence of its cylindrical shape, in which pseudo-area and surface area coincides (Facchetti *et al.*, 2019). Perhaps a similar situation might hold for plant meristem cells, but in this case the difference in pseudo-area and surface area makes testing this hypothesis more challenging.

6.3 PPB: possible role as size sensor

To test the possibility that the PPB is involved in size sensing during G2, a TUBULIN ALPHA 5 (TUA5) tagged with mCherry line for visualization of microtubules (TUA5-mCherry) was used (Fig. 6.3) (the line was described in (Gutierrez *et al.*, 2009)). To my knowledge, there was no temporal information on PPB progression, as many studies on the topic have employed fixed tissues (Yabuuchi *et al.*, 2015). Therefore, it was paramount to exclude the possibility that the time between PPB appearance and mitosis would be just too short to correct any growth-derived variability accumulated between S-phase and preprophase. For this reason, time lapse images were taken for a total of 2h duration with 10s intervals (Fig. 6.3a). During this period, very few cells were observed dividing, and those that did already had an established PPB (Fig. 6.3a). Events of PPB disappearance, spindle formation and division, were observable during the time lapse and lasted ~30min when combined (Fig. 6.3a). Indeed, spindle formation is a common, often captured in subsequent experiments (Fig. 6.3b). This experiment showed that the duration between preprophase and division likely surpasses 2h, making the whole process between PPB deposition and anaphase much longer than chromosome segregation, which only lasted 30min. This suggests that any process involved in the preparation for division, such as chromatin condensation and perhaps processing information for commitment, takes much longer than mitosis itself.
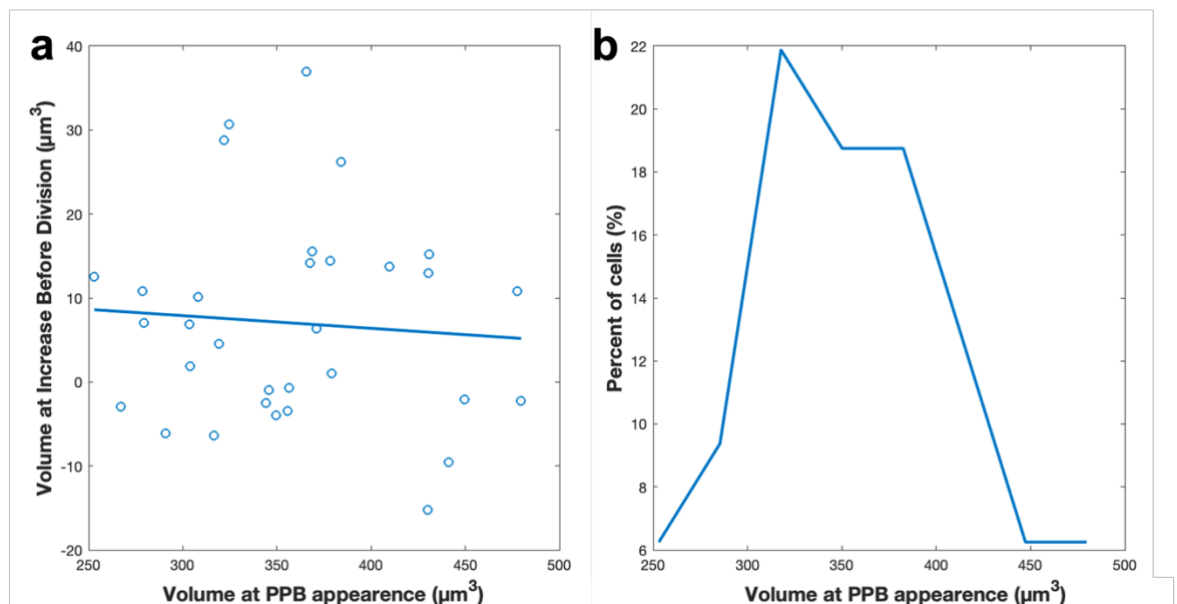
Figure 6.4: Growth between prophase and mitosis did not depend on cell size when the PPB appeared, at least for cells that were large when entering prophase. Data collected form a short time course of 7.5h. a) Correlation between the volume of a cell when the PPB first appeared and the increase of the volume before division, showing no relationship (slope = -0.02) with almost no correlation between the two values (R^2 = 0.006). However, note that the size distribution of those cells ($359\pm61\mu m^3$, mean ± standard deviation) is indicative of the largest cells in the population.

This experiment also informed that, to capture cells depositing PPB and dividing, a longer time course was required. To this end, TUA5-mCherry was crossed to the *UBI10::acyl-YFP* plasma membrane reporter, the same used in Chapter 2 and 3 (Fig. 6.3b). To decide on the length of the time course, I conducted a preliminary experiment in which apexes were imaged every 1.5h for 7.5h. Note that 1.5h resolution can be achieved for short time courses, but for more than 10h, 2h intervals increased survival rate. In this preliminary experiment, 32 cells from 2 apexes were observed depositing the PPB and then dividing, but a similar amount, 39 cells from the same apexes, were observed depositing the PPB without dividing, suggesting that cells might take longer than 7.5h to complete this process. The cells observed undergoing PPB deposition and division were very large and accumulated very little volume after PPB appearance (Fig. 6.4a). In this case there is no correlation between volume at PPB appearance and volume at division (R^2 = 0.005), suggesting that those cells progressed through meiosis regardless of further growth after
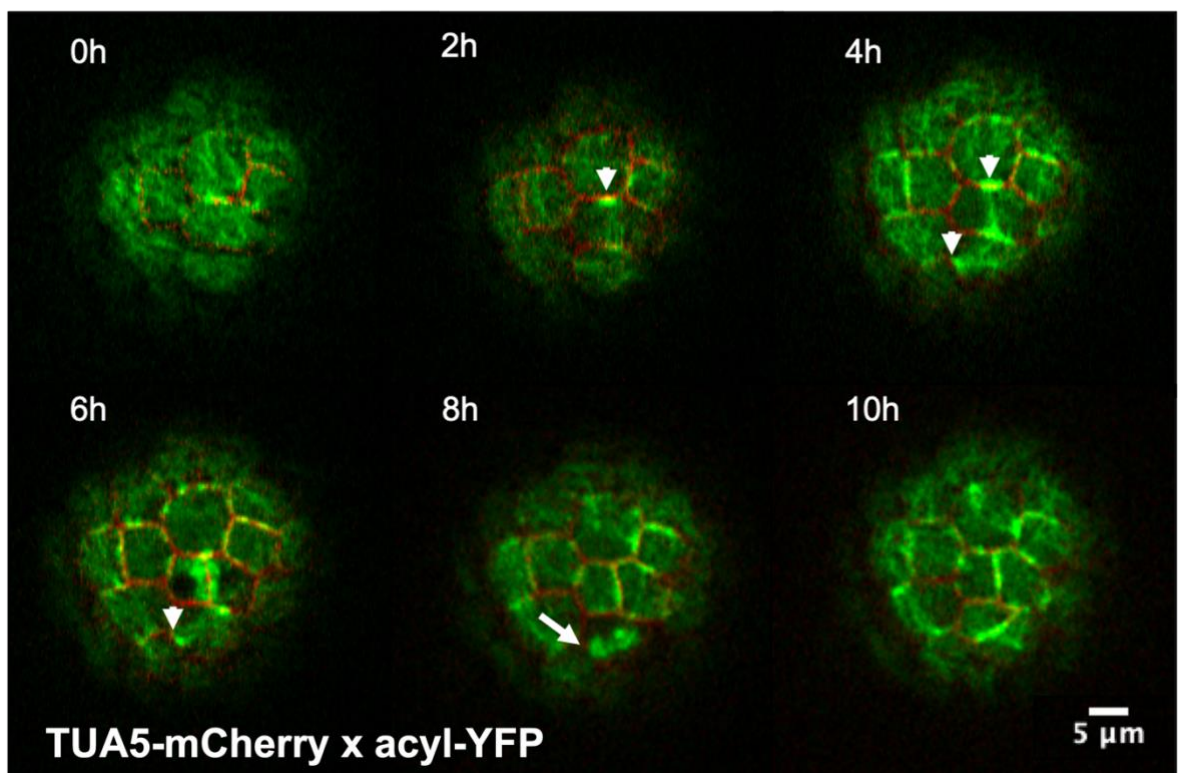
Figure 6.5: Extended time course using a microtubule marker to study PPB dynamics. Confocal slices of the same TUA5-mCherry x acyl-YFP meristem, showing a 10h interval within the 38h of imaging. Notice how two cells, one starting at 2h and the other one starting at 4h, visibly entered preprophase indicated by the appearance of the PPB (arrowheads), but take different times to divide, with the top cell going through prophase in 2 time points, whilst the bottom one required 3. The latter cells also show the presence of the spindle before division (arrow). Scale bar = 5μm.

depositing the PPB. However, those cells belong to the largest class of cells, around the size reported for division: 359±60 μm^3 compared to 272±35μm^3 from the dataset of Chapter 2

(Fig. 6.4b). Thus, either the PPB is deposited just before division, 2 ± 1h according to this experiment, or this experiment was only able to capture those larger cells, which would quickly cycle to meiosis due to their size if the PPB were indeed involved in G2 size sensing, as also suggested by the observation that more than half of the cells observe depositing the PPB did not divide during the course of the experiment.
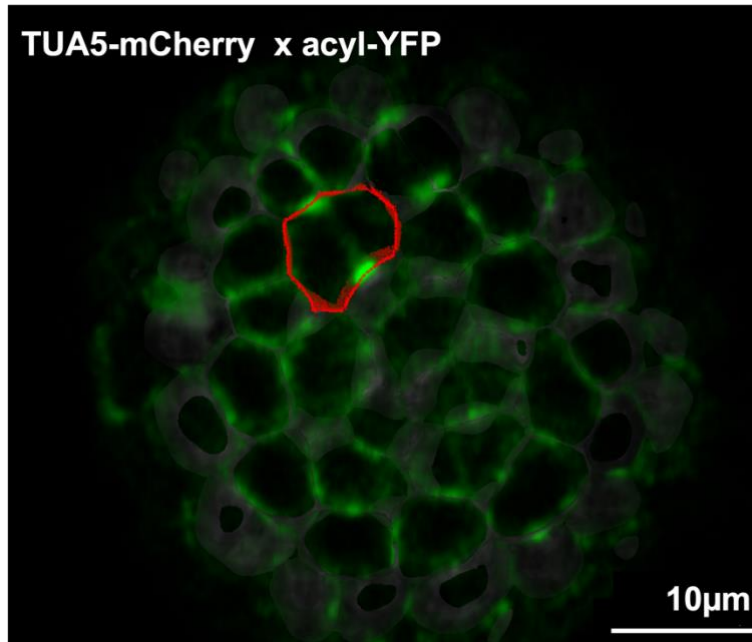
Figure 6.6: Manual selection of PPB cells in MorphoGraphX. Slice of a TUA5-mCherry x acyl-YFP meristem in MorphoGraphX, showing the manual process of selecting cells with a PPB, shown in red. The black "ghostly" film is the cell-mesh produced in MorphoGraphX, used for downstream analysis.

To discriminate between these possibilities, a longer time course of 38h was performed with a resolution of 2h, with the help of Dr Rafael Tavares who imaged the 5 diurnal timepoints. Figure 6.5 shows a confocal slice of the same apex over 10h of the experiment, in which two cells are observed depositing the PPB (arrowheads) and dividing. One of the cells can be seen placing the spindle prior to mitosis (Fig. 6.5, long arrow). Measurements of cell volume at these transitions would require 3D segmentation. Unfortunately, imaging at short time intervals without photodamage required Airyscan technology (Fig. 6.5), which uses filters for acquisition of different channels, as opposed to light scattering techniques (Fig. 6.3b for light scattering comparison), in which the wavelength of each channel can be selected with a 5nm accuracy (see Material and Methods for more information on image acquisition). For this reason, the red signal coming from the microtubules marker often leaked in the yellow channel of the plasma membrane, creating difficulties when segmenting those images. This is visible when comparing the plasma membrane signal in Figure 6.5 with the one in Figure 6.3b, the latter being stronger and more defined. Note

that leaking prevented the use of higher laser power for YFP excitation, which would also increase excitation of mCherry.
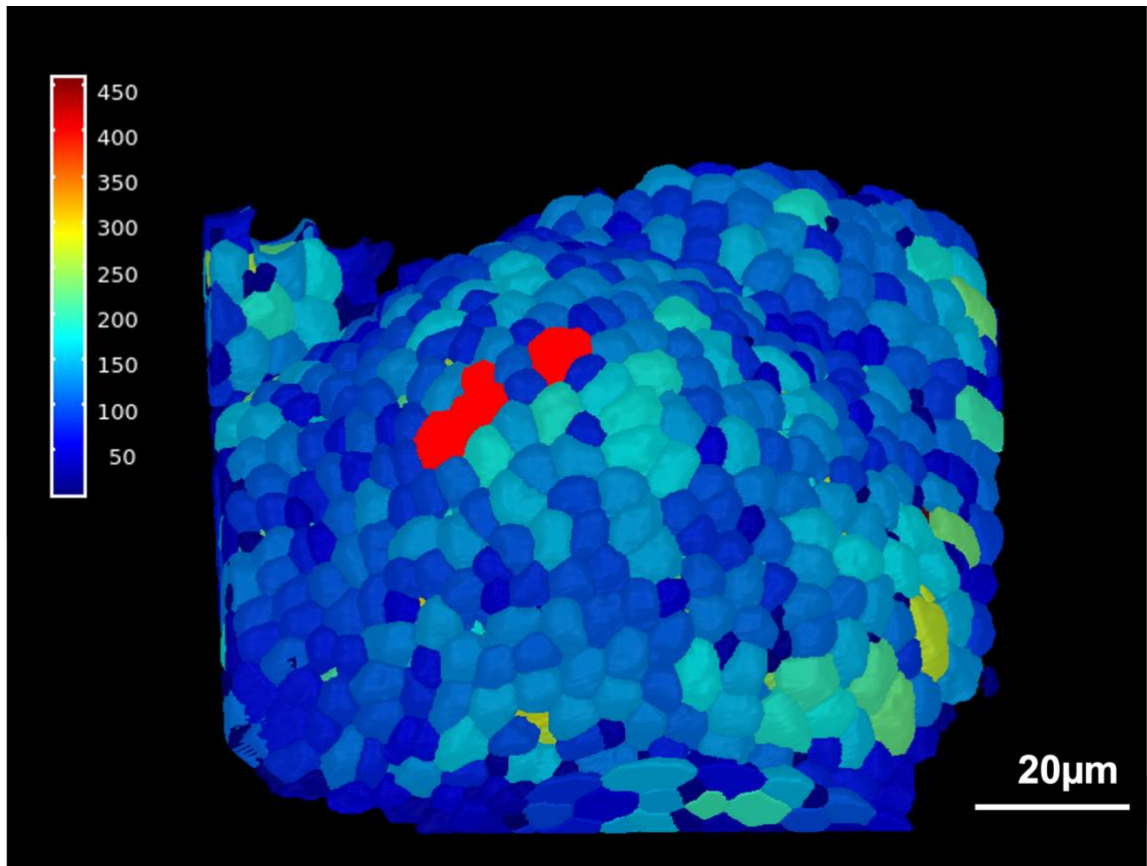
Figure 6.7: Example of apex analysed with MorphoGraphX. 3D cell mesh coloured by cell volume (scale on the left, μm^3) of one time point of the extended time course. Cells in red are those manually selected for PPB presence as shown in Figure 6.6.

Excessive segmentation of imaged cells can be corrected by manually merging virtual cells. To facilitate this process, I utilised the software MorphoGraphX (Fig. 6.6 and 6.7) (Hervieux *et al.*, 2016; Sapala *et al.*, 2018), which not only allows for manual corrections to be performed much more easily, but also implements a trained, neuronal network method for detection of cell walls, which hugely shortened the time required for data analysis. Nevertheless, because of my time constraints, the data will still require much more work to be curated more accurately, because each of the apex (19 images per time points, for a total of 57 images for 3 technical repeats) requires manual correction, and because the generation of accurate parenting, a process heavily hindered by segregation artefacts, also requires manual corrections. Additionally, cells containing the PPB need to be manually selected in three dimensions, which can be done in MorphoGraphX by production a cell-mesh and selecting cells via visualisation of difference confocal stack (Fig. 6.6). Once the
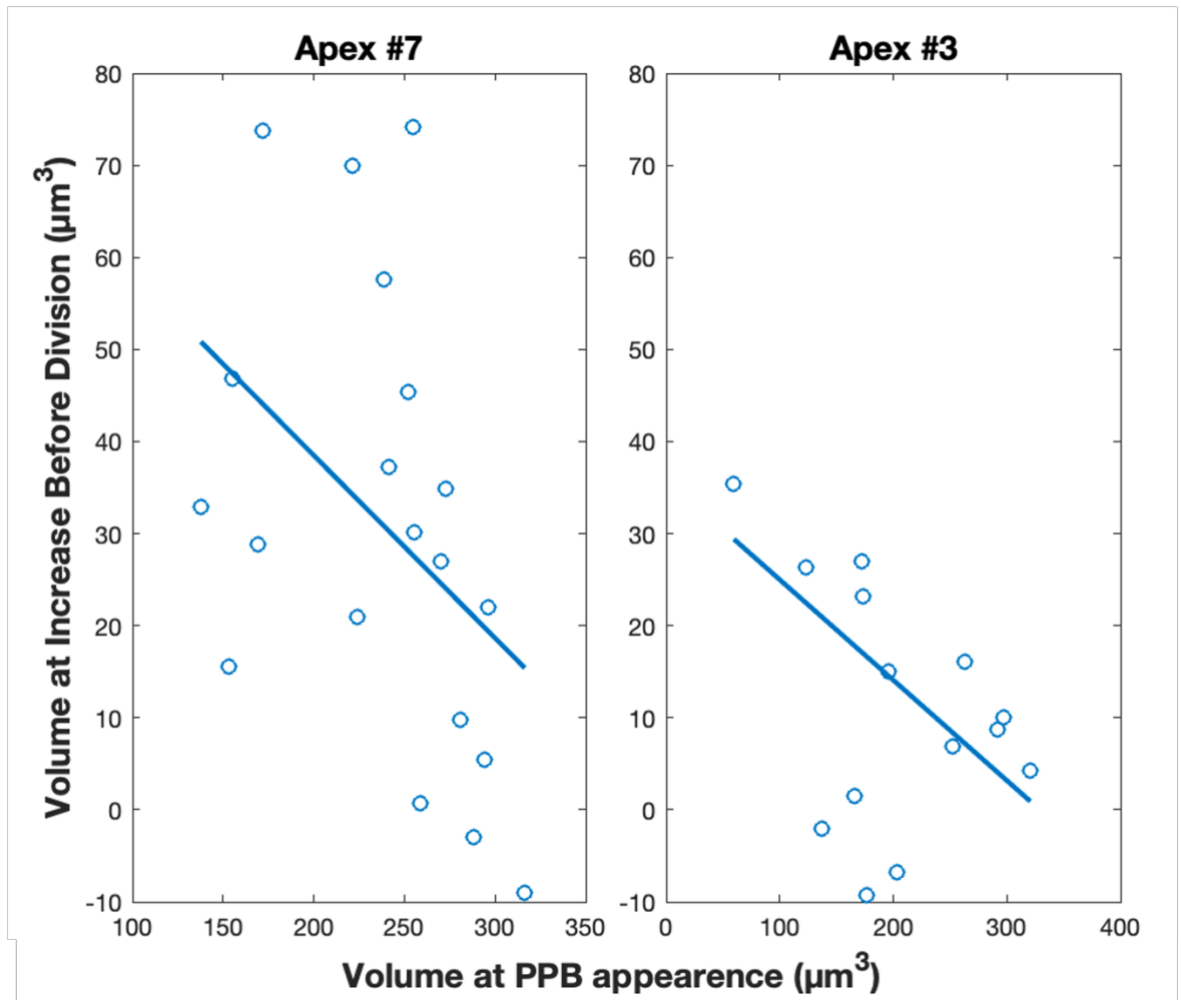
Figure 6.8: Larger cells accumulate less volume between PPB appearance and division. Comparison between the volume of cells when the PPB first appeared and the volume increase before division in two different apexes, using different programs for analysis. The slope of the linear regression is similar for both apexes (slope = - 0.2 in #7 and -0.1 in #3) but the correlation is stronger in #7 (R^2 = 0.18) than in #3 (0.02). Note that the population of preprophase cells is better represented in this data set (ranging from 100 to 350μm^3) compared to the shorter dataset in Figure 6.4, indicating a high variability in preprophase duration.

data are correctly curated, PPB cells can be extracted from the 3D stacks (Fig.6.7) and analysed separately, which I did with custom MATLAB scripts (see material and methods).

So, with the caveat that the data needs more replicates to be analysed and a more accurate curation of the developing apex, Figure 6.8 shows the correlation between volume increase and size at PPB deposition in two different apexes: Apex #3 which I analysed using MorphoGraphX, and Apex #7 analysed independently by Professor Robert Sablowski using custom Python scripts and Fiji (Serrano-Mislata, Schiessl and Sablowski, 2015). In both cases, there seems to be a negative relationship between cell size at PPB deposition and size at division (#7 slope = -0.2 and #3 slope = -0.1), with Apex #7 showing a stronger correlation (R^2=0.18) and Apex #3 showing a weaker one (R^2=0.02). Unfortunately, I do not

think this is enough to confirm nor reject the hypothesis of size control during preprophase, and more apexes need to be analysed for this purpose. Nevertheless, the high variability in the interval between PPB appearance and division (7.7 ± 5h), suggests that this process is not simply on a timer and that there is active regulation of progression through preprophase. The hypothetical size regulation would have to act through the cell cycle machinery, acting between the boundaries of PPB positioning and cell cycle progression. With these considerations in mind, let us now focus our attention on the inhibitors of G2 progression: the SMRs.
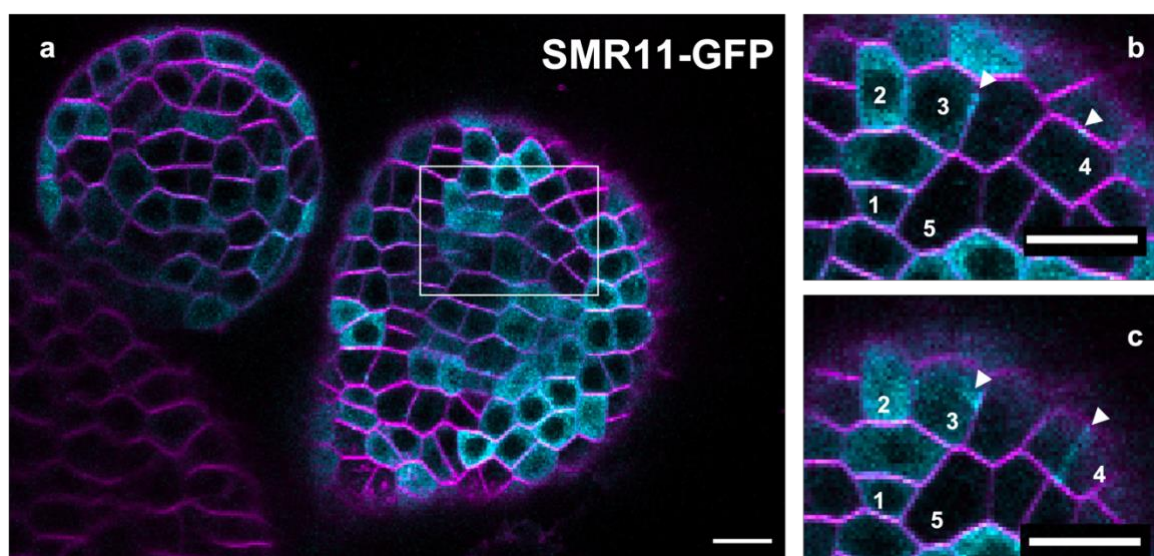
Figure 6.9: SMR11 subcellular localisation changes during the cell cycle. Confocal slice of a line expressing SMR11-GFP showing subcellular localisation of the protein. The white rectangle in (a) represents the view in (b) and (c), which are two different slices of the same confocal stack. SMR11 concentration starts low (cell 1) and increases, presumably during G1 (cell 2) without entering the nucleus. During preprophase, SMR interacts with the PPB (cell 3) and disappears from the cytoplasm (cell 4) during this period. Before dividing, SMR11 is no longer detectable inside the cell (cell 5). Scale bar = 10µm.

6.4 SMR protein family

To test whether members of the SMRs family could perform a role as G2/M size sensors, SMR11 was chosen as a potential candidate due to its known expression in the meristem (Yang, Wightman and Meyerowitz, 2017). A GFP-tagged line was produced to study the subcellular localisation of SMR11 and test whether it associates with the PPB. SMR11 subcellular localisation appeared to be dependent on cell size and, presumably, on cell cycle progression (Figure 6.9). In small cells, presumably those in early G1, SMR11 expression was low, but it visibly occupied the cytoplasm, and it was excluded from the nucleus (Fig. 6.9b and c, cell 1). Later in the cell cycle, in what I would assume was late G1

or early G2, SMR11 cytoplasmic concentration seemed to increase, whilst still being excluded from the nucleus (Fig. 6.9b and c, cell 2).
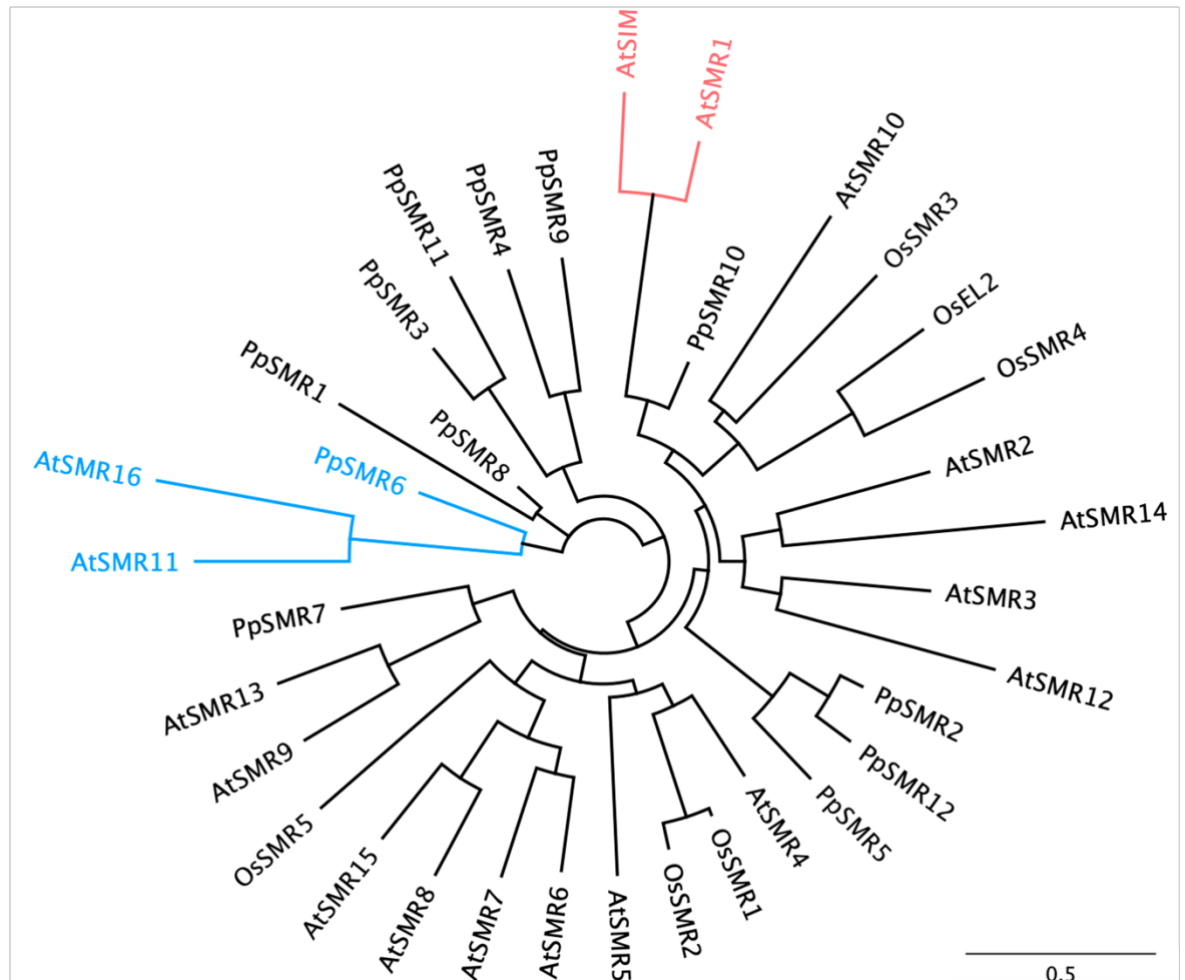
Figure 6.10: Sequence similarity in the SMR family. Tree based on protein sequence similarities of SMR members, comparing sequences form Arabidopsis (At), *Physcomitrium patens* (Pp) and rice (Os). SIAMES (SIM), which gives the name to the family, and its most similar member SMR1 (also known as LGO) are highlighted in red. SMR11, SMR16, subject of this study, are most similar to other moss SMRs than other Arabidopsis proteins, like PpSMR6, and are highlighted in blue. Scale bar = 0.5 substitution per site, calculated as number of substitutions per 100 amino acids.

SMR11 localisation in the cytoplasm could explain why these proteins do not have an inhibitory effect during G1 (Churchman *et al.*, 2006) – they are simply unable to interact with CDKa, which is localised in the nucleus during this period. This simple mechanism would give SMR11 a way to be produced during G1, without interfering with size homeostasis regulated by KRP4. At some point during PPB appearance, SMR11 can be seen localised both in the cytoplasm and on the PPB (Fig. 6.9b and c, cell 3), suggesting that either SMR11 has a role in the control of PPB assembly, or that it could be involved in the hypothetical role of the PPB in size sensing. Later in G2, SMR11 seemed to only be visible in its PPB-bound state (Fig. 6.9b and c, cell 4), suggesting either a progressive accumulation

in the PPB or removal of the cytoplasmic population. Finally, in very large cells, those that were presumably about to divide, SMR11 was not visible, possibly because the PPB has been disassembled and the cell was ready for chromosome segregation (Fig. 6.9b and c, cell 5). An extensive time lapse of SMR11 with a CDT1 marker would greatly support these observations. Nevertheless, considering that SMR11 is expected to be an inhibitor of G2/M progression, and due to its known expression in the meristem, its cell cycle dependent cell localisation, its behaviour perfectly fitted a role as a surface area, or pseudo-area, sensor in G2, making this protein of great interest. In this scenario, the putative infomration on cell size carried out SMR11, might be delived into the nucleus by CDKa, known to localise there during G2, but also at the PPB (Boruc *et al.*, 2010).
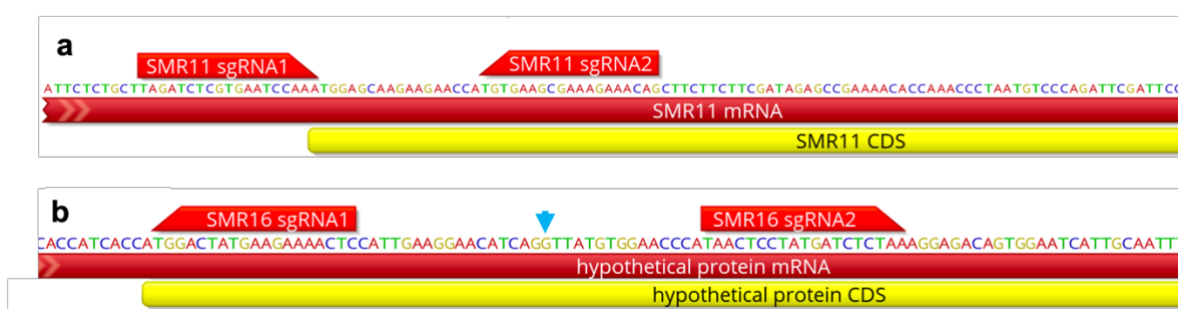
Figure 6.11: CRISPR design for SMR11 and 16. Close up of protein coding regions of SMR11 (a) and 16 (b), showing the direction and location of the sequences used to construct small guide RNAs (sgRNAs). The cyan arrow shows a site commonly found to be mutated when genotyping CRISPR lines. Long red bar shows mRNA and yellow bar shows coding sequence (CDS).

6.5 CRISPR of SMR11/16

Encouraged by the information on the cellular localisation and behaviour of SMR11, to study the possible role of SMRs in size sensing during G2, a mutational approach was taken. To exclude possible redundancy of SMR11, a phylogenetic tree was produced using sequences from *Oryza sativa* and *Physcomitrium patens*, to identify possible closely related members of the family (Fig. 6.10). Consistent with previously conducted PCA (Kumar *et al.*, 2015), SMR11 clustered together with SMR16, suggesting that, if any SMR performs a redundant function to SMR11, SMR16 would be the most likely candidate. Interestingly, SMR11 and 16 share more sequence similarity with some of the moss proteins than with the remaining members of the Arabidopsis family, with 7 of the 12 *P. patens* SMRs clustering together with SMR11 and 16, suggesting a possible conserved role in these distant organisms. Therefore, a CRISPR approach was taken, aimed to knock out SMR11 and 16 at once. Small RNA guides were designed to target the beginning of the coding

sequence of both genes (Fig. 6.11) and various transgenic lines were produced and analysed.

I selected for transformants using the Fast Red seed coat marker (Shimada, Shimada and Hara-Nishimura, 2010) after two independent rounds of transformations, both of which yielded fewer transgenic seeds than in my other CRISPR experiments (those involved in the production of *krp3-11* mutant, Chapter 5) (~20 red seeds in this case, versus an average of more than 100), suggesting low recovery, possibly due to lethality. The survival after sowing was also very low and only half of the seeds reached maturity (12 plants). One of these showed a stunted growth phenotype, never produced pollen and, therefore, seeds. The carpels showed large cells growing and bulging out (Fig. 6.12), a phenotype potentially connected with SMRs inhibitory role in endoreduplication (Kumar *et al.*, 2015).

Figure 6.12: Phenotype of CRISPR *smr11,16-7* mutant. Gynoecia of the same individual, showing the phenotype of the mutagenized plant, presumably associated with mutations in *SMR11* or *16*. Note the giant cells (arrowhead) bulging out of the carpel epidermis.

To detect any mutations in SMR11 and SMR16, I cloned and sequenced the regions expected to be affected by CRISPR mutagenesis. In many cloning attempts, the only mutation I ever identified in SMR16 was a SNP in position 65, which resulted in a glutamate to aspartate mutation (Fig. 6.11b, cyan arrow). In contrast, SMR11 sequences were often mutated, ranging from SNPs to large insertions and deletions (Fig. 6.13). The variability in sequences was observed within the same plants, indicating that the majority of the tissue analysed (inflorescences) was chimeric. This was also true for the mutant *smr11/16-7*, whose phenotype is shown in Fig 6.12. In this plant, two *smr11* alleles were recovered, both

of which had mutations that removed the start codon (Fig. 6.13, bottom panel). In one of the alleles (SMR11-7-3, Fig. 6.13, bottom panel), the start codon was missing but, if an alternative ATG was present further upstream, the predicted protein could be in frame. In the other allele (SMR11-7-2.3, Fig. 6.13, bottom panel), multiple stop codons preceded the bulk of the reading frame, so translation of SMR11 should be prevented (Fig. 6.13, bottom panel). This sequencing experiment suggested that there might not be the need to target *SMR16* for mutation to reveal the consequences of *SMR11* loss of function. However, loss of *SMR11* function could result in a sterility. Further progress in revealing the function of SMR11 may require an inducible loss of function approach, as described in Chapter 4 for *FBL17*.
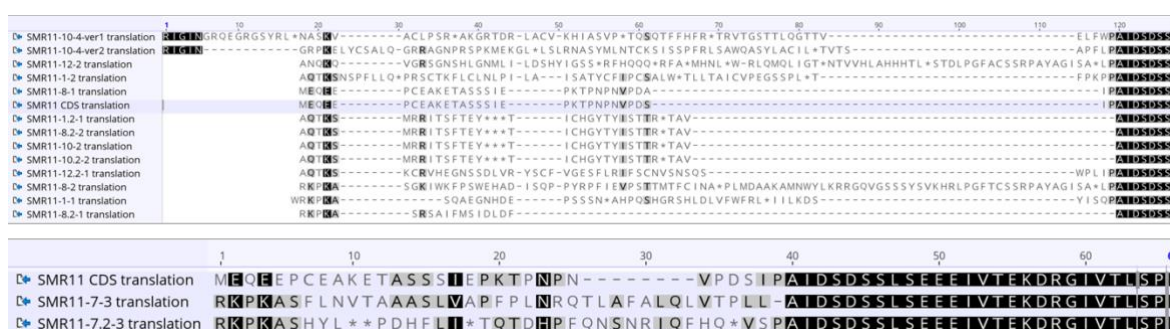
Figure 6.13: Possible protein products of detected SMR11,16 CRISPR alleles. After genotyping of various CRIPSR-mutagenized plants, the sequences were used to predict the encoded protein sequences. The wild-type protein (SMR11 CDS translation) is highlighted in blue in the top panel. Many of the alleles found could result in a knockout of SMR11. The bottom panel highlights *smr11,16-7*, shown in Figure 6.12. Blosum62 score matrix was used for alignment and consensus, which is coloured by Bosum62 similarity as follows: black = 100%, dark grey = 80 to 100%, light grey = 60 to 80%, no colour less than 60%.

6.6 Discussion

In this chapter, I sought to test the idea of an area sensing mechanism in G2 that involves the PPB, putatively using this structure as an internal scale. However, much still needs to be done to test this hypothesis. One critical aspect, which was not fully considered here, is that the supposed scaling of G2 cells is of a geometric quantity that mathematically resembles surface area in *S. pombe*, but in reality is likely to be a more complex measurement, which scales like the volume divided by the size of the PPB, in a system analogous to the one shown for the cortical band in fission yeasts (Pan *et al.*, 2014; Facchetti *et al.*, 2019). Therefore, improved experiments that utilise cell shape mutants should compare the ratio between cell volume and the PPB size, rather than surface area alone. This can be done using *pok1/*2, in which PPB still form correctly (Müller, Han and

Smith, 2006). Ideally, this experiment would be conducted in live tissues, rather than on fixed samples, with a low-resolution time course and the purpose of selecting dividing cells only, reducing the variability in the distribution of size associated with cell population-bases studies, like the one conducted here for *pok1/2*. If the hypothesis were supported, it would present a mechanism connecting volume at S-phase to the area at division, using PPB as an internal metric. As mentioned before, since the size of the PPB will depend on the size and shape of the cell during PPB deposition, the size information carried through G2 would contain information from preprophase. In this way, a PPB-based mechanism would not have intrinsic, constant information to measure size, rather serve as a mean to measure the ratio between different geometric quantities of a cell.
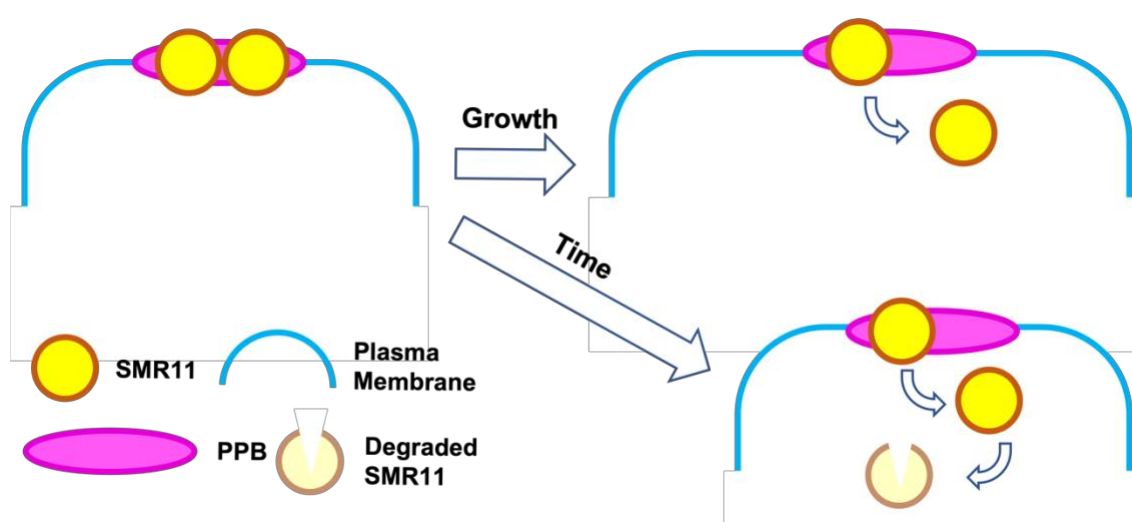
Figure 6.14: Hypothetical mechanisms for SMR11 action. SMR11 accumulated on the PPB (top left) and its concentration on it would be dependent on cell volume during PPB deposition. In the growth-based mechanism, dissociation of SMR11 from the PPB would be triggered by growth (top right), whilst in the "hourglass" mechanism, dilution would be driven by proteolysis of cytosolic SMR11 (bottom right).

Although the possible role of SMR11 in size sensing during G2 could not be tested, it was interesting to see that SMR11 associates with the PPB throughout preprophase. In fact, SMR11 was chosen for its expression in the meristem (Yang, Wightman and Meyerowitz, 2017) and its observed subcellular behaviour was surprisingly similar to the one expected for a protein performing this function. SMR11 concentration visibly increased from birth to preprophase until the PPB appeared. At this point, the amount of SMR11 proteins would contain information on cell volume, but this information could not be interpreted by the cell, because it would still be in the form of cytosolic concentration. In this way, the PPB would offer a way to transform the information locked in SMR11 concentration in the form of quantity, by delocalising the SMR11 on the PPB. At this point, the concentration of SMR11 on the PPB would be proportional to the volume at PPB deposition and could be

read by components of the cell cycle that localise in this area, like CDKs (Boruc *et al.*, 2010) (Fig. 6.14). Of course, growth would cause dissociation of SMR11 from the PPB (Fig. 6.14), until its inhibitory effect on CDKs is released, in a mechanism connecting volume at the entry of preprophase with surface area at division. Note that the size regulation performed by Cdr2 works inversely to this putative mechanism, in which SMR11 concentration on the PPB is lowest after commitment. The slow disappearance of SMR11 during mitosis could be part of a reinforcing feedback loop that ensures removal of SMR11 after commitment of progression through the cell cycle. After division, SMR11 accumulation begins once more, ready for the next round.

It is possible that disappearance of SMR11 at the end of G2 is not a consequence of commitment to mitosis, rather part of the mechanism by which SMR11 control mitotic progression. If a component acted to remove SMR11 from the cytoplasm, but not on the PPB, similarly to shielding of KRP4 on DNA, SMR11 proteins would act like the grains in an hourglass, slowly disassociating from the PPB to be destroyed in the cytoplasm (Fig. 6.14). Although this scenario might appear like a timer mechanism, leading to mitosis in a time dependent manner, the amount of SMR11 stored on the PPB is hypothesised to be proportional to volume, and so would be the time of progression to mitosis. In this scenario, the SMR11/PPB mechanism would not necessarily be considered a cell size control mechanism, rather a mechanism for cell cycle proregression that translates information on size to information on time for cell cycle progression. More experiments, combined with a detailed mathematical understanding of different behaviours will be critical in dissecting the molecular mechanism that might link the amount of SMR11 to commitment to division.

It is possible that the G1/S size control mechanism described in previous chapters completely pre-empts any size regulation during G2, so that in meristem cells the impact of such a mechanism would normally be minimal. Nevertheless, it is fascinating to speculate that multiple mechanisms could be recruited to different extents by different developmental programs. So, different geometric quantities could be used to link cell size to cell cycle progression, depending on the function of different cell types. I hope that future studies on cell size control will take into account this possibility and show the many ways that cells can measure their size.

6.7 References

Boruc, J. *et al.* (2010) 'Systematic Localization of the Arabidopsis Core Cell Cycle Proteins Reveals Novel Cell Division Complexes', *Plant Physiology*, 152(2), pp. 553–565. doi: 10.1104/pp.109.148643.

Churchman, M. L. *et al.* (2006) 'SIAMESE, a plant-specific cell cycle regulator, controls endoreplication onset in Arabidopsis thaliana', *The Plant cell*. 2006/11/10. American Society of Plant Biologists, 18(11), pp. 3145–3157. doi: 10.1105/tpc.106.044834.

Facchetti, G. *et al.* (2019) 'Reprogramming Cdr2-Dependent Geometry-Based Cell Size Control in Fission Yeast', *Current Biology*, 29(2), p. 350–358.e4. doi: https://doi.org/10.1016/j.cub.2018.12.017.

Garmendia-Torres, C. *et al.* (2018) 'Multiple inputs ensure yeast cell size homeostasis during cell cycle progression', *eLife*. Edited by A. Musacchio. eLife Sciences Publications, Ltd, 7, p. e34025. doi: 10.7554/eLife.34025.

Gutierrez, R. *et al.* (2009) 'Arabidopsis cortical microtubules position cellulose synthase delivery to the plasma membrane and interact with cellulose synthase trafficking compartments', *Nature Cell Biology*, 11(7), pp. 797–806. doi: 10.1038/ncb1886.

Hervieux, N. *et al.* (2016) 'A Mechanical Feedback Restricts Sepal Growth and Shape in Arabidopsis', *Current Biology*. Elsevier Ltd, 26(8), pp. 1019–1028. doi: 10.1016/j.cub.2016.03.004.

Jones, A. R. *et al.* (2017) 'Cell-size dependent progression of the cell cycle creates homeostasis and flexibility of plant cell size', *Nature Communications*. Nature Publishing Group, 8, p. 15060. doi: 10.1038/ncomms15060.

Kumar, N. *et al.* (2015) 'Functional Conservation in the SIAMESE-RELATED Family of Cyclin-Dependent Kinase Inhibitors in Land Plants', *The Plant Cell*, 27(11), pp. 3065–3080. doi: 10.1105/tpc.15.00489.

Livanos, P. and Müller, S. (2019) 'Division Plane Establishment and Cytokinesis', *Annual Review of Plant Biology*. Annual Reviews, 70(1), pp. 239–267. doi: 10.1146/annurev-arplant-050718-100444.

Louveaux, M. *et al.* (2016) 'Cell division plane orientation based on tensile stress in Arabidopsis thaliana', *Proceedings of the National Academy of Sciences*, 113(30), p. E4294 LP-E4303. doi: 10.1073/pnas.1600677113.

Müller, S., Han, S. and Smith, L. G. (2006) 'Two Kinesins Are Involved in the Spatial Control of Cytokinesis in Arabidopsis thaliana', *Current Biology*, 16(9), pp. 888–894. doi: https://doi.org/10.1016/j.cub.2006.03.034.

Nurse, P., Thuriaux, P. and Nasmyth, K. (1976) 'Genetic control of the cell division cycle in the fission yeast Schizosaccharomyces pombe', *Molecular and General Genetics MGG*, 146(2), pp. 167–178. doi: 10.1007/BF00268085.

Pan, K. Z. *et al.* (2014) 'Cortical regulation of cell size by a sizer cdr2p', *eLife*, 2014(3), pp. 1–24. doi: 10.7554/eLife.02040.

Pickett-Heaps, J. D. and Northcote, D. H. (1966) 'Organization of microtubules and endoplasmic reticulum during mitosis and cytokinesis in wheat meristems', *Journal of Cell Science*. Company of Biologists, 1(1), pp. 109–120.

Rasmussen, C. G., Sun, B. and Smith, L. G. (2011) 'Tangled localization at the cortical division site of plant cells occurs by several mechanisms', *Journal of Cell Science*, 124(2), pp. 270–279. doi: 10.1242/jcs.073676.

Salic, A. and Mitchison, T. J. (2008) 'A chemical method for fast and sensitive detection of DNA synthesis in vivo', *Proceedings of the National Academy of Sciences*, 105(7), p. 2415 LP-2420. doi: 10.1073/pnas.0712168105.

Sapala, A. *et al.* (2018) 'Why plants make puzzle cells, and how their shape emerges', *eLife*. Edited by S. McCormick. eLife Sciences Publications, Ltd, 7, p. e32794. doi: 10.7554/eLife.32794.

Serrano-Mislata, A., Schiessl, K. and Sablowski, R. (2015) 'Active Control of Cell Size Generates Spatial Detail during Plant Organogenesis', *Current Biology*. The Authors, 25(22), pp. 2991–2996. doi: 10.1016/j.cub.2015.10.008.

Shimada, T. L., Shimada, T. and Hara-Nishimura, I. (2010) 'A rapid and non-destructive screenable marker, FAST, for identifying transformed seeds of Arabidopsis thaliana', *The Plant Journal*. John Wiley & Sons, Ltd, 61(3), pp. 519–528. doi: https://doi.org/10.1111/j.1365-313X.2009.04060.x.

Walker, K. L. *et al.* (2007) 'Arabidopsis TANGLED Identifies the Division Plane throughout Mitosis and Cytokinesis', *Current Biology*, 17(21), pp. 1827–1836. doi: 10.1016/j.cub.2007.09.063.

Weart, R. B. *et al.* (2007) 'A Metabolic Sensor Governing Cell Size in Bacteria', pp. 335–347. doi: 10.1016/j.cell.2007.05.043.

Weiss, D. S. (2004) 'Bacterial cell division and the septal ring', *Molecular Microbiology*. John Wiley & Sons, Ltd, 54(3), pp. 588–597. doi: https://doi.org/10.1111/j.1365-2958.2004.04283.x.

Yabuuchi, T. *et al.* (2015) 'Preprophase band formation and cortical division zone establishment: RanGAP behaves differently from microtubules during their band

formation', *Plant Signaling and Behavior*, 10(9), pp. 1–11. doi: 10.1080/15592324.2015.1060385.

Yang, W., Wightman, R. and Meyerowitz, E. M. (2017) 'Cell Cycle Control by Nuclear Sequestration of CDC20 and CDH1 mRNA in Plant Stem Cells', *Molecular Cell*. Elsevier Inc., 68(6), p. 1108–1119.e3. doi: 10.1016/j.molcel.2017.11.008.

Yi, D. *et al.* (2014) 'The Arabidopsis SIAMESE-RELATED cyclin-dependent kinase inhibitors SMR5 and SMR7 regulate the DNA damage checkpoint in response to reactive oxygen species', *The Plant cell*. 2014/01/07. American Society of Plant Biologists, 26(1), pp. 296–309. doi: 10.1105/tpc.113.118943.

Chapter 7: Discussion

7.1 Summary and conclusion

In this work, I sought to investigate the mechanism responsible for cell size homeostasis, using the Arabidopsis meristem as model system. First, I develop a novel imaging protocol in which extensive time lapse experiments can be carried out at high time resolution, allowing for imaging of living tissue every 2h. This approach was critical to observe how cell cycle progression was linked to cell size and answer the question on when during the cell cycle is cell size variability corrected. Using a new cell cycle marker (described in (Desvoyes *et al.*, 2020)) I was able to discriminate between different cell cycle phases and show that cell size variability, which was highest at birth, was reduced at S-phase, and remained comparable until division. This strongly suggested that any mechanism for reduction in cell size variability acted between birth and S-phase, likely counteracting variability by linking cell size to the progression into the G1/S transition. It also suggests that another mechanism, likely of a different nature, acts in G2 to prevent further accumulation of variability before division.

With this information, I moved my attention to the plant inhibitors of the G1/S progression, inspired by previous work that emphasised dilution of inhibitor as primary mechanism for cell size-dependent cell cycle progression in other organisms (Umen and Goodenough, 2001; Schmoller *et al.*, 2015; Zatulovskiy *et al.*, 2020). After showing that RBR behaves very unlike its non-land plants counterparts, I observed KRP4 being diluted during G1, and then being accumulated in G2. This behaviour was in line with the one expected for a cell size sensor, but required a further step, involving a system to ensure size independent accumulation during G2, as well as equal inheritance at division. The observation that KRP4 is bound to chromatin throughout the cell cycle, seemed to be the answer of both problems, suggesting a mechanism that uses DNA as internal metric to measure and partition KRP4 amount. To ensure that KRP4 production matched DNA amount, a mechanism was suggested in which overproduction of KRP4 during G2 was followed by removal of excess of the protein. The E3-ligase FBL17 was selected as candidate for performing this role and using mutant lines I was able to show that FBL17 is required for size independent accumulation of KRP4, and that mutation in the *FBL17* gene resulted in loss of cell size homeostasis, loss particularly affecting larger cells.

To better understand the phenotype observed in the *fbl17* mutants and predict mutation of other genes, I developed a quantitative mathematical model, which I was able to solve analytically to show the relationship between cell size at the G1/S transition and KRP4 amount at birth. The model highlighted that the two population of KRP4, the DNA-bound one and the nucleosolic one, play a "tug of war" in favour and against cell size homeostasis, respectively. The model also explained that volume at birth enhances the effect of nucleosolic KRP4, explaining the effect on cell size variability in the *fbl17* mutants and was ablet to recapitulate the cumulative effect of the *krp3* and *krp4* mutants, the former being generated in this work using CRISPR technology. Thus, I was able to identify and describe a mechanism for cell size homeostasis that acts at the G1/S, which uses DNA as an internal standard to counteract cell size variability accumulated during division.

7.2 Intracellular metrics: three components to measure size

As part of this work, I presented a molecular mechanism in which genomic content is used as an intracellular metric to measure cell volume. KRP4 is the protein used to relay this information to the cell cycle machinery, in the form of inhibition to entry into the S-phase. Critically, FBL17 is required to ensure that the amount of KRP4 matches the genomic content. So, in this system, each of the components plays a unique role in size control. First, there is DNA, which act as a "ruler", the standard, the internal scale that sets the metric. It is so fascinating, and poetic in a way, that DNA performs such an important role in size control. The role of DNA as the holder of genetic information (Franklin and Gosling, 1953; Watson and Crick, 1953) is fundamental to our understanding of biology; here, I showed that DNA contains another type of information, related to cell size, embedded in its physical presence inside the cell. In this comparison, KRP4 performs a role analogous to that of a transcription factor, or an RNA-polymerase, accessing and releasing this information to the rest of the cell. Indeed, KRP4 has the role of a molecular relay, delivering the information accessed during G2, when KRP4 receives information on the amount of DNA present in the cell, to the daughter cells during G1, when KRP4 is slowly released from DNA in proportion to cell size. The information retrieved by KRP4 in G2 requires FBL17, whose role is to ensure that KRP4 is using the right unit of measure. Indeed, in *fbl17* mutants, KRP4 is still able to carry the information it accessed during G2, but cannot discriminate between DNA and nucleosol, thus delivering the wrong information to the cell.

It is to expect that any mechanism for cell size regulation would require these three components: a standard, a molecular relay and a gauger. In the plant meristem, these three players are separate, but other mechanisms could use the same molecule to perform more than one function. An example of this can be observed in the mechanism proposed for Cdr2 (Pan *et al.*, 2014), in which the role of standard is played by the cortical band, while Cdr2 performs the dual function of measuring the size and delivering the information to the cell. A contrasting example is the mechanism involving the FtsZ ring in bacteria, which also plays a dual role, in this case as standard and molecular relay, whilst the gauging role is played by the molecule UgtP, which measures information related to metabolic activity against the size of the contractile ring (Weart *et al.*, 2007). In fact, FtsZ acts as internal standard in an analogous way to the cortical band of fission yeast, providing a subcellular region of fixed size, but unlike the cortical band, it also delivers the size information by contracting, initiating cytokinesis.

Of course, this view might be simplistic, because many other factors can act through each one of the components, individually or simultaneously affecting standard, measuring process or information delivery. Some intrinsic factors have already been discussed in Chapter 5, where mathematical modelling of the KRP4 dynamics highlighted the impact that affinities between molecules can have on the output of size regulation. Indeed, the intrinsic constants of binding and unbinding are part of the cellular metric and play a similar role performed by different standard of measurement, like kilograms versus pounds, which measure the same quantity, but use different scales. The extent to which this feature is used by the cell will require dissection of individual dynamics, which I hope will be the subject of future studies. Nevertheless, in the case of Cdr2, the importance of these dynamics constants has been emphasised by target mutations that changed scaling of Cdr2 from surface area to cell length (Facchetti *et al.*, 2019). Endoreduplication performs a similar role, yet more direct than changing of dynamics constants would, scaling up the internal standard by increasing DNA amount. It is interesting to notice however, how cells can be "fooled" to sense that everything is smaller than it actually is, simply by changing the metric for measuring size. An intelligent designer would have organised this very differently, as we do with rulers, asking the reader to measure different amounts, rather than changing the scale.

The further role performed by DNA in size control is to ensure equal inheritance of KRP4 by daughter cells. In this case, however, the function of DNA converges with that of KRP4 in delivering the information to G1 cells, rather than performing the role of standard itself. This subtle, yet critical, distinction is emphasised in the proposed model for Whi5, in which the role of the standard is not played by DNA, but chromosomes are still used as means for equal inheritance between daughter cells (Swaffer *et al.*, 2021). The information on size, which is delivered by Whi5 in the form of protein concentration, is contained in the Whi5 promoter, which transcribes the protein in a size independent manner, unlike other proteins (Swaffer *et al.*, 2021). Therefore, the activity of the Whi5 promoter acts as the internal scale used by yeast cells to measure size, providing size independent information and performing a similar role to chromatin in plants and cortical band in fission yeast. In this way, the gauging component in the system is the time during G2 required for production of Whi5 mRNA, which if constant, results in a reproducible accumulation of Whi5 (Schmoller and Skotheim, 2015). Thus, the role of DNA in the proposed mechanism for size homeostasis in budding yeast is not as an internal standard, like it is in the plant meristem, but rather as a vehicle for delivery of the size information which is held by Whi5.

An interesting property of the Whi5 mechanism described above is that increasing variability in the time of Whi5 production could result in the coupling between Whi5 levels and cell volume, leading to loss of size homeostasis. Additionally, loss of size-independent production of Whi5 mRNA would mean loss of the internal size standard, and consequently loss of size regulation. However, changes in the *Whi5* promoter region, which resulted in scaling of the RNA amount with volume, did not lead to loss of size homeostasis (Barber, Amir and Murray, 2020). This observation generated scepticism in the community about the role of Whi5 as a size sensor and the following years will show how this issue will be resolved. Thus, the major weakness of the mechanism suggested for Whi5 is the utilization of production length as gauging component for size regulation, implying that any error in controlling this length, would impact variability in size. In contrast, in the plant meristem FBL17 contributes to the robustness of the system by counteracting KRP4 accumulation, so that any variability in KRP4 accumulation is corrected by protein degradation – in the Whi5 mechanism, the opposite is true, with the gauging mechanism contributing to variability in protein production, instead of counteracting it.

To conclude, I suggest that mechanisms for measuring cell size require three components to achieve control, and manipulating each of them would have a different impact on size regulation. The nature of these components might coincide, however, and part of the role might be shared between molecules. You might now be wondering how the cell could measure features other than cell volume. Inspired by the elegant biotechnological work carried in fission yeast (Facchetti *et al.*, 2019), let us discuss this idea further.

7.3 Transforming information between metrics: interfacing between quantities

In our macroscopic world it is obvious that measuring different quantities requires different units, like using seconds to measure time or grams to measure mass. A less obvious observation is that the measuring devices we use often operate by transforming one unit into another to relay this information to us. For example, a pocket watch is clearly designed to measure time, but this information is provided in the form of radians, degree angles, to be interpreted by ourselves as seconds, minutes, and hours. Cells are not different and require information to be transformed in the form of molecule concentration to be interpreted. In the example provided in this text, KRP4 just transforms information on concentration of a molecule to the concentration of another, from nucleic acid concentration to protein concentration. Note that the unit for concentration is molarity, expressed as number of molecules per volume, or μm^{-3}. So the measurement of volume is intrinsic in protein concentration.

Considering the evidence of the interaction between CDKa and chromatin during the mitotic (Boruc *et al.*, 2010) and meiotic (Yang *et al.*, 2020) cycle, as well as chromatin localisation of protein required for CDKa activity (Vanstraelen *et al.*, 2004; Boruc *et al.*, 2010), it is likely that this information is further relayed via the interaction between CDKa and KRP4 on chromatin. So even if at a first glance the communication between G2 and G1 appears to be just the conversion of one concentration to another, a more complex system that uses chromatin as interface between genomic amount and cell volume might be in place. In fact, as we saw in Chapter 5, the dynamic of binding during G2 is different from that in G1, not only because the production of KRP4 is different, but because the binding rates are. I speculated that this difference in binding rate exists to allow KRP4 to perform different functions, to obtain the information in G2 and then release it during G1. So, perhaps the differential binding of KRP in G1 and G2 is directed by a different CYC/CDK pair, present in those two cell cycle phases. After all, a CYC binding domain is also present in the

primary sequence of KRPs (Torres-Acosta, Fowke and Wang, 2011), so interactions with CDK and CYC would not only be part of the cell cycle mechanism, but also work at the interface of the cell size signal communicated between KRP4 on chromatin and the rest of the cell. Note that this is different from the mechanism of binding to chromatin and shielding from FBL17, likely directed via Motif 8, as discussed in Chapter 4. This highlights the importance of future studies of the molecular nature of KRP4 association with chromatin, which would reveal the details of this critical mechanism for cell size regulation.

Other, more complex examples in which cells interface between different quantities are found in biology. One of this is the fascinating way in which cyanobacteria relay information on time using protein concentration (Rust *et al.*, 2007). Briefly, phosphorylation of the protein KaiC occurs in a burst and sets up the beginning of the clock – KaiC is then slowly dephosphorylated, until a minimum concentration is reached, when KaiC is phosphorylated once again (Rust *et al.*, 2007). Thus, the concentration of phosphorylated KaiC contains information on the time passed since the last burst of phosphorylation, in a system that transforms information on time to information on protein concentration. In this system, the rate of dephosphorylation of KaiC is the molecular metric that measures time, and it contains the information of time in its unit, that comprises the term "per second", s^{-1}. In fact, if dephosphorylation is dependent on the concentration of a single phosphatase, the unit of the rate of dephosphorylation would be $\mu m^3 s^{-1}$, which contains information for both concentration and time. So in a way, the dynamic constants can also provide an interface between two quantities, volume and time in this example, for molecular mechanism to translate information on one into the other.

In terms of measuring size, this flexibility is crucial when studying systems that measure quantities other than volume, because any quantitative information measured by the cell will need to be translated in terms of concentration. In the example found in fission yeast, one could say that the further role of the cortical band is to transform three-dimensional information encoded into Cdr2 concentration into two-dimensional information by interfering with Cdr2 dynamics (Pan *et al.*, 2014). As explained in detail in (Facchetti *et al.*, 2019), Cdr2 phosphorylation scales with volume because of the nature of protein-protein interactions. By interacting with the pool of phosphorylated Cdr2, the cortical band collects this volumetric information in a way that is proportional to its diameter, performing the division of volume by length (Facchetti *et al.*, 2019), i.e. $\mu m^3 / \mu m = \mu m^2$, effectively

extracting information on area from protein concentration. Interestingly, this system can be hijacked, so that interaction of Cdr2 with the cortical band occurs via the cell membrane, instead of cytoplasm, so that the information fed to the cortical band is surface area – so when the size is measured, the dividing operation returns information on length (Facchetti *et al.*, 2019), $\mu m^2/\mu m = \mu m$, rather than surface area. So, the role of the cortical band is to allow for information to be transformed between geometric quantities, effectively measuring the ratio between volume and cell diameter.

The idea of an interface for the comparison of one quantity to another to measure different quantities within the cell, like Cdr2 volumetric accumulation against cortical band size, or the KiC dephosphorylation constant, can be extended beyond the measuring of cellular components into measuring multicellular tissues. As a matter of fact, organ size is controlled genetically and macroscopic information that spans multiple cells has to be reduced and interpreted by single cells. Models that explain how cells expand using information fields generated by polarity have been recognised in leaves (Sauret-Güeto *et al.*, 2013) and there are plenty that discuss the role of auxin (for two recent reviews (Leyser, 2018; Du, Spalding and Gray, 2020)), but how information on organ size is relayed to single cells remains ambiguous. Models on carpel elongation after pollination have suggested a molecular component, unknown thus far, that diffuses from the tip of the carpel in a basipetal fashion and effectively counts the number of cells along the organ (Zhu *et al.*, 2020). The cell counting occurs because diffusion of this component through the membrane of each cell slows its movement, effectively being the only medium affecting diffusion (Zhu *et al.*, 2020). In this way, the plasma membrane transforms information on diffusion of this putative molecule into information on cell number along the carpel and, ultimately, organ size. Critically, consistent organ size in this system should depend on cell size homeostasis, which is used as starting point and internal metric, combined with information on diffusion rate, to archive predictable organ length.

Therefore, cells seem to require information to be presented to them in the form of molecular concentrations, but biological features, like subcellular structures or binding constants, can be implemented as interfaces between a diverse array of geometric and abstract quantities, to transform one information to another. This could be how the PPB functions in G2, integrating information from volume at early G2, and on cell surface prior to division. The possible interaction between volume and surface area makes this system

very appealing, because surface to volume ratio (SV) is perhaps more important in terms of fitness than cell volume (Gallet *et al.*, 2017), providing a more obvious trait for natural selection to operate. Thus, the role of the PPB could be more complex than just measuring surface area, but instead provide a system to compare different geometric quantities during cell cycle progression, a feature that would help to clarify the role of cell size control at G2. As a matter of fact, the reduction of variability performed by KRP4 is enough to ensure homeostasis in meristem cells, as any accumulated variably in G2 would just add to the one at division, and be easily corrected by the next S-phase. Additionally, size regulation at G2 is clearly not enough to recover homeostasis when this is lost, as shown by the *fbl17* mutants. Furthermore, mutants that change the threshold of G1/S transition, like *cycd* (Jones *et al.*, 2017) and *krp* mutants, support the role of the G2 size sensor as one that integrates information from the G1/S to the commitment to division, rather than as absolute size control to achieve homeostasis.

Finally, systems that interface between two distinct quantities might provide a further layer for cell size regulation, one whose function is not to achieve homeostasis, optimal size, or reduction of variability, but rather a system to compares different geometric quantities and compute the relationship between the two. Therefore, what other mechanism might exist for regulation of cell size and how did this have been shaped and changed over millions of years of evolution, is a question that will aid the understanding of how cells might be able to measure diverse quantities.

7.4 Evolution of size homeostasis in plants: a tale of two inhibitors

The uniqueness of KRPs in plants, and the role of RBR-like proteins in size homeostasis in other organisms (Umen and Goodenough, 2001; Schmoller *et al.*, 2015; Zatulovskiy *et al.*, 2020), begs the question of how cell size control evolved in the plant lineage.

7.4.1 RBR: the ancestral regulator with multiple functions

Even though the *Chlamydomonas* mechanism for size homeostasis uses the RBR homologue MAT3, the way it is used to measure genomic content and size is very different from other RBR-like mechanisms, which employ dilution of an inhibitor to measure size (Schmoller and Skotheim, 2015; Zatulovskiy *et al.*, 2020). The most parsimonious explanation of this discrepancy would see the ancestor of all eukaryotes possessing an RBR-like protein with a similar role seen in yeast and humans, with the evolution of CDKG being a derived trait in the algal lineage (Li *et al.*, 2016), perhaps consequent to *Chlamydomonas*

unique life cycle (Fig. 7.1). In fact, the unique presence of CDKG in *Chlamydomonas* expands this hypothesis and leaves open the possibility that the ancestral role of MAT3 within the plant lineage might have been more similar to the RBR-like proteins in animals and fungi, leaving open the question of how RBR-like proteins evolved within the plant lineage.

Additionally, since a role of RBR concentration in cell size homeostasis in the plant meristem seems unlikely, it is not clear how RBR-like proteins moved away from size control in the plant lineage. An example of the latter phenomenon can be found in the green alga *Volvox carteri* (hereafter Volvox). *MAT3* mRNA in Volvox shows sexually dimorphic splicing, with female mature RNA being more similar to the one observed in *Chlamydomonas* MAT3 (Ferris *et al.*, 2010). Although a possible function of Volvox MAT3 in size sensing has not been disputed nor confirmed, the unique splicing of MAT3 in male cells, and its association with the *MATING LOCUS* responsible for sexual dimorphism and zygote development (Goodenough, Lin and Lee, 2007), suggests a more complex function for MAT3 in fate differentiation (Fig. 7.1). The monophyletic relationship between Volvox and *Chlamydomonas* compared to land plants (Li *et al.*, 2021), combined with the reported role for MAT3 in the green algae, implies one of two hypotheses. In the first one, the last common ancestor between green algae and land plants had already evolved a more complex RBR-like protein, able to act both as size sensor and as fate determining protein, a function that foreshadowed more complex interactions of RBR (Desvoyes and Gutierrez, 2020). In this scenario, *Chlamydomonas* would have lost the latter function of RBR, in favour of the sole role in cell cycle progression, presumably as part of a process of adopting its unique life cycle. In the alternative scenario, the complexity of RBR interaction and functionality beyond size control are derived traits, convergently evolved in land plants and green algae. In this hypothesis, the ancestral state of the plant RBR is like the one of the RBR-like protein in animal and yeast (Fig. 7.1). I would argue for the validity of this latter scenario, and I would like to discuss its legitimacy by exploring the characterised role of RBR in Arabidopsis.

The complexity of the evolution of this pathway is further highlighted when it is considered that those cases for the algal RBR-like proteins are specific for the gametophytic stage, thus comparison should be made for gametophyte development in other plants, with the only well understood examples belonging to Arabidopsis. The female gametophyte of *rbr* mutants in Arabidopsis undergoes supernumerary nuclear division, unable to arrest the

process of nuclear proliferation (Ebel, Mariconti and Gruissem, 2004). The highly derived and unique development of the angiosperm's female gametophytes blurs the definition of size control in this example, but one could say that the role of RBR to set the threshold for correct division number seems conserved between *Chlamydomonas* and Arabidopsis. This observation questions the nature of the ancestral state of RBR-like protein in size sensing, perhaps suggesting that, withing the plant lineage, the ancestral way of achieving size homeostasis was to count the number of divisions after reaching a certain size, rather than by volumetric control of cell cycle progression (Fig. 7.1). Alternatively, size sensing might have evolved to be different in green algae, as their unique life cycle of daily growth and nightly division presented different challenges. Algae spend most of their life cycle as haploid gametophytes and have unicellular sporophytes. However, this changed during
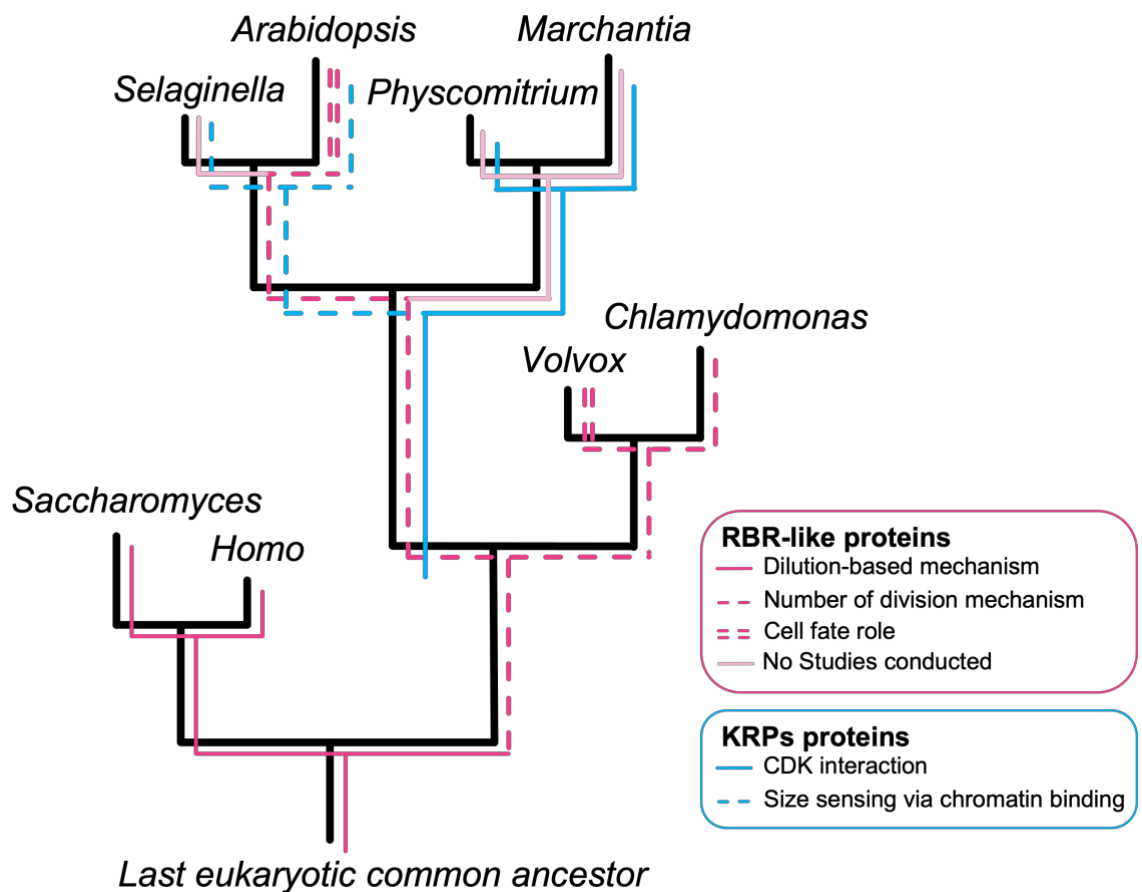
Figure 7.1: Proposed evolutionary pathway of cell size control in plants. The phylogenetic relationship between different organisms was overlayed with the inferred trajectory of the evolution of cell size control. Although the ancestral regulation is thought to be performed by an RBR-like protein, in the last common ancestor of green algae and land plants (pink solid line), the mechanism might be changed in a mechanism to count division, (pink dashed line) rather than affecting cell cycle progression. RBR-like in plants also seems to have evolved a function in cell fate, convergently at least twice (pink double dashed line). KRPs on the other hand, likely evolved in the last common ancestor of all land plants, but their role in size homeostasis might have not involved chromatin binding (blue solid line). This mechanism however, likely evolved in the ancestor of all vascular plants (blue dashed line).

plant colonisation of the land, when the sporophyte become the dominant phase of the life cycle, at least in the tracheophyte lineage. As the sporophyte evolved to become more complex, cell size regulation become an important characteristic. Therefore, assuming that controlling cell size by growth during the day and counting division at night was a feature of the land plant ancestor, perhaps this becomes a not so successful strategy anymore and a new mechanism needed to evolve.

To support this view, the role of RBR in the sporophytic generation in Arabidopsis, other than as an inhibitor of cell cycle progression, seems to be completely different and is more congruent with the fate determining role of the Volvox MAT3. RBR has been shown to interact with multiple transcription factors, key to cell fate transition during development, like FAMA during stomata identity acquisition (Matos *et al.*, 2014) SCARECROW in roots (Cruz-Ramírez *et al.*, 2012) and XYLEM NAC DOMAIN1 during vascular development (C. Zhao *et al.*, 2017). Importantly, each of those interactions are achieved thanks to the LxCxE motif found on these proteins, a conserved motif in eukaryotic CYCLINs for interaction with RBR, emphasising how easily proteins can evolve to interact with RBR by using an existing interface and a short motif for binding. It would be therefore not surprising if a fate-determining role of RBR would have evolved multiple times in the plant lineage (Fig. 7.1).

In contrast, a role for RBR in size sensing in the sporophyte of Arabidopsis, at least in the meristem, was discarded in light of its cellular behaviour (Chapter 3) suggesting the fascinating hypothesis that any role of RBR in cell size control in plant has only been adopted for the gametophyte generation, while the sporophyte used RBR for cell identity establishment and, of course, size-independent S-phase progression. A possible hypothesis to explain this evolutionary trend is that the role in cell fate added too many constraints on RBR function, which might conflict with a role in cell size regulation and created a selective pressure for an alternative mechanism for cell size control in the sporophyte to evolve. A further possibility is that the mechanism of cell size control shown in *Chlamydomonas* of counting cell divisions, become too derived to allow different growth strategies, creating pressure to develop a new size control mechanism more suitable for cycling cells. In this scenario, RBR functionality would be operating throughout gametophytic development, but only at specific stages, perhaps those following meiosis, like in Arabidopsis. Unfortunately, the lack of understanding of the roles of RBR in bryophytes (Fig. 7.1) prevents a rigorous formulation of a hypothesis for the evolution of RBR in size sensing

within the land plants lineage, and studies on RBR-like proteins in other plant systems will be critical to properly address this question.

7.4.2 KRP4: the land-plant size sensor

A consequence of the suggested absence of RBR-based size regulation in the sporophyte is that another protein evolved to perform this role in the sporophyte. The counterpart to RBR as size sensors in vascular plants are, of course, the KRPs, particularly KRP3,4 and 5. These regulators of size homeostasis in the plant meristem are the first examples of this in the sporophyte. In trying to address the evolutionary history of KRPs, it is important to consider the moss gene *PpPRL12*, encoding a hybrid protein containing sequences similar to both KRP and to the proteasomal subunit RPN5. The similarities between *rpn5* and *fbl17* mutants in Arabidopsis (Book *et al.*, 2009) suggest the appealing hypothesis that PpPRL12 might perform both the CDKa inhibitory function, via the KRP-like Motif 1, and a self-regulatory function, via the proteasomal subunit-like domain (PSL). It is easy to imagine a system where PpPRL12 interacts with chromatin via the PSL domain, but the same domain directs PpPRL12 to the proteosomes otherwise. This system would be enough to establish equal inheritance of PpPRL12 without the need for FBL17, whilst acting as a size-dependent inhibitor of S-phase progression during G1, performing a dual role in relay and gauging mechanisms, similar to the role performed by Cdr2 Even if this is very speculative, it creates a narrative of the natural history of the KRP-FBL17 module that does not require the existence of two distinct proteins to function and evolve from a single polypeptide. In this scenario, it is even possible that FBL17 originally evolved to function as counteractor of CDT1 accumulation to prevent genomic instability (Desvoyes *et al.*, 2019), only later being opted as regulator of KRP4 in the context of cell size homeostasis.

An alternative scenario for the evolution of cell size homeostasis using KRP4 sees ancestral cells accumulating KRP4 during G2, without the presence of FBL17, or to a motif performing a similar role. However, this would clearly not be possible, because any observation made for the *fbl17-1* mutants would also apply here. One could argue in favour of a scenario in which cells do not grow in G2, so KRP4 production can be slower, so cells would have enough time to saturate DNA prior to division. However, this would not be enough to generate homeostasis because non-growing cells cannot dilute the protein they produced, so the limit for protein concentration is infinite (see Equation **Error! Reference source not found.** in Chapter 5 with $\lambda = \mu = 0$). In fact, rather counterintuitively the time required to

reach a steady concentration of a protein is only linked to degradation and growth rate but not protein production, suggesting that for a mechanism like the one described here to evolve, a protein performing a function similar to KRP4 and one performing a similar function to FBL17 have to be present simultaneously. Or, of course, a protein performing both functions, as speculated for PpPRL12. Alternatively, the cells could increase growth rate considerably, so dilution would act as degradation, but the cell would grow dramatically, counteracting any positive effect on size homeostasis. Whether the putative role of PpPRL12 is ancestral to other land plants, or it is a derived trait of bryophytes remains controversial as the recent acceptance of bryophyte monophyly led to the consensus of many characteristics of this taxon are derived rather than ancestral (Puttick *et al.*, 2018; de Sousa *et al.*, 2019; Harris *et al.*, 2020). This implies that the state of KRP in bryophytes might be a manifestation of the ancestral state, or the result of reductive evolution – the KRP in bryophytes might even be fully derived and unique to this taxon.

Proteins recognisable as KRPs seem to have evolved at some point during land plant colonisation, as highlighted by the presence of proteins with a CDKa biding motif found in the bryophyte's KRPs (Fig. 7.1). However, the DNA binding motif associated with size sensing, like the one found in the Arabidopsis KRP3,4 and 5, was only found in lycophytes and other tracheophytes (Fig. 7.1). The presence of KRP3,4,5 class in *S. moellendorffii* is enough evidence to support that a size sensing machinery, similar to the one described in this work, evolved in vascular plants before the split with lycophytes. It is possible that this mechanism evolved to function in the more complex tracheophyte meristems, as it does in Arabidopsis where it is critical to maintaining cell size homogeneity (Serrano-Mislata, Schiessl and Sablowski, 2015). Interestingly, *S. moellendorffii* has a unique KRP not found in angiosperms, annotated as SmCDKI3, in which the only homologous sequence is the CDKa binding motif, suggesting divergent evolution of this family**.** Finally, *Marchantia*'s KRP has a CDKa binding motif, but not a PRL motif, leaving open the possibility that the size sensing by KRPs either evolved after the split between vascular plants and *Bryophytes*, or was lost in the latter (Fig. 7.1).

Perhaps a more complete view of the evolution of size sensing in plants should not focus on RBR or KRPs, but rather try to understand how these two interact in plant development, not only as the obvious S-phase transition cascade, but on their plausible role as size sensor in different organs. For example, in the *krp4,6,7* triple mutant multiple cells in the

developing ovule acquire megaspore mother cell identity, so this mutant has multiple female gametophytes (X. Zhao *et al.*, 2017). Although this phenotype is similar to the one shown for *rbr* mutants, division in the gametophytes in the *krp4,6,7* triple mutant are comparable to the wild type, even if development is arrested, in part due to WUSCHEL misexpression (X. Zhao *et al.*, 2017). This is of course unlike *rbr* mutants, which show supernumerary nuclear fissions in the female gametophyte (Ebel, Mariconti and Gruissem, 2004). Therefore, the role in establishing division numbers prior to mother cell identity might be shared by RBR and KRPs, or even performed in orchestration between the two, but the same role in the successive divisions seem to be specifically performed by RBR. Similarly, KRP6,7 perform a role in male gametophyte development by preventing division of the vegetative cell, released by FBL17 (Kim *et al.*, 2008), but *rbr* mutation results in the supernumerary division of the vegetive cell of the male gametophyte (Johnston *et al.*, 2008), suggesting an overlapping role in the control of division number in this cell type. Recent work on the acquisition of megaspore mother cells identity have highlighted the importance of cell geometry, cell elongation and cell size (Hernandez-Lagana *et al.*, 2021), suggesting the possible involvement of these cell cycle inhibitors at the interface between cell cycle and cell fate establishment.

Even though in these examples it is hard to precisely dissect the role as inhibitors of cell cycle progression from the role as cell size regulators, it is clear that the roles of RBR and KRPs might overlap in gametophyte fate establishment and development, suggesting that a similar relationship might have underlined their evolutionary history. In the case of a KRP similar to the one found in *Physcomitrium*, which could putatively function as the gauging component, RBR might instead be the relay part of the mechanism, by measuring DNA content in a similar function to the one performed by MAT3. In this scenario, binding of KRP to chromatin might result from a complex between RBR and CDK, in a similar fashion to the CDKG system in Chlamydomonas (Li *et al.*, 2016). These are of course just speculations, but they emphasise the importance of considering both RBR and KRPs when conducting future studies on the evolution of cell size regulation in plants.

7.5 Beyond size sensing with KRPs: tuning cell size regulation

In the light of the importance of average cell size and cell size variability in development, it is important to discuss how the KRP4/FBL17 system might operate to control those two entities separately during development. We have already seen how the mechanism of KRP4

size sensing, which uses DNA content as internal metric, might account for the observed increase in cell size following endoreduplication, but other pathways might also orchestrate cell size regulation via KRPs. Any of the regulators of S-phase entry, like CYCDs, CDKs and RBR, could contribute to increase or lower the threshold required for KRP4 to trigger the phosphorylation cascade leading to cell cycle progression. In fact, ultimately CDK activity is the interface between cell signalling and cell cycle progression (Jones *et al.*, 2017), so affecting this, for example via increased production of CYC, would affect the size threshold relayed by KRP4.

Interestingly, we saw that since the concentration of nucleosolic KRP4 is independent of the volume, this cannot be used for size control – overwhelming free KRP4 with chromatin-bound KRP4 is critical to achieve size homeostasis. However, volume independency of any other cell cycle regulator would result in a size-independent change in the threshold of S-phase transition, without interfering with the process of homeostasis. Thus, the absence of a relationship between free KRP4 concentration and cell size, a feature that could brake homeostasis, is also a reason that allows other cell cycle regulators to perform the different function of affecting average cell size. For this reason, interactions between TOR and E2F consequent to glucose detection (Xiong *et al.*, 2013), might affect the KRP4 threshold by increasing the required dilution of KRP4 to trigger S-phase, resulting in an increase of average cell size without affecting cell size homeostasis, in line with experimental observations of sugar-dependent cell size increase (Jones *et al.*, 2017). It would be easy in this way for plants to actively manipulate the average cell size in their cells and organs to meet a specific metabolic demand by interaction between the growth regulation pathway and the cell cycle progression machinery, whilst preserving size homeostasis in the meristem. It would be interesting to test this hypothesis by showing whether the concentration of KRP4 at S-phase entry is lower in sucrose-treated apexes, despite comparable amounts of inherited KRP4.

In contrast, pathways regulating KRP4 accumulation or binding dynamics during G2 would hinder cell size homeostasis dramatically, because they are part of the gauging mechanism ensuring accurate matching between KRP4 and DNA. One could even speculate that the KRP4 production observed during G1 plays a role in increasing cell size variability, although this production seems to be volume-independent, thus contributing to cell size average and not variability (Chapter 5). More work in understanding the mechanism of KRP4

production in G1 would help addressing this question. Nevertheless, regulatory pathways affecting KRP4 production or degradation during G2, through FBL17 for example, would of course result in an increase of average cell size at the G1/S transition, but would also increase the dependency between volume at S and volume at birth, effectively increasing variability in the cell population, as observed in the *fbl17* mutants (Chapter 5). Certainly, this seems an unwanted effect, detrimental for homeostasis, but if increased in cell size variability is needed during development, such a process could be easily used by plant cells to do so. In the introductory Chapter 1, I presented recent work carried on the possible roles of cell size variability within tissues, so it would be fascinating to discover that the same mechanism that ensures size homeostasis is also able to generate variability, perhaps necessary for correct tissue development.

Additionally, during bud emergence an observable increase in cell size is accompanied by an increase in cell size variability (Jones *et al.*, 2017). Whether the change in the regularity of cell volume is a consequence of the flexibility required to ensure proper formation of a new organs, part of a mechanism that requires high variability, the consequence of heterogenous cell types, or just the effect of increased growth in this tissue, remains an open question. A similar phenomenon, achieved differently mechanistically, is observed during sepal primordia emergence, where increased cell size and cell size variability is accompanied by decupling of cell size from cell cycle progression, specifically during the G1/S transition (Schiessl *et al.*, 2012). It has been proposed that JAG decouples S-phase entry from cell size by repressing KRP proteins, particularly KRP4, but testing this hypothesis has not been possible, likely due to genetic redundancy in the KRP family (Schiessl, 2014). In fact, emerging sepal cells are larger than those in the flower meristem, in spite of downregulation of KRP4 (Schiessl, Muino and Sablowski, 2014), contrasting with *krp4* mutant cells, which are smaller (Chapter 5), suggesting that the role of JAGGED (JAG) is in part to remove homeostasis control in this organ. I speculate that lack of homeostasis is required for folding of the tissue, because the effect of isotropically dividing cells would equalise the anisotropic mechanical stress generated by the folding sepals (Zhao *et al.*, 2020), hindering the process of bending. This is similar to what happens in emerging trichomes, which are unable to bulge out when dividing (Hervieux *et al.*, 2017). In support of this idea, in *jag* mutants the cells of emerging sepals are similar to those in the meristem and folding does not occur (Schiessl *et al.*, 2012). Thus, rather than folding being the result of size variability, it is possible that homogeneous division caused by size homeostasis

would dissipate the mechanical stress accumulated by anisotropic growth, so in this case cell size variability would be the necessary consequence of a mechanism for sepal development. The observation that increase in cell size variability in bud and sepal primordia is accompanied by an increase in cell size and growth rate, would suggest the alternative hypothesis that suppression of the cell size homeostasis machinery is required for an increase in growth rate in these organs (Schiessl, 2014), perhaps allowing those cells to cycle more freely without restrictions.

In these examples, even though the function of the uncoupling between cell size and cell cycle progression remains unclear, it undoubtedly results in an increase in the average cell size. During stomata development instead, the uncoupling of cell size from cell cycle progression works in the opposite way, allowing for division to occur at much smaller sizes than the surrounding cells (Geisler, Nadeau and Sack, 2000). The stomata lineage initiates by cell fate transition, which is followed by asymmetric cell division. The smallest cells of the two acquires meristemoid identity and continue dividing a variable number of times, generating one or two stomata (for a review of stomatal development, see (Pillitteri and Torii, 2012)). In contrast to what we observed in the meristem cell, where the larger sister of an asymmetric division always divides first, during stomatal development the opposite is true, suggesting that overriding of the KRP4 pathway is required for correct acquisition of meristemoid identity.

Perhaps an overriding mechanism is present during the development of the whole leaf and an insight into this possibility came from *fugu* mutants, retrieved through a mutant screen for altered leaf morphology but retained organ size (Ferjani *et al.*, 2007). *fugu* take their name from the Japanese word for "puffer fish", because in these mutants, leaves have fewer but larger cells, which account for similar leaf size when compared to wild type (Ferjani *et al.*, 2007). Interestingly, one of these mutants is an overexpressor of KRP2, showing how different KRPs might influence cell size or proliferation, regardless of size homeostasis. Regardless of the nature of the increase in cell size or decrease in cell number, those mutants suggest that mechanisms for measuring cell size in developing organs can act non-cell autonomously, perhaps overriding cell autonomous pathways. Importantly, in the *fugu* mutants, the cell size of the palisade cells only increases during the cell expansion phase of leaves development (Ferjani *et al.*, 2007), corroborating the idea that this is a unique feature found in leaves, rather than a general feature of plant tissues. Nevertheless,

in some of those mutants, including the mutant with KRP2 overexpression, leaf size is smaller than observed in the wild type, suggesting that even if a mechanism that controls organ size might act non-cell autonomously and hijack the cell autonomous pathway for cell size regulation, perhaps this cannot be completely overridden and still retains some degree of independency.

The connection between development, cell size regulation and cell size homeostasis is a captivating topic that will continue to fascinate me and developmental biologists alike for many years. However, answering this question has been challenging, mainly because mechanistic evidence for cell size control was very scarce. I hope that this work will open a door towards this direction, allowing us to answer the question on how cell size regulation and plant development are concomitantly orchestrated.

7.6 References

Barber, F., Amir, A. and Murray, A. W. (2020) 'Cell-size regulation in budding yeast does not depend on linear accumulation of Whi5', *Proceedings of the National Academy of Sciences*, 117(25), p. 14243 LP-14250. doi: 10.1073/pnas.2001255117.

Book, A. J. *et al.* (2009) 'The RPN5 subunit of the 26s proteasome is essential for gametogenesis, sporophyte development, and complex assembly in Arabidopsis', *The Plant cell*. 2009/02/27. American Society of Plant Biologists, 21(2), pp. 460–478. doi: 10.1105/tpc.108.064444.

Boruc, J. *et al.* (2010) 'Systematic Localization of the Arabidopsis Core Cell Cycle Proteins Reveals Novel Cell Division Complexes', *Plant Physiology*, 152(2), pp. 553–565. doi: 10.1104/pp.109.148643.

Cruz-Ramírez, A. *et al.* (2012) 'A bistable circuit involving SCARECROW-RETINOBLASTOMA integrates cues to inform asymmetric stem cell division', *Cell*, 150(5), pp. 1002–1015. doi: 10.1016/j.cell.2012.07.017.

Desvoyes, B. *et al.* (2019) 'FBL17 targets CDT1a for degradation in early S-phase to prevent Arabidopsis genome instability', *bioRxiv*, p. 774109. doi: 10.1101/774109.

Desvoyes, B. *et al.* (2020) 'A comprehensive fluorescent sensor for spatiotemporal cell cycle analysis in Arabidopsis', *Nature Plants*, 6(11), pp. 1330–1334. doi: 10.1038/s41477-020-00770-4.

Desvoyes, B. and Gutierrez, C. (2020) 'Roles of plant retinoblastoma protein: cell cycle and beyond', *The EMBO Journal*. John Wiley & Sons, Ltd, 39(19), p. e105802. doi:

https://doi.org/10.15252/embj.2020105802.

Du, M., Spalding, E. P. and Gray, W. M. (2020) 'Rapid Auxin-Mediated Cell Expansion', *Annual Review of Plant Biology*. Annual Reviews, 71(1), pp. 379–402. doi: 10.1146/annurev-arplant-073019-025907.

Ebel, C., Mariconti, L. and Gruissem, W. (2004) 'Plant retinoblastoma homologues control nuclear proliferation in the female gametophyte', *Nature*, 429(6993), pp. 776–780. doi: 10.1038/nature02637.

Facchetti, G. *et al.* (2019) 'Reprogramming Cdr2-Dependent Geometry-Based Cell Size Control in Fission Yeast', *Current Biology*, 29(2), p. 350–358.e4. doi: https://doi.org/10.1016/j.cub.2018.12.017.

Ferjani, A. *et al.* (2007) 'Analysis of Leaf Development in fugu Mutants of Arabidopsis Reveals Three Compensation Modes That Modulate Cell Expansion in Determinate Organs 1 [W]', *Plant Physiology*, 144(June), pp. 988–999. doi: 10.1104/pp.107.099325.

Ferris, P. *et al.* (2010) 'Evolution of an expanded sex-determining locus in Volvox', *Science*, 328(5976), pp. 351–354. doi: 10.1126/science.1186222.

Franklin, R. E. and Gosling, R. G. (1953) 'Molecular configuration in sodium thymonucleate', *Nature*. Nature Publishing Group, 171(4356), pp. 740–741.

Gallet, R. *et al.* (2017) 'The evolution of bacterial cell size: the internal diffusion-constraint hypothesis', *The ISME Journal*, 11(7), pp. 1559–1568. doi: 10.1038/ismej.2017.35.

Geisler, M., Nadeau, J. and Sack, F. D. (2000) 'Oriented Asymmetric Divisions That Generate the Stomatal Spacing Pattern in Arabidopsis Are Disrupted by the too many mouths Mutation', *The Plant Cell*, 12(11), pp. 2075–2086. doi: 10.1105/tpc.12.11.2075.

Goodenough, U., Lin, H. and Lee, J.-H. (2007) 'Sex determination in Chlamydomonas', *Seminars in Cell & Developmental Biology*, 18(3), pp. 350–361. doi: https://doi.org/10.1016/j.semcdb.2007.02.006.

Harris, B. J. *et al.* (2020) 'Phylogenomic Evidence for the Monophyly of Bryophytes and the Reductive Evolution of Stomata', *Current Biology*. Elsevier, 30(11), p. 2001–2012.e2. doi: 10.1016/j.cub.2020.03.048.

Hernandez-Lagana, E. *et al.* (2021) 'Organ geometry channels reproductive cell fate in the Arabidopsis ovule primordium', *eLife*. Edited by S. McCormick and J. Kleine-Vehn. eLife Sciences Publications, Ltd, 10, p. e66031. doi: 10.7554/eLife.66031.

Hervieux, N. *et al.* (2017) 'Mechanical Shielding of Rapidly Growing Cells Buffers Growth Heterogeneity and Contributes to Organ Shape Reproducibility.', *Current Biology*. England, 27(22), p. 3468–3479.e4. doi: 10.1016/j.cub.2017.10.033.

Johnston, A. J. *et al.* (2008) 'A Dynamic Reciprocal RBR-PRC2 Regulatory Circuit Controls Arabidopsis Gametophyte Development', *Current Biology*, 18(21), pp. 1680–1686. doi: https://doi.org/10.1016/j.cub.2008.09.026.

Jones, A. R. *et al.* (2017) 'Cell-size dependent progression of the cell cycle creates homeostasis and flexibility of plant cell size', *Nature Communications*. Nature Publishing Group, 8, p. 15060. doi: 10.1038/ncomms15060.

Kim, H. J. *et al.* (2008) 'Control of plant germline proliferation by SCFFBL17 degradation of cell cycle inhibitors', *Nature*, 455(7216), pp. 1134–1137. doi: 10.1038/nature07289.

Leyser, O. (2018) 'Auxin Signaling', *Plant Physiology*, 176(1), pp. 465–479. doi: 10.1104/pp.17.00765.

Li, X. *et al.* (2021) 'Large Phylogenomic Data sets Reveal Deep Relationships and Trait Evolution in Chlorophyte Green Algae', *Genome Biology and Evolution*, 13(7). doi: 10.1093/gbe/evab101.

Li, Y. *et al.* (2016) 'A new class of cyclin dependent kinase in Chlamydomonas is required for coupling cell size to cell division', *eLife*. eLife Sciences Publications, Ltd, 5, pp. e10767–e10767. doi: 10.7554/eLife.10767.

Matos, J. L. *et al.* (2014) 'Irreversible fate commitment in the Arabidopsis stomatal lineage requires a FAMA and RETINOBLASTOMA-RELATED module', *eLife*. Edited by R. Amasino. eLife Sciences Publications, Ltd, 3, p. e03271. doi: 10.7554/eLife.03271.

Pan, K. Z. *et al.* (2014) 'Cortical regulation of cell size by a sizer cdr2p', *eLife*, 2014(3), pp. 1–24. doi: 10.7554/eLife.02040.

Pillitteri, L. J. and Torii, K. U. (2012) 'Mechanisms of Stomatal Development', *Annual Review of Plant Biology*. Annual Reviews, 63(1), pp. 591–614. doi: 10.1146/annurev-arplant-042811-105451.

Puttick, M. N. *et al.* (2018) 'The Interrelationships of Land Plants and the Nature of the Ancestral Embryophyte', *Current Biology*. Elsevier, 28(5), p. 733–745.e2. doi: 10.1016/j.cub.2018.01.063.

Rust, M. J. *et al.* (2007) 'Ordered phosphorylation governs oscillation of a three-protein circadian clock', *Science (New York, N.Y.)*. 2007/10/04, 318(5851), pp. 809–812. doi: 10.1126/science.1148596.

Sauret-Güeto, S. *et al.* (2013) 'JAGGED controls Arabidopsis petal growth and shape by interacting with a divergent polarity field', *PLoS biology*. 2013/04/30. Public Library of Science, 11(4), pp. e1001550–e1001550. doi: 10.1371/journal.pbio.1001550.

Schiessl, K. *et al.* (2012) 'JAGGED controls growth anisotropy and coordination between

cell size and cell cycle during plant organogenesis', *Current Biology*. Elsevier Ltd, 22(19), pp. 1739–1746. doi: 10.1016/j.cub.2012.07.020.

Schiessl, K. (2014) *The role of the transcription factor JAGGED in early floral organogenesis*. University of East Anglia. Available at: https://ueaeprints.uea.ac.uk/id/eprint/49812/%5C.

Schiessl, K., Muino, J. M. and Sablowski, R. (2014) 'Arabidopsis JAGGED links floral organ patterning to tissue growth by repressing Kip-related cell cycle inhibitors', *Proceedings of the National Academy of Sciences*, 111(7), pp. 2830–2835. doi: 10.1073/pnas.1320457111.

Schmoller, K. M. *et al.* (2015) 'Dilution of the cell cycle inhibitor Whi5 controls budding-yeast cell size', *Nature*, 526(7572), pp. 268–272. doi: 10.1038/nature14908.

Schmoller, K. M. and Skotheim, J. M. (2015) 'The Biosynthetic Basis of Cell Size Control', *Trends in Cell Biology*. Elsevier Ltd, 25(12), pp. 793–802. doi: 10.1016/j.tcb.2015.10.006.

Serrano-Mislata, A., Schiessl, K. and Sablowski, R. (2015) 'Active Control of Cell Size Generates Spatial Detail during Plant Organogenesis', *Current Biology*. The Authors, 25(22), pp. 2991–2996. doi: 10.1016/j.cub.2015.10.008.

de Sousa, F. *et al.* (2019) 'Nuclear protein phylogenies support the monophyly of the three bryophyte groups (Bryophyta Schimp.)', *New Phytologist*. John Wiley & Sons, Ltd, 222(1), pp. 565–575. doi: https://doi.org/10.1111/nph.15587.

Swaffer, M. P. *et al.* (2021) 'Transcriptional and chromatin-based partitioning mechanisms uncouple protein scaling from cell size', *Molecular Cell*. doi: https://doi.org/10.1016/j.molcel.2021.10.007.

Torres-Acosta, J. A., Fowke, L. C. and Wang, H. (2011) 'Analyses of phylogeny, evolution, conserved sequences and genome-wide expression of the ICK/KRP family of plant CDK inhibitors', *Annals of Botany*, 107(7), pp. 1141–1157. doi: 10.1093/aob/mcr034.

Umen, J. G. and Goodenough, U. W. (2001) 'Control of cell division by a retinoblastoma protein homolog in Chlamydomonas', *Genes and Development*, 15(13), pp. 1652–1661. doi: 10.1101/gad.892101.

Vanstraelen, M. *et al.* (2004) 'A plant-specific subclass of C-terminal kinesins contains a conserved a-type cyclin-dependent kinase site implicated in folding and dimerization', *Plant physiology*. 2004/07/09. American Society of Plant Biologists, 135(3), pp. 1417–1429. doi: 10.1104/pp.104.044818.

Watson, J. D. and Crick, F. H. C. (1953) 'Molecular Structure of Nucleic Acids: A Structure for Deoxyribose Nucleic Acid', *Nature*, 171(4356), pp. 737–738. doi: 10.1038/171737a0.

Weart, R. B. *et al.* (2007) 'A Metabolic Sensor Governing Cell Size in Bacteria', pp. 335–347. doi: 10.1016/j.cell.2007.05.043.

Xiong, Y. *et al.* (2013) 'Glucose-TOR signalling reprograms the transcriptome and activates meristems', *Nature*. 2013/03/31, 496(7444), pp. 181–186. doi: 10.1038/nature12030.

Yang, C. *et al.* (2020) 'The Arabidopsis Cdk1/Cdk2 homolog CDKA;1 controls chromosome axis assembly during plant meiosis', *The EMBO Journal*. John Wiley & Sons, Ltd, 39(3), p. e101625. doi: https://doi.org/10.15252/embj.2019101625.

Zatulovskiy, E. *et al.* (2020) 'Cell growth dilutes the cell cycle inhibitor Rb to trigger cell division', *Science*, 471(July), pp. 466–471.

Zhao, C. *et al.* (2017) 'XYLEM NAC DOMAIN1, an angiosperm NAC transcription factor, inhibits xylem differentiation through conserved motifs that interact with RETINOBLASTOMA-RELATED', *New Phytologist*. John Wiley & Sons, Ltd, 216(1), pp. 76–89. doi: https://doi.org/10.1111/nph.14704.

Zhao, F. *et al.* (2020) 'Microtubule-Mediated Wall Anisotropy Contributes to Leaf Blade Flattening', *Current Biology*, 30(20), p. 3972–3985.e6. doi: https://doi.org/10.1016/j.cub.2020.07.076.

Zhao, X. *et al.* (2017) 'RETINOBLASTOMA RELATED1 mediates germline entry in Arabidopsis', *Science*. American Association for the Advancement of Science, 356(6336), p. eaaf6532. doi: 10.1126/science.aaf6532.

Zhu, M. *et al.* (2020) 'Robust organ size requires robust timing of initiation orchestrated by focused auxin and cytokinin signalling', *Nature Plants*, 6(6), pp. 686–698. doi: 10.1038/s41477-020-0666-7.

Chapter 8: Material and Methods

8.1 Growth conditions

For seed sterilisation, dry seeds were placed into Eppendorf® tubes and 10x of the seed volume of sterilising solution was added. Sterilising solution was prepared fresh, dissolving 50 mg dichloroisocyanuric acid (Sigma-Aldrich®) in 4ml of water before adding 4ml of 100% (v/v) ethanol. Seeds were incubated on a rotator for 15 min and washed three times with 100% (v/v) ethanol. Seeds were left to dry before being moved on 1% (m/v) agarose low EEO (Melford) MS medium (4.41g/L of Murashige & Skoog Medium Including vitamins (Deuchefa), 10g/L of glucose and 3mL of 166g/L of MES hydrate pH 6.0 (Sigma-Aldrich®), pH 5.7). When selectable markers were used, MS medium was supplemented with one of the following: 50µg/L of hygromycin B (Roche), 50µg/L kanamycin monosulphate (Formedium™), 10µg/L of phosphinothricin (Deuchefa), aka. Basta®, 37.5µg/ml of sulfadiazine sodium salt (Sigma-Aldrich®), or 0.7%(v/v) gentamicin solution (Sigma-Aldrich®). For *fbl17*, dry sterilised seeds were suspended in 0.2% low EEO (m/v) agarose low EEO and moved on MS medium via pipetting, ensuring that seed were spaced approximately 2mm apart for future visual selection.

Seeds were left stratifying for 4 days at 4˚C in the dark. Sterilised seeds on plates were moved to 20˚C 16h light growth chambers. For *fbl17*, 2-3 weeks old seedlings were visually inspected individually for *fbl17-1* related phenotype and moved to soil at maturity, 3-4 weeks after sawing. Seeds not requiring sterilisation were sown on damp filter paper prior to stratification. After stratification, the seeds were moved to soil, and grown at 20˚C 16h light for seeds production or 16˚C 24h light for 4 to 6 weeks for dissection.

Dissected apexes (see plant material), were grown on 0.8% (m/v) agarose low EEO (Melford) ACM media (based on (Hamant, Das and Burian, 2014)) (2.2g/L of Murashige & Skoog Medium Including vitamins, (Duchefa), 10g/L sucrose (Thermo Scientific™), 10mL of 50g/L of MES hydrate pH 5.8, (Sigma-Aldrich®), 100µg/L carbenicillin disodium salt (Formedium™), 50 µM *trans*-Zeatin (Sigma Aldrich®), pH 5.8) and grown at 20˚C 24h light for the duration of the experiment. For live imaging with more than one time point and for EdU staining, apices were left to recover in the medium for 24 h. For EdU staining, after 24h recovery the apexes were left for 3 h in 0.8% (m/v) ACM medium as above, supplemented with 10 µM EdU, prior to ethanol dehydration (see confocal microscopy

below). For experiments using inducible transgenes, 10µM β-estradiol (Sigma- Aldrich®) was included in the medium and the apexes were left growing for 48h before imaging.

8.2 Plant materials

See Table 8.1 for list of original seed materials and their origin.

Meristems were dissected from bolting plants between 2 to 8cm tall. Flowers and flower buds were removed from the growing stem, from older to younger, using fine tweezers until the buds were too small to be removed in this way. For fixing, samples were move in 15% (v/v) ethanol for dehydration (see tissue staining and mPS-PI). For live imaging, apexes were then excised using tweezers and moved into a 50x20mm deep petri dish, containing 20mL of 2% (m/v) agarose low EEO (Melford), previously perforated at the centre to accommodate excised apexes, standing upright. Water containing 100µg/L of carbenicillin disodium salt (Formedium™) was added to cover the samples, which were dissected using a BD Micro Fine™ plus U100 insulin needle syringe as a tool to cut emerging flower buds, until the meristem was visible. The last few buds were often not visible underwater, so water was removed, and the apexes were dissected in the open air, until the larger bud was no bigger than a quarter of the apical meristem. To avoid desiccation damage, the samples were not exposed to the air for more than 30s. Dissected meristems were either moved to ACM medium (see growth conditions above) for long term imaging, imaged straight after dissection, or treated accordingly prior to imaging (see confocal microscopy below).

Insert/Mutation	Genetic Background	Origin
pUBQ10::acyl-YFP	Col-0	Provided by Professor Henrik Jönson (Willis et al., 2016)
acyl-YFP x 3xMarker	Col-0	Provided by Porfessor Crisanto Gutierrez (Desvoyes et al., 2021)
pRBR::RBR-GFP	Col-0	Priovided by Dr Beatrix Horváth (Magyar et al., 2012)
KRP4-GFP	krp4-2 -/-; Ler-0	(Schiessl et al., 2012)
KRP4-Cherry	jag -/+; krp4-2 -/-; Ler-0	Made by Dr Katharina Schiessl
krp4-2	krp4-2; Ler-0	Gen trap line, GT1143 (Springer, 2000)
fbl17-1/+	fbl17-1/+; Col-0	GAB-Kat line, GABI_170E02 (Li et al., 2007)
pFBL17::FBL17-GFP	fbl17-1; Col-0	Provided by Professor David Twell (Kim et al., 2008)
KRP1 to 7-GFP	Col-0	Provided by Professor Masaaki Umeda, unpublished
pok1/2	pok1/2; Col-0	Provided by Professor Laurie Smith, (Müller et al., 2006)
TUA5-mCherry	Col-0	Provided by Professor Crisanto Gutierrez (Gutierrez et al., 2009)

Table 8.1: Plant materials. List of plants materials used for this work, including reference with origin.

Tissue collection for nucleic acids extraction was performed by excising the required tissue, leaf in the case of genotyping and stem for mRNA or CRISPR related analysis, which was

placed in a 2ml tube (Eppendorf™) containing a 2mm metal ball and snap frozen using liquid nitrogen. TissueLyser LT (QIAGEN) was used to macerate the tissue, which was either processed immediately (see genetic analysis, cloning and transformation) or stored at -70°C before processing.

8.3 Genetic analysis, cloning and transformation

Geneious Prime (Biomatters) was used to design primers and constructs, produce phylogenetic trees and DNA alignments. See Table 8.2 for the list of non-commercial plasmid used.

For genomic DNA (gDNA) extraction, 200µl of extraction buffer (200, Tris pH 7.5, 250mM sodium chloride, 25mM EDTA pH 8.0, 0.5% (v/v) SDS solution (Severn Biotech Ltd)) was added to the macerated tissue (relative to ~1cm long leaf, see plants material above) and incubated for 30min at 50°C. Samples were spun for 5min at 14k RCF. 150µl of the supernatant were mixed with equal volumes of isopropanol, incubated at room temperature for 5min and spun for 5min at 14k RCF. The supernatant was discarded, and the pellet was incubated for 15min at 50°C with the lid open. The dried pellet was resuspended vigorously with 200µl of sterile water, incubated at room temperature for 1min and spun for 5min at 14k RCF. 150µl of the supernatant were mixed with 50µl of water and stored at 4°C.

For RNA extraction and complementary DNA (cDNA) synthesis, the RNeasy® Plant Mini Kit (QIAGEN) was used to extract mRNA from macerated tissue (~200µg of inflorescence tissue, see plants material above). 5µg of mRNA was used in 30µl reaction for DNase treatment using Ambion™ DNase I (Invitrogen™) and incubated for 1h at 37°C. 8µl of deactivation liquid (included in Ambion™ DNase I) was added, the mixture mixed vigorously, and spun for 2m at 14k RCF. 27µl of the supernatant was collected and up to 5µg of the so obtained RNA were treated with SuperScript™ III (Invitrogen™) for reverse transcription. 1µl of RNase H (Thermo Scientific™) was added to the cDNA mix to remove RNA and incubated for 20min at 37°C and stored at 4°C.

For polymerase chain reaction (PCR), 8%(v/v) gDNA or 2%(v/v) cDNA were mixed with 800µM primers, 800µM dNTPs and Q5® High-Fidelity DNA Polymerase and its buffer (NEB®) as suggested by instructions. Solutions was incubated on a thermocycler set as 98°C for

5min, then 35 cycles of 98˚C for 30sec, 58˚C for 30sec and 72˚C for 1min per kb were repeated, before 5min incubation at 72˚C. PCR products were run on a 0.8% (m/v) agarose low EEO (Melford) gel with 500µg/L of ethidium bromide (Thermo Scientific™) for 30 to 40min at 100V.

Plasmid Name	Description	Origin
pER8	β-Estradiol-Inducible	(Zuo *et al.*, 2000)
pICSL86900OD	Accpetor vector with nos:nptII:ocs	The Sainsbury Laboratory's SynBio
pICLS70001	sgRNA template	The Sainsbury Laboratory's SynBio
pICSL90002	U6-26 Promoter	The Sainsbury Laboratory's SynBio
pICH47751	Position 3-F	The Sainsbury Laboratory's SynBio
pICH47761	Position 4-F	The Sainsbury Laboratory's SynBio
pICH47772	Position 5-F	The Sainsbury Laboratory's SynBio
pICH47781	Position 6-F	The Sainsbury Laboratory's SynBio
LBJJ358-2	Ubi10:Cas9:Ags cassette	Provided by Professor Jonathan Jones
pAGM8031	Level M Position 1 Acceptor	The Sainsbury Laboratory's SynBio
pICSL11015	pFAST-Red selection cassette	The Sainsbury Laboratory's SynBio
pAGM8081	Level M Position 6 Acceptor	The Sainsbury Laboratory's SynBio
pICH50927	Level M End-Link 6	The Sainsbury Laboratory's SynBio
pICSL4723-P1	Level P Accpetor	The Sainsbury Laboratory's SynBio
pICH79300	Level P End-Link 6	The Sainsbury Laboratory's SynBio

Table 8.2: Plasmids DNA. List of non-commercial plasmid DNA used in this work. Other than acceptor vectors, the majority of those plasmids are part of the CRISPR cloning system used at The Sainsbury Laboratory.

For cloning using pGEM®-T Easy vector system (Promega), DNA bands were excised from a gel and purified using NucleoSpin™ Gel and PCR Clean-up Kit (Macherey-Nagel™). 200ng of eluted DNA were mixed with 1mM dATP, 1x TAQ Buffer and TAQ polymerase (QIAGEN), and incubated at 68˚C for 30min. Ligation with pGEM®-T Easy was carried out as explained in the manual, by incubation overnight at 16˚C.

For restriction digest-based cloning, vector plasmid DNA and plasmid DNA containing the gene of interest were digested using restriction enzymes, at concentrations suggested by the manufacturers. For the pER8 inducible lines (see Table 3: primers), the restriction enzyme uses were *Asc*I (NEB®) and *Apa*I (NEB®). The mix of DNA and restriction enzymes was incubated for 1h at 37˚C. The mix containing the vector DNA was treated with Alkaline Phosphatase (Merck Life Science UK) as instructed by manufacturer, incubating for 30min at 37˚C. Both the phosphatase-treated vector and the digested gene of interest were excised from a gel (see above) and ligated using T4 ligase enzyme (NEB®) as instructed by the manufacturer, with a ratio of 3:1 of gene to vector and incubated overnight at 16˚C. 1µl of the mix was used for transformation (see below).

For Golden Gate cloning, The Sainsbury Laboratory deposited plasmid database (Engler *et al.*, 2014) was used for the majority of reactions, as explained in detail in (Engler *et al.*, 2014). Briefly, a Golden Gate mix (5ng/µl of plasmid DNA, 2µg/µl bovine serum albumin (Roche), T4 ligase enzyme and buffer (NEB®) as suggested by the manufacturer's instructions, *Bsa*I (NEB®) as suggested by the instructions) was incubated in a thermocycler as follows: 35 cycles of 37˚C for 3min and 16˚C for 4min were followed by 5min at 50˚C and 80˚C for enzyme denaturation. 1µl of the mix was used for transformation (see below).

For preparation of electrocompetent cells, a single *Escherichia coli DH5α* colony was inoculated in 10ml of liquid LB broth (5g/L LB Broth Miller, Formedium™) and incubated overnight at 37˚C. 4ml of the overnight culture were inoculated in 50ml liquid LB broth overnight and 10ml were inoculated in 2L liquid LB broth overnight at 16˚C to an optical density of 0.2, when a 10x diluted culture was measured with 600nm wavelength. Cells were centrifuged at 3k RCF for 30min at 4˚C and resuspend on ice with half the original amount of ice-cold water. The process was repeated until the volume of water used for resuspending was less than 20ml, when pellets were resuspended in 2ml of ice cold 10%(v/v) glycerol. Cells were stored as 40µl aliquots at 70˚C. For *Agrobacterium tumefaciens* GV3101, a single colony was inoculated in 10ml of liquid LB broth, including 20µg/L rifampicin (Melford) and 100µg/L gentamicin sulphate (Sigma-Aldrich®), and incubated overnight at 28˚C. The whole culture was used to inoculate 500ml of liquid LB broth overnight at 28˚C, to an optical density of 0.6, when measured for 600nm. The cells were centrifuged at 4k RCF for 10min at 4˚C and resuspended on ice with the same volume of ice-cold water. This wash step was repeated 5 times, by halving the volume of water used for resuspending the cells. Cells were centrifuged one last time and resuspended in 4ml of ice cold 10%(v/v) glycerol, and stored as 40µl aliquots at -70˚C.

For bacteria transformation, 1µl of plasmid DNA was mixed with 40µl of electrocompetent cells and electroporated using Gene Pulser™ (Bio-Rad™) (2.4v, 0.25µFD, 200Ω for *E. coli* and 400Ω for *A. tumefaciens*) using an electroporation cuvette with a 2mm gap (GENEFLOW). 1ml liquid LB broth was added to the electroporated bacteria, which were incubated for 1h at 37˚C (*E. coli*) or 2.5h at 28˚C (*A. tumefaciens*). Bacteria were plated on 3.6% agar LB medium (10g/L Tryptone, 5g/L Yeast extract, 10g/L sodium chloride) including antibiotics, depending on selection, as follows: 50µg/L kanamycin monosulphate (Formedium™), 100µg/L ampicillin sodium salt (Sigma-Aldrich®), 100µg/L spectinomycin

dihydrochloride pentahydrate (Sigma-Aldrich®). *A. tumefaciens* GV3101 plates always included 20μg/L rifampicin (Melford) and 100μg/L gentamicin sulphate (Sigma-Aldrich®).

Primer name	Sequence	Description
pER8 Seq F	ACCCTTCCTCTATATAAGGAAGTTC	Sequencing pER8 constructs
pER8 Seq R	CATTGAACTTGACGAACGTTG	Sequencing pER8 constructs
KRP4 CDS F	GT GGTCTC T GGAG GGCGCGCC ATGGGGAAATACATAAGAAAGAGCAAAATC	Cloning KRP4 CDS and relative mutations
KRP4 K52R R	GT GGTCTC G ATCT AGCTCGAGTTAAAACACCAAG	Cloning of KRP4 CDS and introduction of Lys to Arg mutation
KRP4 K52R F	GT GGTCTC T AGAT CTCTAGCTCTTCAACAACAACAAC	Cloning of KRP4 CDS and introduction of Lys to Arg mutation
KRP4 Δ8 R	GT GGTCTC C AAGT GAAGAAGAGGAAGAAGGTG	Cloning of KRP4 CDS and deletion of Motif 8
KRP4 Δ8 F	GT GGTCTC C ACTT CAACAACAACAACAACGCTG	Cloning of KRP4 CDS and deletion of Motif 8
KRP4 CDS R	GT GGTCTC A ACCT CC ATCATCTACCTTCGTCCATTCAAAC	Cloning KRP4 CDS and relative mutations
C-eGFP F	GT GGTCTC T AGGT ATGGTGAGCAAGGGC	Cloning GFP to tag KRP4 CDS and relative mutations
eGFP noTerm R	GT GGTCTC T AGCG GGGCCC TTACTTGTACAGCTCGTCCATGC	Cloning GFP to tag KRP4 CDS and relative mutations
krp4-2 F	GGTGAATCCTCTATTGCTTTAATGG	Genotyping krp4-2 mutants
krp4-2 R	CTTATCAAACTGCATGGTGTGG	Genotyping krp4-2 mutants
Ds5-1	GAAACGGTCGGGAAACTAGCTCTAC	Genotyping krp4-2 mutants
fbl17-1 F	TTCAACTGTCCAAATCTTACGG	Genotyping fbl17-1 mutants
fbl17-1 R	TAACTTTGGACATTGTAGCACC	Genotyping fbl17-1 mutants
GABI BP	ATATTGACCATCATACTCATTGC	Genotyping fbl17-1 mutants
KRP3-sgRNA1	TGT GGTCTC A ATTG TGAAGAAATCAAAGATAAC GTTTTAGAGCTAGAAATAGCAAG	CRISPR of KRP3
KRP3-sgRNA2	TGT GGTCTC A ATTG TGGTTCGAACACCTGGACT GTTTTAGAGCTAGAAATAGCAAG	CRISPR of KRP3
KRP5-sgRNA1	TGT GGTCTC A ATTG TTTGACATTGATTGACACT GTTTTAGAGCTAGAAATAGCAAG	CRISPR of KRP5
KRP5-sgRNA2	TGT GGTCTC A ATTG TTAGAGCCGGATACGACGA GTTTTAGAGCTAGAAATAGCAAG	CRISPR of KRP5
sgRNA R	TGTGGTCTCAAGCG TAATGCCAACTTTGTAC	sgRNA common reverse primer for CRISPR
krp3-11 F	GAAATCAAAGATCCAGGTGTTCG	Genotyping krp3-11 mutants
KRP3 F	GATATCAGCGTCATGGAAGTCTC	Genotyping krp3-11 mutants
krp3-11 R	TCAACGCGAGACCTGGAACC	Genotyping krp3-11 mutants
krp5 F	CATTAAGAAGTCAAAAGTCGCCG	Genotyping krp5 mutants
krp5 R	TGATTTTGAATCACTTATCATGCTC	Genotyping krp5 mutants
SMR11 sgRNA1	TGT GGTCTC A ATTG TAGATCTCGTGAATCCAAA GTTTTAGAGCTAGAAATAGCAAG	CRISPR of SMR11
SMR11 sgRNA2	TGT GGTCTC A ATTG CTGTTTCTTTCGCTTCACA GTTTTAGAGCTAGAAATAGCAAG	CRISPR of SMR11
SMR16 sgRNA1	TGT GGTCTC A ATTG GAGTTTTCTTCATAGTCCA GTTTTAGAGCTAGAAATAGCAAG	CRISPR of SMR16
SMR16 sgRNA2	TGT GGTCTC A ATTG TAACTCCTATGATCTCTAA GTTTTAGAGCTAGAAATAGCAAG	CRISPR of SMR16
smr11 Gen F	GGCGCAAACCAAAAGCAAG	Genotyping smr11 mutants
smr11 Gen R	GAAGAATCGGAATCAATGGCAGG	Genotyping smr11 mutants
smr16 Gen F	TTTTCCAGATATTGTGACACCATC	Genotyping smr16 mutants
smr16 Gen R	GTGAGAACCATAACCAGATTCCTC	Genotyping smr16 mutants
pSMR11 F	GTGGTCTC T GGAG CTAATCGTTATTCATTTGTCACCCACTG	Cloning SMR11 to fuse it to GFP
pSMR11 F1 R	GTGGTCTC C TCAA CTAGACCGTTGTTATTAATC	Cloning SMR11 to fuse it to GFP
pSMR11 F2 F	TCGTGAATTGATTAATAACAAC GGTC	Cloning SMR11 to fuse it to GFP
pSMR11 R	GT GGTCTC A AGTA TTGGATTCACGAGATCTAAGCAG	Cloning SMR11 to fuse it to GFP
SMR11 CDS F	GTGGTCTC T AATG GAGCAAGAAGAACCATGT	Cloning SMR11 to fuse it to GFP
SMR11 Ter R	GTGGTCTC T AGCG CCATGAAAGACCAAGCAAAGATC	Cloning SMR11 to fuse it to GFP

Table 8.3: Primer list. List of primers used in this work. These include, primers used for genotype and sequence constructs, as well as primers used in the making of CRISPR lines.

Arabidopsis transformation was carried out as previously reported (Clough and Bent, 1998), as follows: an *A. tumefaciens* colony with the construct of interest was inoculated in 10ml LB liquid medium plus antibiotics (same as LB plates see above) and incubated for 48h at 28˚C. 5ml of this culture was used to inoculate 500ml LB liquid medium plus antibiotics and incubated overnight at 28˚C. Cells were spun at 3k RPM for 20min, the supernatant discarded, and resuspended in 400ml of dipping solution (5% (w/v) sucrose, 0.05% (v/v) Silwet L-77 (De Sangosse Ltd)). Siliques from 5 to 6 weeks old Arabidopsis plants were removed with scissors and the inflorescence was dipped in the bacteria mixed dipping solution for 2 to 3min. Plants were left overnight at room temperature covered from light, then moved to 20˚C 16h light for seed production.

8.4 Tissue staining

For live imaging, samples were incubated in water for 5min, washed and incubated in 50µg/ml of with FM™4-64 (Invitrogen™) for 10min. Samples were then washed twice with water before imaging.

mPS-PI (modified pseudo-Schiff-propidium iodide) staining protocols (including EdU and Alexa Fluor™ 488 succinimidyl ester staining) were carried out as previously reported (Schiessl *et al.*, 2012) as follows: samples were dehydrated in ethanol by serial incubation for 15min with 15%, 30%, 50%, 70%, 85%, 95% and 100% (v/v) ethanol. Samples were then incubated overnight in 100% (v/v) ethanol. In case the apexes were not fully dissected, dissection was completed as described above (see plant materials), but 100% ethanol was used instead of water. Apexes were then excised but beneath the oldest remaining floral meristem, approximately 150µm below the meristem dome, and moved into a 70µm nylon cell strainer (Corning®) placed in a 6-well CytoOne® plate (starlab), submerged in 100% ethanol. Apexes were rehydrated by serial incubation for 15min with 95%, 85%, 70%, 50%, 30%, and 15% before washing with water twice for 10min. Samples were then moved in an α-amylase solution (300µg/ml of α-amylase (Sigma-Aldrich®), 20mM phosphate buffer pH7, 2mM sodium chloride, 0.25mM calcium chloride) and incubated overnight at 36˚C. Samples where then washed twice in water.

For Alexa Fluor™ 488 succinimidyl ester staining, samples were washed twice with bicarbonate buffer (0.1M sodium bicarbonate buffer, pH 8.3). Samples were then incubated with 40µg/ml with Alexa Fluor™ 488 succinimidyl ester dye (Invitrogen™) in

bicarbonate buffer for 1h protected from light, before being washed three times with water.

For EdU staining, samples were washed twice with TBS (8g/L sodium chloride, 200mg/L potassium chloride, 3g tris base (Thermo Scientific™), pH 7.4). Samples were incubated in 10µM Alexa Fluor™ 488 Azide (Invitrogen™) in 100mM Tris, pH 8.5 for one hour while protected from light. Samples were moved to staining mix (100mM Tris, pH 8.5, 1mM copper sulphate, 10µM Alexa Fluor™ 488 Azide, 100mM ascorbic acid) and incubated for 30min protected from light, before being washed twice in water.

For mPS-PI staining, the samples were moved into 1% (m/v) periodic acid (Sigma-Aldrich®) and incubated for 30min at room temperature. Samples were washed twice with water, moved into Schiff reagent (1.9%(m/v) sodium bisulfite (Sigma-Aldrich®), 0.0125% hydrogen chloride solution, 20µg/ml propidium iodide (Invitrogen™)) and incubated for 2h protected from light. Samples were washed twice with water an mounted on a 15x1mm single cavity slides (Agar Scientific). Excess water was removed using filter paper, and 20µl of chloral hydrate solution (4g chloral hydrate, 0.5 ml glycerol, 1 ml water) was added to cover the samples. Samples were incubated for 20min, the excess chloral hydrate was removed and 90µl of Hoyer's medium (40 g chloral hydrate, 10 ml water, 4 ml glycerol, 6 g Gum Arabic (Sigma-Aldrich®)), previously centrifuged at maximum speed for 20min, was added to cover the sample. A cover slip was placed atop the cavity and shifted to position the sample upwards. Samples were left hardening overnight prior to imaging.

For DAPI staining, dissected apexes were incubated for 20min in 100µg/ml of FM™ 4-64FX, fixable analog (Invitrogen™). Samples were washed in PBS buffer (0.99g/L of phosphate saline buffer pH 7.4, Formedium™) and moved in 3%(v/v) formaldehyde in PBS buffer. Samples were incubated on ice and left under vacuum for 2min, prior to incubation for 30min on ice at room pressure. The apexes were then washed 3 times in PBS and moved in 1µg/ml of DAPI (Sigma-Aldrich®) in PBS and incubated for 1hat room temperature. Samples were washed once with PBS and once with water and finally imaged in water (see confocal microscopy).

8.5 Confocal microscopy

Fluorophore excitation wavelengths were set as follows: 406nm for DAPI, 458nm for CFP, 488nm for GFP, YFP and FM™4-64, and 514nm for mCherry and RFP. For imaging of fixed samples, a 40x 1.3 Plan-Neofluar oil immersion objective was used. For imaging of live samples, a 40x 1.1 water immersion C-Apochromat objective was used. For ZEISS LSM780 or 880 in confocal mode, emission filters were adjusted manually depending on the samples, with 572–625 nm for PI and 505-600 nm for Alexa 488 dye. For Airyscan imaging on the ZEISS LSM880, the emission filters were used as follows: band pass 420-480nm, long pass 570nm for GFP and YFP; band pass 495-550nm, long pass 570nm for mCherry; band pass 420-480nm, long pass 525nm for CFP.

8.6 Image analysis

To segment images, and to locate, measure and track the segmented cells, a combination of Fiji macros and Python scripts were used as previously described (Serrano-Mislata, Schiessl and Sablowski, 2015), with minor changes for optimisation. In short, images were converted from .lsm to .tif using Fiji macros and segmented using the watershed algorithm implemented in SimpleITK. FIJI macros were also used to landmark cells in 3D, required to detect the central zone of the meristem and for automatic image alignment (D'Ario *et al.*, 2021). Raw data were collected in .cvs tables and analysed further (see below).

For MorphoGraphX, .tif images were segmented using inbuilt functionalities (Sapala *et al.*, 2018; Zhu *et al.*, 2020). Briefly, images where segmented with the help of a computational neuronal network algorithm (Çiçek *et al.*, 2016) and segmented using SimpleITK segmentation functions. A 3D mesh was generated, and alignment was conducted manually across time points. Cells showing preprophase bands were selected manually and raw data were collected in .csv tables to be analysed further (see below).

8.7 Data analysis and mathematical modelling

All the raw data produced with Python scripts and MorphoGraphX were analysed using custom scripts in MATLAB. Briefly, the most used functions: the plot() function was used to produce various graphs, polyfit() was used to produce linear regressions, tTest() for comparisons and kstest2() for two-sample Kolmogorov-Smirnov test. Other scripts were generated to locate individual cells in lineages array (for the long-time courses for example) and plot them.

For the mathematical model implementation, a function for the differential equations described in Chapter 5 was implemented and the MATLAB function ode15() was used to find the numerical solution based on set thresholds described in Chapter 5, before asymmetric division was carried out. A function would use the solution of this divided cell to create and grow a new cell, with a new solution. The details of cell cycle progression, asymmetric division and thresholds used are described in more detail in Chapter 5.

The following references complement Tables 8.1 and 8.2: (Desvoyes *et al.*, 2019)(Willis *et al.*, 2016)(Magyar *et al.*, 2012)(Springer, 2000)(Li *et al.*, 2007)(Kim *et al.*, 2008)(Müller, Han and Smith, 2006)(Gutierrez *et al.*, 2009)(Zuo, Niu and Chua, 2000)

8.8 References

Çiçek, Ö. *et al.* (2016) '3D U-Net: learning dense volumetric segmentation from sparse annotation', in *International conference on medical image computing and computer-assisted intervention*. Springer, pp. 424–432.

Clough, S. J. and Bent, A. F. (1998) 'Floral dip: a simplified method for Agrobacterium-mediated transformation of Arabidopsis thaliana.', *The Plant journal : for cell and molecular biology*. England, 16(6), pp. 735–743.

D'Ario, M. *et al.* (2021) 'Cell size controlled in plants using DNA content as an internal scale', *Science*, 372(6547), p. 1176 LP-1181. doi: 10.1126/science.abb4348.

Desvoyes, B. *et al.* (2019) 'FBL17 targets CDT1a for degradation in early S-phase to prevent Arabidopsis genome instability', *bioRxiv*, p. 774109. doi: 10.1101/774109.

Engler, C. *et al.* (2014) 'A Golden Gate Modular Cloning Toolbox for Plants', *ACS Synthetic Biology*. American Chemical Society, 3(11), pp. 839–843. doi: 10.1021/sb4001504.

Gutierrez, R. *et al.* (2009) 'Arabidopsis cortical microtubules position cellulose synthase delivery to the plasma membrane and interact with cellulose synthase trafficking compartments', *Nature Cell Biology*, 11(7), pp. 797–806. doi: 10.1038/ncb1886.

Hamant, O., Das, P. and Burian, A. (2014) 'Time-Lapse Imaging of Developing Meristems Using Confocal Laser Scanning Microscope BT - Plant Cell Morphogenesis: Methods and Protocols', in Žárský, V. and Cvrčková, F. (eds) *Plant Cell Morphogenesis*. Totowa, NJ: Humana Press, pp. 111–119. doi: 10.1007/978-1-62703-643-6_9.

Kim, H. J. *et al.* (2008) 'Control of plant germline proliferation by SCFFBL17 degradation of cell cycle inhibitors', *Nature*, 455(7216), pp. 1134–1137. doi: 10.1038/nature07289.

Li, Y. *et al.* (2007) 'GABI-Kat SimpleSearch: an Arabidopsis thaliana T-DNA mutant database with detailed information for confirmed insertions', *Nucleic acids research*. 2006/10/24. Oxford University Press, 35(Database issue), pp. D874–D878. doi: 10.1093/nar/gkl753.

Magyar, Z. *et al.* (2012) 'Arabidopsis E2FA stimulates proliferation and endocycle separately through RBR-bound and RBR-free complexes', *The EMBO Journal*, 31(6), pp. 1480–1493. doi: 10.1038/emboj.2012.13.

Müller, S., Han, S. and Smith, L. G. (2006) 'Two Kinesins Are Involved in the Spatial Control of Cytokinesis in Arabidopsis thaliana', *Current Biology*, 16(9), pp. 888–894. doi: https://doi.org/10.1016/j.cub.2006.03.034.

Sapala, A. *et al.* (2018) 'Why plants make puzzle cells, and how their shape emerges', *eLife*. Edited by S. McCormick. eLife Sciences Publications, Ltd, 7, p. e32794. doi: 10.7554/eLife.32794.

Schiessl, K. *et al.* (2012) 'JAGGED controls growth anisotropy and coordination between cell size and cell cycle during plant organogenesis', *Current Biology*. Elsevier Ltd, 22(19), pp. 1739–1746. doi: 10.1016/j.cub.2012.07.020.

Serrano-Mislata, A., Schiessl, K. and Sablowski, R. (2015) 'Active Control of Cell Size Generates Spatial Detail during Plant Organogenesis', *Current Biology*. The Authors, 25(22), pp. 2991–2996. doi: 10.1016/j.cub.2015.10.008.

Springer, P. S. (2000) 'Gene traps: tools for plant development and genomics', *The Plant cell*. American Society of Plant Physiologists, 12(7), pp. 1007–1020. doi: 10.1105/tpc.12.7.1007.

Willis, L. *et al.* (2016) 'Cell size and growth regulation in the *Arabidopsis thaliana* apical stem cell niche', *Proceedings of the National Academy of Sciences*, 113(51), pp. E8238–E8246. doi: 10.1073/pnas.1616768113.

Zhu, M. *et al.* (2020) 'Robust organ size requires robust timing of initiation orchestrated by focused auxin and cytokinin signalling', *Nature Plants*, 6(6), pp. 686–698. doi: 10.1038/s41477-020-0666-7.

Zuo, J., Niu, Q. and Chua, N. (2000) 'An estrogen receptor-based transactivator XVE mediates highly inducible gene expression in transgenic plants', *The Plant Journal*. Wiley Online Library, 24(2), pp. 265–273.